THE DESIGN AND INVESTIGATION OF AN EXTREMELY LOW FREQUENCY (ELF) TRANSMISSION DATA LINK

AYMAN AHMED ALAIWI

A thesis submitted to the University of Huddersfield in partial fulfilment of the requirements for the degree of Doctor of Philosophy

The University of Huddersfield
July 2013

Publications and Achievements (*See Appendix*)

1- Alaiwi, A., Sibley, M., Mather, P. and Holmes, V. (2009) Extremely low frequency based communication link. In: *Computing and Engineering, Emerging Technologies in Computing and Engineering*. (2009) Huddersfield. Proceedings of Computing and Engineering Annual Researchers' Conference 2009: CEARC'09, December 2009.

2- Alaiwi, A., Sibley, M. and Mather, P. (2013) Demonstration of data transmission using an Extremely Low Frequency (ELF) Carrier. In*: Computing and Engineering, Emerging Technologies in Computing and Engineering*. (2013) Huddersfield. Proceedings of Computing and Engineering Annual Researchers' Conference 2013: CEARC'13, December 2013.

3- Alaiwi, A., Sibley, M. and Mather, P. 2013, *Improvements to Receivers and Method of Use Thereof*. Application #: PS-BF-G47213. Patent number to be confirmed by the lawyer - BAILEY WALSH & CO LLP. (3M Buckley Innovation Centre).

4- Alaiwi, A., Sibley, M. and Mather, P. (2013) Demodulation of PSK signals using cross-correlation techniques. *IEEE Transaction on Communication.* To be submitted once the patent number (above) is confirmed.

5- Alaiwi, A., Sibley, M. and Mather, P. (2013) Demodulation of 16-QAM signals using cross-correlation techniques. *IEEE Transaction on Communication.* To be submitted once the patent number (above) is confirmed.

(Contact Dr. Martin Sibley or Dr. Peter Mather if you have any doubts about publications 3, 4 & 5)

ABSTRACT

The telecommunication engineering field is playing a big role in the technology revolution, with most new technologies, smart phones and computers etc requiring 3G internet connection to be constantly in communication worldwide. A high spectral efficiency spectrum and maximising the number of users and transmission rate within a frequency band are the most critical design objectives and challenge to improve the reliability and performance of wireless communications systems.

The use of the Extremely Low Frequency (ELF) band has largely been confined to submerged submarine communications and its application to civilian data transmission has been neglected. ELF signals propagate through the ground itself using earth rods for long distances without regeneration compared to Radio Frequency (RF). There are two major noise sources in the ELF band, namely flicker noise (1/f) and 50Hz radiation of power feed cables underground. This thesis has described the theoretical aspects of adopting the ELF band and the ground itself as transmission medium in a communication link based on Orthogonal Frequency Division Multiplex (OFDM) scheme. The use of 16-Quadrature Amplitude Modulation (16-QAM) and OFDM in ELF link enhances the transmission capacity at such low frequencies and reduces the multi-path interference. The link could handle at least 1000 bit/s (bps) and replace the complexity and reduces the power needed for RF link in some applications.

This thesis investigated the practical implementations of Binary Amplitude Shift Keying (BASK), 8-Phase Shift Keying (8-PSK) and 16-QAM with 20 Hz carrier and a data rate of *4 symbols/s* from context to practice using Field Programmable Gate Array (FPGA). The highly flexible nature of FPGAs allows the systems designers to integrate any signal processing function. FPGAs replace the use of Digital Signal Processing (DSP) processors in many applications. Very high speed circuit Hardware Description Language (VHDL) language, Matlab, Altera DSP Builder and Altera Quartus II were used to design the ELF link.

A thorough literature review showed that demodulating phase data is generally performed using carrier recovery. The current technology generally incorporates a complex mathematics 'tan' function and Costas loop to detect the phase changes of the 8-PSK and 16-QAM signals. The 8-PSK and 16-QAM are widely used in Wide-band Code Division Multiple Access (WCDMA), High-Speed Download Packet Access (HSDPA), World-wide Inter-operability for Microwave Access (WiMAX) and Wireless Local Area Network (WLAN) Broadband wireless access technologies. Alternative method has been proposed to use cross correlation to detect the phase modulated data. Patent literature review showed that there is no such patent or known prior art related to the proposed technique. This novel technique does not extract the carrier for demodulation purposes and offer improved phase detection performance as well as superior resistance to Additive-White-Gaussian-Noise (AWGN) compared to a carrier recovery scheme operating at low Signal-to-Noise-Ratio (SNR).

The proposed demodulation scheme significantly reduces the implementation resources to demodulate 8-PSK and 16-QAM. As a consequent, this technique will yield cost reduction in products using 8-PSK and 16-QAM demodulators, namely Broadband internet and Digital TV. Furthermore, the cross correlations would have potential impacts on the development of ELF link using OFDM scheme that would require significantly less resources compared to recent OFDM systems.

ACKNOWLEDGMENT

In The Name of Allah, The Compassionate, Most Merciful. All Praise belongs to Allah, the Lord of the worlds and the Maker of all creation, and may Peace and benedictions be upon His servant and messenger, His beloved and elect, our master, our prophet, and our sir, Abul Qasim Mohammed, may Allah bless him and his pure, immaculate, and infallible Progeny, Ahlulbayt (A.S.). Alhamdulillah, all praises to Allah for the strengths and His blessing in completing this thesis. I thank God for all opportunities, trials and strength that have been showered on me to complete my thesis. I am grateful to "Allah", for bestowing me with affectionate parents, Sister Eman, IT Teacher and Brother Mohammed, BIS Student, whose love, dedication and inspiration encouraged me to undergo higher studies. Their sacrifice, heartiest, countless blessings and firm faith have made this documentation a puny remuneration to translate their and my dreams into reality.

I am extremely grateful to the University of Huddersfield for the Fee-Waiver Scholarship. Special thanks go to Haji Hassan Group W.L.L. for providing the Education Loan. It is my privilege to place on record my profound gratitude and thanks to the members of my supervisory committee viz; Dr. Martin Sibley, Reader, and Dr. Peter Mather, Senior Lecturer. I wish to express my sincere appreciation to my mentor tutor; Dr. Violeta Holmes.

I am particularly and greatly indebted to my fiancé (Zainab Alfaraj – Al Awamiyah, Engineer to be), for her love, support, encouragement, patience and understanding to the critical time of my research. Special thanks also go to my father-in-law (Ahmed Alfaraj – Al Awamiyah, Electrical Engineer), for his continuous support and encouragement.

I can hardly overlook the co-operation, timely help and moral support extended by my friends and colleagues especially Mr. Mohammed Mojbel – A'ali, Automotive Engineer and Teacher, Mr. Mirza Eid – Sanad, Driving Trainer, Mr. Ali Ayoub – Sayhat, Mechanical Engineer, Mr. Emad Al-Shafei – Sayhat, Chemical Engineer and PhD Researcher, Sayed Saleh Sharaf – Jed Hafs, Maintenance Engineer, Mohammed Khamis, Communication Engineer, Mustafa Ramadan, Logistic Driver, Sulaiman Alshaabani – Alduraz, Server Engineer, Kumail Majeed Alshehabi – Alduraz, Security man , Mr. Brian Haigh – Huddersfield, Historian and Project Officer. Acknowledgements are inherently endless and incomplete, and I request indulgence from many friendly and helpful people whom I could not name here, due to paucity of space.

Content **Page**

Content (cont.) **Page**

Content (cont.) **Page**

Content (cont.) **Page**

Content (cont.) **Page**

List of figures

List of tables

Symbol	Definition
3G	third-generation
3GPP	3rd Generation Partnership Project
ADC	Analogue-to-Digital Converter
ADSL	Asynchronous Digital Subscriber Line
AGC	Automatic-Gain-Controller
AIBS	American Institute of Biological Sciences
AM	Amplitude Modulation
ASK	Amplitude Shift Keying
AWGN	Additive White Gaussian Noise
BASK	Binary Amplitude Shift Keying
BCRC	British Cave Rescue Council
BER	Bit-Error-Rate
BPF	band pass filter
bps	bit-per-second
BPSK	Binary Phase Shift Keying
CDMA	Code Division Multiple Access
CNR	Carrier-to-Noise-Ratio
COFDM	Coded Orthogonal Frequency Division Multiplex
CRO	Cave Rescue Organisation
CTIA	Cellular Telecommunications Industry Association
DAB	Digital Audio Broadcasting
DAC	Digital-to-Analogue Converter
DFT	Discrete Fourier Transform

Symbol	Definition
DIP	Dual in-link Package
DPLL	Digital Phase-Locked-Loop
DPSK	Differential Phase Shift Keying
DS-CDMA	Direct Sequence Code Division Multiple Access
DSP	Digital Signal Processing
DVB	Digital Video Broadcasting
DVB-T	Digital Video Broadcasting – Terrestrial
EbNR	Bit-to-Noise-Ratio
ELF	Extremely Low Frequency
EMC	Electromagnetic Compatibility
EsNR	Symbol-to-Noise-Ratio
ETT	European Transaction on Telecommunications
FCC	Federal Communications Commission
FDD	Full Division Duplex
FDMA	Frequency Division Multiple Access
FFT	Fast Fourier Transform
FH-CDMA	Frequency Hopping Code Division Multiple Access
FIR	Finite Impulse Response
FPGA	Field Programmable Gate Array
FSK	Frequency Shift Keying
HDSL	High-bit-rate Digital Subscriber Line
HIPERLAN	High Performance Local Area Network
HPF	High Pass Filter

Symbol	Definition
HSPDA	High-Speed Downlink Packet Access
IC	Integrated Circuits
ICI	Inter-Carrier-Interference
IEEE	Institute of Electrical and Electronics Engineers
IFFT	Inverse Fast Fourier Transform
IP	Intellectual Property
ISI	Inter-Symbol-Interference
ITU	International Telecommunication Union
JFET	Junction Field-Effect Transistor
LF	Low Frequency
LO	local oscillator
LPF	low pass filter
LSB	Least Significant Bit
LUTs	Look-Up-Tables
MBC	Murray Broadcasting Company
MC-CDMA	Multi-Carrier Code Division Multiple Access
MC-DS-CDMA	Multi-Carrier Direct Sequence Code Division Multiple Access
MIA	Multiple access interference
MOSFET	Metal-Oxide Semiconductor Field-Effect Transistor
MSB	Most Significant Bit
MUX	Multiplexer
NCO	Numerically Controlled Oscillator
NRC	National Research Council

Symbol	Definition
OFDM	Orthogonal Frequency Division Multiplex
OOK	On-Off Keying
PAPR	Peak-to-Average-Power-Ratios
PCM	Pulse Code Modulation
PCS	Personal Communication Service
PIMRC	International Symposium on Personal, Indoor and Mobile Radio Communications
pk-pk	peak-to-peak
PLL	Phase-Locked-Loop
PN	Pseudo-Noise
Pr	Probability
PRBS	Pseudo Random Binary Sequence
P/S	Parallel to Serial
PSK	Phase Shift Keying
QAM	Quadrature Amplitude Modulation
QPSK	Quadrature Phase Shift Keying
RDS	Radio Data System
RF	radio frequency
SER	Symbol Error Rate
SNR	signal-to-noise-ratio
S/P	Serial-to-Parallel
SPST	Single-Pole-Single-Throw
SR	Schumann resonance

Symbol	Definition
SSB	Single Side Band
TDMA	Time Division Multiple Access
TIA	Telecommunications Industry Association
UART	Universal Asynchronous Receiver/Transmitter
UK	United Kingdom
UPR	User Performance Requirements
US	United States
UWB	Ultra Wide Band
VCA	Voltage-Controlled-Amplifier
VCO	Voltage-Controlled-Oscillator
VF	Voice Frequency
VHDL	Very high speed circuit Hardware Description Language
VLF	Very Low Frequency
WCDMA	Wide-band Code Division Multiple Access
WiMAX	World-wide Inter-operability for Microwave Access
WLAN	Wireless Local Area Network

Symbol	Definition
A	Peak amplitude of carrier
a_1	ODD data NRZ
a_2	EVEN data NRZ
a_n	Modulator data input
β	Detected phase
B	Bandwidth
B_s	Information bandwidth (CDMA)
b_n	Modulator data input
c_n	Modulator data input
C	Speed of light
$d_i(t)$	The data sequence Non-Return-to-Zero (NRZ)
d_n	Modulator data input
E_1	Energy of logic 1
E_0	Energy of logic 0
erf	Error function
erfc	complementary error function
E_b	Energy per bit
E_s	Energy per symbol
f_c	Carrier frequency
g	LPF/integrator output
H	Continuous variable
j	Complex imaginary part notation
k_p	The proportionality factor relating the phase shift to the signal voltage

Symbol	Definition
m_i	Modulation index
m	The mean value of density and symmetry point
M	M-ary constellation points
N_o	Noise density, *watt/Hz*
n_{nb}	Narrowband noise
n	Number of sample
P_c	Carrier power
P_i	Sideband power
P_e	Probability of error
P_N	Noise power
P_d	Data power
$P_{e_{BPSK}}$	Probability of error of the BPSK scheme
$P_{e_{DPSK}}$	Probability of error of the DPSK scheme
$P_{e_{M-PSK}}$	Probability of error of the M-PSK scheme
$P_{e_{16-QAM}}$	Probability of error of the 16-QAM scheme
P_G	Processing gain
Q	a function to calculate the error rate
R_b	Bit rate
S_m	ASK signal
$s(t)$	Baseband information
$S_c(t)$	PSK signal
S_i	Modulator output/Correlator input

Symbol	Definition
S_o	Correlator output
S_{QAM}	QAM signal
t	Time, continuous variable
T_b	Bit period
T_c	Time of cross correlation
T_s	Symbol period
ω_c	Carrier angular frequency
w_1	Continuous variable
w_2	Continuous variable
w_3	Continuous variable
w_4	Continuous variable
$X(n)$	Real part sample
x	Continuous variable of the function
$x(t)$	In-phase noise
x_o	Recovered data
x_i	Modulator data
$Y(n)$	Imaginary part sample
y_0	Threshold of ASK
$y(t)$	Quadrature noise
y	Continuous variable in $P_{e_{M-PSK}}$ equation
$\mathrm{Z_n}$	Current sample
$\mathrm{Z_{n-1}}$	Delayed sample
$\overline{\mathrm{Z_{n-1}}}$	Complex conjugate of a delayed sample

Symbol	Definition
$\Delta\theta$	Phase difference
θ_e	Phase error
ΔdB	Gain difference
θ_0	Phase angle, representing logic 0
θ_1	Phase angle, representing logic 1
θ	Average angle
$\Delta\theta$	Phase deviation/modulation index
σ	Standard deviation (spread of density)
$(x-m)$	The deviation of x from the mean value
θ_t	Transmitter angle
θ_r	Receiver angle
$\Delta\theta_t$	Deviation of transmitted angle
$\Delta\theta_r$	Deviation of received angle
π	Mathematical constant, 3.142 and equivalent to 180^0
λ	Wavelength
γ	Conductivity

1. Introduction

The field of telecommunication engineering is playing a big role in the technology revolution, with most new technologies, smart phones and computers etc requiring third-generation (3G) internet connection to be constantly in communication worldwide. A high spectral efficiency and maximising the number of users and transmission rate within a frequency band are the most critical design objectives and challenges to improve the reliability and performance of wireless communications systems.

Modulation is the process of converting a series of data bits to signals that can be transmitted over a communications medium. The modulation can be carried out by altering the magnitude, frequency, or phase of a signal. Digital data transmissions include Amplitude Shift Keying (ASK), Frequency Shift Keying (FSK), Phase Shift Keying (PSK) and others. A combination of phase and amplitude modulation is considered to be the most efficient in terms of wireless communication system capacity, with the 16-Quadrature Amplitude Modulation (QAM) technique being one of the most efficient techniques.

PSK and 16-QAM are widely used in Wide-band Code Division Multiple Access (WCDMA), High-Speed Downlink Packet Access (HSDPA), World-wide Inter-operability for Microwave Access (WiMAX) and Wireless Local Area Network (WLAN) broadband wireless access technologies [1]. The HDSPA, WiMAX and WLAN are part of the 3rd Generation Partnership Project (3GPP) WCDMA, Institute of Electrical and Electronics Engineers (IEEE) 802.16 and IEEE 802.11 standards respectively [1]. Applications of 16-QAM includes mobile and fixed broadband internet [1]. In addition, for domestic broadcast applications, 64-QAM and 256-QAM are often used in digital cable television and cable modem applications. In the UK, 16-QAM and 64-QAM are currently used for digital

terrestrial television using Digital Video Broadcasting (DVB-T) [2]. The 16-QAM is one of the standard modulation schemes in Orthogonal Frequency Division Multiplex (OFDMs') [3] applications such as DVB-T and High Performance Local Area Network (HIPERLAN) [4].

This thesis is concerned with the use of these advanced techniques in an Extremely Low Frequency (ELF) link. Chapter 2 is a literature review including background to the use of the ground as a transmission medium, current use of the ELF band, digital data transmissions and multi-carrier communication systems. It was found that the ground can be used as transmission medium using buried earth rods. The use of the ELF band has largely been confined to submerged submarine communications and its application to civilian data transmission has been neglected. A Field Programmable Gate Array (FPGA) can be used to design, simulate, build and test the ELF Transmission Data Link. The highly flexible nature of FPGAs allows the systems designers to integrate any signal processing function and FPGAs can replace the Digital Signal Processing (DSP) processors in many applications. OFDM can be used to enhance the transmission rate of a given bandwidth and offers high spectral efficiency due to the large number of digital modulation sub-carriers that form nearly rectangular frequency spectrum. In contrast, Spread spectrum systems allow multiple access simultaneously and privacy within the same channel but significantly reduces the speed of the same channel. These techniques are explored for use in an ELF link.

Chapter 3 is concerned with the practical implementation of an ASK transmitter and receiver with 20 Hz carrier. The data rate is 4 *symbols/s* and 1 *bit/symbol*. The advantage of using ASK is that it is more straightforward to generate/recover data compared to PSK and FSK.

A Literature review has shown that demodulating phase data is generally performed using carrier recovery. The current technology generally incorporates a complex mathematics 'tan' function to detect the phase changes of the 8-PSK and 16-QAM signals. This requires carrier signal recovery circuitry and Look-Up-Tables (LUTs) to distinguish phase levels and changes on the received signals. Consequently, large memory blocks are required to perform the demodulation processes which requires significant levels of Integrated Circuit (IC) resources to be implemented. Consequently, this inspired the need for a novel and simpler function than the carrier recovery, which is where the concept of cross correlation to detect the phase changes is investigated in chapter 4. Patent literature review showed that there is no such patent or known prior art related to the presented system design in chapters 4 and 5.

Chapter 4 discusses the use of an FPGA to implement 8-PSK transmitter and receiver with 20 Hz carrier. PSK can only be demodulated using coherent detectors. The data rate is 4 *symbols/s* and 3 *bit/symbol*. Chapter 5 combines the ASK and 8-SPK designs in Star 16-QAM transmitter and receiver FPGA design with 20 Hz carrier. The data rate is 4 *symbols/s* and 4 *bit/symbol*. A cross-correlation theory and its FPGA implementations will be used in chapters 4 and 5 to extract the phase modulated data. Chapter 6 discusses overall conclusions of previous chapters, the issues and applications related to the use of ground as transmission medium, ELF band and multi-carrier (i.e. OFDM) communication systems in implementing a complete ELF Transmission Data Link based on the facts presented in the literature review and the implementations of the digital modulation schemes in chapters 3, 4 and 5.

1.1 Statement of the thesis

The thesis sets out the main objective of designing and building 8-PSK and Star 16-QAM using 20 Hz carrier and cross correlation to detect the phase data from context to practice. This will be done through stages by designing ASK and 8-PSK transmitters and receivers. After that, the ASK and 8-PSK designs will be utilized to build a Star 16-QAM transmitter and receiver. Furthermore, the theoretical aspects of adopting the ELF band and the ground itself as transmission medium in a communication link based on OFDM scheme will be discussed. The cross correlation technique would have potential impacts on the development of ELF links using an OFDM scheme - it would require significantly less resources compared to recent OFDM systems. This link can be used in any system where the response time is not critical. Possible applications include sensing and broadcasting the weather of mountain areas, remote control and telemetry of oil wells, valves and motors, power substations, and switches in train tracks. Various features could be embedded to the link such as text, voice and video messaging for subterranean and rural areas.

2. Literature Review

2.1 Background to ground as transmission medium

2.1.1 Wireless communications in the 19th Century

In the 1830s, Michael Faraday from England and Joseph Henry from America discovered possibilities of wireless telephone [5]-[8]. Firstly, the electric current generates static electricity that may under certain conditions discharge as a spark – the so-called spark gap transmitter [9]. The second possibility is that the current generates a magnetic field around and perpendicular to a coil connected to the circuit. This field will in turn stimulate current in a second separate coil nearby. Variations in the current through the first coil will create proportional variations in the current through the second and this is called electromagnetic induction. In 1842, Henry detected wireless electricity from a coil 200 yards away [8]. The third possibility of wireless transmission is that the electric current through the first coil generates a magnetic field that radiates electromagnetic waves through the atmosphere. This is done when one end of the coil is grounded and the other terminates in an elevated metal plate or grid. This is electromagnetic radiation. Although the waves propagate to distances that far exceed the electromagnetic induction field, they require a more sophisticated detector at the receiver [10]. This is the system in use today.

Telecommunication inventors tried to employ electrical technologies, including natural conduction, modulated light, induction and finally electromagnetic waves. Samuel F.B. Morse was the first inventor who used a canal as natural conduction by running insulated wires underwater: Morse came up with the name wireless telegraph [7], [8], [11], [12].

> "*In Germany, Sommerling and Steinhil had shown that water or earth could serve as conductor for an electrical circuit*" *(Closed circuit). [13]*

Hence, telegraphs replaced the second wire in the system with ground conduction. Samuel believed that replacing a wire by the earth or water then the second wire can be replaced as well. He used two plates in one side of the river and two on the other side and successfully managed to send signals to the other side of the river (wireless telegraph by natural resource conduction). The span of transmission was 80 yards only (0.046 mile). Morse's assistant later transmitted messages across the Susquehanna River at Havre de Grace, Maryland a distance of 1 mile. They found that the larger the metal plates and more widely spaced they were, the longer the transmission distance and the higher the quality of the signals [7], [8], [11], [12].

In the mid 1860s, the dentist Mahlon Loomis from Washington DC successfully tested his wireless telegraph [8], [12]. His system used two light weight metal grids hoisted on kites from hilltops. These grids were connected to the ground directly using metal wires. The top side was a superior electrical conductor and the electricity there had opposite charge from that of the earth. Loomis reckoned that his system was merely a completed circuit and all he needed was a device like the telegraph. In 1866, he tested this apparatus successfully at a distance of 14 miles and received a United States (US) patent on it six years later [8], [12].

William Henry Ward of Auburn, New York, learned of the Loomis Wireless Telegraph and used a vented taper with a horizontal vane at the top that rotated in the wind [8], [12], [13]. It was constructed of two dissimilar metals so the vane produced a low-voltage electric signal in moist air. Hence, combination of wind and hot air rising through the core of tower would propel the signal to the next tower and that is called the wireless by convection.

After that, Alexander Graham Bell created a refinement of the Morse wireless for experimental communication between two boats [7], [12]. He tested this telephone system on

the Potomac River near Washington in 1879 at a distance of up to a quarter of a mile but obtained poor results. He suspected that the poor quality was because the telephone transmitter was at fault. By then, he wanted to invent optical wireless telephone using the naturally photo-electric element selenium in the receiver to turn light intensity and fluctuation into an electric telephone signal. He worked with Charles Sumner Tainter at his lab in Washington. After two years of perfecting the invention, he named it the Photophone and was awarded the first US patent for a Wireless telephone in December 1880 [7], [12]. The American Bell Telephone never progressed beyond the novelty stage as the mechanism was too complicated.

A later version of the invention used radiant energy rather than the light as transmission medium. This was done by a French electrician who called it Radiophone which was the first use of the term radio for a wireless telephone. Also, Lloyd Espenschied an Electric engineer pointed out that with its claim to modulate the radiant energy by sound, Bell's invention was the basis of Amplitude Modulation (AM) radio [9].

In 1866, the Scottish mathematician James Clerk Maxwell published a treatise on the nature of light and predicted the existence of electromagnetic waves at various frequencies and wavelengths [6]-[8], [10], [11], [14].

In the 1870s, Thomas Edison and Elihu Thompson in the United States and David Hughes in Britain encountered unexplained wireless electric phenomena that were probably radiated waves and Edison called it an "etheric force" [7]-[9], [12]. American inventors seemed to make more progress in the 1880s. Thomas Edison, Lucius Phelps and Granville Woods all received patents for wireless telegraphs and Amos Dolbear secured one for wireless

telephone based on induction [7], [8], [12], [13]. Dolbear was a professor at Tufts College in Massachusetts and discovered wireless telephony quite by accident. He described the event:

> *"While at work at the single terminal receiver ..... , the cord became detached from the line while I was unaware of it, and I still heard the speech from the transmitter plainly. Upon noticing this I began backing away from the end of the wire from the transmitter, letting the single cord hang free in the air. I could hear the talking in the most remote part of the room ...." [13].*

In the 1880s, several inventors wanted to create a telegraph system to communicate with moving trains. The main reason for having instant communication with the trains was to save the life of people and property. Granville Woods of Cincinnati was apparently the first to devise a wireless induction telegraph for this purpose in early 1881 [13]. William Wiley Smith of Indianapolis received the patent for such a device and attempted to communicate with existing telegraph lines running parallel to the train tracks, but its design was inferior. Lucius Phelps of New York advanced the technology further than his competitors. Later, Edison and Phelps formed the Consolidated Railroad Telegraph Company [7], [8], [12], [13].

Both Granville Woods and Lucius Phelps' system were quite similar [13]. A telegraph inside a railroad car was connected to a coil underneath. The secondary coil ran down the middle of the track, about 2 feet from the primary and was connected to a telegraph in the station. As the distance between the coils was short and relatively constant, the magnetic field remained strong enough for the system to work well. The main problem of this technology was the cost and not the design where the design required installing and maintaining delicate telegraph lines along the tracks as well as the equipment on the car. In 1888, German scientist Heinrich

Hertz finally proved the existence of electromagnetic waves by building equipment to transmit and receive them in his lab [6], [8], [11], [14].

2.1.2 Wireless communication through the ground – Stubblefield's contribution

Mr. Nathan Beverly Stubblefield (1860-1928) was a farmer from Kentucky-US. He was the first person to broadcast the human voice using a telephone system attached to ground electrodes [9]. At that time he had to pay a franchise fee to American Bell Telephone or invent his own equipment that did not conflict with any Bell patent, unless he waited until 1983 when the initial Bell patent would become public property. Hence he was encouraged to devise his own telephony. Stubblefield tried the acoustic telephones where signals vibrate the wires but the acoustic signals were audible and noisy.

His approach to natural conduction wireless communication was consistent with what Morse had used in 1842 and with Bell's experiments 20 years earlier [7], [8], [11], [12]. He found that he could easily double the transmission distance for his induction wireless [13], [15].

Stubblefield's telephones were attached to boxes whose contents were not divulged and wires connecting the boxes to a pair of metal rods that were sunk in the ground as shown in figure 2.1. Stubblefield's son usually operated the transmitter by whispering, whistling and blowing. Stubblefield discovered that receivers worked almost anywhere he could drive the ground rods and he often set-up multiple listening posts for simultaneous reception [9], [13], [15]. The users of Stubblefield Telephone at that time praised it for its good efficiency and clarity of transmission.

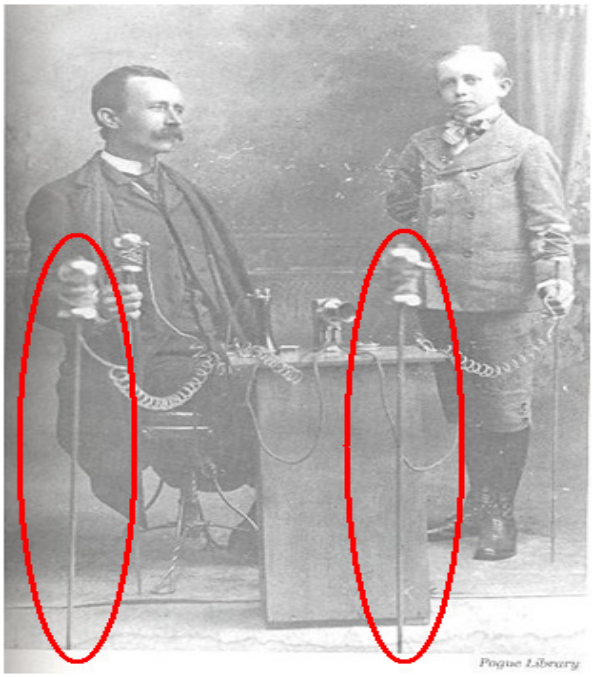

Figure 2.1: Mr. Stubblefield and his son with his telephone system attached to metal rods [13]

On New Year's Day of 1902, Stubblefield and his son demonstrated the usefulness of the technology and its broadcasting capability with a transmitter on the courthouse square. 1000 listeners at five receivers around the town heard the results of what was quite possibly the first wireless broadcast [9], [13], [15]. On January 1st 1902, the Paducah Sun-Democrat published that Mr. Stubblefield had achieved the wireless telegraphy and his system could be placed at the centre of the US with proper earth connections so that the signals flash to all parts of US. Thus at a cost of a few dollars, each home in the country may be equipped with a receiver and earth connection to receive the weather forecasts and the news of the day. Also, it could be used to send emergency information as a means to communicate between ships at sea to avoid wrecks. In March 1902, Stubblefield showed to scientists and people how easily he could communicate from ship to shore with his system. He set up a central station in a boarding house and tested the transmission over many places on the river and successfully received the signals. Stubblefield said he had achieved in a basic form something greater

even than Marconi [15]. His system was transmitting through wires dropped from the stern of a small boat on the river and receiving through a wire that was grounded on the shore [13], [15].

In 1902, wireless was still very new. The equipment of Marconi, Lodge, Popov, Slaby and others lacked the amplification that would make voice transmission possible [6], [8], [11], [12]. Marconi had succeeded in sending one letter of Morse Code across the Atlantic a month before Stubblefield's demonstration [13], [15].

A reporter [13], [15] tested Stubblefield's system and said it was like a person 12-foot apart from him while Stubblefield's son was 500 yards (0.284 mile) away. The reporter made sure that it was wireless by removing the steel rods from the ground and thrusting them into the ground again. After that, Stubblefield's son started a routine by saying "Hello ..." and the reporter had heard the same quality he heard a while ago. In addition to this test, they went 1 mile away and the reporter himself stuck the steel rod and they tested the transmission quality and the reporter found a good quality of voice can be heard as he heard before when they were 500 yards away from Stubblefield's son. After that, Stubblefield was offered to do a business for his invention by Gerald Fennell on behalf of the Wireless Telephone Company of America which had been formed in February 1902 [13]. Stubblefield made a portable receiver using 2 induction coils of about 15 inches in diameter so that the receiver picked up the signals from the steel rod through the primary coil and eventually to the secondary coil attached to the receiver. He demonstrated the new system for dignitaries like the founder of General Electric, Edwin Houston, the general manager of the Philadelphia Key Stone Telephone Company, Albert Grump, Henry Clay Fish the treasurer of Wireless Telephone

Company of America, Professor Archibald Fredrick Collins a local wireless inventor and some journalists [13], [15].

Stubblefield experienced problems when he tried his system in Manhattan Island. Stubblefield's son said that they never could find good connection because the soil was rocky. They faced a new challenge as well due to the 60 Hz of the power cables buried below the level of the ground. However, they had poor signal-to-noise-ratio (SNR). The interference was louder than the transmitted sound where the system received all electric signals in a 30-50kHz band and could not be tuned to another channel and there was no way to turn the noise off [13], [15]. This confirmed that any ELF data link that uses the ground as a transmission medium would suffer from power feed cables radiation.

In 1892, Stubblefield successfully demonstrated his wireless system to Dr. Rainey Wells the former Calloway County attorney and president of Murray State College. In 1935, Wells said, "I have been given a telephone receiver but without wires when even the telephones were rare and I clearly heard "Hello Rainey" booming out of the receiver" [13], [15].

Stubblefield's son stated that his father had not used radio frequency (RF). His system uses a portable telephone connected to a primary coil. On the other hand, a secondary coil was connected to a buried electrode to transmit the human voice through the ground. His transmitter system needed the primary coil in order to complete the induction circuit with the secondary coil so that as long as he stayed inside the electromagnetic induction field of the transmitter site, the listener on the other site would be able to pick up the signals from the ground. Modern broadcasting is based on the process of modulating a signal upon a continuous high frequency carrier wave. Hence, Stubblefield is not the father of modern radio

broadcasting [15]. However, it is confined that he used the ELF and Voice Frequency (VF) band 0 to 3 kHz [16] to transmit the human voice through the ground [9], [13], [15].

In 1992, Bob Lochte a Professor in the Department of Journalism and Mass Communication at Murray State University and Larry Albert a TV Engineer with an interest in historical research, replicated Stubblefield's system and unlike him they decided to not conceal the circuitry from the public at the time of demonstration. In February 1992, Professor Bob Lochte and Larry Albert successfully demonstrated Stubblefield's replicated system that confirmed the history of Nathan B. Stubblefield [13].

2.1.3 Subterranean communication

Cave radio systems are in fact low frequency inductive communication systems [17]-[19]. They are mostly used by United Kingdom (UK) rescue team [17], [19]. Low frequency radio penetrates through conductive media like rock permitting through-earth communication [17], [19]. The through-earth communication could be done using compact loops or earth electrodes [17], [19]. Rescue teams communicate between the cave and surface to summon additional manpower, equipment, medical assistance or any kind of support to save lives and casualties [17], [19]. Cave radios were developed by cavers themselves [17], [19]. In the 1960s, Harold Lord a caver of the Mines Research Establishment in Sheffield conducted experiments with cave communication [17], [19]. Lord's system was impractical as it was too heavy and required large batteries [17], [19]. In the 1970s, Bob Mackin of Lancaster University and a member of the Cave Rescue Organisation (CRO) introduced the first cave radio, the so-called Molefone [17]-[20]. It managed to communicate between cave and surface using portable equipment to a depth of 100m [17], [18]. In the 1990s, the British Cave Rescue Council (BCRC) formed a team to develop a new cave radio based on a design by Leeds-based radio amateur John Hey [17]-[19]. The developed cave radio is called the HeyPhone and has been in use by all UK rescue teams since 2001 [17]-[19].

Figure 2.2: John Hey (left) the founder of HeyPhone in his workshop, a HeyPhone (right) in use on the surface above Carlswalk Caverns in Derbyshire - UK [18], [19]

HeyPhone units have been hand-built by John Hey [17], [18] as shown in figure 2.2. The communication range using HeyPhone cave radio is 800m using earth electrodes compared to loop antennas [17]-[19]. The Molefone and HeyPhone systems use Single Side Band (SSB) [19], [21] based on an 87 kHz carrier frequency which is part of Low Frequency (LF) [17]-[22]. Graham Naylor is a British caver who developed 'System Nicola' that is widely used in France in parallel with the development of HeyPhone [17], [18], [20]. Naylor's system provides software functions rather than circuitry that provide flexibility and features to rescuer such as text messaging [17], [20]. Nicola is preferred over the current technologies because the system relies on programming IC chips in which the units are upgradable [17], [18], [20].

2.1.4 Summary

Mr. Nathan Stubblefield (1860-1928) was the first person to broadcast the human voice in 1900 using a telephone system that attached to earth rods and on New Year's Day of 1902 Stubblefield and his son Bernard demonstrated this system to the people in Kentucky-US. In March 1902, he successfully showed to scientists and other people how easily he could communicate from ship to shore using wires dropped from the stern of ship and the receiver at shore connected to ground via earth rod near the Potomac River-US. Stubblefield experienced problems when he tried his system in Manhattan Island-US because the soil was rocky and the bad SNR caused by 60 Hz of the power cables. Stubblefield's son stated that his father did not use radio frequencies in his system. In 1992, Bob Lochte, a Professor in the Department of Journalism and Mass Communication at Murray State University and Larry Albert a TV Engineer with a historical research replicated Stubblefield's system and successfully demonstrated it. This confirmed that Nathan B. Stubblefield has used the ELF and VF band (0 up to 3 kHz) to transmit the human voice through the ground [9], [13], [15]. This confirms that it propagates through the ground using buried earth rods which is an advantage to adopt this band in a communication link uses the ground as transmission medium. Cave radio systems are low frequency inductive communication systems and mostly used by UK rescue team, the so-called Molefone and HeyPhone [17]-[19]. LF radio penetrates through conductive media like rock permitting through-earth communication using earth electrodes [17], [19]. The use of loop antennae achieved a range of 100m whereas earth electrodes greatly improved the communication range to 800m [17]-[19]. The Molefone and HeyPhone systems use SSB [19], [21] communication technique based on 87 kHz carrier frequency which is part of LF [17]-[22]. Nicola system adds more features to HeyPhone such as text messaging [17], [20].

2.2 Current use of ELF band

Nowadays, the ELF range of up to 300 Hz is mostly used by the US and Russian Navies. This is because ELF frequencies can penetrate deeply through the sea water and the lower the frequency being transmitted, the more deeply it penetrates the sea water. Consequently, they use the ELF to communicate with their submerged submarines in oceans and seas. The data received by the submerged submarines through the sea water are few bits a minute and these bits construct commands within few minutes for the Navy people to do specific tasks such as indicating that they should move slowly and close to the surface of the water for RF transmissions so that they are less susceptible for enemy detection under the sea water [22]-[27].

The US Navy began testing two ELF radio transmitters more than 30 years ago at Clam Lake, located in the Chequamegon National Forest in Northern Wisconsin-US. These transmitters are used to communicate with deep diving submarines and are operated by the Naval Computer and Telecommunications Area Master Station – Atlantic. The site consists of more than 28 miles of over-head transmission line that form the electrical antenna to radiate ELF signals from the two transmitters [22]-[24].

2.2.1 Advantages of ELF over RF

ELF penetrates the seawater to great depth while the RF signals are attenuated below the seawater surface. ELF is virtually jam proof from both natural and man-made interference and it allows the submarine to remain submerged at depth and speed while communicating with the national command authority [22], [23].

Frequencies of about 20 kHz of the Very Low Frequency (VLF) band penetrate seawater to depths of only tens of feet. The Navy's ELF system operates at about 76 Hz and the enhanced penetration of waves in seawater allows signals to reach depths of hundreds of feet permitting communications with submarines while maintaining stealth [22].

2.2.2 History of US Navy's ELF transmitters

In the late 1950s, researchers and scientists stated that, compared to RF, ELF could penetrate the ocean and permit communications with submerged submarines. However, the Navy needed to determine the possibility of building such a communication system to send messages to their submerged submarines as the ELF has a long wavelength that requires massive antenna. If this system worked as hoped, the submarines would not need to rise to near surface for RF communications [22], [23].

Initially, very large transmitter and antenna was envisioned to send orders to the submarine fleet using ELF. The conceptual design, called Project Sanguine, included more than 100 transmitter bunkers and an antenna array covering more than 3000 square miles. The initial theoretical and experimental work of this project was done between 1958 and 1963 at the David Sarnoff Laboratory of RCA in Princeton-US. In 1962, a field test site was built with facilities in North Carolina and Virginia. In 1963, the site was used to demonstrate the concept by sending signals deeply to submerged submarines that were 2,500 miles away [23], [25], [26].

In 1968, the Navy constructed a test facility in the Chequamegon National Forest in Northern Wisconsin-US and conducted initial scientific studies of biological and ecological effects of ELF transmissions using above-ground and buried antenna. In addition, the Navy conducted research called the Interference Mitigation Program into procedures to reduce the impacts of ELF transmissions on power lines, telephone lines, fences, utilities and other long metallic objects due to the induced voltage. The Navy tested these systems using the bands 40 to 50 Hz and 70 to 80 Hz [23], [25], [26].

Figure 2.3: Wisconsin ELF transmitter site (Left), view (right) of a typical ELF antenna [23]

In 1977, the studies of biological and ecological impacts of using ELF band were compiled by National Research Council (NRC) [26]. The NRC concluded that the likelihood of serious adverse biologic effects of using ELF was very small. In the mid-1980s, the Navy initiated an unprecedented literature review and ecological monitoring program in conjunction with the development of the ELF system. In addition, the American Institute of Biological Sciences (AIBS) was requested to provide an evaluation and analysis of the literature published in January 1977 about the ELF non-ionizing electromagnetic radiation effects carried by NRC.

In 1985, the AIBS concluded in its report [23], [26] that:

> *"It is unlikely that exposure of living systems to ELF electric and magnetic fields in the range of those associated with the Navy's ELF Communications system can lead to adverse effects on plants and animals".*

In 1984, Navy Secretary John Lehman confirmed that the ELF system is essential to the national defence, allowing the Trident and Poseidon submarines to remain undetected. These types of submarines must also maintain continuous communication with the President and Secretary of Defence. However, with other communication systems submarines have to rise

to near the surface in order to deploy a receiving antenna. This requirement increases the exposure to detection and restricts the speed and depth of operation. The ELF system removes these restrictions on communicating with submarines and therefore it represents a critical safeguard against a scientific breakthrough in submarine detection by another nation using aircraft or satellite systems that use non-acoustic phenomena such as Kelvin wakes and internal waves near the surface [23].

In 1989, the Michigan-US site became fully operational and the Wisconsin-US site was renamed the Naval Radio Transmitter Facility Clam Lake. On October 1, 1989 the entire ELF communication system became fully operational and began synchronised transmitting of an ELF broadcast to the submarine fleet “24 hours a day, 7 days a week” [23].

2.2.3 Principle operation of the US Navy's ELF transmitter

The ELF system was radiating 8 watts signals from the dual site and signals travelled around the world being reflected off the atmospheric layer between the earth's surface and lower ionosphere layer. As these electromagnetic waves pass over the ocean's surface, part of their energy passes into the ocean. Submarines were equipped with ELF receivers to receive and decode these signals at depth of 100 feet and travelling at operational speeds. The disadvantage of using the ELF system to communicate with submarines is that the ELF system provides *one-way* (transmitters sites to submarines) message system only and is slow. Submarines cannot transmit ELF signals due to the large power requirements, the large transmitter and large antenna required to transmit ELF signals. This problem can be avoided by sending commands to the submarines to rise to the surface for RF communications such as satellite communications systems [23].

Each ELF antenna works as horizontal electric dipole and both of the transmitting sites synchronize their transmission to provide wide coverage to the oceans in which the US submarines operate. The conductivity of the bedrock layer (Precambrian metamorphic) and overlaying rocks (Palaeozoic) located in the transmission site provide geological formation channels that allow the current to flow deeply into the ground and increase the antenna size for more efficient transmission [23]. The areas chosen for the ELF system have low conductivity and the electrical current flows deep up to 100 meters before returning to the opposite antenna terminal ground. The Navy estimates the local economic expenditure of the Clam Lake Facility to be about $6m annually. They spend about $400,000 annually on electricity from the local Wisconsin power utility [23].

2.2.4 Natural ELF waves

ELF waves are initiated by lightning strikes that make the electrons in the atmosphere oscillate and resonate in the region between the ionosphere and the surface. In addition, the circumference of the earth is 40,075.02 km – a wavelength corresponding to a frequency of 7.5 Hz. This frequency and higher resonance modes of 14, 20, 26 and 32 Hz appear as peaks in the ELF spectrum are called the Schumann resonance (SR) range. “On this basis, they can be located by any ELF receiver worldwide (Huang et al, 1999; Hobara et al, 2006), characterized by a vertical charge moment in physical units (C-Km), and counted as lightning flash” [27].

2.2.5 ELF used in electricity

The electricity all over the world is operated at either 50 or 60 Hz. Feed cables [28], [29] are buried to transmit the 11,000 volts of electricity from the power substations to the cities and towns. The long feed cables operating at 50 or 60 Hz are radiating waves above and inside the ground. For critical safety reasons most of the electrical equipment is tied to the ground using earth rods in order to discharge the electricity leakages to the ground. Most of these danger cases are caused by short circuit, overload and fault to earth. The fault to earth is similar to the short circuit and occurs if the line conductor becomes connected somehow to the earthed metalwork that is tied to the ground itself allowing the current to flow through the ground at 50 or 60 Hz [28], [29]. This causes interference in the ELF band.

2.2.6 Summary

ELF is the band of frequencies up to 300 Hz and is allocated by the Federal Communications Commission (FCC) for general purposes free of charge [22], [30]. The use of the ELF band (3-300 Hz) has largely been confined to submerged submarine communications, operated by the US and Russian navies. Although ELF transmission was first demonstrated in 1900, its application to civilian data transmission has been neglected. The US Navy found that ELF has a better penetration depth than RF does - the lower the frequency being transmitted the deeper it penetrates the seawater. The US Navy radiate ELF waves using large transmitter facilities. The signals propagate between the lower part of the ionosphere and the earth's surface and part of these waves pass into the ocean. Submarines are equipped to receive and decode these waves. Biological and ecological impact studies of using ELF on human and plant were conducted by NRC-US and the AIBS-US and they concluded that there are no serious adverse effects of using ELF band. It is expected that any communication system using the ELF band will suffer from noise caused by the electric feed cables, electric leakage through the earth rods and the lightning strikes that make the electrons in the atmosphere to oscillate between the ionosphere and earth's surface [23], [25]-[27].

2.3 Digital data transmissions

Digital communications are replacing Analogue communication. Digital systems can be designed to enhance the speed of transmission compared to analogue systems. Digital systems are able to distinguish between approximated discrete points of a signal rather than discriminating between fine variations of a signal in analogue systems [31]. Therefore, digital systems are much faster and more reliable than analogue systems. The digital modulation can be carried out by altering the magnitude, frequency, or phase of a signal. Digital data transmissions include ASK, FSK, PSK and others.

2.3.1 Amplitude Shift Keying (ASK)

ASK is the digital form of AM [32], [33] so the carrier wave has to be of a higher frequency than the modulating wave. A simple ASK represents 2 logical states. Figure 2.4 shows the states represented by varying the amplitude of the carrier as in AM. Two amplitude levels represent the two states of logical 1 and 0. The data rate of ASK can be enhanced using more than two amplitude levels such $2^2 = 4$ levels to represent 2-bit, $2^3 = 8$ levels to represent 3-bit and so on. ASK is simple compared with the other digital transmission techniques but has a disadvantage of being more susceptible to error because of the noise affecting the amplitude of the carrier [32], [33]. ASK occupies a bandwidth of twice the data rate as shown in figure 2.4.

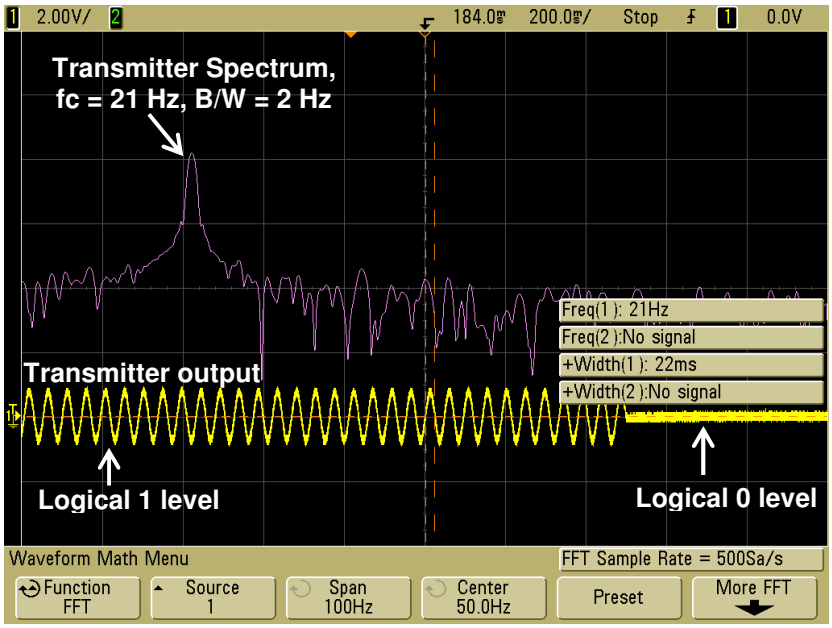

Figure 2.4: ASK transmitter output and spectrum bandwidth

2.3.2 Frequency Shift Keying (FSK)

FSK uses two frequencies to represent logic 1 and 0. It occupies a bandwidth of 2 carrier frequencies [32], [33] as shown in figure 2.5. The switching between 2 carriers causes each carrier to occupy a bandwidth twice the data rate. Therefore, FSK is an inefficient bandwidth system.

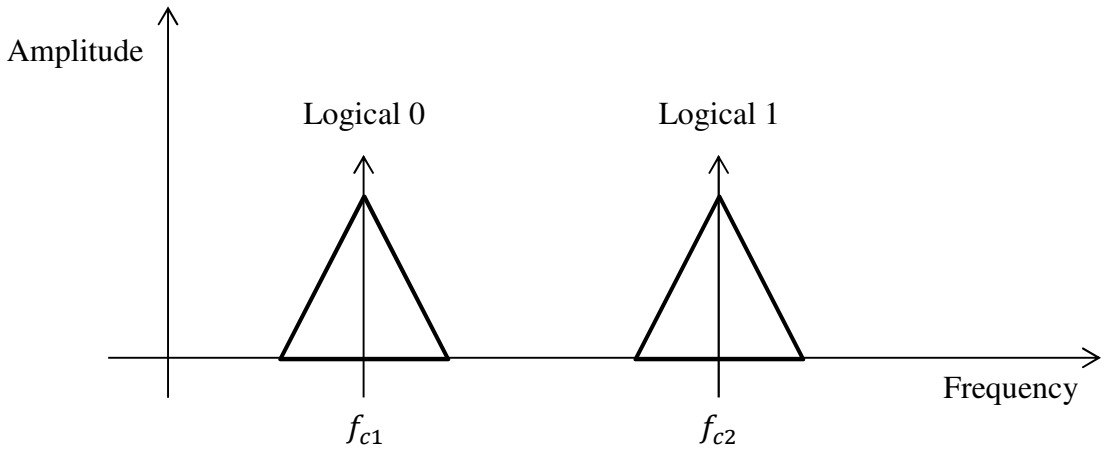

Figure 2.5: Frequency domain of FSK transmitter [32], [33]

2.3.3 Phase Shift Keying (PSK)

PSK uses phase angles to represent binary states with a constant frequency carrier and amplitude [32], [33]. Figure 2.6 shows the basic form of PSK constellation that is called Binary PSK (BPSK) that requires 2^1 phase angles to represent 1-bit using 0^o and 180^o. It occupies a bandwidth twice the bit rate. The transmission rate of PSK can be increased without increasing the bandwidth by keeping the phase change per time the same as BPSK and increasing the number represented by a phase change which is called a symbol. For example, a 2-bit symbol requires $2^2 = 4$ phase angles to represent the 2-bit alphabet. This type of PSK is called Quadrature PSK (QPSK) or 4-PSK as shown in figure 2.6. The angles are spaced equally at 90^o to avoid cross talk.

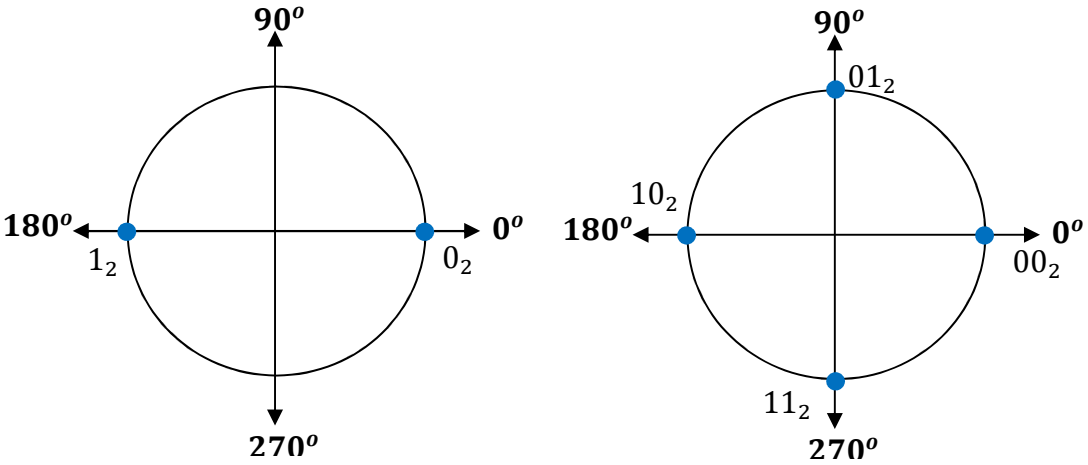

Figure 2.6: BPSK (Left) and QPSK (right) constellation points [33], [34]

The bandwidth of QPSK remains the same as BPSK but the symbol rate of QPSK is double, so the transmission rate is doubled [32], [33]. Similarly, 8-PSK and higher orders can be implemented in the same manner of BPSK and QPSK to occupy the same bandwidth and increase number of bits per symbol. So, 8-PSK is able to transmit 3-bit per symbol. Clearly, 8-PSK shown in figure 2.7 is faster than BPSK and QPSK by 3 times and 1.5 times respectively but more susceptible to link degradation.

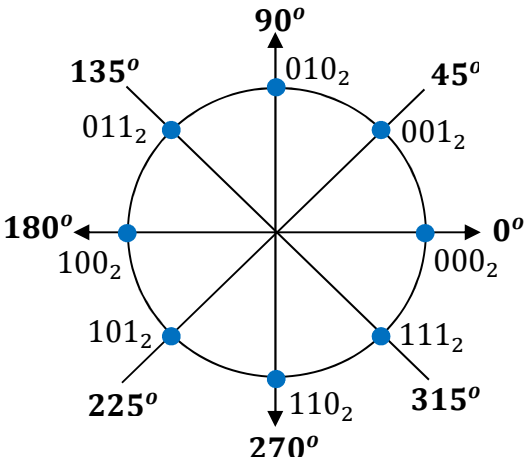

Figure 2.7: 8-PSK constellation points [34]

Another form of PSK is called Differential PSK (DPSK). This form of PSK differentially encodes the data in the phase of the carrier rather than the absolute phase as in BPSK, QPSK or 8-PSK [32], [33]. DPSK compared to the other forms of PSK records the changes in the binary stream. DPSK can be constructed using the same concept of BPSK, QPSK and 8-PSK transmitter and receiver except that a differential encoder and decoder at both sides are required.

2.3.4 Quadrature Amplitude Modulation (QAM)

A combination of phase (PSK) and amplitude (ASK) modulation is considered to be the most efficient in terms of wireless communication system capacity, so called QAM [32], [33], [35]. The QAM technique occupies the same bandwidth of BPSK and enhances the transmission rate by utilizing at least two amplitude levels of the ASK and two phase levels of the PSK of a carrier frequency, resulting in four possible states (4-QAM) of 2-bit per symbol [32], [33]. For example, 16-QAM allows each carrier signal change to represent 4-bit a time. So, the bit rate can be higher than the number of signal changes (baud rate) without increasing the bandwidth. This scheme is very useful for the ELF link to utilise the limited bandwidth. In modems the data can be transferred at speed of 28,800 bps within the telephone bandwidth [36].

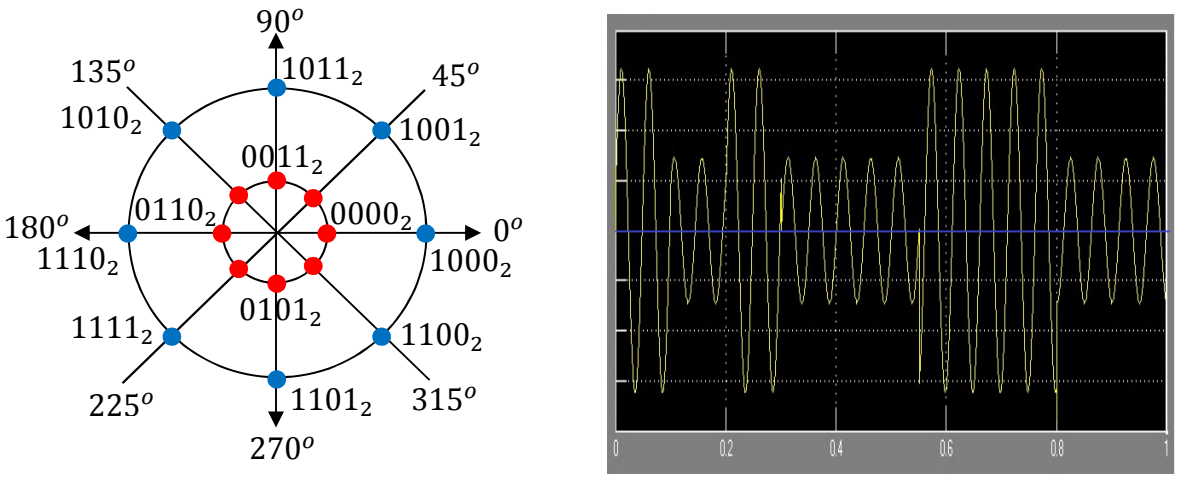

Figure 2.8: Star 16-QAM constellation points (left) [34], 16-QAM signal using DSP Builder

Figure 2.8 shows the constellation of star 16-QAM of the transmitter/receiver being designed and the transmitter output using MATLAB and Altera's DSP Builder. The higher-order QAM make the constellation points close together, making the receiver unable to distinguish the symbols in noisy phase environment [32], [33]. Therefore, the higher-order QAM the more bandwidth efficient, but is more susceptible to phase noise and distortion [32], [33].

The 16-QAM technique is one of the most efficient techniques. The 16-QAM transmitter encodes 4-bit, 16 state data (2^4 = 16 states) onto 8 different phases state of the carrier (PSK), separated by 45^o as illustrated in figure 2.8. The 4^{th} bit is amplitude modulated on the carrier (ASK), which enables migration between the red and blue points, shown in figure 2.8. The 16-QAM is widely used in WCDMA, HSDPA, WiMAX and WLAN broadband wireless access technologies [1]. The HDSPA, WiMAX and WLAN are part of the 3GPP WCDMA, IEEE 802.16 and IEEE 802.11 standards respectively [1].

Applications of 8-PSK and 16-QAM include mobile and fixed broadband internet [1]. In addition, for domestic broadcast applications, 64-QAM and 256-QAM are often used in digital cable television and cable modem applications. In the UK, 16-QAM and 64-QAM are currently used for digital terrestrial television using DVB-T [2].

The 16-QAM receiver can be designed to demodulate the amplitude data by introducing a 180^o delay on the carrier amplitude and the absolute value is compared to the current carrier amplitude absolute value to determine the amplitude (ASK) data. Demodulating the phase data is crucial and is generally performed using complex mathematics, 'tan' function, Phase-Locked-Loop (PLL) or a combination of 'tan' and Digital PLL (DPLL) [35], [37]-[44].

2.3.5 Complex number technique for demodulation

Complex number technique [34] includes the use of delayed sample and complex conjugate to find the phase changes. However, if the received signal changes, in terms of phase, by 90° from the initial position of 45° resulting in a phase of 135° according to the polar form, shown in figure 2.9, then the signal will be 0.7071+ j 0.7071 (45°) in complex notation before it moves to -0.7071 + j 0.7071 (135°) by +j (90°). This can be performed using a delayed sample of the received signal; taking the complex conjugate and multiplying it by the current received sample as proven mathematically below and system shown in figure 2.10 to find the phase differences [34], [45], [46].

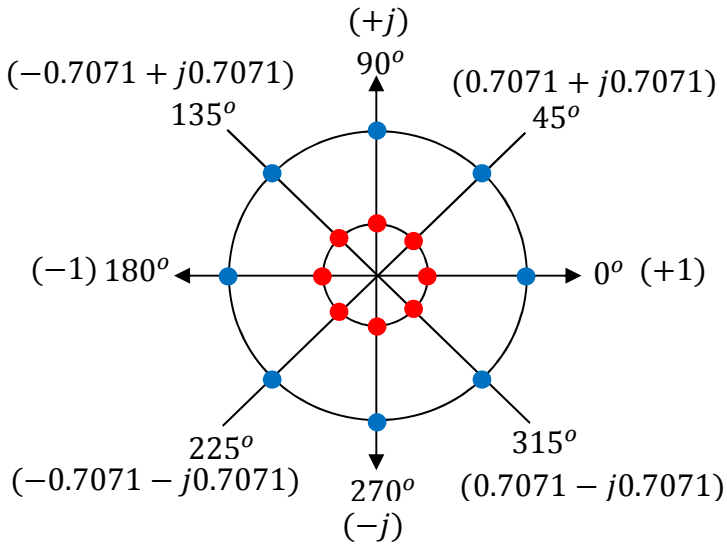

Figure 2.9: Complex notation of the 16-QAM constellation [34]

Mathematically,

$Z_{n-1} = 0.7071 + j\ 0.7071$ Delayed a sample (45°)

$\overline{Z_{n-1}} = 0.7071 - j\ 0.7071$ Delayed complex conjugate (315° or -45°)

$Z_n = -0.7071 + j\ 0.7071$ The new phase (135°)

hence,

$\Delta\theta = \angle(Z_n . \overline{Z_{n-1}}) = \angle(Z_n) + \angle(\overline{Z_{n-1}})$ Phase difference

$= (-0.7071 + \text{j}\ 0.7071) \times (0.7071 - \text{j}\ 0.7071)$

$= -0.5 + \text{j}\ 0.5 + \text{j}\ 0.5 - \text{j}^2\ 0.5$

$= 0 + \text{j}$ The resulting phase is 90^o

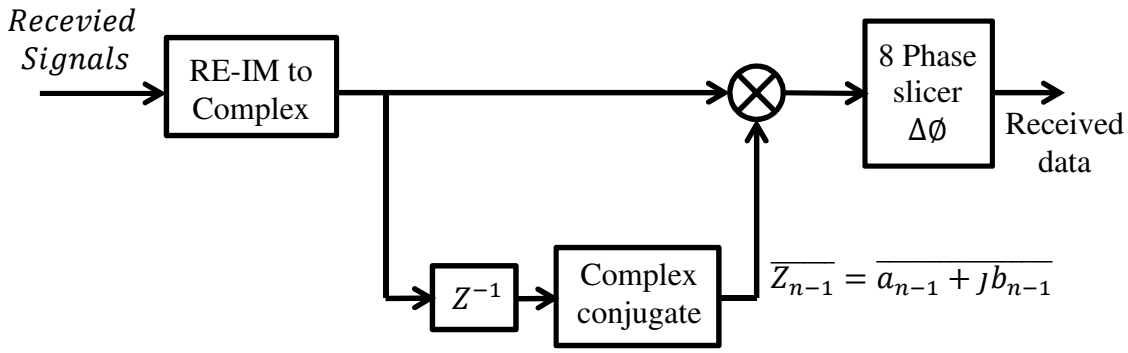

Figure 2.10: Phase detector using complex numbers [34]

Advantages of complex numbers technique:

1- Simple multiplication function required.

Disadvantages of complex numbers technique:

1- Requires Real-Imaginary to Complex conversion. Hence, an high specification processor is required.

2- The results of the multiplier need to be interpreted through complex phase slicer circuitry.

3- Phase slicer needs system variable LUT (scale) depending on the peak-to-peak (pk-pk) received signals even if an Automatic-Gain-Controller (AGC) is utilised, hence continual calibration of the system is required.

2.3.6 'tan' function and digital PLL for demodulation

PLL can be used to detect the phase changes [39], [40], [44]. A basic PLL includes a phase detector, Voltage-Controlled-Oscillator (VCO) and a filter. The output of the VCO is directly compared with the input to the PLL through a phase comparator. The resulted signal undergoes a low pass filter (LPF) resulting in a voltage reference to the VCO to keep track of the incoming phase. Therefore, a PLL can be used individually to find the phase changes in 16-QAM.

The PLL technique can be enhanced using 'tan' function in parallel with DPLL. The concept of 'tan' function is where the received signals are changed in terms of phase, with the phase calculated using inverse 'tan' function and DPLL as shown in figure 2.11. Firstly, the received signals are separated to '*sin'* and '*cos'* and multiplied by the recovered carrier of DPLL. The resulting signals undergo filtering through an LPF then are passed through an 'atan' function to find the phase difference. The phase difference drives the Numerically Controlled Oscillator (NCO) to lock to the carrier signal.

Published journal papers, technical and literature reviewed [35], [37], [39], [40], [43] in this thesis shows that this system requiring a 'tan' function to demodulate 16-QAM signals is generally used. The review also showed that 16-QAM demodulation is currently performed using the 'tan' function.

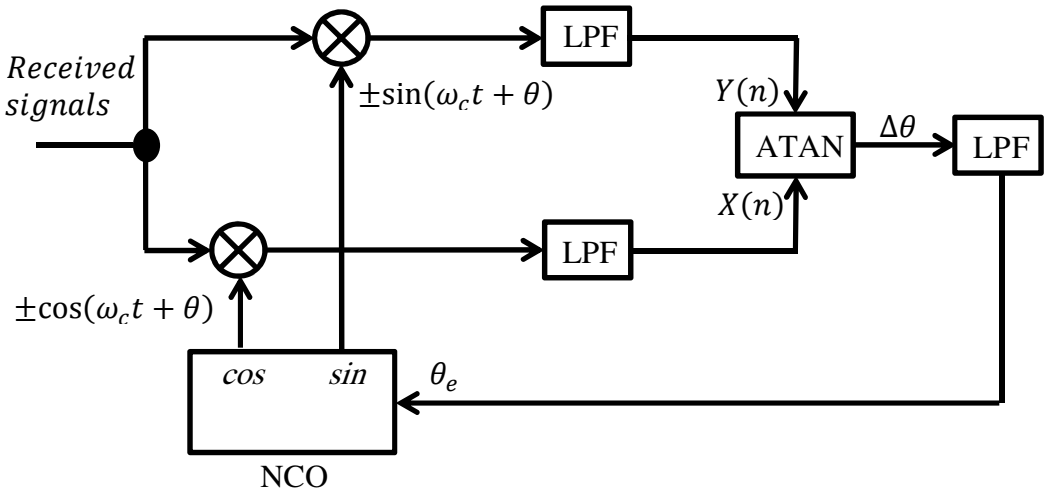

Figure 2.11: Phase demodulation using DPLL and 'tan' function [39], [43]

Advantages of using 'tan' function:

1- High performance and accuracy.

Disadvantages of using 'tan' function:

1- DPLL, carrier recovery and LPFs add more complexity to the system, hence, requires large amounts of system resources.

2- High specification processor is required to perform the 'tan' function.

3- The result of the 'atan' needs to be interpreted through a complex phase slicer.

4- Phase slicer needs system variable LUT (scale) depending on the pk-pk received signals even if an AGC is utilised, hence continual calibration of the system is required.

2.3.7 Summary

ASK is the digital form of AM which, in its simplest form, uses 2 logical states. ASK is simple compared FSK and PSK digital data transmission techniques and occupies a bandwidth of twice the data rate [32], [33]. FSK occupies a bandwidth of 2 carrier frequencies to represent 1-bit, each carrier occupies a bandwidth of twice the data rate and is bandwidth inefficient [32], [33]. PSK uses phase angles to represent binary states with a constant frequency carrier and amplitude [32], [33]. BPSK is the basic form of PSK that represents 1-bit and QPSK that represents 2-bit. QPSK, 8-PSK and higher orders can be implemented to occupy the same bandwidth of BPSK and increase the number of bits per symbol. A combination of ASK and PSK is called QAM which is considered to be the most efficient in terms of wireless communication system capacity and bandwidth [32], [33], [42]. QAM enhances the transmission rate of PSK forms without increasing the bandwidth which is very useful in a limited bandwidth such as ELF. Applications of 8-PSK and 16-QAM includes mobile and fixed broadband internet [1]. Demodulating the phase data is crucial and is generally performed using complex mathematics, ‘tan’ function, PLL or a combination of ‘tan’ and DPLL [35], [37]-[44].

2.4 Multi-Carrier Communication systems

Mobile or indoor radio channels are multipath channels that challenge researchers to devise ways to distinguish the original signals (direct path) from the large number of reflected waves. This degradation of the performance requires as well designed wireless system to cope with these adverse effects. Moreover, a high spectral efficiency spectrum is a critical design objective. Another critical design objective is the channel should handle multiple users within the same frequency band [1], [34], [47]-[49]. These last two properties are of interest to the ELF communications link being designed.

2.4.1 Orthogonal Frequency Division Multiplexing History

The OFDM concept was proposed by Chang in 1966 for dispersive channels [34], [48]. Most of the conventional modulation techniques are sensitive to Inter-Symbol-Interference (ISI) unless the channel symbol rate is small compared to the delay spread of the channel in the multipath environment [50]. OFDM is significantly less sensitive to ISI, because a special set of signals is used to build the composite transmitted signal [50]. The researchers Weinstein, et al [34], [48] have made a valuable contribution to the evolution of OFDM research. Europe has adopted and standardised OFDM as the Digital Audio Broadcasting (DAB) and Digital Video Broadcasting (DVB) standards and similar standards exist in Japan and are under discussion for China. HIPERLAN has selected OFDM as the transmission technique and it is part of the IEEE 802.11 WLAN standard [4], [34], [48].

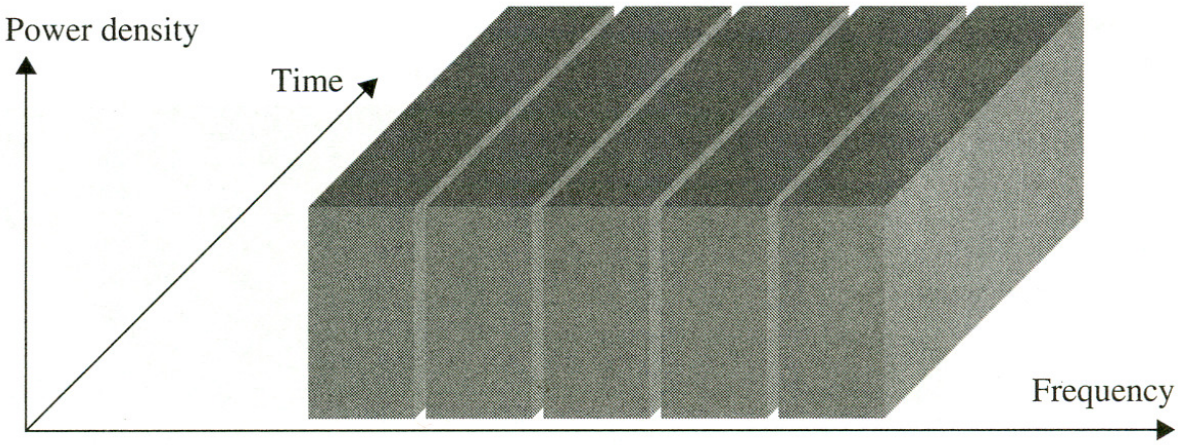

Figure 2.12 FDMA spectrum [47]

OFDM is similar to the Frequency Division Multiple Access (FDMA) [34], [48] where the FDMA divided the bandwidth into multiple channels as shown in figure 2.12 which was then allocated to users. It is estimated that 50% of the bandwidth is wasted when FDMA is used due to the spacing between each single channel to prevent channels from interfering with one another.

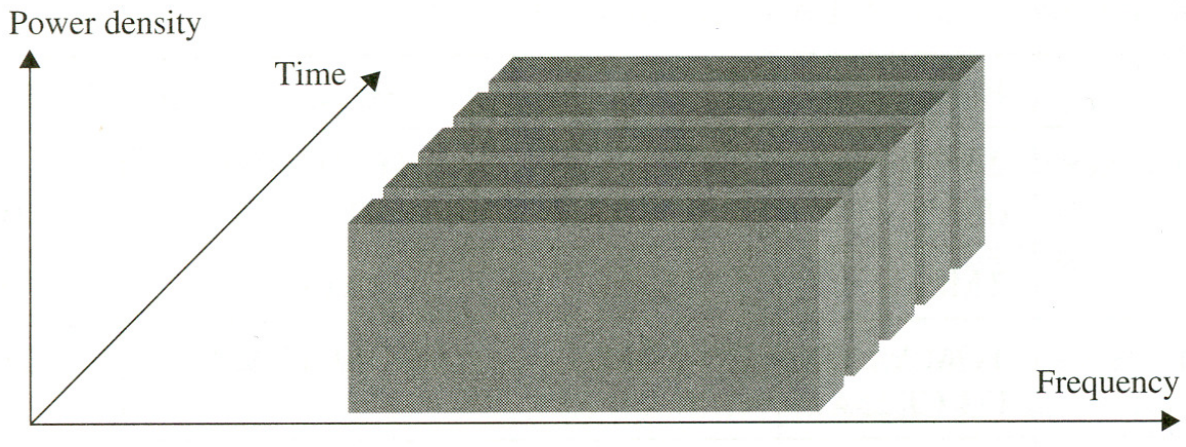

Figure 2.13: TDMA spectrum [47]

Time Division Multiple Access (TDMA) [34], [48] allows multiple users to access the same channel by transmitting their data in time slots as shown in figure 2.13. However, this limits the number of users that can be sent efficiently in each channel especially in low speed links.

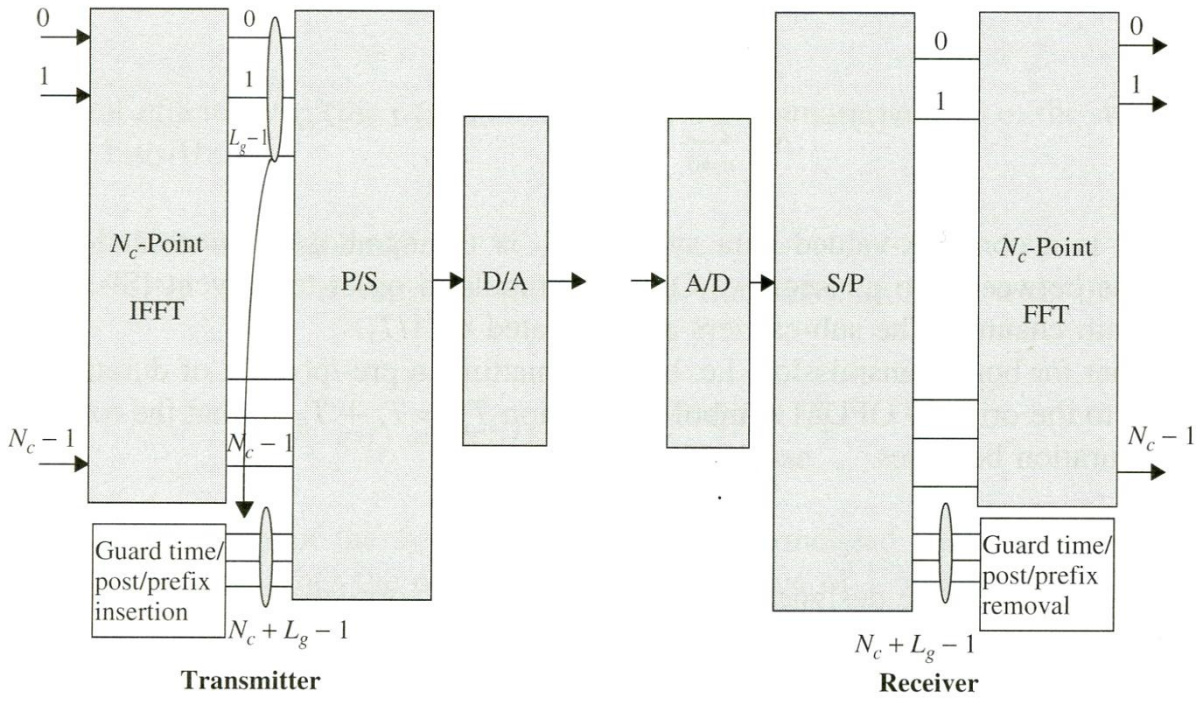

Figure 2.14: OFDM transmitter and receiver structure [47]

OFDM overcomes these problems by [3], [34], [48] using the bandwidth more efficiently by spacing a number of sub-carriers in the original bandwidth and make them orthogonal using the Fast Fourier Transform (FFT) to send the data in parallel form as shown in figure 2.14. Sub-carriers (sub-channels) are spaced accurately according to the rate of the data stream that is to be transmitted per sub-carrier so that the nulls of a sub-carrier occur at neighbour's sub-carriers to maintain the orthogonality as shown in figure 2.15.

Bello, Zimmermann, Powers and Zimmerman, Chang and Gibby have employed OFDM systems in military applications since the 1960s [34], [48]. Coded OFDM (COFDM) is similar to OFDM except that forward error correction is applied to the signal before transmission [48]. This overcomes the problems associated in recovering signals that are corrupted by frequency selective fading, channel noise and other propagation effects.

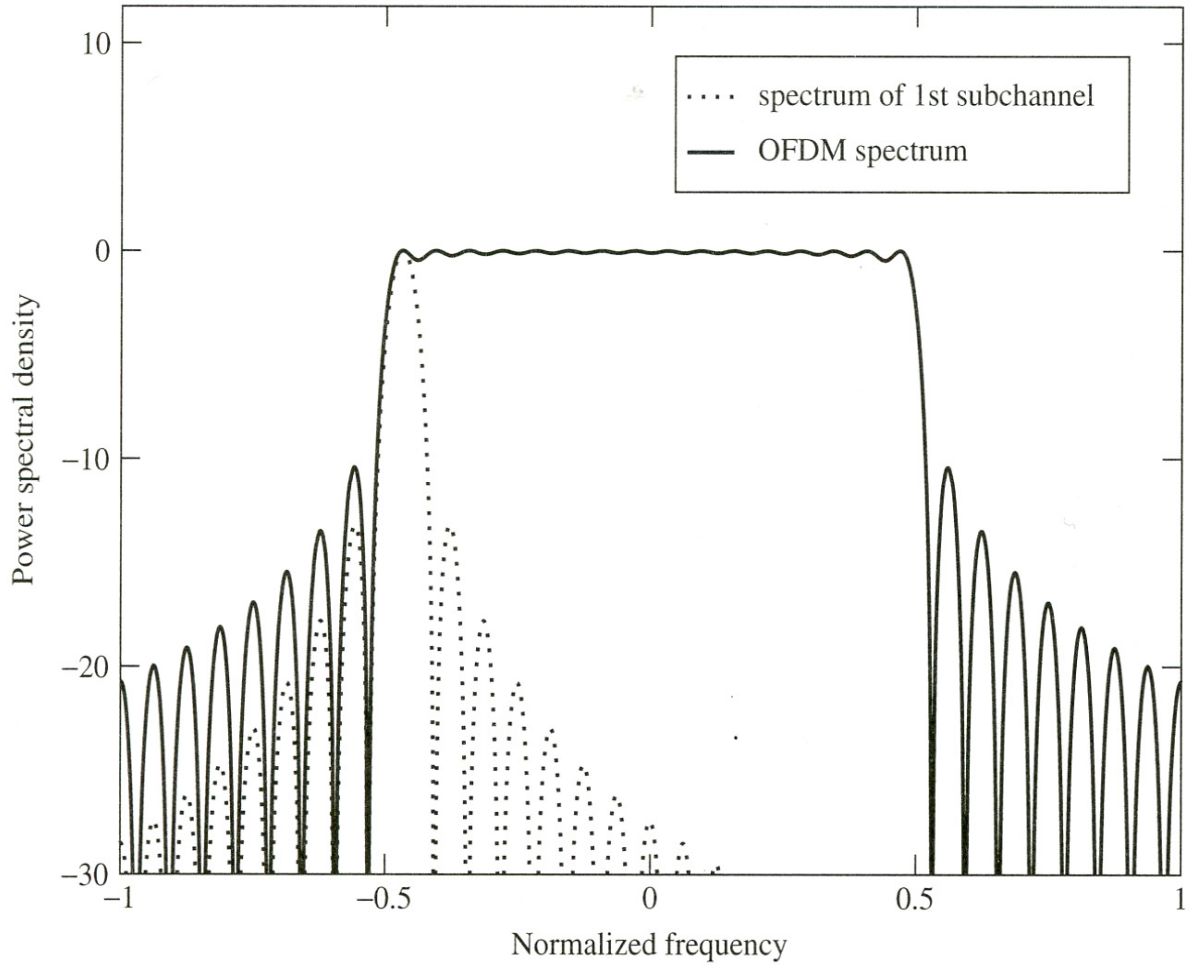

Figure 2.15: OFDM spectrum, nulls of a sub-carrier occur at neighbour's sub-carriers [47], [51]

In 1971, Weinstein and Ebert reduced the complexity of OFDM by employing the Discrete Fourier Transform (DFT) to replace the use of sub-carriers generators and demodulator. In 1980, an equalizer to suppress the ISI and Inter-Carrier-Interference (ICI) caused by timing and frequency errors was suggested by Hirosaki [34], [48], [49]. In addition, Peledin investigated the simplified OFDM modem implementations [34], [48], [49].

More recently, the Erlangen University, Germany, conducted research into the applications of OFDM by Kolb, Schussler, Preuss and Ruckriem [48]. Also, Cimini and Kalet published analytical and early unprecedented experimental results on the performance of OFDM modems in mobile communications channels [48].

OFDM is employed in the Asynchronous Digital Subscriber Line (ADSL) and High-bit-rate Digital Subscriber Line (HDSL) systems and it has also been suggested for power line communications systems due to its resilience to time dispersive channels and narrow band interferers. It is widely used in Europe in DAB and DVB standards [1], [34], [49]. Table 2.1 summarises the advantages and disadvantages of OFDM.

OFDM advantages	OFDM disadvantages
1- High spectral efficiency. 2- Can be easily implemented using FFT. 3- Form nearly rectangular frequency spectrum. 4- Guard interval avoids ISI and ICI. 5- Reduce the complexity of the receiver.	1- Suffers from high PAPR. 2- Requires highly linear amplifier. 3- Guard interval makes loss in spectral efficiency. 4- More sensitive to Doppler spreads compared to single-carrier modulated system. 5- Requires an accurate frequency and time synchronization.

Table 2.1: OFDM advantages and disadvantages [1], [34], [47], [49]

2.4.2 Spread Spectrum Techniques

"Literally, a spread spectrum system is a system in which the transmitted signal is spread over a wide frequency band, much wider than the minimum bandwidth required to transmit the information being sent" [1]. This is done by chipping the data to be modulated and transmitted using high Pseudo-Noise (PN) code which is independent of the data as shown in figure 2.16.

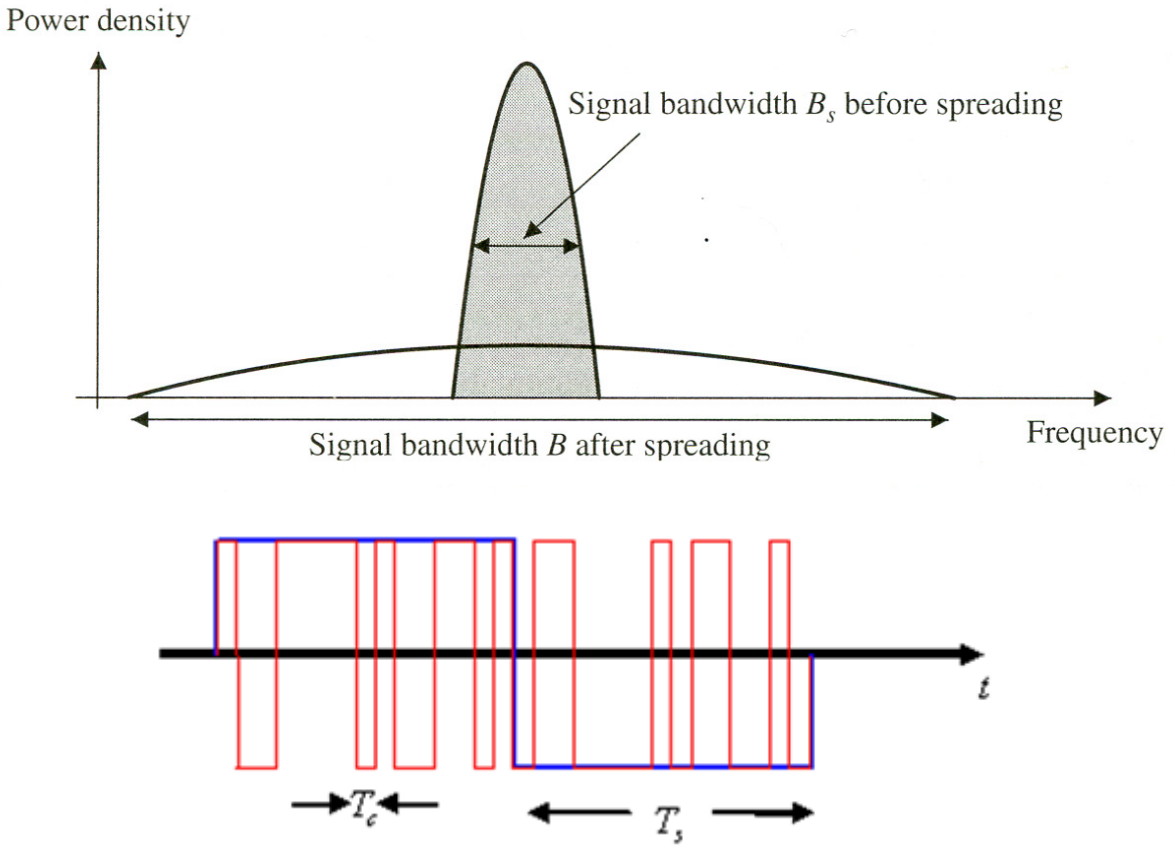

Figure 2.16: CDMA spectrum (top), PN code chipping the data (bottom) [47], [52]

The receiver is to be synchronized to the code being transmitted in order to de-spread and recover the data being transmitted. Code Division Multiple Access (CDMA) is an example of Spread spectrum. In the mid 1950s, the spread spectrum was initiated in military applications to anti-jam tactical communications, guidance systems and experimental anti-multi-path systems. Applications of spread spectrum include anti-jamming, interference rejection, low

probability of intercept, multiple access, multi-path reception, diversity reception, high resolution ranging and accurate universal timing [1], [47].

Spread Spectrum has been studied in the United States in 1989 by the Cellular Telecommunications Industry Association (CTIA) for the next cellular generation technology requirements. In September 1988, the CTIA laid out the User Performance Requirements (UPR) for the next generation of wireless service applications to offer voice and data privacy, ease of transition and compatibility with existing analogue system, ability to introduce new features, high voice quality and tenfold increase over analogue system capacity [53].

In 1989, TDMA was adopted by the Telecommunications Industry Association (TIA) as the radio interface standard. After that, a company called QUALCOMM developed a CDMA system that was compliant with CTIA requirements. In December 1991, QUALCOMM presented the trial results of CDMA with the participating carriers and manufacturers in New York City. Also, QUALCOMM successfully performed large-scale capacity tests in San Diego. In 1992, the CTIA Board of Directors adopted a resolution to the wideband systems and requested TIA to accept this contribution. TIA accepted and recommended that the TR45 committee standardize the wideband spectrum digital technologies. In July 1993, IS-95 was initiated. In 1994, South Korea adopted CDMA and thereafter Sprint Personal Communication Service (PCS) adopted CDMA in 1994. In 1995, Hong Kong operated the first commercial network and QUALCOMM launched the first commercial cdmaOne handset. South Korea commercially launched cdmaOne in 1996. Thereafter, commercial services have begun in both cellular and PCS bands all over the world [1], [53], [54].

In 1997, the IS-95B standard was completed including 64,000 bit-per-second (bps) data transmission capability. In 1998, the TIA endorsed CDMA2000 to be 3G solution and submitted for the International Telecommunication Union (ITU) as part of the International Mobile Telecommunication-2000 standard process for global 3G standards. LG Telecom launched first CDMA data services. In 1999, more than 80 CDMA operators in 35 countries have nearly 42 million subscribers. IUSACELL - Mexico was the first Latin American operator to offer Wireless Internet Services in 2000 where QUALCOMM, Samsung and Sprint PCS made their first 3G CDMA2000 voice call. In 2002, countries have begun to launch commercial CDMA2000 services globally. A large number of subscribers use CDMA services starting from 100 million subscribers to more than 240.2 million subscribers in 2004. A million subscribers use CDMA2000 in 2001 and reached more than 200 million commercial CDMA2000 subscribers worldwide in 2005 and is ongoing. In addition, 143 CDMA2000 operators are commercially deployed in 67 countries on 6 continents. Furthermore, 950 CDMA2000 devices are offered commercially since 2000. Moreover, there are 64 CDMA2000 device manufacturers which confirms the efficiency of offering multiple access without interference while handling millions of users globally divided to micro-cells [1], [54].

There are two primary types of spread spectrum technique known as Direct Sequence (DS)-CDMA and Frequency Hopping (FH)-CDMA. The principal operation of the DS-CDMA is that the information with bandwidth B_s is spread over a bandwidth B, where $B \gg B_s$. However, the processing gain is proportional to the spreading bandwidth in which specified as

$$P_G = \frac{B}{B_s}$$

so that the higher the processing gain, the lower power density needed to transmit the information. When the bandwidth used is very large, as in Ultra Wide Band (UWB) systems, the signal can be transmitted in such a way that it appears like noise. The main problem of using DS-CDMA is that a user could mask all the other users at the receiver if its power level is too high compared to the other users trying to access the receiver. Hence accurate power control is an inherent part of any DS-CDMA system [1], [47].

The signal information is spread using PN codes with good cross- and auto-correlation properties. The PN code is mixed with the data to spread the power of the information signal over a wide bandwidth as shown in figure 2.16. In order to recover the signals being spread and transmitted, a replica of the PN code is used at the receiver and once synchronization is maintained, the original data can be recovered. In a multi-user environment, each user is assigned to a specific PN code and the receiver needs only knowledge of the user's PN code to synchronize to it. If a long PN code is used, the signals would look like noise and the synchronization becomes more difficult unless a pilot signal is sent to aid the acquisition [1], [52].

The FH-CDMA is similar to the DS-CDMA where both use the same concept of PN code except that the information signal bandwidth is unchanged and hopped in FH-CDMA over a number of channels instead of spreading the signals over a continuous bandwidth in DS-CDMA, as shown in figure 2.17. Recovering the FH-CDMA signals is difficult and the receiver must know the hopping pattern in advance. The PN code ensures that all frequencies in the total available bandwidth are optimally used. Thus, FH-CDMA is not ideal for long transmission due to the multi-path and interference of the other systems [1], [52].

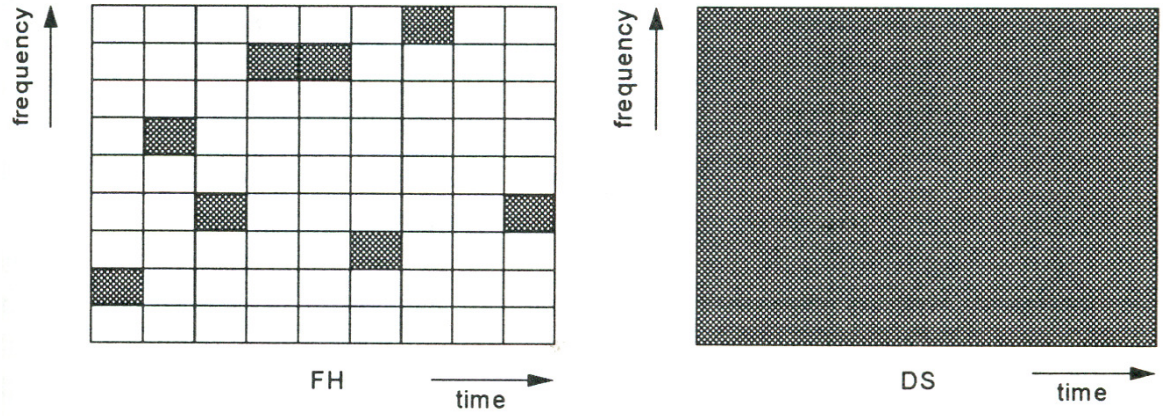

Figure 2.17: DS-CDMA compared to FH-CDMA in frequency and time domain [1], [52]

DS-CDMA offers easy frequency planning, high immunity against interference if a high processing gain is used, flexible data rate adaptation and multiple access [47]. Multiple Access Interference (MAI) occurs as the number of simultaneously active users increases. However, the DS-CDMA could handle reasonable number of users at limited processing gain and once the number of users exceeds the limit, the system performance reduces and it may not able to distinguish the signals. This can be felt in crowded places when a group of people use the same network simultaneously that causes pressure on the micro-cell station to handle them simultaneously.

> *"In order to exploit all multi-path diversity it is necessary to apply a matched filter receiver approximated by a rake receiver with a sufficient number of arms. In addition, the receiver has to be matched to the time-variant channel impulse response. Thus, proper channel estimation is necessary. This leads to additional receiver complexity with adaptive receiver filters and a considerable signalling overhead" [47].*

In the case of single-tone or multi-tone interference, additional operations have to be done at the receiver, such as notch filtering in the time domain or in the frequency domain (based on the FFT) to partly decrease the amount of interference. However, this extra processing leads to additional receiver complexity [47].

2.4.3 Multi-Carrier CDMA

There are many equivalent ways to describe Multi-Carrier (MC)-CDMA. MC-CDMA is a form of CDMA or spread spectrum; however the spreading code is applied in the frequency domain rather than in time domain as in DS-CDMA [47], [55]. Thereafter, FFT is performed to maintain the orthogonality. Therefore, MC-CDMA is a form of OFDM and sometimes also called OFDM-CDMA [48], [55]. MC-CDMA usually uses a specific code called a Walsh Hadamard sequence (orthogonal code). In contrast to DS-CDMA, MC-CDMA can handle N simultaneous users with good Bit-Error-Rate (BER) using standard receiver techniques [47], [55]. However, multiple users can share the same spectrum as well as in DS-CDMA due to multipath channels; DS-CDMA should use a highly complex interference cancellation technique in order to accommodate the same N simultaneous users in MC-CDMA [47], [55]. In contrast, OFDM applies coding (COFDM) to avoid bit errors on subcarriers in deep fade so that the number of subcarriers needed is larger than the number of bits or symbols transmitted simultaneously whereas the MC-CDMA replaces this encoder by an NxN matrix operation [48], [55].

MC-CDMA was first proposed in 1993 at the IEEE International Symposium on Personal, Indoor and Mobile Radio Communications (PIMRC) to combine the OFDM and CDMA. Since that time, hundreds of research articles have been written about its promise in the field of mobile radio communications. MC-CDMA is the contribution of Yee, et al [47], [48], [54]-[56]. In addition, Fazel and Papke [47], [48], [54]-[56] carried out the investigation of convolutional coding in conjunction with OFDM-CDMA. Prasad and Hara [47], [48], [52], [54]-[56] compared, and published books on, various methods of combining OFDM and CDMA techniques, identifying there different structures and aspects, namely MC-CDMA and multi-carrier direct sequence CDMA (MC-DS-CDMA). In addition, an International

Workshop on Multi-Carrier Spread Spectrum was initiated in 1997 and thereafter every 2 years. These workshops are published in the European Transaction on Telecommunications (ETT) journals. The first live demonstration of the MC-CDMA was in 2001 in the third International Workshop on Multi-Carrier Spread Spectrum. OFDM-CDMA methods suffer from the same disadvantage of OFDM which is the high peak-to-average-power-ratios (PAPR), which are dependent on the frequency domain spreading scheme, as investigated by Choi, Kuan and Hanzo.

Both MC-CDMA and MC-DS-CDMA allow users to share the same bandwidth at the same time using PN code to separate the data of users [54]. In addition, both schemes apply OFDM modulation to reduce the ISI per sub-channel [48]. The ISI is significant in spread spectrum where high chip rates occur. The main difference between both schemes in term of operation is the allocation of the chips where the MC-CDMA apply the PN code in the frequency direction over several parallel sub-channels and the MC-DS-CDMA apply the PN code in the time direction over several multi-carrier symbols [47].

MC-CDMA transmits a data symbol over several narrowband sub-channels and the sub-channels are multiplied by the PN code. This can be realized using low complex OFDM operation. MC-CDMA offers a flexible system design as the spreading code does not have to be equal to the number of sub-carriers [48].

MC-DS-CDMA converts the high rate data symbol serial-to-parallel to low rate sub-streams on each sub-channel and thereafter applies the PN code on the sub-channels in the time direction which leads to DS-CDMA on each sub-channel. MC-DS-CDMA systems have been proposed with different multi carrier modulation schemes even without OFDM and the

general term used is MC-DS-CDMA [47]. It can be categorised into two schemes. The first scheme is broadband sub-channels and the second scheme is the narrowband sub-channels. The first scheme typically applies only few numbers of sub-channels where each sub-channel can be considered as DS-CDMA. The second scheme typically uses high numbers of sub-carriers can be efficiently realized using OFDM. Table 2.2 compares the advantages and disadvantages of MC-CDMA and MC-DS-CDMA.

MC-CDMA		MC-DS-CDMA	
Advantages	Disadvantages	Advantages	Disadvantages
Simple implementation with Hadamard Transform and FFT Low complex receivers High spectral efficiency High frequency diversity gain due to spreading in the frequency direction	High PAPR, especially in the uplink Synchronous transmission	Low PAPR in the uplink High time diversity gain due to spreading in the time direction	ISI and/or ICI can occur, resulting in more complex receivers Less spectral efficiency if other multi-carrier modulation schemes than OFDM are used

Table 2.2: Advantages and drawbacks of MC-CDMA and MC-DS-CDMA [47]

2.4.4 Summary

A high spectral efficiency spectrum and maximising the number of users and transmission rate within a frequency band are the most critical design objectives and challenge to improve the reliability and performance of wireless communications systems. Multipath channels degrade the performance of the single carrier modulation technique. However, most of the conventional modulation techniques are sensitive to ISI unless the channel symbol rate is small compared to the delay spread of the channel in the multipath environment [1], [34], [47]-[49].

OFDM offers high spectral efficiency due to the large numbers of sub-carriers that form a nearly rectangular frequency spectrum [1], [34], [47]-[49], [55]. It can be easily realized using FFT. A guard interval is used in OFDM symbol to reduce the complexity of receiver that avoids ISI and ICI. But, OFDM suffers from a high PAPR that requires highly linear amplifiers otherwise the out-of-band power will be enhanced. COFDM is similar to OFDM except that forward error correction is applied to the signal before transmission to avoid bit errors on subcarriers in deep fade so that the number of subcarriers needed is larger than the number of bits or symbols transmitted simultaneously. This is an advantage in high frequency transmission links such as the DAB, DVB and DVB-T systems used in Europe [1], [34], [47]-[49], [55].

Spread spectrum is a rapidly growing technology and widely used in wireless communications to allow multiple access simultaneously and privacy within the same channel whereas OFDM itself does not. DS-CDMA and FH-CDMA are the primary types of spread spectrum. The DS-CDMA spread the narrowband channel over a continuous bandwidth by mixing the data with a PN code whereas the narrowband signal in the FH-

CDMA is hopping over a wide bandwidth using the PN code instead of spreading the signals over a continuous bandwidth. DS-CDMA is preferred to FH-CDMA for long transmission distance due to the interference and multipath signals of the other systems. DS-CDMA requires accurate power control so that no user masks all the users if its power is too high comparing to the other users at the receiver side [1], [47].

DS-CDMA offers easy frequency planning, high immunity against interference if a high processing gain is used, flexible data rate adaptation and multiple access. MAI occurs as the number of simultaneously active users increases in which the single carrier CDMA limited the number of users according to the processing gain [47].

The combination of OFDM and CDMA offers a robust system that is immune to multipath waves, reduces ISI and ICI, allows multiple access and privacy. This combination, known as MC-CDMA, usually uses the Walsh Hadamard orthogonal code. MC-CDMA is similar to DS-CDMA except that MC-CDMA performs the spreading code in the frequency domain. MC-CDMA can achieve good BER for N users using standard receiver techniques comparing to single carrier DS-CDMA that requires highly complex receiver for the same N users. MC-CDMA is better than COFDM in terms of multiple access and it replaces the encoder of COFDM by an NxN matrix to avoid bit errors [47], [55].

MC-DS-CDMA is a descendent of MC-CDMA in that both allow users to share the same bandwidth at the same time using PN code to separate the data of users. The main difference is that the MC-CDMA applies the PN code in the frequency domain whereas the MC-DS-CDMA applies it in the time domain. However, MC-CDMA can be realized using low complex OFDM operation and offers a flexible system design as the spreading code does not

have to be equal to the number of sub-carriers. MC-DS-CDMA can be realized with or without OFDM which depends on the number of sub-carriers used as large number sub-carriers can be efficiently realized using OFDM [47].

2.5 Overall summary, methodology and conclusions

It was discussed in this chapter that the ground can be used as transmission medium using buried earth rods [9], [13], [15], [17]-[19]. As a consequence, a bad SNR is expected from the ground due to rocky soil and the power feed cables' frequencies such 50 Hz and 60 Hz [9], [13], [15]. The use of earth electrodes compared to loop antenna greatly improved the communication range to 800m using SSB communication technique based on 87 kHz carrier frequency [17]-[22]. ELF is a neglected band in the civil communication applications, free of FCC fee license [22], [30] and propagates for long distances without regeneration due to its long wavelength compared to RF. Biological and ecological impact studies of using ELF on human and plant have concluded that there are no serious adverse effects of using ELF band [25], [26]. For these reasons, the ELF band can be used in a communication link where the ground itself is a transmission medium using earth rods in between the transmitter and receiver. A high spectral efficiency spectrum and maximising the number of users and transmission rate within a frequency band are the most critical design objectives and challenge to improve the reliability and performance of wireless communications systems [1], [34], [47]-[49]. The 16-QAM of the digital communication schemes would enhance the transmission rate at such low frequencies compared to ASK and 8-PSK. OFDM enhances the transmission rate of a given bandwidth and offers high spectral efficiency due to the large number of digital modulation sub-carriers that form a nearly rectangular frequency spectrum but suffers from a high PAPR that requires highly linear amplifiers [1], [34], [47]-[49], [55]. Spread spectrum systems allow multiple access simultaneously and privacy within the same channel compared to OFDM. The MC-CDMA offers a robust system that is immune to the multipath waves, reduces the ISI and ICI, allows multiple access and privacy [47], [55]. In contrast to OFDM, the spread spectrum significantly reduces the speed of the usable data.

2.5.1 Methodology

The ELF link that was inspired by the literature review can be implemented using 16-QAM with help of OFDM to transmit the data in parallel form which would enhance the transmission rate at such low frequencies and reduce the multi-path interference. Transceivers can be designed using FDD form to allow 2 way transmission simultaneously especially for the remote control applications [57]. FPGA can be used to design, simulate, build and test the transceivers in laboratory. Altera Cyclone III EP3C120 FPGA development board [58] is a ready DSP platform for communication and signal processing via 2 Analogue-to-Digital Converters (ADCs), 2 Digital-to-Analogue Converters (DACs), External and Internal clock sources, Dual-in-line Package (DIP) switches and push-buttons switches. MathWorks and Altera [59]-[62] are co-operating to provide an easy designing platform that provides flexibility to import VHDL codes to be a part of a Simulink design file. These features are available from Altera using DSP Builder software [59]-[62] that is integrated in Simulink after installation. Altera DSP Builder [59]-[62] provides Intellectual Property (IPs) made by Altera team themselves to allow engineers and researchers to speed-up the development of new applications using Simulink of MathWorks. A complete design that uses DSP Builder functions can be simulated in Simulink to test the functionality of the design prior the compilation of Altera Quartus II project to program the FPGA development board [59]-[62]. Therefore, Matlab/Simulink of MathWorks and DSP Builder of Altera were used to develop the ELF transmission data link.

Figure 2.18 shows a basic OFDM transceiver design based on the FPGA selected. The transmitter side of the transceiver is expected to transmit the data by Serial-to-Parallel (S/P) converting the data of the source first. Then, the n parallel data are modulated on n subcarriers using 16-QAM modulation technique. After that, the modulated subcarriers

undergo DSP processing using Inverse FFT (IFFT) to maintain the orthogonality of OFDM in the time and digital domain. After that, the digital domain of OFDM is converted to analogue domain using DAC and then filtered using high order active band pass filter (BPF) to remove the aliasing caused by the sampling frequency on the output of the DAC so that the OFDM signals are sent purely analogue to the channel. The filters have to be linear in terms of phase because of phase data in QAM modulation. A high linear power amplifier can be used to increase the power of the transmitted signals.

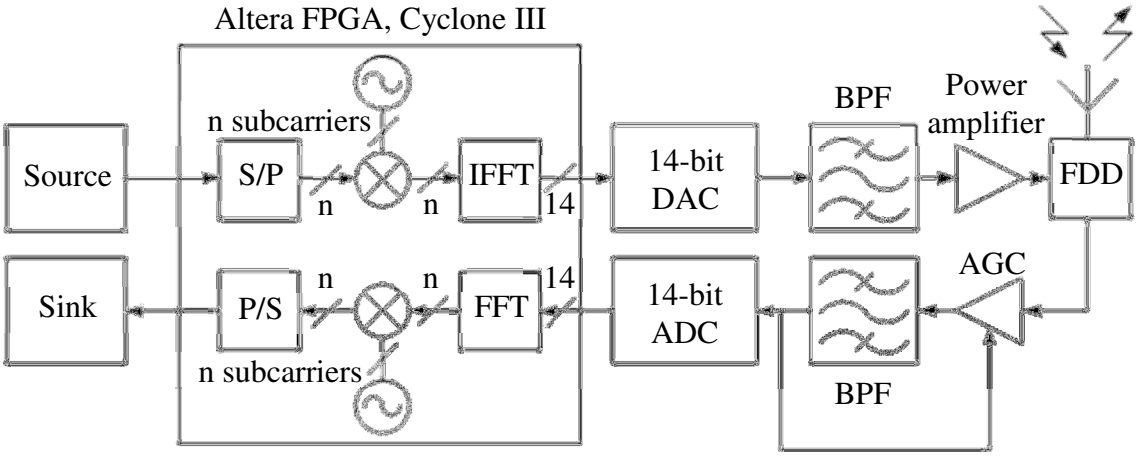

Figure 2.18: Basic OFDM design using FPGA

The receiver side shown in figure 2.18 is behaving in the reverse direction of the transmitter and is expected to pre-filter out the noise using high order active BPF with linear phase response. The analogue signals are to be converted back to digital domain using ADC. The amplitude input of the ADC is limited; therefore a high linear AGC amplifier is a need to keep the input to the ADC within the limit and prevent the system from high PAPR or otherwise the out-of-band power will be enhanced [1], [34], [47], [49]. The output of ADC undergoes FFT processing to separate the n subcarriers. The n separated subcarriers are 16-QAM demodulated individually. The n demodulated data are Parallel-to-Serial (P/S)

converted back to the sink. Digital filters with linear phase response can be used prior to the FFT processing to enhance the quality of the received signals.

2.5.2 Applications of ELF link

This is a generic link which can be used in any system in which the responding time is not critical [57]. Possible applications include sensing and broadcasting the weather of mountain areas as RF is not reliable in these areas due to multipath signals [57] where a complex RF receiver is required. Also, it could be used for remote control and telemetry of oil wells valves and motors, and power substations to avoid overload [57]. It could also be used in the remote control of points in train tracks located in countryside areas where RF needs high power transmission and reception.

2.5.3 Limitations and motivations

It was found from the literature that demodulating the phase data of 16-QAM is crucial and is generally performed using complex mathematics [34], [35], 'tan' function [35], [39], [43] PLL [38]-[44] or a combination of 'tan' and DPLL [39], [43]. Consequently, this inspired the need for a simpler function than the carrier recovery functions, which is where the concept of cross correlation to detect the phase changes was investigated and presented in chapter 4. Patent literature review showed that there is no such patent or known prior art related to the presented system design in chapter 4. The author of this thesis has conducted initial investigation and calculations shown in appendix A, B and C using Microsoft (MS) Excel to replace the use of 'tan' function and concluded that demodulation of phase data can also be undertaken using the cross correlation function that needs a maximum of 4 multipliers, which requires significantly less multipliers than carrier recovery, thus IC resources.

To the author's knowledge, cross correlation will be used, for the first time in the 16-QAM demodulator system, to replace the carrier recovery to detect the phase changes on the received signal. It is expected that this would yield a significant reduction in terms of complexity and the silicon required to integrate the 16-QAM receiver onto an IC. The reduced complexity of the receiver leads to a reduced number of resources required, for the design, and thus power consumption of the system.

Applications of 8-PSK and 16-QAM includes mobile and fixed broadband internet [1], [4]. It is widely used in WCDMA, HSDPA, WiMAX and WLAN broadband wireless access technologies [1]. The HDSPA, WiMAX and WLAN are part of the 3GPP WCDMA, IEEE 802.16 and IEEE 802.11 standards respectively [1]. In the UK, 16-QAM and 64-QAM are currently used in DVB-T systems [2], [4]. Therefore, cross correlation technique is expected

to yield a cost reduction in products using 16-QAM demodulators, namely broadband internet and Digital TV.

Chapters 3, 4 and 5 are concerned with the development of Star 16-QAM link and cross correlation to demodulate the phase data. Chapter 6 discusses the issues and applications related to the use of ground as transmission medium, ELF band and multi-carrier communication systems in implementing a complete ELF Transmission Data Link based on the facts presented in the literature review and the implementations of the digital modulation schemes in chapter 3, 4 and 5.

3. Amplitude Shift Key (ASK) transmitter/receiver

As discussed in chapter 2, use of the ELF band has largely been confined to submerged submarine communications, and its application to civilian data transmission has been neglected. This chapter describes the design and build of a data link operating with a 20 Hz carrier using ASK at a data rate of 4 bps. This link will be advanced and taken forward in chapter 5 to combine it with 8-PSK link of chapter 4 to utilise the bandwidth for 16-QAM transmission that enhance the capacity of the ELF link. Chapter 6 discusses the possibility of utilising 16-QAM in OFDM link to enhance the bit rate at such low frequencies. Possible applications of this link include remote control of traffic gates, motorway signage, plant equipment, subterranean communication, telemetry, diversions of train tracks, etc.

3.1 Theory

3.1.1 ASK transmitter

Digital systems are able to distinguish between approximated discrete points of a signal [31]. Therefore, digital systems can be considered to be much faster and more reliable than analogue systems. Digital modulation can be carried out by altering the magnitude (ASK), frequency (FSK), or phase (PSK) of a signal. The advantage of using ASK is that it is more straightforward to generate/recover data compared to PSK and FSK. ASK is the digital form of AM [32], [33] so the frequency of the carrier signal has to be higher than that of the modulating wave. ASK equation can be derived using AM [33], [63] equations:

$$S_m(t) = A[1 \pm m_i]\cos(\omega_c t) \qquad (1)$$

Where,

A	Peak amplitude voltage of the carrier
m_i	Modulation index, ratio of amplitude when sending logical states 1 or 0
ω_c	Angular frequency of the carrier, $2\pi f_c$ rad/sec
t	Time of modulation in seconds

The modulation index m_i must be less than or equal to 1 or otherwise $A[1 - m_i]$ would over modulate the signal [33]. It is best to use $m_i = 1$ in digital communication to maximize the system performance [33]. When $m_i = 1$, the amplitude is shifting between $2A$ and 0 in ASK to send logical 1 and 0 respectively. Thus, it is sometimes called On-Off Keying (OOK). ASK is simple compared with the other digital transmission techniques but has a disadvantage of being more susceptible to error because of the noise hitting the amplitude of the carrier [32], [33], [63]. ASK occupies a bandwidth of twice the data rate.

From equation 1, the carrier amplitude is A, the transmitted carrier power when $m_i = 0$ is then,

$$P_c = \frac{A^2}{2} \text{ watt} \quad (2)$$

So, the total average power using $m_i = 1$,

$$P_c = 2A^2 \text{ watt, when sending logical 1} \quad (3)$$

$$P_c = 0 \text{ watt, when sending logical 0} \quad (4)$$

Moreover, if the 1's and 0's are equally likely [33], then the average power ratio $P_c = A^2$ watt where $\frac{A^2}{2}$ watt occur when transmitting 1's and the remainder $P_i = \frac{A^2}{2}$ watt is the power of the sidebands as shown in figure 3.1, so called *information* with sidebands [33].

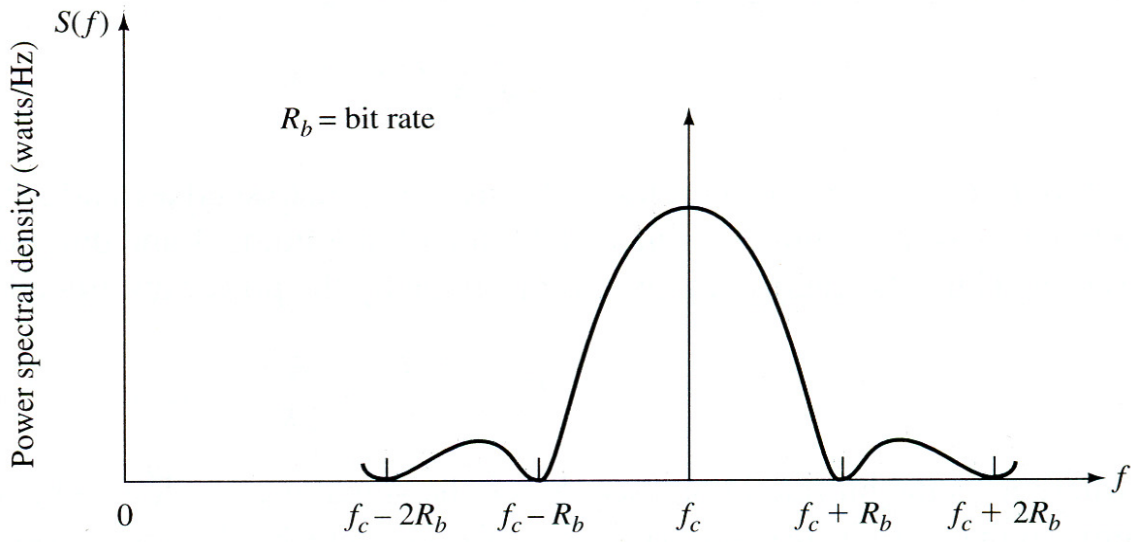

Figure 3.1: OOK power spectral density [33]

ASK generates the AM wave directly using an analogue switch and an oscillator [33]. A digital word keys the output of the oscillator via the analogue switch as shown in figure 3.2.

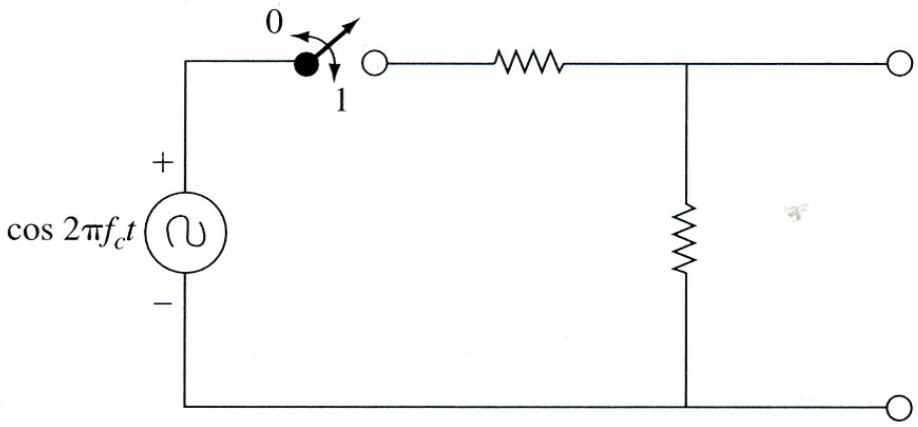

Figure 3.2: Typical ASK transmitter [33]

3.1.2 ASK coherent receiver

The modulated carrier of the ASK can be demodulated using a matched filter detector [33] as shown in figure 3.3. The local oscillator (LO) has to be synchronised with the transmitted carrier [3], [33]. The matched filter detector is the best for binary digital communication [33]. A threshold has to be set at the output of the matched filter since the ASK transmitter is sending a sinusoidal burst of amplitude A and zero to represent logical 1 and zero respectively. With reference to the trigonometric identities [45], [46], [64] in equations 5, the output of the *correlator* can be predicted by summing the identities:

Identities, $\cos(H \pm B) = \cos(H)\cos(B) \mp \sin(H)\sin(B)$ (5)

The sum, $\cos(H)\cos(B) = \frac{1}{2}[\cos(H - B) + \cos(H + B)]$

So, $Correlator = A\cos(\omega_c t) \times \cos(\omega_c t)$

$= \frac{A}{2}[\cos(2\omega_c t) + 1]$ (6)

Therefore, the output of the synchronous matched filter detector is a unipolar sinusoidal wave shifted by 1 ranging in amplitude between 0 and $\frac{A}{2}$ volts after filtering. The output of the matched filter has to be compared to a threshold between the energy E_1 and E_0 of logical 1 and 0 respectively.

$$y_0 = \frac{E_1 - E_0}{2} \quad (7)$$

When a logical 1 is transmitted, the amplitude of the carrier is then A and the duration of the transmission T_b (bit period) is sent [33], [63]. So,

Carrier power, $$P_{c_1} = \frac{A^2}{2} \quad (8)$$

Carrier energy, $$E_1 = \frac{A^2 T_b}{2} = \frac{A^2}{2R_b} \quad (9)$$

Carrier energy, $$E_0 = 0$$ since zero signal is sent (10)

The threshold (7) is the average energy per bit given by,

$$y_0 = \frac{A^2 T_b}{4} = \frac{A^2}{4R_b} \quad (11)$$

Figure 3.3 shows a synchronous coherent detector of ASK where the baseband signal is reconstructed with respect to the threshold derived.

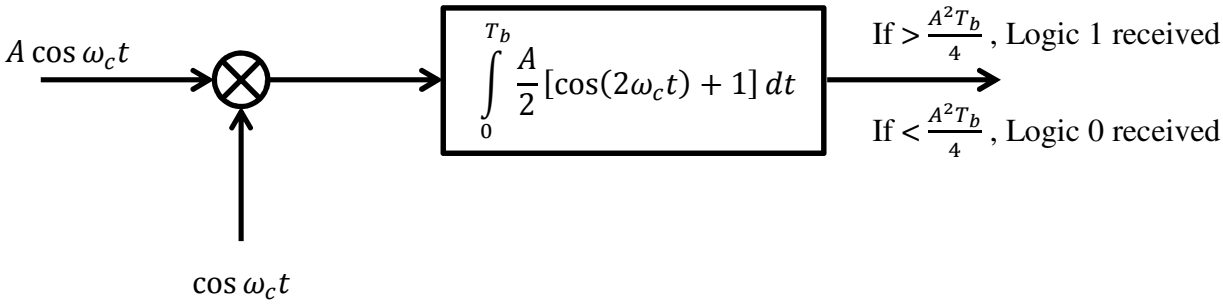

Figure 3.3: Coherent ASK receiver [33]

The performance of the ASK coherent detector [33] is measured using the average energy per bit that was calculated in (11) and the error function table [33] shown in appendix D to estimate the probability of error P_e. The error function is given by,

$$P_e = \frac{1}{2} erfc\left(\sqrt{\frac{y_0}{2N_o}}\right) = \frac{1}{2} erfc\left(\sqrt{\frac{A^2 T_b}{8N_o}}\right) = \frac{1}{2} erfc\left(\sqrt{\frac{A^2}{8N_o R_b}}\right) \qquad (12)$$

Where,

N_o Channel noise density measured in watt/Hz

The matched filter detector [33] is not a difficult technique but experiences difficulties when long strings of 0's are sent. It could generate random error bit in this case in which the carrier needs to be resynchronised when the transmitter turns on back.

3.1.3 ASK non-coherent receiver

The non-coherent detector does not require carrier recovery as in coherent receivers [33]. Therefore, the non-coherent detector is much simpler to construct compared to the coherent detector. The simplest form of a non-coherent detector is the envelope detector as shown in figure 3.4. The envelope detector is a non-linear system making the output not Gaussian distributed [33]. Thus, the analysis of non-coherent digital detector is complicated.

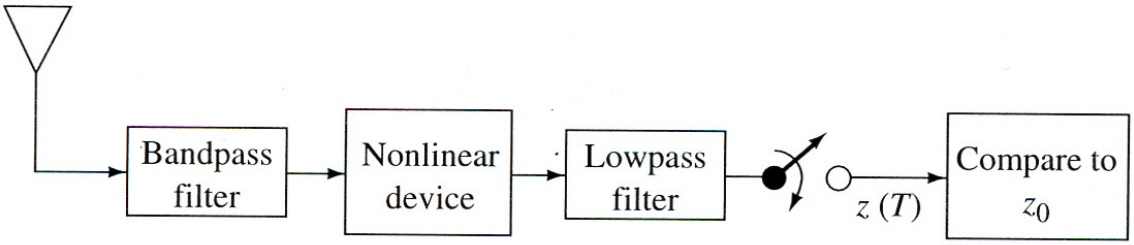

Figure 3.4: Non-coherent ASK receiver [33]

The error rate can be calculated accurately for coherent detectors but non-coherent has an approximate error rate that can be calculated using,

$$P_e = \frac{1}{2}\left(e^{-\frac{A^2 T_b}{8N_o}}\right) = \frac{1}{2}\left(e^{-\frac{A^2}{8N_o R_b}}\right) \qquad (13)$$

3.1.4 Performance of Coherent and non-coherent ASK detectors

The performance of the ASK detector can be estimated using an assumed value of noise density N_o of the channel (14) and equations 12 and 13 to compute the probability of error P_e of coherent and non-coherent detectors against the SNR. The amplitude A can be calculated for various $x\ dB$ values of SNR using (21) to apply A in (12) and (13) in order to compute and compare the probability of error P_e.

Assume,

$$N_o = 5 \times 10^{-10}\ watt/Hz \tag{14}$$

Given,

$$f_c = 20\ Hz \tag{15}$$

$$x\ dB = 10\ \log_{10}\left(\frac{P_c}{P_N}\right)\ or\ \ 10\ \log_{10}\left(\frac{S}{N}\right) \tag{16}$$

$$P_N = N_o f_c \text{ watt} \tag{17}$$

So,

$$P_N = 5\ \times\ 10^{-10}\ watt/Hz\ \times 20\ Hz$$

$$= 10\ \times\ 10^{-9}\ watt \tag{18}$$

Hence,

$$\frac{x\ dB}{10} = \log_{10}\left(\frac{P_c}{P_N}\right)$$

$$10^{\frac{x\ dB}{10}} = \frac{P_c}{P_N}$$

$$P_c = 10^{\frac{x\ dB}{10}} P_N \tag{19}$$

Combining (8) in (19),

$$\frac{A^2}{2} = 10^{\frac{x\ dB}{10}} P_N \qquad (20)$$

So, from (18)

$$A = \sqrt{10^{\frac{x\ dB}{10}} \times 20 \times 10^{-9}} \qquad (21)$$

The probability of error was computed for both detectors in appendix E and compared graphically in figure 3.5. The same procedure was applied when $f_c = 288\ Hz$ and $R_b = 18\ bps$ in appendix E and figure 3.5. Clearly, the coherent detector performs better than non-coherent detector. The difference in SNR for the same amount of P_e of various x gains can be calculated as well to evaluate the power needed for non-coherent detector to perform as the coherent detector.

From (13) and (17),

$$\ln(2P_e) = -\frac{A^2}{8N_o R_b} = -\frac{A^2 f_c}{8NR_b}$$

Rearranging,

$$\frac{S}{N} = \frac{-4R_b \times \ln(2P_e)}{f_c} = \frac{A^2}{2N} \qquad (22)$$

From (16),

$$x\ dB = 10\ \log_{10}\left(\frac{-4R_b \times \ln(2P_e)}{f_c}\right) \qquad (23)$$

The gain required for non-coherent detector to perform as a coherent detector was calculated in appendix E using equation 23 for various P_e points and computed the difference between

the gain of coherent and non-coherent as shown in figure 3.5. Clearly, there is a linear region in traces orange and green where the gain difference between coherent and non-coherent detectors is almost $\Delta dB = 0.78\ dB$ to coherent detector at 20 Hz carrier and $\Delta dB = 0.78\ dB$ at 288 Hz. The non-coherent detector performs better than coherent detectors at higher SNRs than 14 dB at 20 Hz.

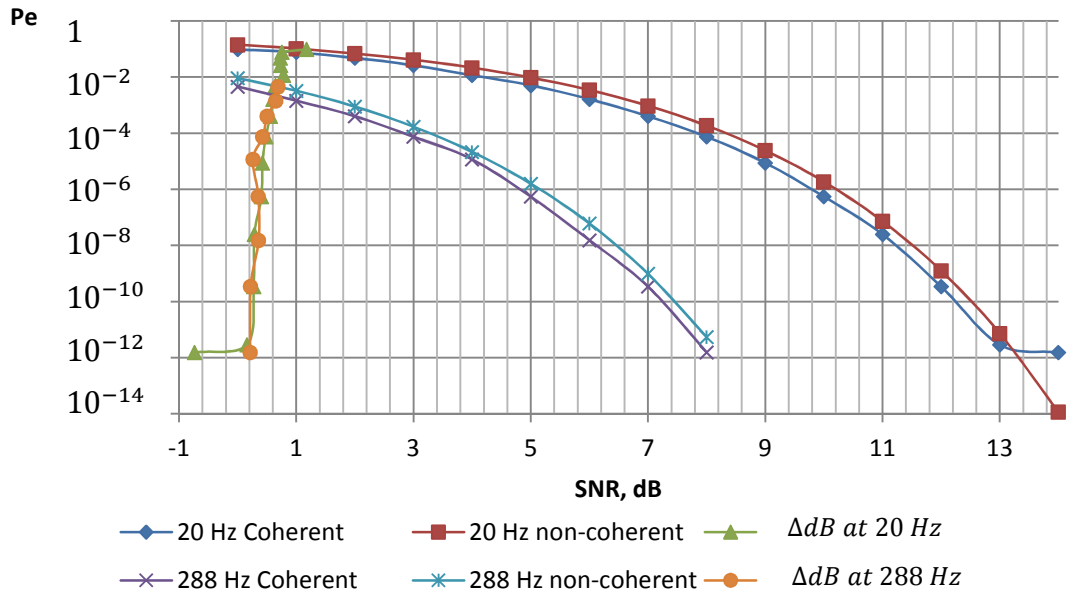

Figure 3.5: Performance of ASK receiver

3.2 Implementation of ASK link

3.2.1 Transmitter

For simplicity of design, a nominal 20 Hz carrier based ASK system, with transmission rate of 4 bps, was chosen to prove the capability of ELF to transmit digital data. This differs from Stubblefield's experiment [9], [13], [15] in which the human voice was transmitted. A non-coherent 20 Hz transmitter and receiver were designed and constructed with custom built transmit and receive Universal Asynchronous Receiver/Transmitter (UARTs) encoded/decoded 2 bits of data using combinational logic and registers. Figure 3.6 illustrates the generation of a digital word by the UART consisting of a start sequence of 1.5 bits, an 8-bit address code, 2 bits of data and a stop sequence of 0.5 bit in Pulse Code Modulation (PCM) form. The 1.5 start bits and 0.5 stop bit define the mark-space ratio and avoid mistaking the address code for start/finish bits.

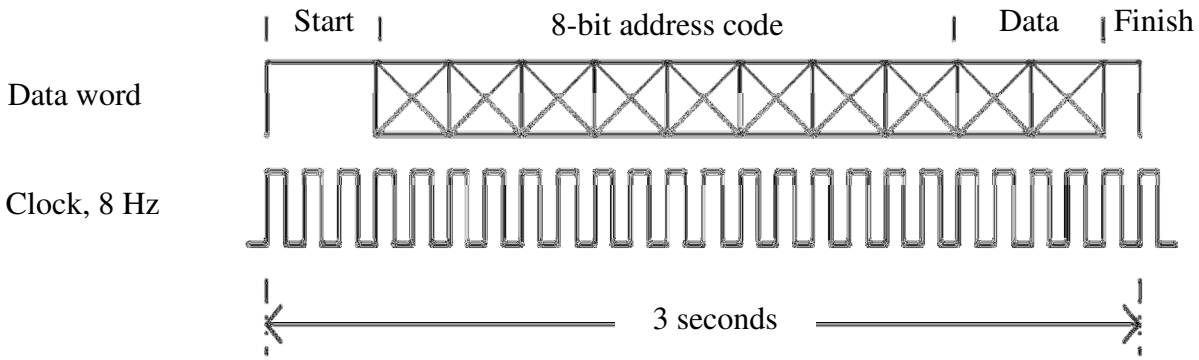

Figure 3.6: PCM word generated by the transmit UART

The digital word keys the output of a Wien-bridge oscillator, operating at a nominal 20 Hz, using a Single-Pole-Single-Throw (SPST) switch as shown in figure 3.7. A BPF filter removes the harmonics [65] caused by the carrier switching and JFET input operational amplifiers were used to minimise 1/f noise [66], [67].

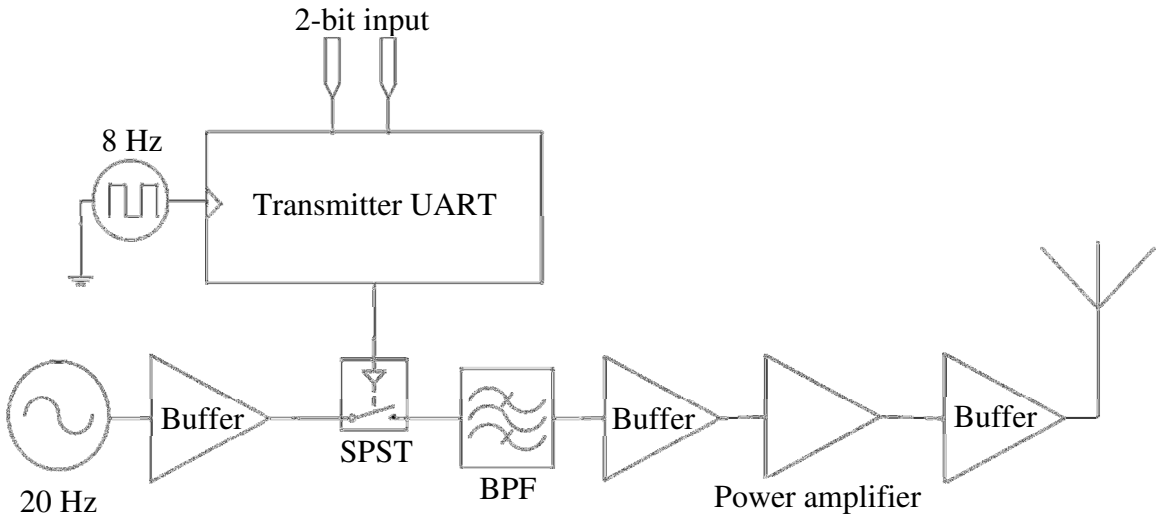

Figure 3.7: ASK transmitter design

The transmitter and receiver were constructed using readily available electronic components including a Wien-Bridge oscillator and an analogue switch controlled by a transmitter UART. A data rate of 4 bit/sec was used. The constructed transmitter (appendix F) had a carrier frequency of 21 Hz shown in figure 3.8 due to components tolerance affecting the closed-loop of the Wien-Bridge oscillator. Figure 3.8 shows the states represented by varying the amplitude of the ASK carrier as in AM. The carrier occupied a bandwidth of 8 Hz that is twice the bit rate R_b and each sideband occupied 4 Hz. The SPST analogue switch produced harmonics due to the data clock not being phase locked to the carrier. Therefore a third order active BPF filter with 60 dB/decade roll-off at 13 and 29 Hz cut-off frequencies would reject the harmonics of the modulated carrier, prevent any UART transmitter low frequency harmonics, and reduce flicker noise.

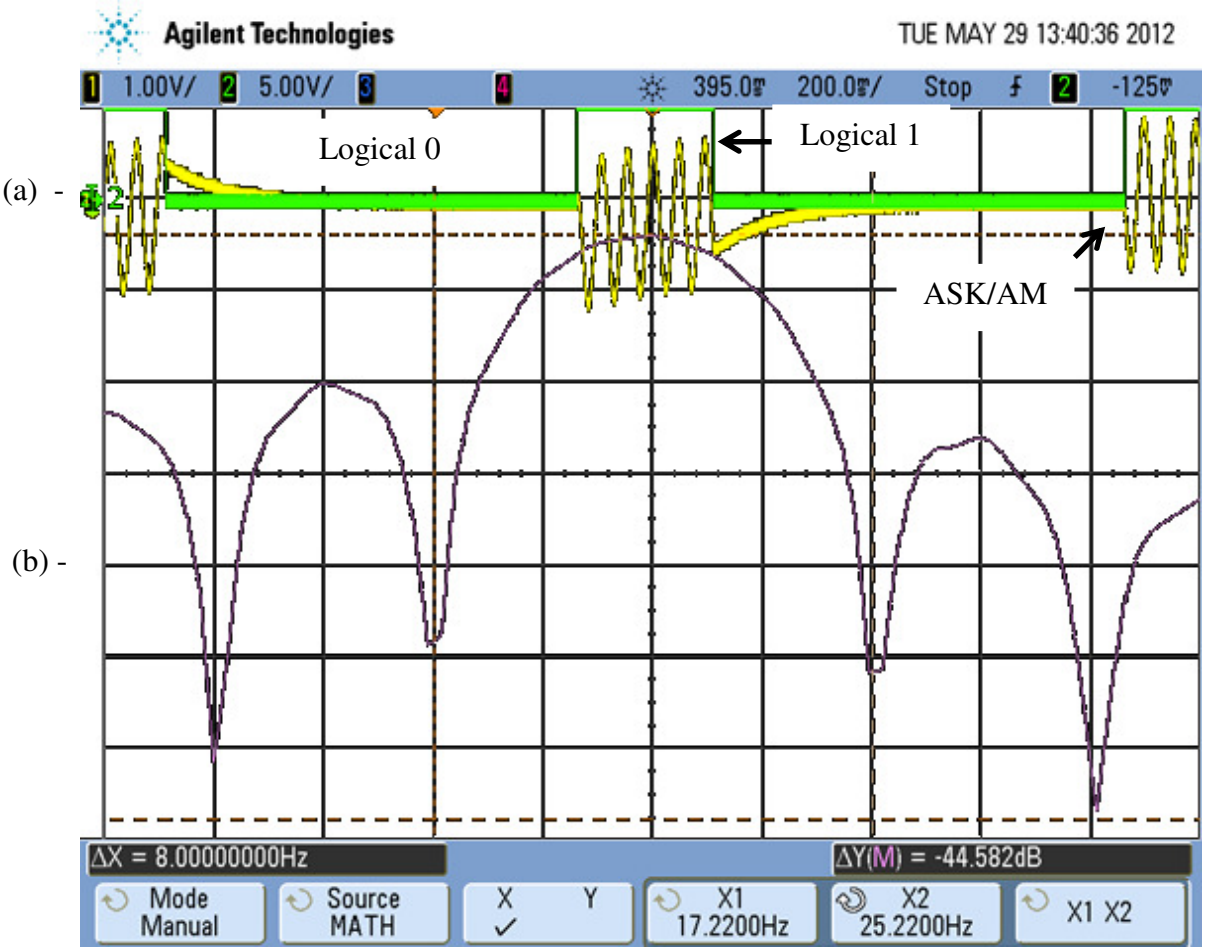

Figure 3.8: (a) UART data key the carrier, (b) carrier spectrum

3.2.2 Receiver

For simplicity of design, a non-coherent detector (see appendix F) was used to demodulate the ASK signals as shown in figure 3.9. The received signals were demodulated through full-wave precision rectifier, envelope detectors, analogue comparator and the recovered data were retimed using PLL through the receiver UART (see appendix F).

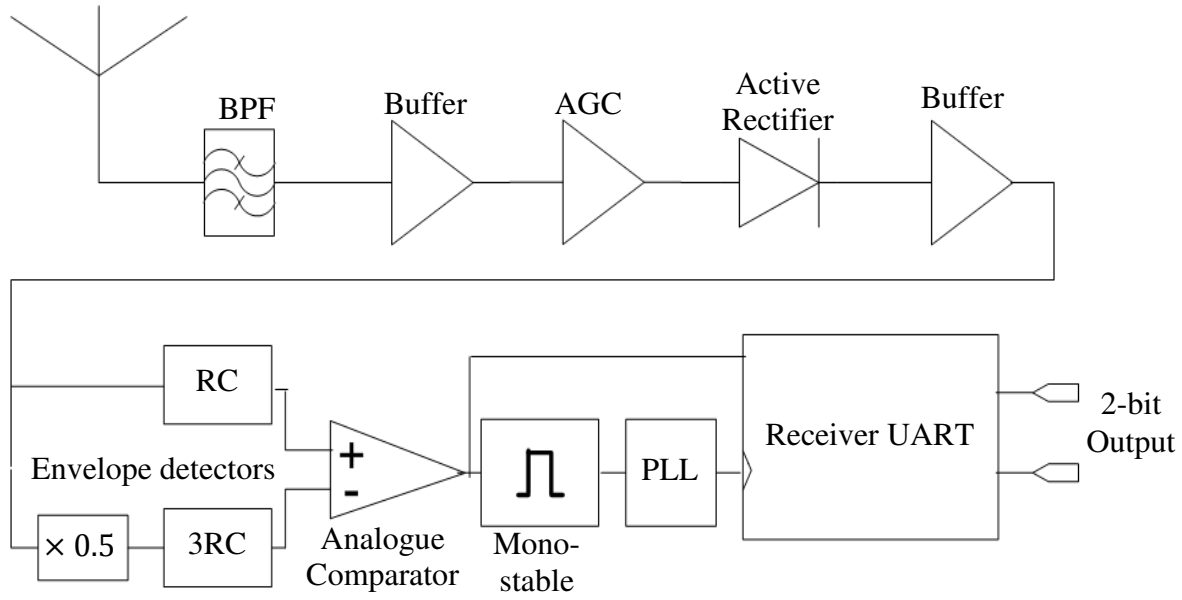

Figure 3.9: Noncoherent ASK receiver

The BPF filter in figure 3.9 removes any harmonics of 50 Hz harmonics and the 1/f noise. The AGC keeps the data amplitude within specified limits. The active filters and a full-wave precision rectifier were implemented using low-noise JFET-input OP-AMPs to minimise the flicker noise. Low cut-in voltage germanium diodes were used to minimise the voltage drop in the rectifier which is followed by a voltage-follower and 2 envelope detectors. The RC network in the second envelope detector has a time constant 3 times that of the first envelope detector to provide a definite threshold to the comparator as shown in figure 3.10.

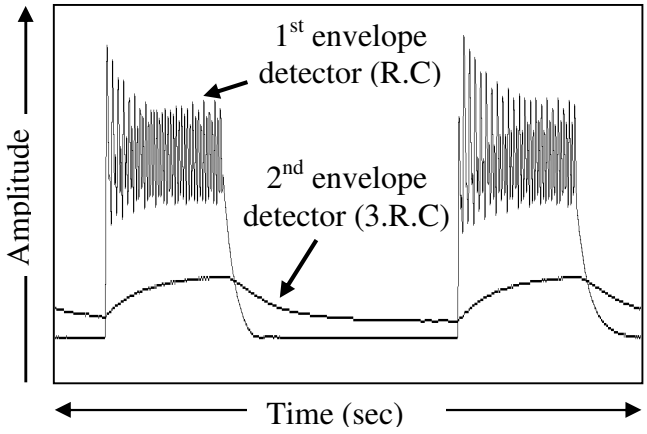

Figure 3.10: Input to envelop detectors

The voltage comparator and PLL slice the data. The Monostable and PLL aid retiming of the recovered data into the receive UART to check the address code and decode the data. The receive UART removes the start/finish bits and checks the 8 bits of address code before outputting the 2 data bits when the receiver address matches that of the incoming word. The data was successfully transmitted across the laboratory as shown in figure 3.11.

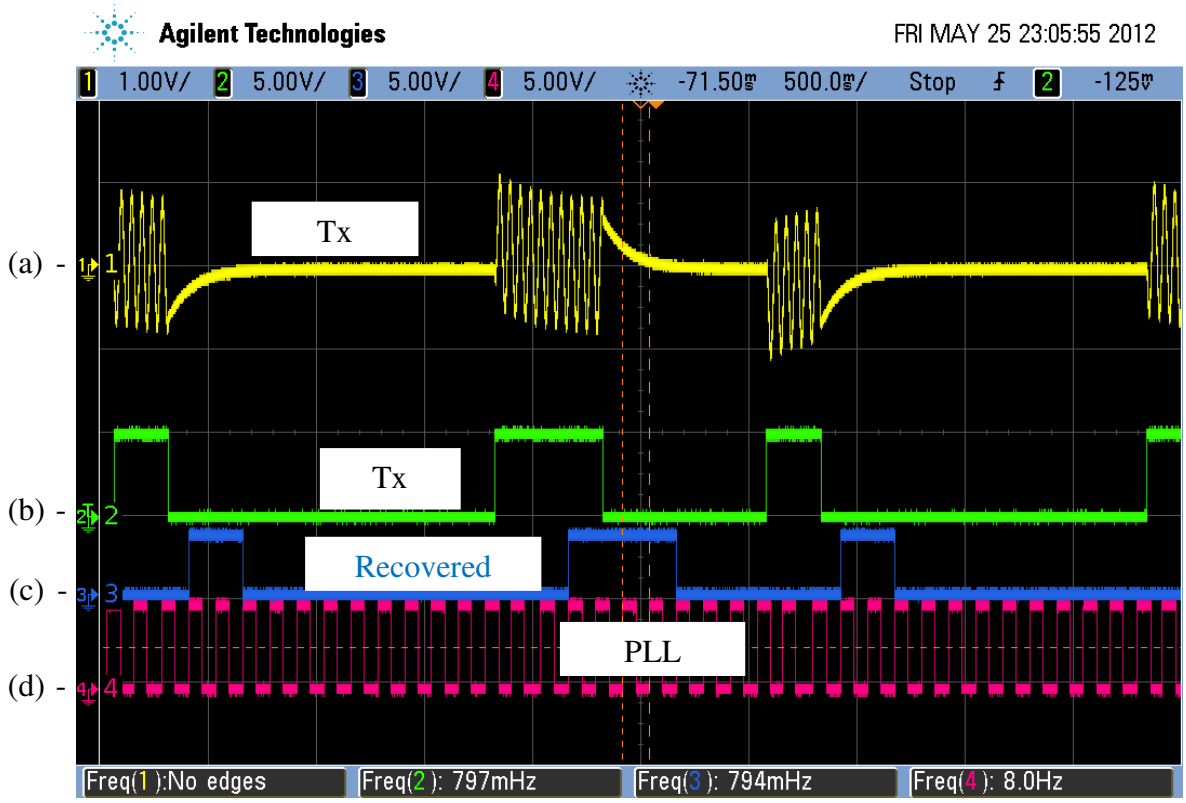

Figure 3.11: (a) Transmitted carrier, (b) UART word, (c) Recovered data, (d) PLL

3.3 Comments on ASK transmitter/receiver

This chapter discussed and evaluated the possibility of a low speed data communication link operating with a 20 Hz carrier using the ASK digital modulation technique at a data rate of 4 bps. The transmitter and receiver were constructed using readily available electronic components. The advantage of using ASK is that it is more straightforward to generate/recover data compared to PSK and FSK. The disadvantage of ASK is it is more susceptible to error because of the noise adding to the amplitude of the carrier. ASK occupies a bandwidth of twice the data rate.

The transmitted signals can be demodulated using a matched filter detector which is the best for binary digital communication. The matched filter detector experiences difficulties when long strings of 0's are sent in which the carrier needs to be resynchronised when the transmitter turns back on. The non-coherent detector simply does not require carrier recovery as in coherent receivers. An assumed value of noise density was used to compare the performances of coherent and non-coherent detectors and it was confirmed that the coherent detector performs better than non-coherent detector. The gain differences between the coherent and a non-coherent detector were calculated to evaluate the power needed for non-coherent detector to perform as the coherent detector. It was noticed that the non-coherent detector needs a linear gain difference of $\Delta dB = 0.78\, dB$ to coherent detector at 20 Hz carrier. The non-coherent detector performs better than coherent detectors at higher SNRs than 14 dB at 20 Hz carrier.

Data was successfully transmitted across the laboratory. The passive components are sensitive at low frequencies where tolerances affect the efficiency and performance of the

link. However, FPGA, Matlab and Altera Design suite provide flexibility and accuracy in designing circuits. This link will be advanced and taken forward in chapter 5 to combine it with 8-PSK link of chapter 4 to utilise the bandwidth for 16-QAM transmission that enhance the capacity of the ELF link.

4. Phase Shift Key (PSK) transmitter/receiver

Chapter 3 discussed the use of a non-coherent ASK detector for ELF transmission. It was found that coherent detectors perform better than the non-coherent. This chapter describes the design and build of a data transmission link operating with a 20 Hz carrier but using an 8-PSK coherent detector. PSK can only be demodulated using coherent detectors [33] such as the matched filter [3] discussed in chapter 3. This link has a baud rate of *4 symbols/s*, so that the bandwidth of 8-PSK remains the same as ASK in chapter 3. Each symbol consists of 3-bit. Chapter 5 shows how the 16-QAM signal changes in terms of phase and amplitude as a result of combining 8-PSK and ASK at a rate of 4 *symbols/sec* that enhance the capacity of the ELF link without increasing the bandwidth. The 8-PSK link can be designed using an FPGA which is an attractive option because of its performance, power consumption and flexibility [39], [43]. Recently, the FPGA technology experienced dramatic improvements and revolutionary changes [39], [43]. The highly flexible nature of FPGAs allows system designers to integrate any signal processing function [39], [43]. FPGA manufacturers provide a ready DSP platform for communication and signal processing via ADCs, DACs, and External and Internal clock sources. For example, the MathWorks and Altera [59]-[62] provide an easy designing platform that provides flexibility to import VHDL code to be a part of a Simulink design file. Altera DSP Builder [59]-[62] provides IPs made by Altera team themselves to allow engineers and researchers to speed-up the development of new applications using Simulink. A complete design that uses DSP Builder functions can be simulated in Simulink to test the functionality of the design prior the compilation of Altera Quartus II project to program the FPGA development board [59]-[62]. With Altera DSP Builder, designers can test algorithms, perform, modify or optimise and update whole systems quickly. Therefore, Simulink and Altera DSP Builder were used to develop the 8-PSK and 16-QAM.

4.1 Theory

4.1.1 Binary PSK and carrier recovery

PSK uses phase angles to represent binary states with a constant frequency carrier and amplitude [32], [33]. Figure 4.1 shows the basic form of constellation that requires 2^1 phase angles to represent 1-bit using 0^o and 180^o. It occupies a bandwidth of twice the bit rate as shown in figure 4.2.

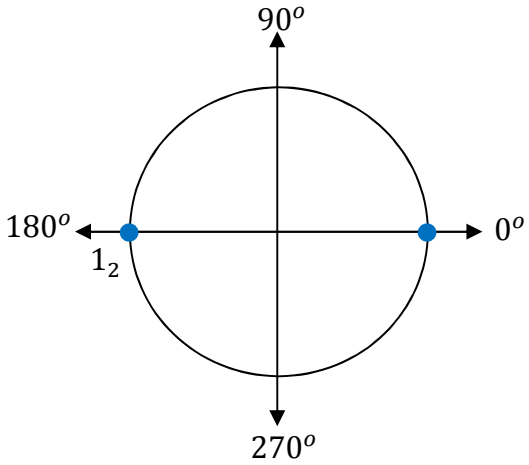

Figure 4.1: BPSK constellation points [33], [34], [68], [69]

The angles of the carrier f_c in BPSK system are controlled using the baseband information $s(t)$. The PSK can be significantly distinguished compared to FSK as the digital signals are drawn from a discrete set of waveforms [33]. This can be described mathematically,

$$S_c(t) = A\ \cos(\omega_c t + \ 2\pi k_p\ S(t)) \qquad (24)$$

Where,

k_p, the proportionality factor relating the phase shift to the signal voltage.

So,

$$S_0(t) = A\ \cos(\omega_c t + \theta_0) \quad (25)$$

$$S_1(t) = A\ \cos(\omega_c t + \theta_1) \quad (26)$$

Where θ_0 and θ_1 in (25) and (26) are constant phase shifts representing the logical 0_2 and 1_2 respectively. These angles can be analytically simplified to show the spectrum of the BPSK shown in figure 4.2.

$$\theta = \frac{\theta_1 + \theta_0}{2} \quad (27)$$

$$\Delta\theta = \frac{\theta_1 - \theta_0}{2}, \quad (28)$$

Where,

θ, Average angle

$\Delta\theta$, phase deviation/modulation index

Rewrite (25) and (26),

$$S_0(t) = A\ \cos(\omega_c t + \theta - \Delta\theta) \quad (29)$$

$$S_1(t) = A\ \cos(\omega_c t + \theta + \Delta\theta) \quad (30)$$

Letting $\theta = 0$, and express (29) and (30) in the general form of,

$$S_i(t) = A\ \cos\big(\omega_c t + \Delta\theta\ d_i(t)\big) \quad (31)$$

Where,

$d_i(t)$, the data sequence Non-Return-to-Zero (NRZ) +1 or -1

Rewriting (31) using (5), gives,

$$S_i(t) = A\ \cos(\omega_c t)\ \cos\big(\Delta\theta\ d_i(t)\big) - A\ \sin(\omega_c t)\ \sin\big(\Delta\theta\ d_i(t)\big)$$

Using Even and Odd properties of cosine and sine where,

$$\cos\big(\Delta\theta\ d_i(t)\big) = \cos(\Delta\theta)$$

$$\sin\big(\Delta\theta\ d_i(t)\big) = d_i(t)\sin(\Delta\theta)$$

So,

$$S_i(t) = A\cos(\Delta\theta)\ \cos(\omega_c t) - A\ d_i(t)\sin(\Delta\theta)\ \sin(\omega_c t) \qquad (32)$$

Clearly, the first term $A\cos(\Delta\theta)\ \cos(\omega_c t)$ is the carrier independent of data and the second term $A\ d_i(t)\sin(\Delta\theta)\ \sin(\omega_c t)$ is the carrier directly dependent on data [37]. So, the power of the carrier P_c and data P_d,

$$P_c = \frac{A^2 cos^2(\Delta\theta)}{2}$$

$$P_d = \frac{A^2 sin^2(\Delta\theta)}{2}$$

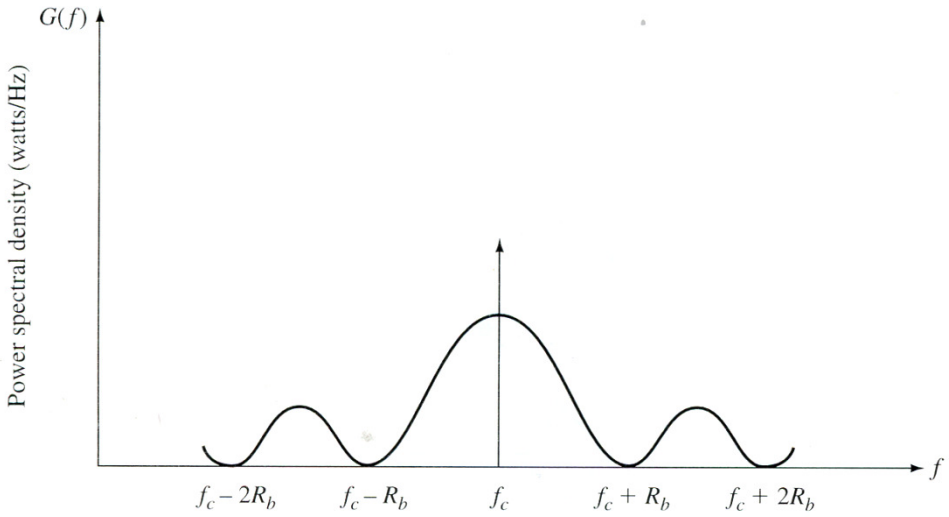

Figure 4.2: BPSK transmitted power [33], [68], [69]

So,

$$Total\ power = P_c + P_d = \frac{A^2}{2}\left[cos^2(\Delta\theta) + sin^2(\Delta\theta)\right]$$

$$= \frac{A^2}{2} \quad (33)$$

Hence, the average energy per bit when the bit period is T_b,

$$E_b = \frac{A^2 T_b}{2} \quad (34)$$

and

$$A = \sqrt{\frac{2E_b}{T_b}} \quad (35)$$

Equation (32) can be simplified for the BPSK shown in figure 4.1, since the phase deviation is $\Delta\theta = 90^o$,

So,

$$S_i(t) = A\, d_i(t)\ \sin(\omega_c t) \quad (36)$$

Hence, the carrier is suppressed in BPSK and with the data $d_i(t)$ NRZ -1 or +1, the transmitted signals are negative of each other as shown in figure 4.3.

$$S_1(t) = -S_0(t) \quad (37)$$

Researchers are paying attention to solve synchronisation problem in phase transmission. PSK systems are only demodulated using coherent detectors where the simplest is the matched filter discussed in chapter 3. The demodulation of BPSK is difficult as the carrier is suppressed. However, an exact phase and carrier frequency have to be recovered to track the abruptly changes of phase. A PLL is a typical phase tracker and carrier recovery system which can be used as shown in figure 4.4 to reconstruct the correctly phased carrier as part of the coherent matched detector.

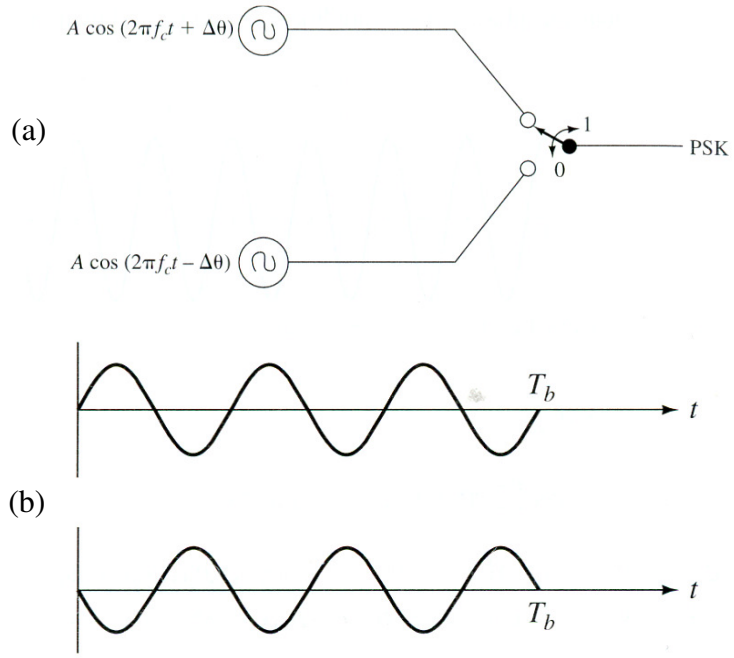

Figure 4.3: (a) BPSK transmitter, (b) BPSK output [33], [68], [69]

Figure 4.4 shows how the received signals deviates the PLL to lock onto the carrier frequency received. The output of the PLL undergoes a 90^o delay prior correlating the reconstructed carrier with the received signals. The output of the correlator undergoes an LPF filter at the baseband information frequency $\frac{1}{T_b}$ to get rid of the carrier frequency components. This can be described mathematically using trigonometric identities [45], [46], [64]:

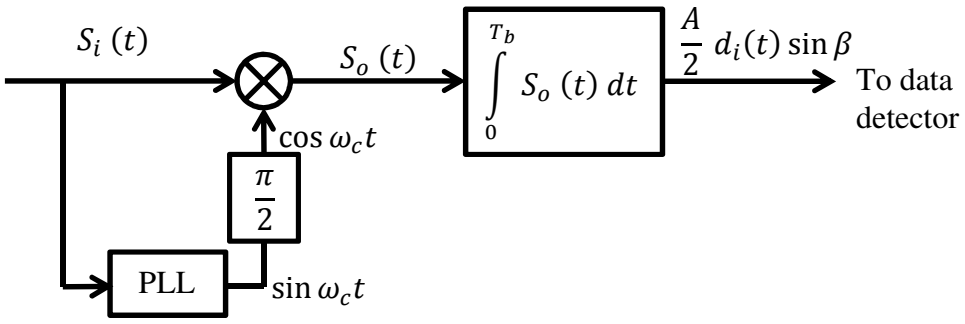

Figure 4.4: BPSK coherent detector using PLL for unsuppressed carrier [33]

Assume unsuppressed carrier, $\beta \neq \frac{\pi}{2}$,

$$S_o(t) = S_i(t) \times \cos(\omega_c t)$$

$$= [A\cos(\beta)\ \sin(\omega_c t) + A\, d_i(t)\sin(\beta)\ \cos(\omega_c t)] \times \cos(\omega_c t)$$

$$= \frac{A}{2}\sin(\omega_c t)\,[\cos(\omega_c t + \beta) + \cos(\omega_c t - \beta)\,] + \frac{Ad_i(t)}{2}\sin(\beta)\,[\cos(2\omega_c t) + 1]$$

$$= \ Carrier\ components + \frac{Ad_i(t)}{2}\sin(\beta)\,[Carrier\ components + 1]$$

So,

$$LPF\ output = \frac{Ad_i(t)}{2}\sin(\beta) \qquad (38)$$

Clearly, the output of the filter is the baseband information for unsuppressed carrier PSK system. But, this is an approximation of the received signals and $d_i(t)$ contains discontinuities that lead to high-frequency components. In fact, the output of the filter is distorted as it is a smoothed version of the baseband data. So, a PLL can be used to reconstruct the carrier in the case of unsuppressed carrier. However, suppressed carrier links require more complex form of carrier recovery where PLL is unable to reconstruct the carrier as the output of the VCO is ideally leading the received signals by 90^o. This can be proven by correlating (36) with PLL output shown in figure 4.4.

So,

$$S_o(t) = S_i(t) \times \cos(\omega_c t)$$

$$= A\, d_i(t)\ \sin(\omega_c t) \times \cos(\omega_c t)$$

$$= \frac{Ad_i(t)}{2}[\sin(2\omega_c t) + \sin(0)]$$

$$= \frac{Ad_i(t)}{2}[Carrier\ components + 0]$$

So,

$$LPF\ output = 0 \qquad (39)$$

This leads to improving the use of PLL in figure 4.4 to implement the Costas loop [33], [68], [69] as shown in figure 4.5. The Costas loop is widely used in carrier recovery and PSK systems [37]-[39], [42], [43]. Costas loops require a *preamble* sequence to lock to the phase of the received signals. The outputs of the upper and lower filters are proportional to the cosine and sine respectively of the phase difference $\Delta\theta$. When the two output terms are multiplied together, the result deviates the VCO operating at the carrier frequency of the transmitter until the VCO and received frequency are matched and locked.

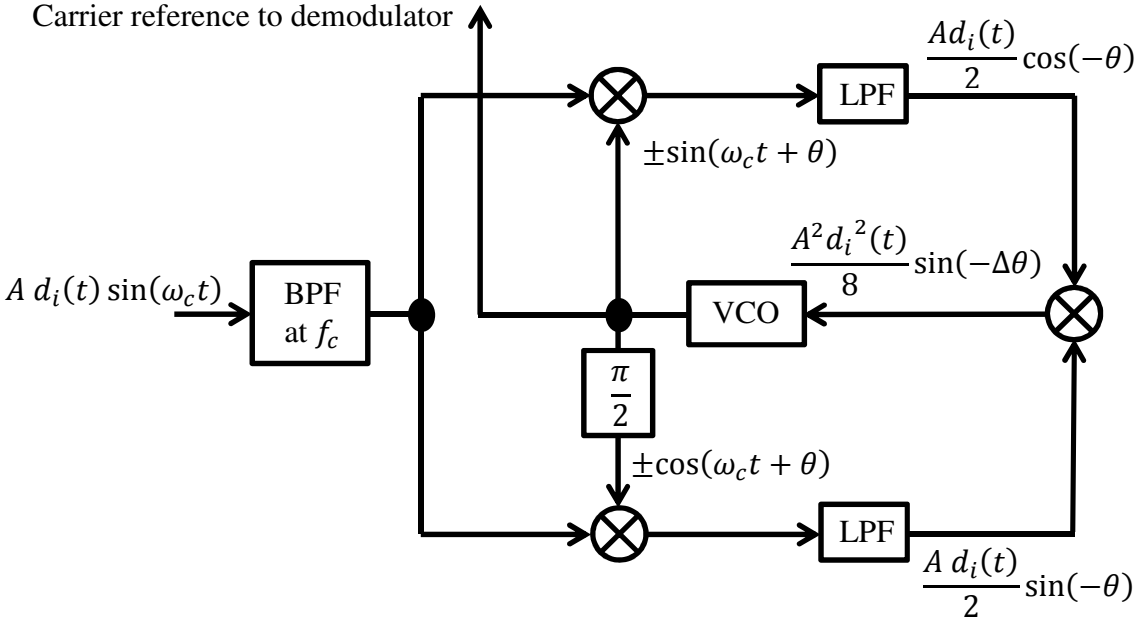

Figure 4.5: Carrier recovery using Costas loop [33]

Mathematically,

$$Upper\ mixer = A\ d_i(t)\sin(\omega_c t)\ \times\ \sin(\omega_c t+\theta)$$

$$= \tfrac{Ad_i(t)}{2}\ [\cos(-\theta)-\cos(2\omega_c t+\theta)\ ]$$

$$LPF = \tfrac{Ad_i(t)}{2}\cos(-\theta) \qquad (40)$$

$$Lower\ mixer = A\ d_i(t)\sin(\omega_c t)\ \times\ \cos(\omega_c t+\theta)$$

$$= \frac{Ad_i(t)}{2} [\sin(2\omega_c t + \theta) + \sin(-\theta)]$$

$$LPF = \frac{Ad_i(t)}{2} \sin(-\theta) \quad (41)$$

$$VCO_{input} = (40) \times (41)$$

$$= \frac{A^2 {d_i}^2(t)}{8} [\sin(-2\theta) - \sin(0)]$$

$$= \frac{A^2 {d_i}^2(t)}{8} \sin(-2\theta) \quad (42)$$

The result in (42) is the phase difference required for the VCO to match the received carrier. If the VCO is locked to the received carrier, the result of one of the filters is 0. Therefore, the result in (42) is then going to be 0, the carrier is then recovered. The Costas loop experiences practical problems such as long time acquisition, possibility of a false lock, a π phase ambiguity due to the squaring loop and requires preamble sequence to aid carrier recovery [33], [68], [69].

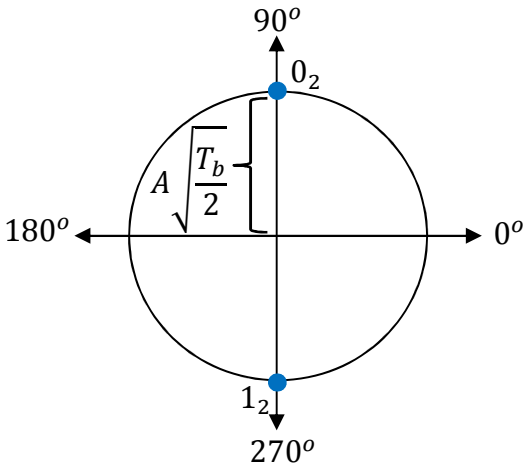

Figure 4.6: BPSK signal space representation [33]

The error performance of any digital communication system is fundamentally related to the distance between points in the signal space diagram [34]. The distance [33], [68], [69] between the two points in figure 4.6, is given by twice the square root of the signal energy per bit period. The distance of the points apart from the origin is useful to calculate the

probability of error using Q-function [33], [68], [69]. This is done using a density function where the most commonly used density function is the Gaussian probability density function [33], [68], [69] shown in equation (43) and sketched in figure 4.7.

$$P(x) = \frac{1}{\sigma\sqrt{2\pi}} e^{\left(\frac{-(x-m)^2}{2\sigma^2}\right)} \tag{43}$$

Where [33], [68], [69],

x,	continuous variable of the function
m,	the mean value of density and symmetry point
σ,	the standard deviation (spread of density)
$(x-m)$	the deviation of x from the mean value

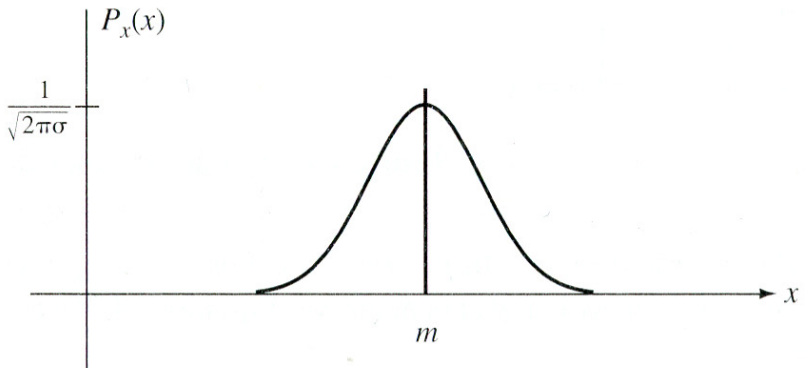

Figure 4.7: Gaussian density distribution [33], [45], [46]

The probabilities within a certain range can be evaluated using closed integral form. However, the closed integral of (43) cannot be evaluated analytically. Therefore, the Gaussian density has been computed and tabulated namely *error function* (*erf*), *complementary error function* (*erfc*) and Q-*function* in Appendix D and G. The *erf*, *erfc* and *Q* functions equations are given in (44), (45) and (46) respectively [33], [68], [69].

$$erf(x) = \frac{2}{\sqrt{\pi}} \int_0^x e^{-u^2}\, du \tag{44}$$

$$erfc\,(x) = \frac{2}{\sqrt{\pi}} \int_x^\infty e^{-u^2}\, du \;=\; 1 - \mathrm{erf}(x) \tag{45}$$

$$Q\,(x) = \frac{1}{\sqrt{2\pi}} \int_x^\infty e^{\frac{-u^2}{2}}\, du \tag{46}$$

Where,

$u = \frac{x-m}{2\sqrt{\sigma}}$, for *erf* and *erfc* functions

$u = \frac{x-m}{\sigma}$, for Q function

So,

$$Q(x) = \frac{1}{2}\left[1 - \mathrm{erf}\left(\frac{x}{\sqrt{2}}\right)\right] = \frac{1}{2}\, erfc\,\left(\frac{x}{\sqrt{2}}\right) \tag{47}$$

The performance of BPSK can be evaluated using the distance of points apart from the origin and the power spectral density N_o of white Gaussian noise [33], [68], [69] that has a mean of $m = 0$, and a variance of $\frac{N_o}{2}$. Although white Gaussian noise is very useful for gaining insight into the underlying behaviour of a system it does not consider the other effects of the phenomena such as fading, frequency selectivity, interference, nonlinearity, etc. However, it is commonly used to simulate the background noise of a link that deflects the transmitted points to evaluate the performance of the link. So, the BPSK link has two points that are symmetrical around the origin which can be defined as (48). Thus, the probability of error can be evaluated using the given parameters and *erf*, *erfc* or Q function:

$x = A\sqrt{\frac{T_b}{2}}$ distance of a point from origin (48)

$\sigma = \sqrt{\frac{N_o}{2}}$ the standard deviation of Gaussian noise (49)

$m = 0$ mean value of Gaussian noise (50)

So,

$$\left(\frac{1}{2}\right)\Pr\{x_1 < m\} + \left(\frac{1}{2}\right)\Pr\{m < x_2\} = \frac{1}{\sqrt{2\pi}} \int_0^{x_1} e^{\frac{(x-m)^2}{2\sigma^2}}\, dx$$

Rewrite using (41),

$$\left(\frac{1}{2}\right)\Pr\{x_1 < m\} + \left(\frac{1}{2}\right)\Pr\{m < x_2\} = \frac{1}{\sqrt{2\pi}} \int_0^{\frac{x_1-m}{\sigma}} e^{\frac{u^2}{2}}\, du$$

$$= Q\left(\frac{x_1-m}{\sigma}\right) \quad (51)$$

$$= Q\left(A\sqrt{\frac{T_b}{N_o}}\right) \quad (52)$$

Hence,

$$P_{e_{BPSK}} = Q\left(A\sqrt{\frac{T_b}{N_o}}\right) = \frac{1}{2}\left[1 - \text{erf}\left(A\sqrt{\frac{T_b}{2N_o}}\right)\right] = \frac{1}{2} erfc\left(A\sqrt{\frac{T_b}{2N_o}}\right) \quad (53)$$

It was discussed that the coherent detector of BPSK requires carrier recovery. Basic forms of coherent detectors are PLL based carrier recovery and Costas loop. It was proved that the Costas loop has the advantage of recovering suppressed carrier over the typical PLL based carrier recovery. Costas loop suffers from practical problems associated with all loops. Alternatively, DPSK is often used to demodulate the BPSK signal. Basically, the DPSK compares the received waveform with a delayed version of itself [33], [68], [69] as shown in figure 4.8. DPSK utilise the coherence of the modulated carrier to observe the changes over one bit interval to the next. This technique does not allow absolute phase determination of the received signal. However, the carrier has to be modulated either differentially so that each change shows logical 1 or the data must be phase locked to the carrier so that the phase changes at multiple periods of the carrier over a bit interval.

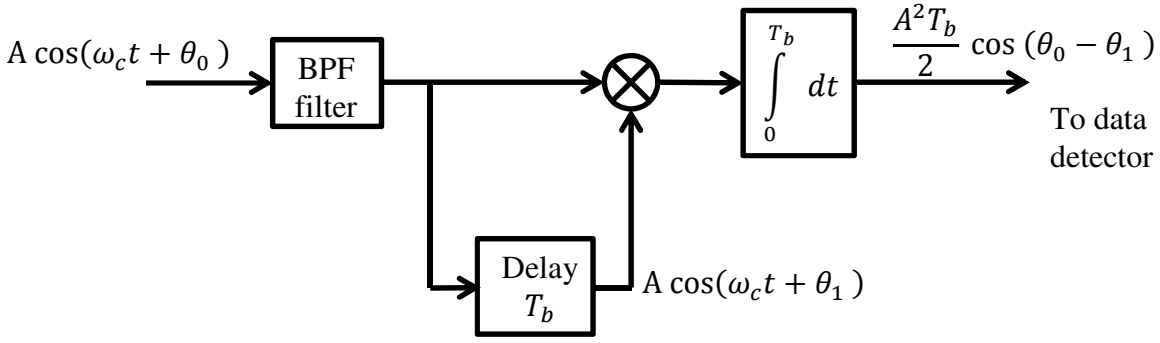

Figure 4.8: BPSK demodulator based on DPSK [33], [68], [69]

Mathematically,

$$Filter\ output = A^2 \int_0^{T_b} \cos(\omega_c t + \theta_0)\ \cos(\omega_c t + \theta_1)\ dt \qquad (54)$$

$$= \frac{A^2}{2} \int_0^{T_b} \cos(2\omega_c t + \theta_0 + \theta_1) + \cos(\theta_0 - \theta_1)\ dt$$

$$\approx \frac{A^2 T_b}{2} \cos(\theta_0 - \theta_1)$$

Referring to figure 4.1, the transmitted phases are 0^o and 180^o to send logical 0 and 1 respectively. Therefore, demodulating a constant phase of 0^o would result in $\frac{A^2 T_b}{2}$ that represents logical 0 and demodulating a constant phase of 180^o would result in $-\frac{A^2 T_b}{2}$ that represents logical 1. The system is said to be a nonlinear detector since the detector multiplies the signal by a delayed version of itself as shown in (54). This follows the ASK non-coherent detector performance. The performance of DPSK detector can be derived using an additive narrowband noise $n_{nb}(t)$ and its delayed version $n_{nb}(t - T_b)$ to the signal as in (55) when a continuous sinusoidal signal is received.

So,

$$Filter\ input = [A\ \cos(\omega_c t) + n_{nb}(t)][A\ \cos(\omega_c t) + n_{nb}(t - T_b)] \qquad (55)$$

The (55) can be expanded using the quadrature components of the narrowband noise:

$$\begin{aligned} Filter\ input = {} & [A\ \cos(\omega_c t) + x(t)\cos(\omega_c t) - y(t)\sin(\omega_c t)] \\ & \times [A\ \cos(\omega_c t) + x(t-T_b)\cos(\omega_c t) - y(t-T_b)\sin(\omega_c t)] \end{aligned}$$

$$\begin{aligned} & = [A + x(t)][A + x(t-T_b)]\, cos^2(\omega_c t) \\ & - [A + x(t)]\, y(t-T_b)\ \cos(\omega_c t)\ \sin(\omega_c t) \\ & - y(t)[A + x(t-T_b)]\ \sin(\omega_c t)\ \cos(\omega_c t) \\ & + y(t)\, y(t-T_b)\ sin^2(\omega_c t) \end{aligned} \qquad (56)$$

$$\begin{aligned} = {} & [A + x(t)][A + x(t-T_b)]\tfrac{1}{2}[\cos(2\omega_c t) + \cos(0)] \\ & - [A + x(t)]\, y(t-T_b)\tfrac{1}{2}[\sin(2\omega_c t) - \sin(0)] \\ & - y(t)[A + x(t-T_b)]\tfrac{1}{2}[\sin(2\omega_c t) + \sin(0)] \\ & + y(t)\, y(t-T_b)\tfrac{1}{2}[\cos(0) - \cos(2\omega_c t)] \end{aligned}$$

Thus,

$$Filter\ output = \tfrac{1}{2}\big([A + x(t)][A + x(t-T_b)] + y(t)\, y(t-T_b)\big) \qquad (57)$$

To simplify the approach, [33] assumed that the interval of two adjacent signals is identical. Therefore, an error bit is received when the output of the filter is negative ($P_e = \Pr\{S_0(T_b) < 0\}$). The analysis in (57) shows two noise components are sampled at two different times. Four different variables were defined by [33] using the average and differences of the noise samples to show the probability density of the filter output.

$$w_1 = A + \frac{x(t)+x(t-T_b)}{2} \quad (58)$$

$$w_2 = \frac{x(t)-x(t-T_b)}{2} \quad (59)$$

$$w_3 = \frac{y(t)+y(t-T_b)}{2} \quad (60)$$

$$w_3 = \frac{y(t)-y(t-T_b)}{2} \quad (61)$$

Each variable is Gaussian distributed where w_1 has a mean of A and the others have a mean of zero [33]. So, the output of the filter can be rewritten as:

$$S_0(t) = ({w_1}^2 + {w_2}^2) - ({w_3}^2 + {w_4}^2) \quad (62)$$

Hence,

$$P_{e_{DPSK}} = \Pr\left\{\sqrt{{w_1}^2 + {w_2}^2} < \sqrt{{w_3}^2 + {w_4}^2}\right\} \quad (63)$$

The square roots were included in $P_{e_{DPSK}}$ to indicate that the first term is Ricean distributed and the second term of $P_{e_{DPSK}}$ is Rayleigh distributed [33], [68], [69]. The Ricean distributed is a square root of the sum of the squares of two quantities. One of them is zero-mean Gaussian distributed and the latter is a result of adding the signal and noise. The Rayleigh distributed is similar to Ricean except that the two quantities in Ricean have zero-mean Gaussian distributed. Therefore, the $P_{e_{DPSK}}$ is similar to ASK non-coherent detector.

$$P_{e_{DPSK}} = \frac{1}{2} e^{\left(-\frac{E}{N_o}\right)} \quad (64)$$

4.1.2 Quadrature PSK

It was discussed and shown in section 2.3.3 and 4.1.1 that BPSK occupies a bandwidth twice the bit rate. It was also discussed that the bit rate can be increased without affecting the bandwidth of BPSK shown in figure 4.2. QPSK is 2 times faster than BPSK without increasing the bandwidth. BPSK sends 1 *bit/symbol* where QPSK sends 2 *bit/symbol* over 2^2 angles separated by 90^o as shown in figure 4.9.

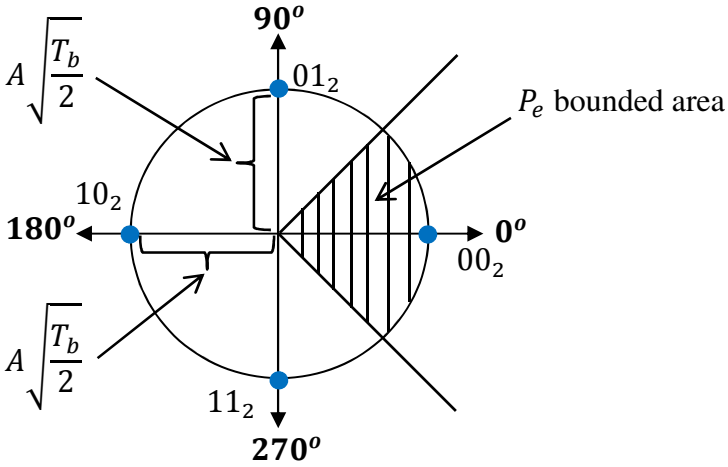

Figure 4.9: QPSK constellation points [33], [34], [68], [69]

The QPSK transmitter is considered as the superposition of two BPSK transmitters [33], [34], [68], [69]. One of them is modulated using the cosine of the carrier and the other is modulated using the sine of the carrier. A demultiplexer splits 2-bit of data stream into an odd and an even part NRZ as shown in table 4.1. The odd part modulates the cosine carrier and the even part modulates the sine carrier at $2T_b$ making the bandwidth equal to that of BPSK.

$x_i(t)$, (2-bit)		NRZ data		Transmitted carrier, $S_i(t)$
ODD	EVEN	a_1	a_2	
0	0	+1	+1	$0.707\cos(\omega_c t + 45^o) + 0.707\sin(\omega_c t + 45^o) = +\cos(\omega_c t) = 0^o$
0	1	+1	-1	$0.707\cos(\omega_c t + 45^o) - 0.707\sin(\omega_c t + 45^o) = +\cos(\omega_c t + 90^o) = 90^o$
1	0	-1	+1	$-0.707\cos(\omega_c t + 45^o) + 0.707\sin(\omega_c t + 45^o) = -\cos(\omega_c t + 90^o) = 270^o$
1	1	-1	-1	$-0.707\cos(\omega_c t + 45^o) - 0.707\sin(\omega_c t + 45^o) = -\cos(\omega_c t) = 180^o$

Table 4.1: Properties of QPSK modulated carrier [33]

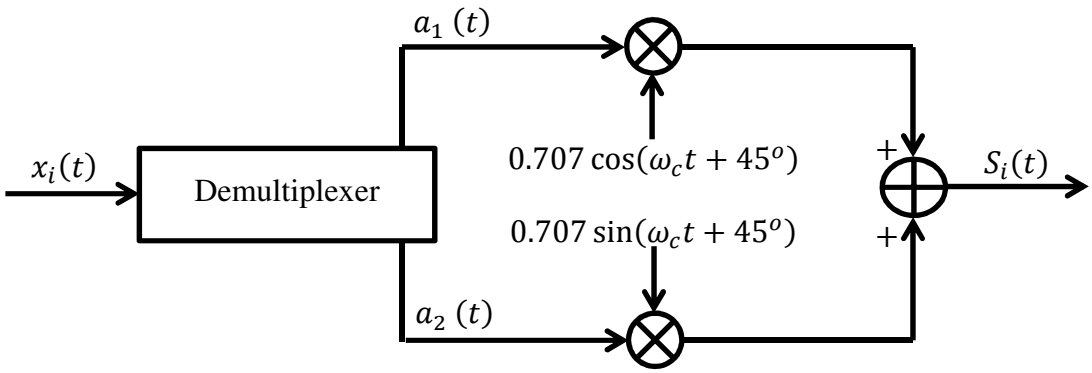

Figure 4.10: QPSK transmitter [33]

Figure 4.10 shows the QPSK transmitter where equation (5) formulates the output of the transmitter. Table 4.1 shows that the transmitted carrier is either shifted by 0^o, 90^o, 180^o or 270^o to represent 2 *bit/symbol*.

It is not surprising that the transmitted power and signal by the QPSK modulator is the same as the power and signal of the BPSK, since QPSK is the superposition of two BPSK transmitters. So, the transmitted signal is said to be suppressed carrier as in (32). QPSK is unlike BPSK in terms of phase detection. The phase of QPSK signals is data dependent [37] therefore the phase detector must produce a signal proportional to the phase difference between the received signal and the recovered carrier [3], [35], [38]-[42], [44]. The QPSK coherent detector is a receiver consisting of four matched filters or correlators. Each correlator is responsible for an angle where it correlates the received signal with a delayed complement phase of that angle. Since two pairs of the transmitted angles are opposite each other, the number of correlators can be reduced to two as shown in figure 4.11 so that each correlator is responsible for two angles that are opposite each other, for example $\pm 90^o$ or $\pm 180^0$. The decision of the received signals is made upon finding the largest magnitude at T_b period and then testing the sign of that output because a negative sign indicates the opposite angle as proven in (54) of the DPSK detector. Thus, the most complex component in the loop is the phase detector [39]. It was discussed in section 4.1.1 and shown mathematically in (39) that a matched filter using the PLL is unable to demodulate the baseband data of a suppressed carrier. Alternatively, the Costas loop (square loop) in figure 4.5 recovers the carrier at 0^o phase difference between the received signal and the VCO output compared to the simple PLL based carrier recovery in figure 4.4.

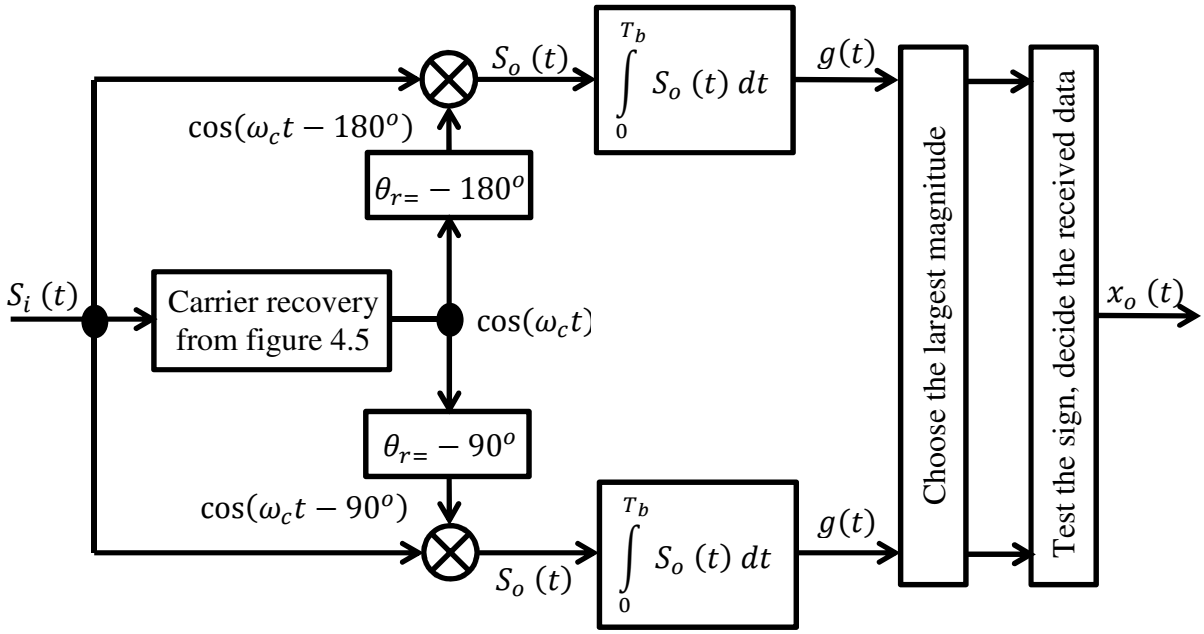

Figure 4.11: QPSK demodulator using Costas loop carrier recovery [33]

Rewriting (36) to represent the transmitted QPSK,

$$S_i(t) = A\ \cos(\omega_c t + \theta_t) \tag{65}$$

Mathematically,

$$S_o(t) = (65) \times\ Recovered\ carrier \tag{66}$$

$$= A\ \cos(\omega_c t + \theta_t)\ \times\ \cos(\omega_c t - \theta_r)$$

$$= \frac{A}{2}\ [\cos(2\omega_c t + \theta_t - \theta_r\ ) +\ \cos(\theta_t + \theta_r\ )]$$

So, the output of the filter is,

$$g(t) = \frac{A}{2} \int_0^{T_b} \cos(2\omega_c t + \theta_t - \theta_r\ ) +\ \cos(\theta_t + \theta_r\ )\ dt$$

$$\approx \frac{AT_b}{2}\ \cos(\theta_t + \theta_r\ ) \tag{67}$$

Using (67), assuming that 270^o being transmitted,

$$Upper\ filter\ \approx \frac{AT_b}{2}\cos(270-180\ )=0 \tag{68}$$

$$Lower\ filter\ \approx \frac{AT_b}{2}\cos(270-90\ )\approx -\frac{AT_b}{2} \tag{69}$$

So, the magnitude output of the upper and lower filters are compared and then the sign is tested prior outputting the received data. Clearly, the matched filter that has a complement phase delay of the transmitted angle results in the absolute amplitude of the received signal having a negative sign indicating that the opposite angle of 90^o is detected i.e. 270^o.

The performance of the coherent QPSK detector can be tested by introducing narrowband noise $n_{nb}(t)$ on the received signal (65) as shown in figure 4.12. The added noise deviates the phase of the transmitted angle by $\Delta\theta_t$. Consequently, the recovered carrier phase (66) suffers from the jitter noise $\Delta\theta_r$ of the VCO caused by the added noise. The effects of the added noise can be described mathematically,

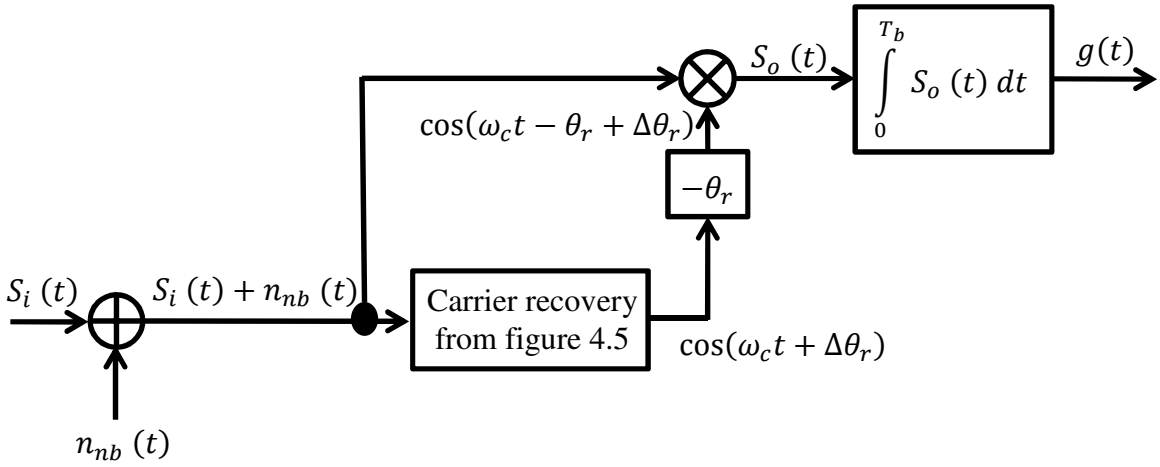

Figure 4.12: Effect of added narrowband noise on matched filter using carrier recovery

So,

$$S_o(t)=\ [A\ \cos(\omega_c t+\theta_t+\Delta\theta_t)+\ n_{nb}(t)][\cos(\omega_c t-\theta_r+\Delta\theta_r)] \tag{70}$$

Expanding (70) using the quadrature components of the narrowband noise:

$$S_o(t) = \begin{bmatrix} A\ \cos(\omega_c t + \theta_t + \Delta\theta_t) + x(t)\cos(\omega_c t + \theta_t + \Delta\theta_t) \\ -y(t)\sin(\omega_c t + \theta_t + \Delta\theta_t) \end{bmatrix}$$

$$\times [\cos(\omega_c t - \theta_r + \Delta\theta_r)\ ]$$

$$= [A + x(t)]\cos(\omega_c t + \theta_t + \Delta\theta_t)\ \cos(\omega_c t - \theta_r + \Delta\theta_r) \quad (71)$$

$$- y(t)\sin(\omega_c t + \theta_t + \Delta\theta_t)\ \cos(\omega_c t - \theta_r + \Delta\theta_r)$$

$$S_o(t) = \frac{[A+x(t)]}{2}[\cos(2\omega_c t + \theta_t - \theta_r + \Delta\theta_t + \Delta\theta_r) + \cos(\theta_t + \theta_r + \Delta\theta_t - \Delta\theta_r)]$$

$$- \frac{y(t)}{2}[\sin(2\omega_c t + \theta_t - \theta_r + \Delta\theta_t + \Delta\theta_r) + \sin(\theta_t + \theta_r + \Delta\theta_t - \Delta\theta_r)]$$

Thus,

$$g(t) = \frac{[A+x(t)]}{2}\cos(\theta_t + \theta_r + \Delta\theta_t - \Delta\theta_r) \quad (72)$$

$$- \frac{y(t)}{2}\sin(\theta_t + \theta_r + \Delta\theta_t - \Delta\theta_r)$$

So, equation (72) shows the output of the matched filter with the added noise. Clearly, the noise deviates the recovered carrier which makes it more likely that the VCO locks to a false quadrant phase. Consequently, the decision maker of the demodulator could mistake the detected angle and hence a bit error would be received. The shaded area in figure 4.9 shows the bounded area of P_e for a particular constellation point.

It was discussed in section 4.1.1 that the error performance of any digital communication system is fundamentally related to the distance between points in the signal space diagram. Clearly, BPSK has the maximum separation between the two constellation points. Figure 4.9

shows that the area between the constellation points in QPSK are relatively smaller than that of the BPSK points as illustrated in the shaded area. The points have the same distance of BPSK points from the origin (48). So, the performance of QPSK can be evaluated using the same distance, standard deviation (49), mean value (50) and Q-function (47) of Gaussian distributed function. QPSK differs from the BPSK as the phases are equally distributed around a circle as shown in figure 4.9 by $\frac{360^o}{M}$ where M is the number of possible symbols. So, a symbol error in QPSK occurs if the detected phase is closer to an incorrect symbol by $\pm\frac{360^o}{2M}$ than to a correct symbol. In fact, the distance between the constellation points in the shaded area in figure 4.9 is complex to estimate due to the angles that are separating them. The authors referenced by [33], [70] have shown a general form of probability of error equation for M-ary PSK links in equation (73).

Equation (73),

$$P_{e_{M-PSK}} = \frac{M-1}{M} - \frac{1}{2}\, erf\left(\sqrt{\frac{A^2T_s}{2N_o}}\,\sin\left(\frac{\pi}{M}\right)\right) - \frac{1}{\sqrt{\pi}}\int_0^{\sqrt{\frac{A^2T_s}{2N_o}}\sin\left(\frac{\pi}{M}\right)} e^{-y^2}\; erf\left(y\,\cot\left(\frac{\pi}{M}\right)\right)$$

Where,

$T_s = T_b \log_2 M$, symbol period

By letting $M = 2$,

$$P_{e_{M-PSK}} = \frac{1}{2}\, erfc\left(\sqrt{\frac{A^2T_s}{2N_o}}\right) = P_{e_{BPSK}}$$

So, for M-ary PSK [33], [34], [68]-[70],

$$P_{e_{M-PSK}} \approx \frac{1}{2}\, erfc\left(\sqrt{\frac{A^2T_s}{2N_o}}\,\sin\left(\frac{\pi}{M}\right)\right) = \frac{1}{2}\, erfc\left(\sqrt{\frac{A^2\,T_b\log_2 M}{2N_o}}\,\sin\left(\frac{\pi}{M}\right)\right) \qquad (74)$$

4.1.3 M-ary PSK

It was shown in section 4.1.2 that the bandwidth of BPSK can be utilised to increase the transmission rate without affecting it using QPSK technique. QPSK is part of M-ary PSK that enhances the transmission rate of BPSK without affecting the bandwidth. QPSK is two times faster than BPSK. This section is concerned with 8-PSK that transmits 3 *bit/symbol* - 3 times faster than BPSK. The phase angles of 8-PSK are equally distributed by 45^o around a circle as shown in figure 4.13.

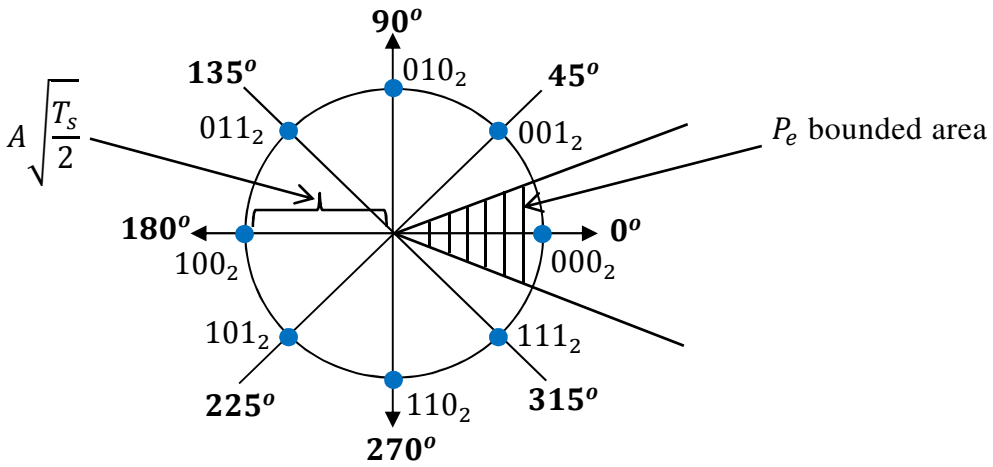

Figure 4.13: 8-PSK constellation points

8-PSK is modulated using a phase mapper with the data source divided in to 3 *bit/symbol*. The symbols are mapped to the phase of the carrier using a 3×8 decoder. The symbols are distributed equally around the circle as shown in figure 4.13 and table 4.2 shows the corresponding angles for each symbol.

3-bit symbol, $x_i(t)$			Mapped phase, θ_t
0	0	0	0^o
0	0	1	45^o
0	1	0	90^o
0	1	1	135^o
1	0	0	180^o
1	0	1	225^o
1	1	0	270^o
1	1	1	315^o

Table 4.2: 8-PSK phase mapper data

Figure 4.14 shows the 8-PSK modulator. The transmitted 8-PSK signal can be represented the same as QPSK in equation (65). The transmitted signal is then a suppressed carrier and the bandwidth is twice the symbol rate as shown in figure 4.2.

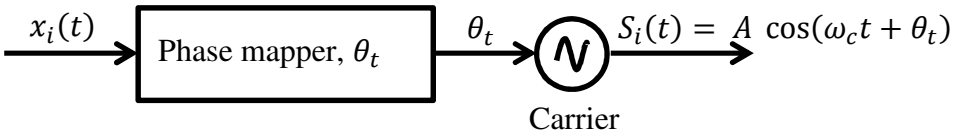

Figure 4.14: 8-PSK modulator

Since the transmitted signal is the same as QPSK, the transmitted power remains the same as BPSK as discussed in section 4.1.1 where half of the power is concentrated in the carrier and

the other half is the modulated phase by the phase mapper. 8-PSK is more complex than QPSK as the symbols are much closer to each other than symbols of the QPSK. Similarly, 8-PSK cannot be demodulated using the PLL based carrier recovery discussed in section 4.1.1 for suppressed carrier. Demodulating 8-PSK can be performed using complex number, Costas loop or digital PLL and 'ATAN' of trigonometric functions.

The complex number approach is similar to the DPSK technique discussed in section 4.1.1. The complex number differs from DPSK in terms of the delayed signal. The DPSK multiplies the received signal by a delay equal to the bit period whereas the complex approach uses a complete full cycle. The delayed sample undergoes a complex conjugate conversion and then multiplied by the received signal [34], [35]. Figure 4.15 shows the 8-PSK demodulator using complex number. The output of the mixer is interpreted through 8 phase slicer before outputting the received symbol.

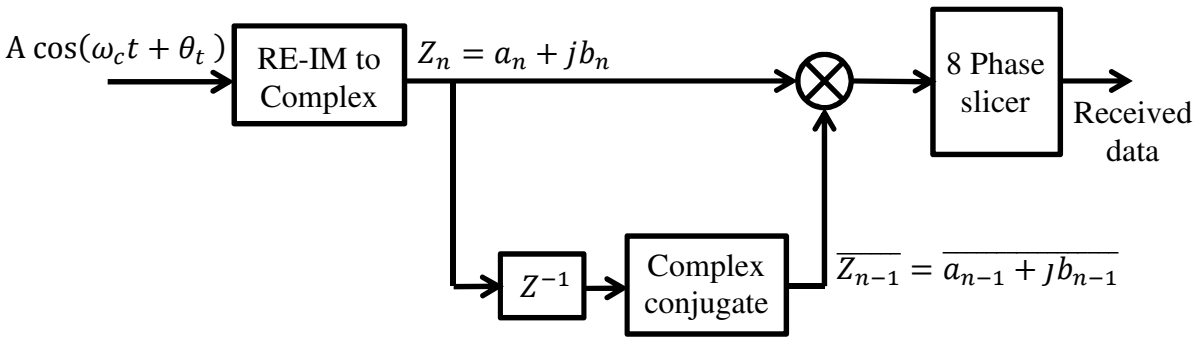

Figure 4.15: 8-PSK demodulator using complex number approach [34]

So, if the received signal changed, in terms of phase, by 90^o from the initial position of 45^o resulting in a phase of 135^o according to the polar form, shown in figure 4.16, then the signal will be 0.7071+ j 0.7071 (45^o) in complex notation before it moves to -0.7071 + j 0.7071 (135^o) by +j (90^o). Then the demodulation of 8-PSK using complex number approach can be proven mathematically with reference to the given information.

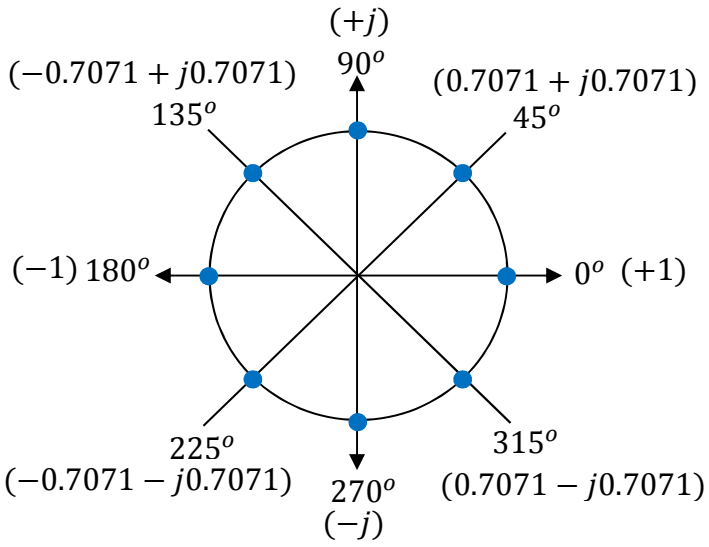

Figure 4.16: Complex notation of the 8-PSK constellation

Mathematically,

$Z_{n-1} = 0.7071 + j\ 0.7071$ Delayed a sample (45^o)

$\overline{Z_{n-1}} = 0.7071 - j\ 0.7071$ Delayed complex conjugate (315^o or -45^o)

$Z_n = -0.7071 + j\ 0.7071$ The new phase (135^o)

Hence,

$\Delta\theta = \angle(Z_n . \overline{Z_{n-1}})$ Phase difference

$= (-0.7071 + j\ 0.7071) \times (0.7071 - j\ 0.7071)$

$= -0.5 + j\ 0.5 + j\ 0.5 - j^2\ 0.5$

$= 0 + j$ The resulting phase is 90^o

The advantage of this technique is that a simple multiplication function is required. However, the system requires Real-Imaginary to Complex conversion which needs to be performed using high specification processor. The sampling frequency has to be a multiple of the *M* carrier frequency to slice the phase angles equally. In addition, the output of the mixer needs to be interpreted through a complex phase slicer circuitry before outputting the received data.

The phase slicer needs system variable LUT (scale) depending on the pk-pk received signals even if an AGC is utilised, hence continual calibration of the system is required.

The coherent QPSK demodulator, shown in figure 4.17, consists of 4 correlators to detect the 8 phase angles. Similarly, each correlator is responsible for two angles that are opposite each other, for example $\pm 45^o$, $\pm 90^o$, $\pm 135^o$ or $\pm 180^o$.

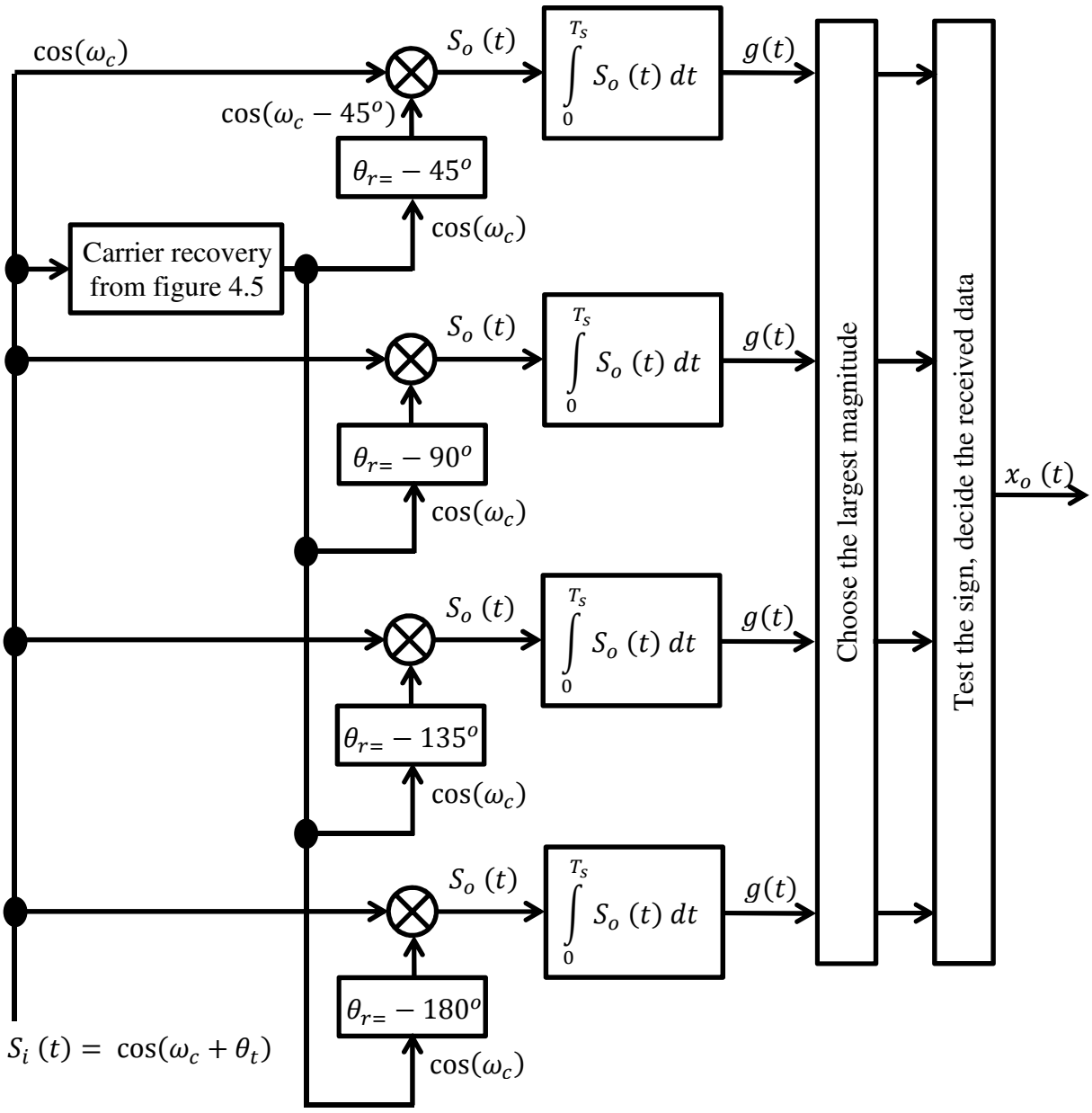

Figure 4.17: 8-PSK demodulator using Costas loop carrier recovery

The magnitude outputs of all filters in figure 4.17 are compared and then the sign is tested prior to outputting the received data at T_s period. A negative sign indicates the opposite angle as shown in (54) and (69). Since the Costas loop is used to demodulate 8-PSK data, the performance of 8-PSK follows the performance of the coherent QPSK detector when narrowband noise $n_{nb}(t)$ is introduced on the received signal as shown in figure 4.12. It was tested mathematically and proven in (72) that the noise deviates the recovered carrier which makes it more likely that the VCO locks to a false quadrant phase, hence a bit error is received.

Recently, researchers are paying attention to solve the synchronisation problem in phase transmission as a result of building a whole communication system. So, it is impractical to advance the demodulator in figure 4.17 to demodulate higher orders of *M-PSK*. The coherent phase detector discussed earlier in this chapter requires phase knowledge which in practice must be estimated. Therefore, the 'ATAN' of the trigonometric function was proposed and is widely used in synchronisation of phase links. The PSK demodulator is to measure the angle between the baseband signal complex envelope and the nearest constellation point using an ATAN computation [39], [43]. This can be done using DSP processors to compute the ATAN function. The FPGAs are a more generic processor that provide DSP functions plus digital design circuitry functions which can be used to implement and test links. The ATAN approach requires complex conversion [39]. The ATAN function is an LUT function and the trade-off point of using FPGA to compute ATAN is the accuracy where high accuracy of ATAN requires high resources of FPGA implementations [39], [43]. The ATAN approach is an advance technique of the Costas loop using DPLL in parallel with ATAN [35], [39], [43] function as shown in figure 4.18 to detect the phase changes instead of the matched filters in

figure 4.17. This technique is very useful for higher *M-PSK* orders and *M-QAM* orders to reduce the resources of FPGA implantations required to implement the matched filters.

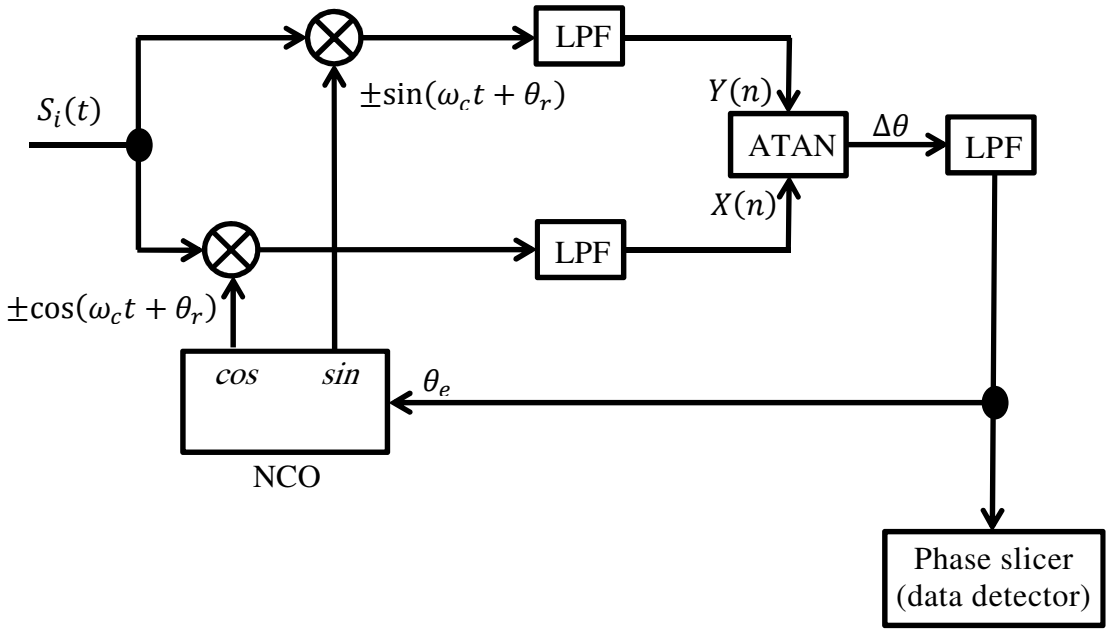

Figure 4.18: Phase demodulator using ATAN function and DPLL [39], [43]

This technique is similar to the complex number approach where the output of the ATAN function needs to be interpreted through an LUT phase slicer before outputting the received data. The DPLL uses a NCO which experiences jitter noise as discussed before in section 4.1.2 when narrowband noise (72) is added to the received signal $S_i(t)$ which cause the received constellation to rotate [34], [69]. Therefore, the output of the ATAN is going to be noisy. The noise can be minimised by using high accuracy ATAN computation [39]. Consequently, high resources of FPGA implementations are required to perform such an operation. Similarly, QAM systems require high accuracy ATAN computation, compensation by using an accurate method of AGC to overcome fading synchronization events or adaptive equalisation is required to phase-different detection [43]. Clearly, higher M-ary PSK orders require high SNR to distinguish phase changes of the transmitted symbols [39].

The P_e of 8-PSK can be estimated using $P_{e_{M-PSK}}$ in (74). Figure 4.13 shows that the area between the constellation points in 8-PSK are relatively smaller than that of the QPSK points as illustrated in the shaded area. The points have the same distance of QPSK points from the origin (48). Similarly, a symbol error in 8-PSK occurs if the detected phase is closer to an incorrect symbol by $\pm\frac{360^o}{2M}$ than to a correct symbol.

Rewriting (74) using Q-function, (48), (49) and (50),

$$P_{e_{M-PSK}} \approx Q\left(\sqrt{\frac{A^2\,T_b \log_2 M}{N_o}}\,\sin\left(\frac{\pi}{M}\right)\right) = \frac{1}{2}\,erfc\left(\sqrt{\frac{A^2\,T_b \log_2 M}{2N_o}}\,\sin\left(\frac{\pi}{M}\right)\right) \quad (75)$$

4.1.4 Performance of PSK communication schemes

The probability of error used to gain an insight into the underlying behaviour of a link is 10^{-5}. The Matlab code in Appendix H was used to evaluate the performance of BPSK, DPSK, QPSK and 8-PSK using equations (53), (63), (74) and (75) respectively. In addition, the performance of Coherent (12) and Non-coherent (13) ASK were computed and compared to the PSK modulation systems as shown in figure 4.19.

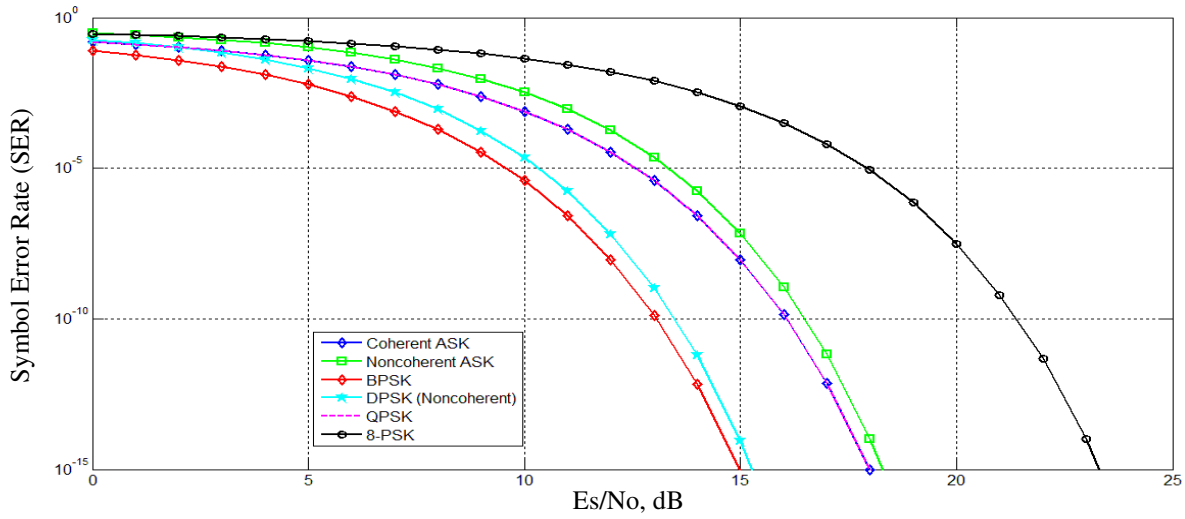

Figure 4.19: Performance of Coherent ASK, Non-Coherent ASK, BPSK, DPSK, QPSK and 8-PSK modulations

The results show that BPSK is the best 1 bit/symbol system at 9.5 dB of SNR among DPSK and ASK systems because they require 10.5 dB and 13 dB respectively to perform as BPSK. QPSK and coherent ASK results are on top of each other in magenta and blue respectively. QPSK is 2 times faster than BPSK and requires an equal trade-off point of SNR power of 12.5 dB to perform as BPSK. 8-PSK is 3 times faster than BPSK but consequently requires an 18 dB. This is because the constellation points of 8-PSK are much closer to each other compared to QPSK which requires more SNR power to be more distinguishable at the receiver side. So, the higher the *M-PSK* is the higher SNR power required to provide the higher performance.

4.2 Implementation of 8-PSK link

4.2.1 Transmitter

The 8-PSK transmitter was designed and implemented using Altera DSP Builder, Matlab-Simulink and Cyclone III FPGA based DSP development board [58]-[62], [71]. The development board provides 14-bit ADC and DAC for analogue interface and an external clock source. The Altera DSP Builder offers MegaCore functions software to parameterize the function that the engineer needs. The NCO MegaCore function wizard allows the engineer to choose the sampling frequency, carrier frequency and amplitude precision plus phase and frequency modulation optionally. An NCO [71] was, with reference to the design shown in figure 4.14, used as a phase modulator of 12-bit precision, generating the carrier frequency 20 Hz with respect to the sampling frequency 16 kHz and an amplitude precision of 12-bit. Chapter 5 uses the 8-PSK modulator, designed in this chapter to implement a 16-QAM modulator. The phase modulator was controlled using phase mapper. The data source was divided into 3 *bit/symbol*. The symbols are mapped to the phase of the carrier using a 3×8 decoder. The symbols are distributed equally around the circle as shown in figure 4.13 and table 4.3 shows the corresponding angles for each symbol and the equivalent code of 12-bit precision. The mapping operation was controlled by a VHDL entity entitled phase_mapper shown in Appendix I.1 and summarised in flowchart 4.1. Theoretically, the phase value is updated every 250 ms by choosing the corresponding phase, accumulate it to the previous phase value and then send it to the phase modulation input of the NCO or otherwise no changes at the input to the NCO. Figure 4.20 shows the transmitter design using Matlab-Simulink and Altera DSP builder functions where NCO and phase_mapper are the key elements of the 8-PSK design shown in figure 4.14.

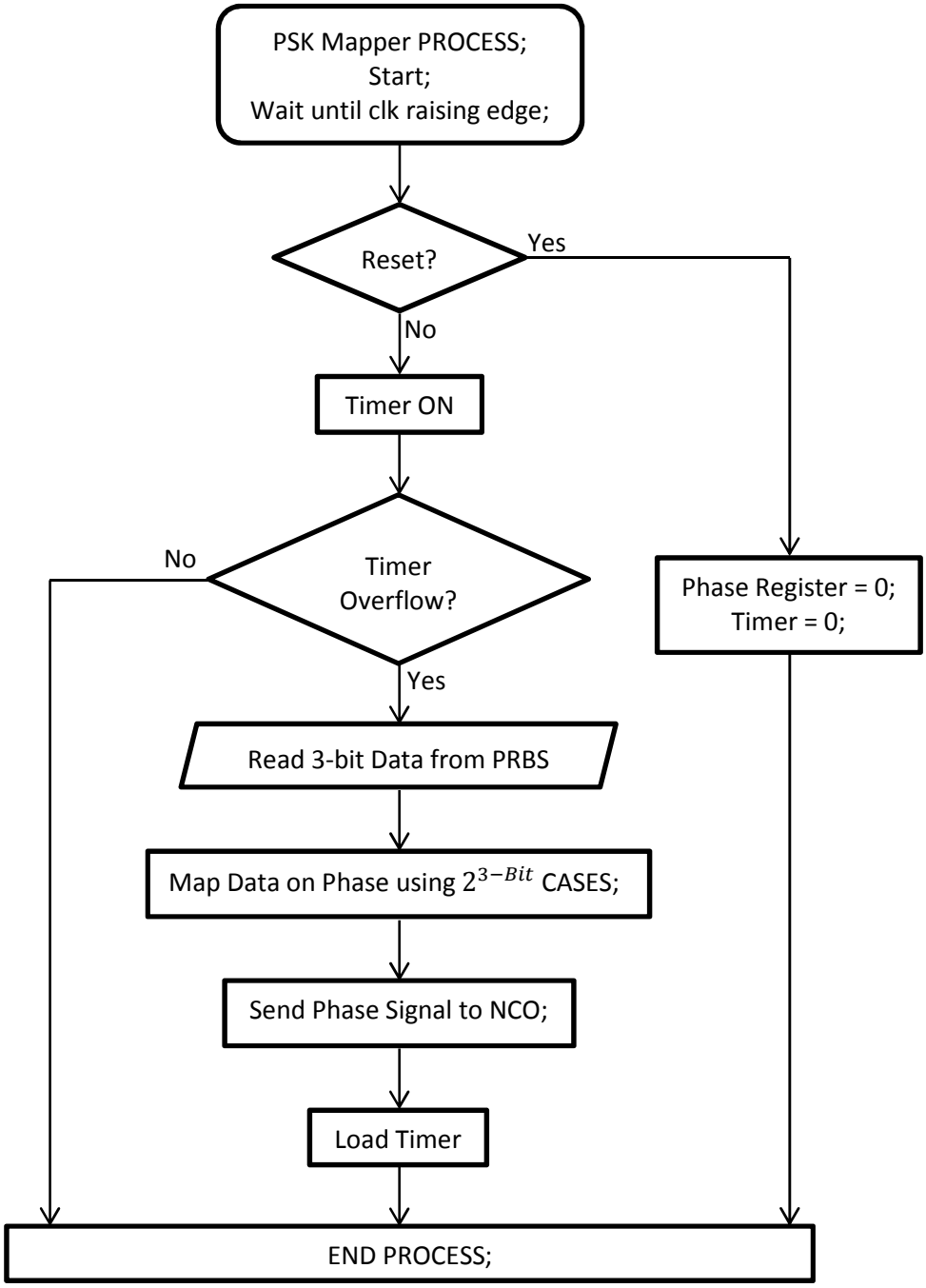

Flowchart 4.1: phase_mapper VHDL process

Data			θ_t	12-bit Equivalent code											
b_n	c_n	d_n		Total	-2048	1024	512	128	64	32	16	8	4	2	1
0	0	0	0^o	0	0	0	0	0	0	0	0	0	0	0	0
0	0	1	45^o	512	0	0	1	0	0	0	0	0	0	0	0
0	1	0	90^o	1024	0	1	0	0	0	0	0	0	0	0	0
0	1	1	135^o	1536	0	1	1	0	0	0	0	0	0	0	0
1	0	0	180^o	-2048	1	0	0	0	0	0	0	0	0	0	0
1	0	1	225^o	-1536	1	0	1	0	0	0	0	0	0	0	0
1	1	0	270^o	-1024	1	1	0	0	0	0	0	0	0	0	0
1	1	1	315^o	-512	1	1	1	0	0	0	0	0	0	0	0

Table 4.3: Binary data and corresponding coded angles

In M-ary PSK, it is most likely that one symbol is mistaken for an adjacent symbol. Gray coding can be used to minimise the bit error. Gray coding numbers are only differing in one bit position. Table 4.4 shows a comparison of corrupted data when symbol has been mistaken for an adjacent symbol. Clearly, Gray code minimise the bit error per symbol by one-third when adjacent phases were detected. Therefore, Gray coding was used to minimise the error rate.

Angle	Direct mapping			Adjacent phase detected (direct)			Gray coded			Adjacent phase detected (Gray)		
0^o	0	0	0	1	1	1	0	0	0	1	0	0
				0	0	1				0	0	1
45^o	0	0	1	0	0	0	0	0	1	0	0	0
				0	1	0				0	1	1
90^o	0	1	0	0	0	1	0	1	1	0	0	1
				0	1	1				0	1	0
135^o	0	1	1	0	1	0	0	1	0	0	1	1
				1	0	0				1	1	0
180^o	1	0	0	0	1	1	1	1	0	0	1	0
				1	0	1				1	1	1
225^o	1	0	1	1	0	0	1	1	1	1	1	0
				1	1	0				1	0	1
270^o	1	1	0	1	0	1	1	0	1	1	1	1
				1	1	1				1	0	0
315^o	1	1	1	1	1	0	1	0	0	1	0	1
				0	0	0				0	0	0

Table 4.4: Comparison of 8-PSK transmission using direct versus Gray code mapping

The design can be tested using the Random Integer Generator source for simulation in Simulink, Pseudo Random Binary Sequence (PRBS) or DIP switches to control the VHDL code on the FPGA chip [58]-[62], [71].

The transmitter design shown in figure 4.20 was simulated using the symbols 000_2 to 111_2 emitted from the source with respect to the constellation points shown in figure 4.13 to prove the phase modulation at 0^o, 45^o.. 315^o. The results are shown in figure 4.21.

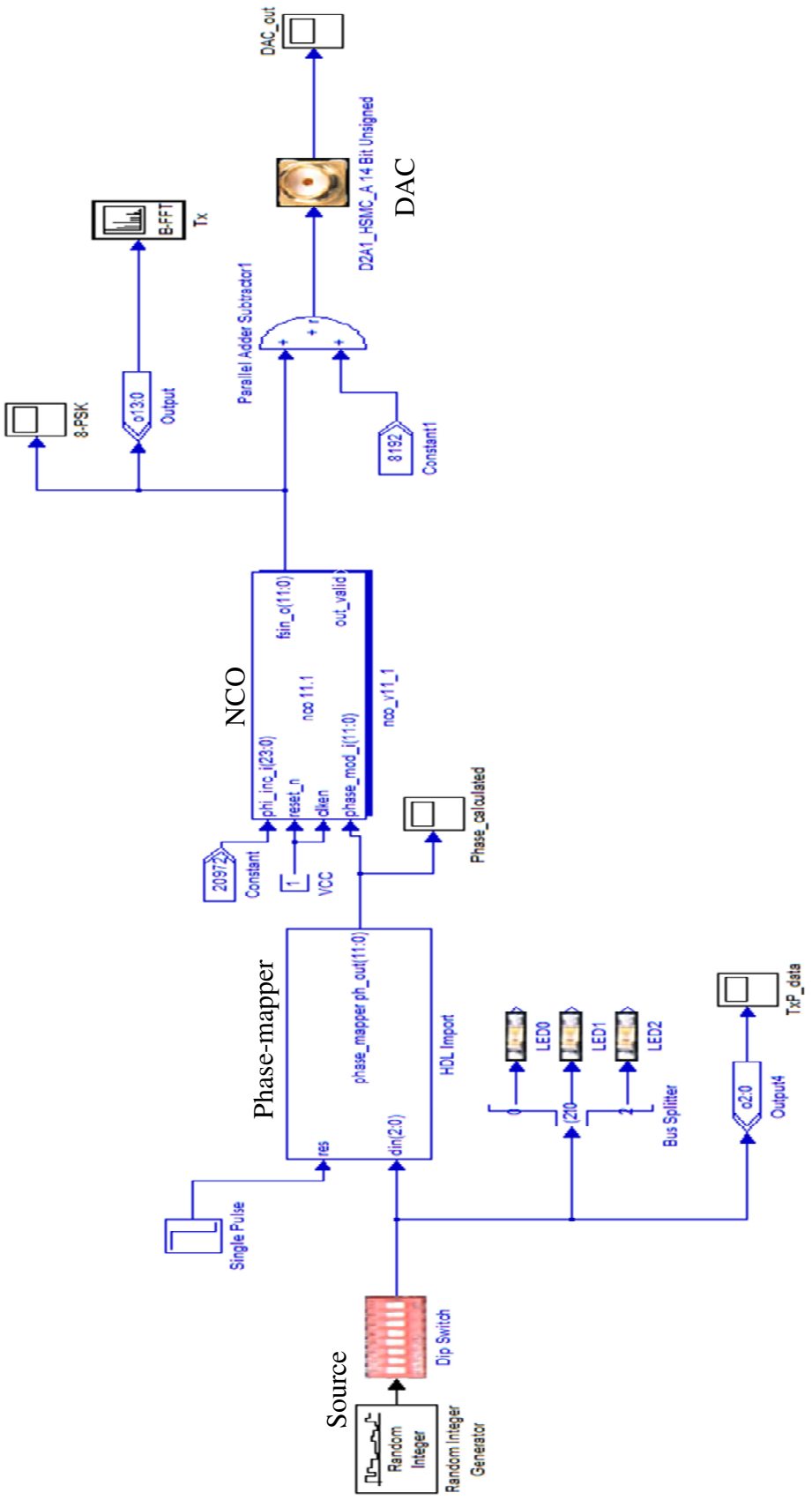

Figure 4.20: 8-PSK transmitter design using Altera DSP Builder and Simulink

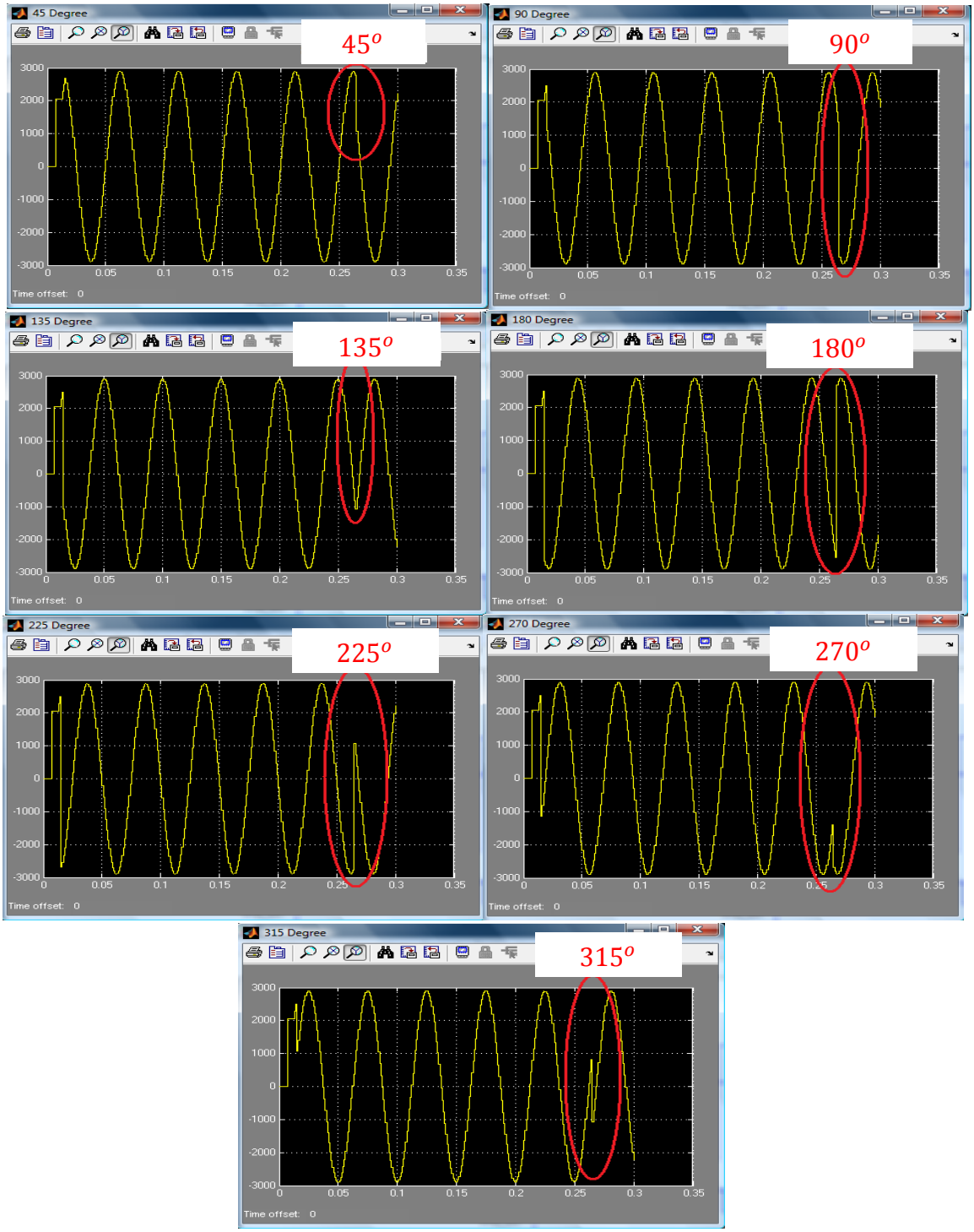

Figure 4.21: Simulink results of the 8-PSK transmitter

The 8-PSK transmitter was fully designed using Altera DSP Builder and downloaded onto the development board from a laptop via a USB cable as shown in figure 4.22. The DAC output was connected to digital oscilloscope and an external sampling clock running at 16 kHz was connected to the development board to drive the whole system.

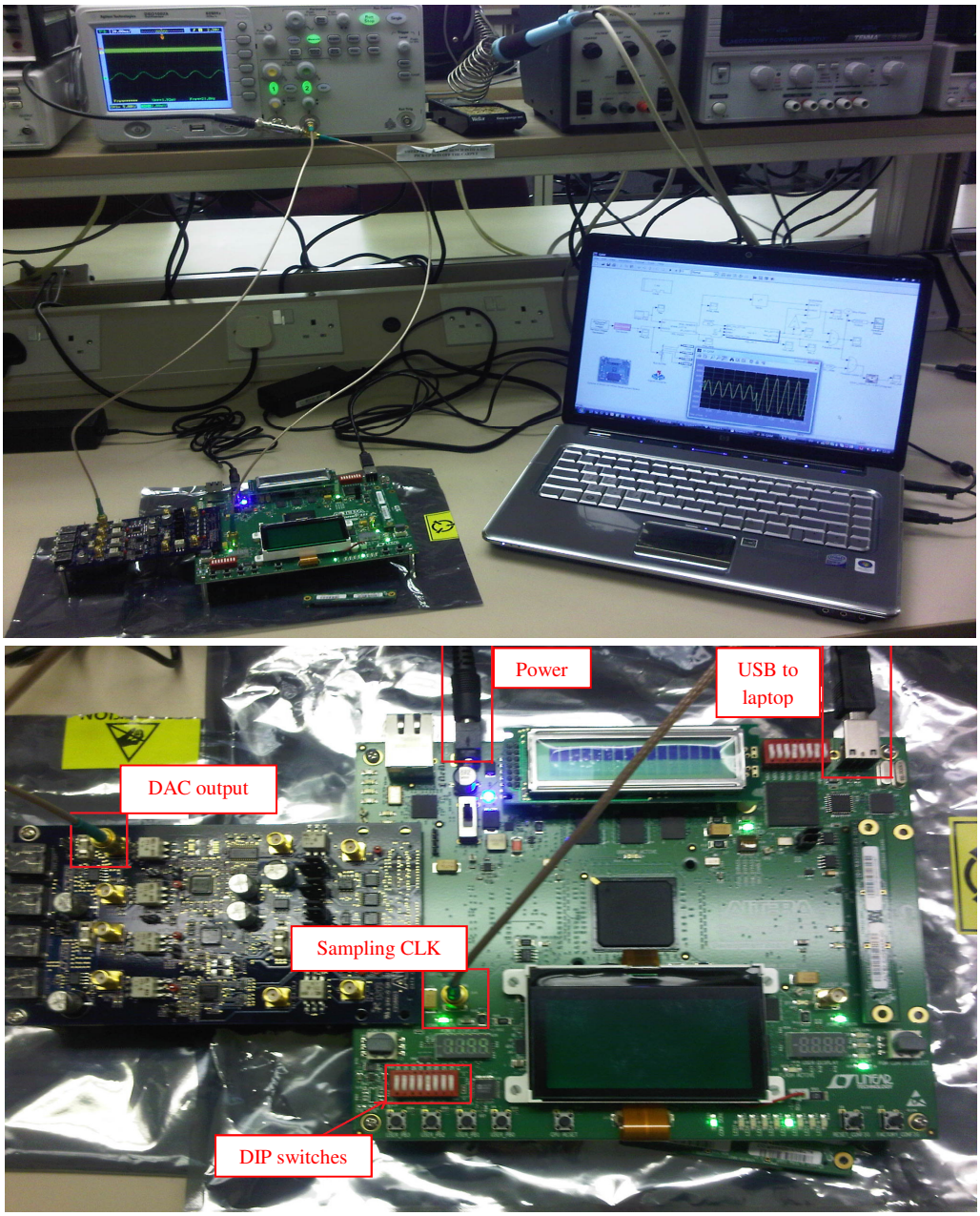

Figure 4.22: Laboratory testing facility of a design on Cyclone III DSP board

Flowchart 4.2 summarises 8-PSK transmitter VHDL processes behaviour.

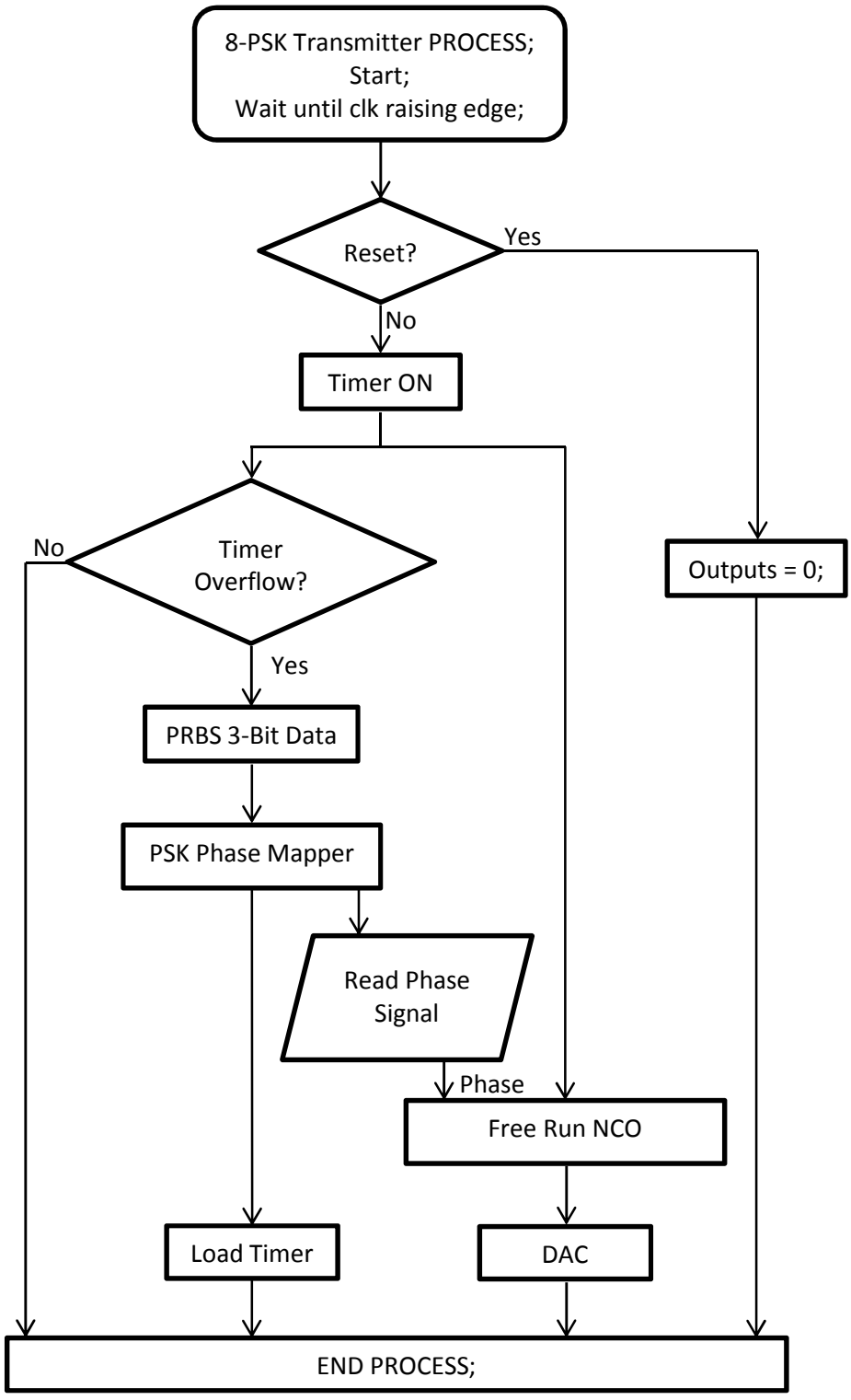

Flowchart 4.2: 8-PSK transmitter VHDL process

It was noticed during the experimentation that the DAC output needs an anti-aliasing linear phase filter to get rid of the sampling frequency components. In addition, the DACs of the development board were not supporting low frequencies such as the carrier frequency used and the output seemed to be attenuated using High Pass Filter (HPF) as shown in figure 4.23 compared to figure 4.24. The DIP switches were used to test the phase shift of each angle individually by selecting the corresponding symbols.

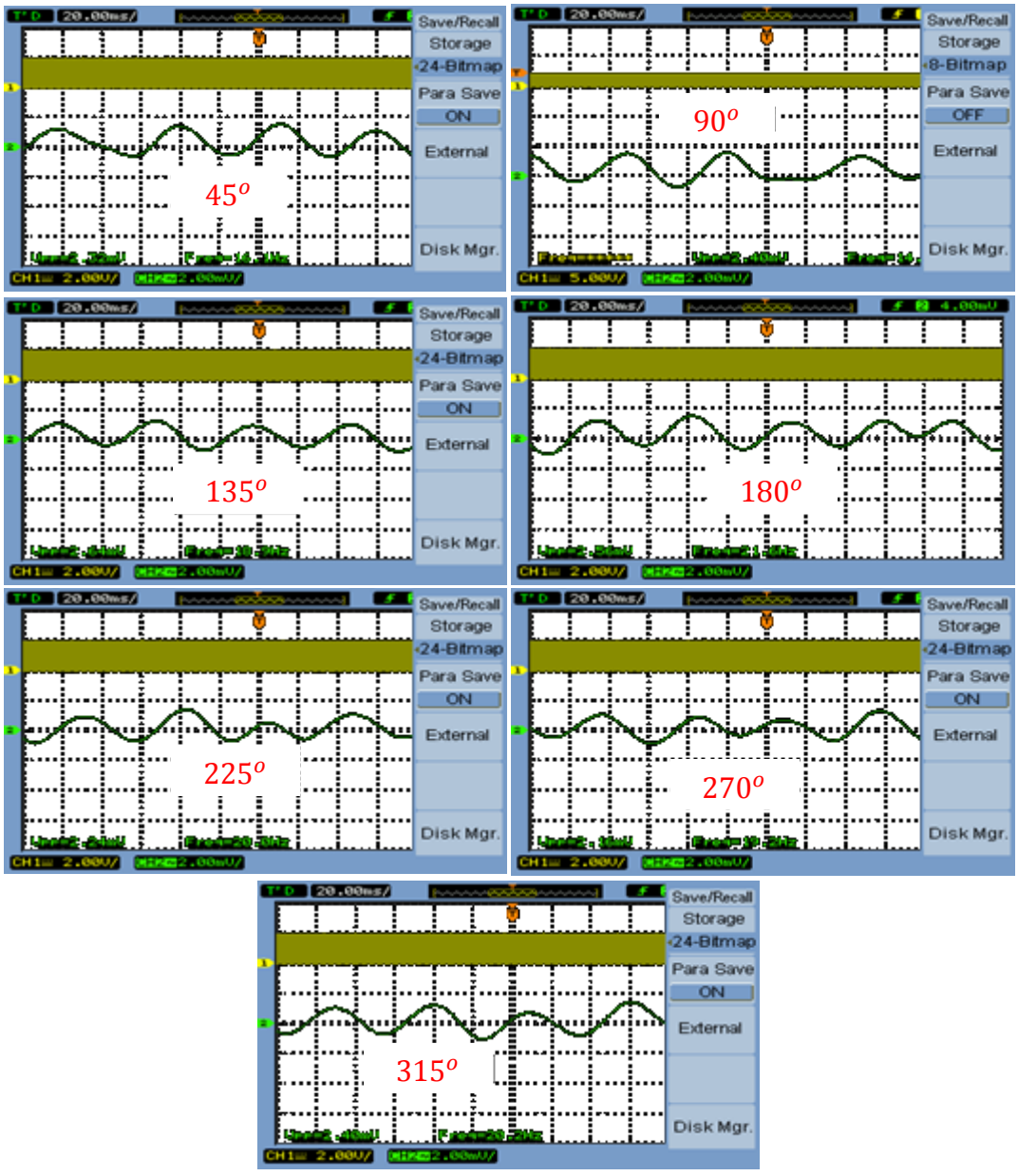

Figure 4.23: Practical results of 8-PSK and the attenuation of the DAC at 20 Hz

Alternatively, the same design was compiled and tested using the internal sampling clock of 50 MHz that generated a carrier frequency of 62.5 kHz. The output of the DAC with high frequencies is much better than that of the low frequencies. Figure 4.24 shows the tested angles using high carrier frequency. The transmitted 8-PSK signal can be represented as (65).

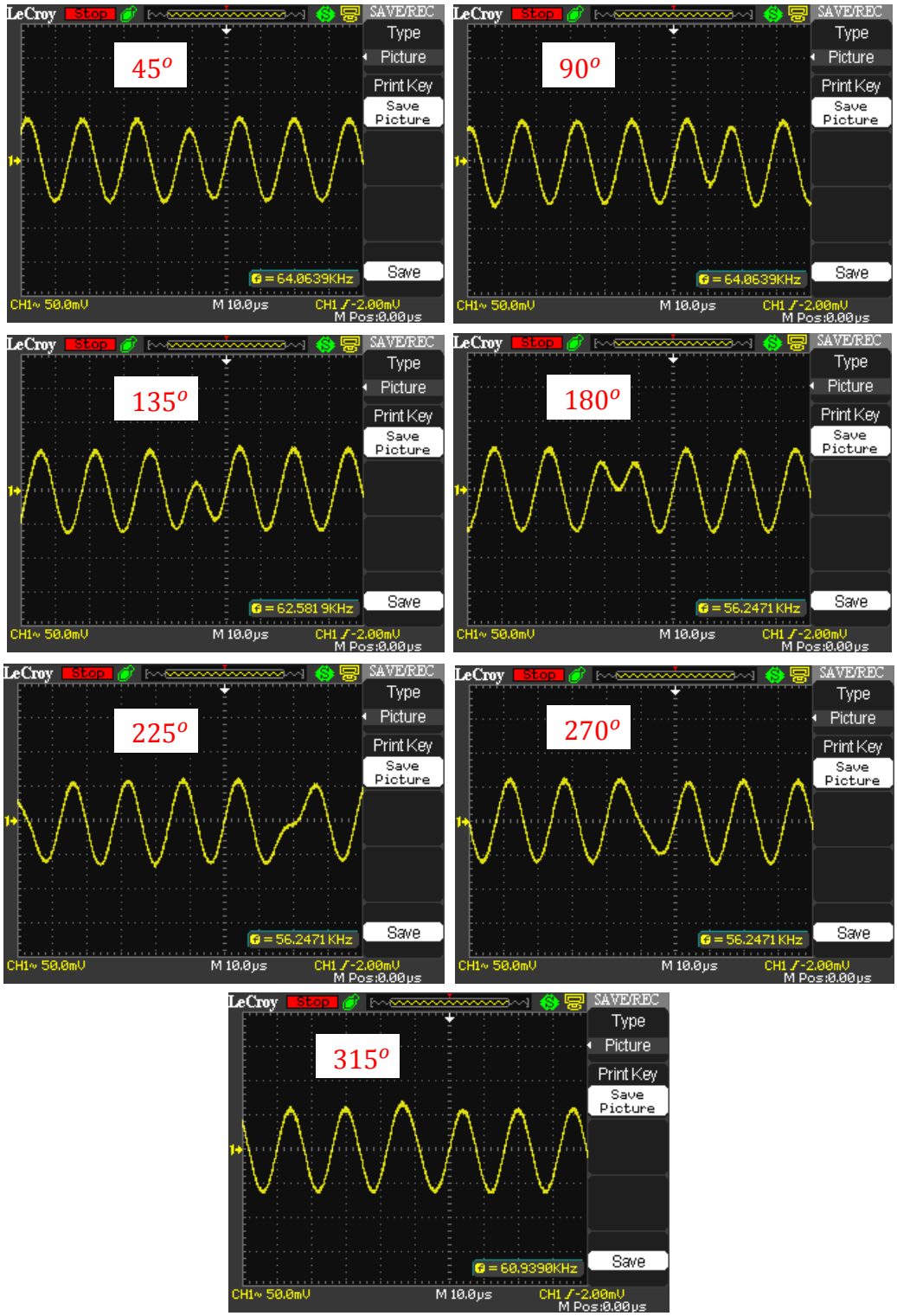

Figure 4.24: Practical results of 8-PSK at 62.5 kHz

4.2.2 Receiver

It was discussed in section 4.1 that demodulating phase data is generally performed using carrier recovery to measure the phase difference between the original and recovered carrier. However, an exact phase and carrier frequency have to be recovered to track the abrupt changes of phase. Basically, the PLL can be used to reconstruct the carrier in the case of unsuppressed carrier links [33] as proven in (39). Moreover, the Costas loop [33], [68], [69] has the advantage of recovering suppressed carrier links over the basic PLL based carrier recovery but experiences practical problems such as long time acquisition, possibility of a false lock and requires preamble sequence to aid carrier recovery. In addition, the DPSK technique does not allow absolute phase determination of the received signal and the data has to be phase locked. Furthermore, the most complex component of the QPSK and 8-PSK receivers is the phase detector because of the signals are data dependent [37], [39] where narrowband noise would deviate the recovered carrier by Costas loop as proven in (72) which makes it more likely that the VCO locks to a false quadrant phase. The complex number [34], [72] technique requires simple multiplication function but also requires a high specification processor to handle complex conversion and calculations. Alternatively, a high accuracy ATAN approach [39], [43] requires higher resources of FPGA implementation or otherwise it follows the performance of the Costas loop when narrowband noise (72) is added to the received signal that cause the received constellation to rotate [34], [69].

Clearly, extracting the carrier is essential in demodulating phase data. This leads to propose a technique that cross correlates the received signals directly without recovering the carrier as discussed earlier in this section. This is similar to the 8-PSK receiver design shown in figure 4.17 but excluding the Costas loop to recover the carrier so that each matched filter is similar to DPSK receiver shown in figure 4.8. This technique is unlike DPSK in utilising the

coherence of cross correlated carrier by the complement transmitted angles to observe the changes over half carrier cycle interval for rapid updates; compared to DPSK that observe the changes over longer intervals. The shorter the time of the cross correlation, the more linear is the system. Otherwise, the cross correlation will follow the performance of DPSK scheme in Ricean and Rayleigh channels. The proposed cross correlation technique optimises the number of implementation resources required to demodulate the PSK data compared to the techniques that use ATAN by omitting carrier recovery circuitry, filters and LUTs to slice the phase data.

The performance of the cross correlation approach can be derived using an additive narrowband noise $n_{nb}(t)$ and its delayed version $n_{nb}(t-\theta_r)$ to the signal as shown in figure 4.25 when a continuous sinusoidal signal is received. The added noise deviates the phase of the transmitted angle by $\Delta\theta_t$. Consequently, the complement angle $(-\theta_r)$ of the cross correlation suffers from the jitter noise $\Delta\theta_r$ caused by the delayed version of $\Delta\theta_t$.

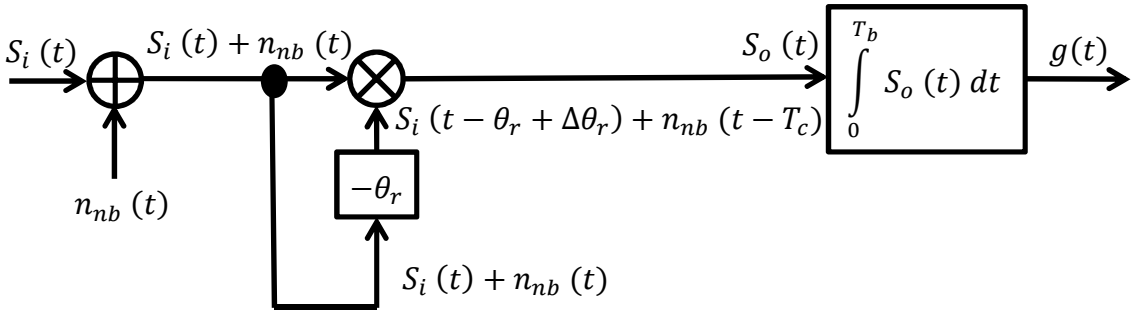

Figure 4.25: Effect of added narrowband noise on cross correlation approach

Mathematically,

$$S_o(t) = [A\ \cos(\omega_c t + \theta_t + \Delta\theta_t) + n_{nb}(t)][A\ \cos(\omega_c t - \theta_r + \Delta\theta_r) + n_{nb}(t - T_c)]$$

Expanding $S_o(t)$ using the quadrature components of the narrowband noise:

$$S_o(t) = \begin{bmatrix} A\ \cos(\omega_c t + \theta_t + \Delta\theta_t) + \ x(t)\cos(\omega_c t + \theta_t + \Delta\theta_t) \\ -y(t)\sin(\omega_c t + \theta_t + \Delta\theta_t) \end{bmatrix}$$

$$\times \begin{bmatrix} A\ \cos(\omega_c t - \theta_r + \Delta\theta_r) + \ x(t - T_c)\cos(\omega_c t - \theta_r + \Delta\theta_r) \\ -y(t - T_c)\sin(\omega_c t - \theta_r + \Delta\theta_r) \end{bmatrix}$$

$$= \ [A + x(t)][A + x(t - T_c)]\cos(\omega_c t + \theta_t + \Delta\theta_t)\ \cos(\omega_c t - \theta_r + \Delta\theta_r)$$

$$- [A + x(t)]\ y(t - T_c)\ \cos(\omega_c t + \theta_t + \Delta\theta_t)\ \sin(\omega_c t - \theta_r + \Delta\theta_r)$$

$$- y(t)[A + x(t - T_c)]\sin(\omega_c t + \theta_t + \Delta\theta_t)\ \cos(\omega_c t - \theta_r + \Delta\theta_r)$$

$$+ y(t)y(t - T_c)\sin(\omega_c t + \theta_t + \Delta\theta_t)\ \sin(\omega_c t - \theta_r + \Delta\theta_r)$$

The $\Delta\theta_r$ is a delayed version of a random phase noise $\Delta\theta_t$ (76). The pre-filtering unit minimises $\Delta\theta_t$ noise. The remaining noise is contaminating the carrier amplitude at higher frequencies that makes fake quadrant lock in carrier recovery systems. Nevertheless, the $\Delta\theta_r$ is cancelled out with $\Delta\theta_t$ when cross correlated using the proposed approach as proven in (77).

$$\Delta\theta_t \approx \ \Delta\theta_r \qquad \text{Delayed version of each other} \qquad (76)$$

$$S_o(t) = \frac{[A+x(t)][A+x(t-T_c)]}{2}[\cos(2\omega_c t + \theta_t - \theta_r + 2\Delta\theta_t) + \cos(\theta_t + \theta_r)]$$

$$- \frac{[A+x(t)]\ y(t-T_c)}{2}\ [\sin(2\omega_c t + \theta_t - \theta_r + 2\Delta\theta_t) - \sin(\theta_t + \theta_r)]$$

$$- \frac{y(t)\ [A+x(t-T_c)]}{2}[\sin(2\omega_c t + \theta_t - \theta_r + 2\Delta\theta_t) + \sin(\theta_t + \theta_r)]$$

$$+ \frac{y(t)\ y(t-T_c)}{2}\ [\cos(\theta_t + \theta_r) - \cos(2\omega_c t + \theta_t - \theta_r + 2\Delta\theta_t)]$$

Thus,

$$g(t) = \frac{[A+x(t)]\,[A+x(t-T_c)] + y(t)\,y(t-T_c)}{2}\cos(\theta_t + \theta_r) \quad (77)$$

$$+ \frac{[A+x(t)]y(t-T_c) - y(t)[A+\,x(t-T_c)]}{2}\sin(\theta_t + \theta_r)$$

When a symbol is phase (θ_t) *transmitted*, the complement angle at the receiver is $(-\theta_t)$,

$$\therefore\ g(t)\ \approx\ \frac{[A+x(t)]\,[A+x(t-T_c)] + y(t)\,y(t-T_c)}{2} \quad (78)$$

Clearly, carrier recovery systems suffer from phase and amplitude noise as proven in (72) where the proposed approach suffers from amplitude noise only as proven in (78). The direct cross correlation results in a guaranteed phase difference in (77). There are $x(t), x(t-T_c)$, $y(t)$ and $y(t-T_c)$ amplitude noise in (77) deflecting and rotating the constellation points away from the origin. However, an AGC and pre-filtering units keep SNR at reasonable level and the highest cross correlated points within the bounded area of the detected angle shown in figure 4.13 over the symbol period.

Therefore, the cross correlation technique does not require a carrier recovery circuitry or LUTs to detect the phase changes, but uses simpler cross correlation detectors. Four detectors are used as shown in figure 4.26 to utilise the coherence of cross correlated carrier by the complement transmitted angles to detect 8 separate phase angles and a timer to update and compare the cross correlated angles every half carrier cycle interval for instant observations. The cross correlated signals are separated into 2 parts and then the absolute value of both parts are obtained with the highest absolute value identifying the received data phase angle. This removes the need of LPFs, which is used to extract the carrier components.

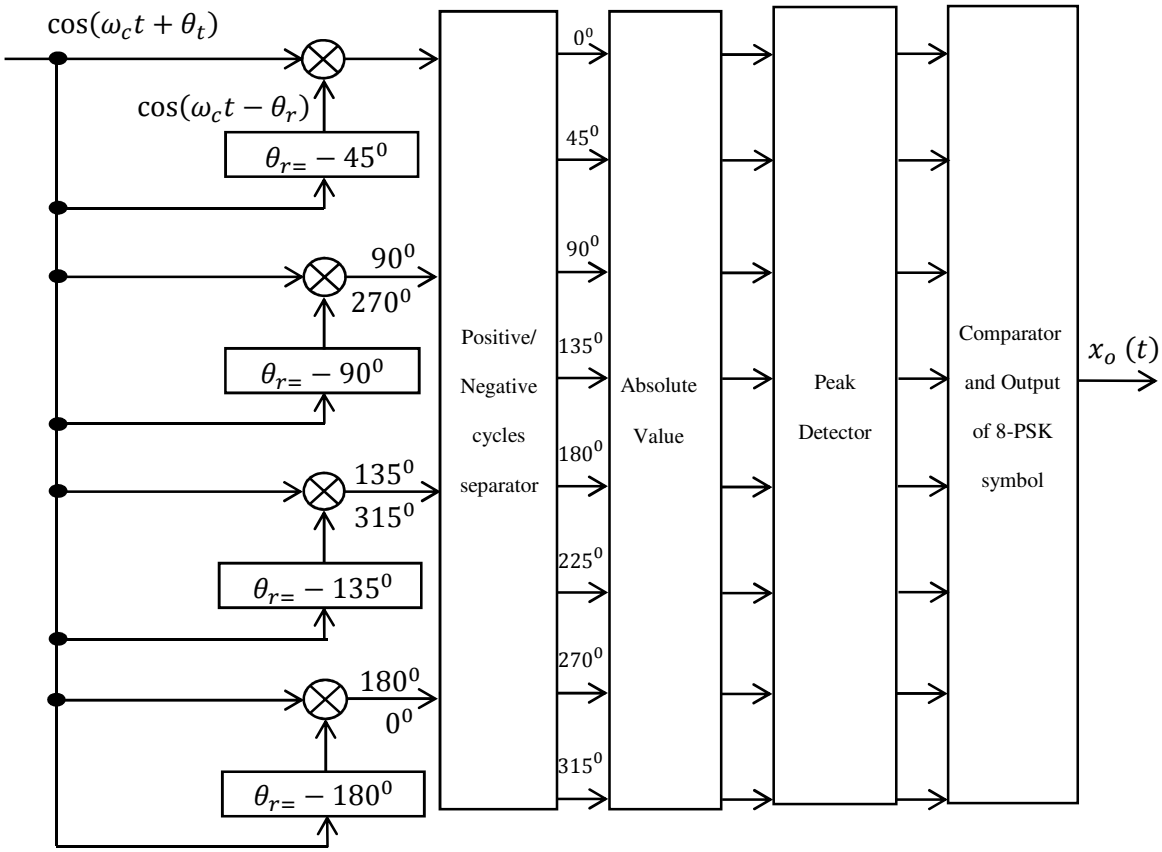

Figure 4.26: 8-PSK receiver design using cross correlation

The cross correlation technique has many advantages compared with other techniques where the results of the detectors are directly compared to determine the phase difference. No carrier recovery, DPLL, ATAN function nor LPFs are required, which saves on circuit resources. Furthermore, it is less complex compared to systems which use the 'tan' function and complex numbers. The disadvantage of cross correlation is that multiple multiplier blocks are required. Moreover, pre-filtering and AGC are essential for all telecommunication techniques.

Figure 4.27 reflects the 8-PSK receiver design shown in figure 4.2 and summarised in flowchart 4.3. The 8-PSK receiver was designed and implemented using Altera DSP Builder, Matlab-Simulink and Cyclone III FPGA based DSP development board [58]-[62], [71]. The

development board provides 14-bit ADC maximum 512 mVp-p. The digitised signal undergoes cross correlation, positive/negative separation, updating the highest cross correlated points and finally comparison of cross correlated signals.

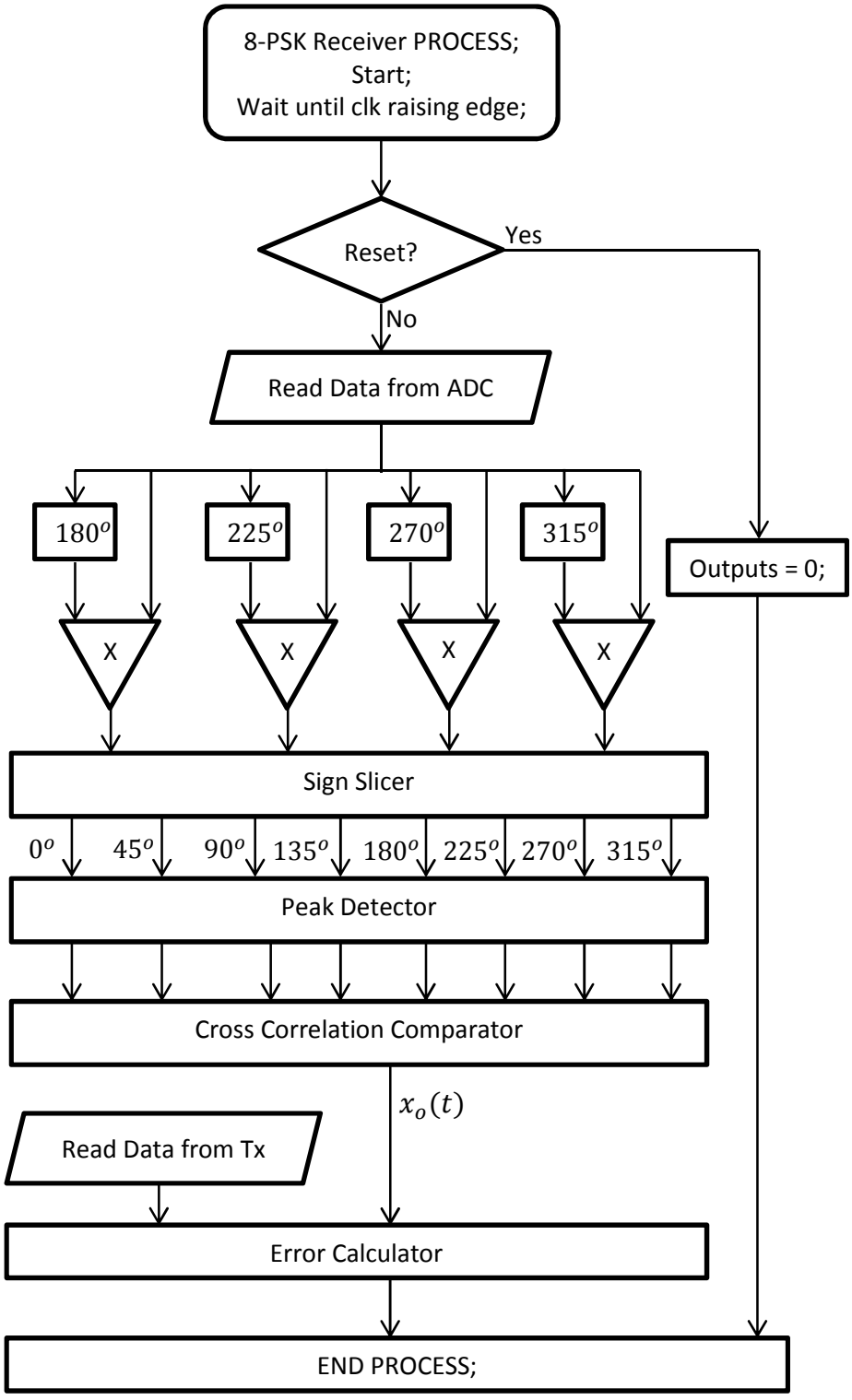

Flowchart 4.3: 8-PSK receiver VHDL process using cross correlation

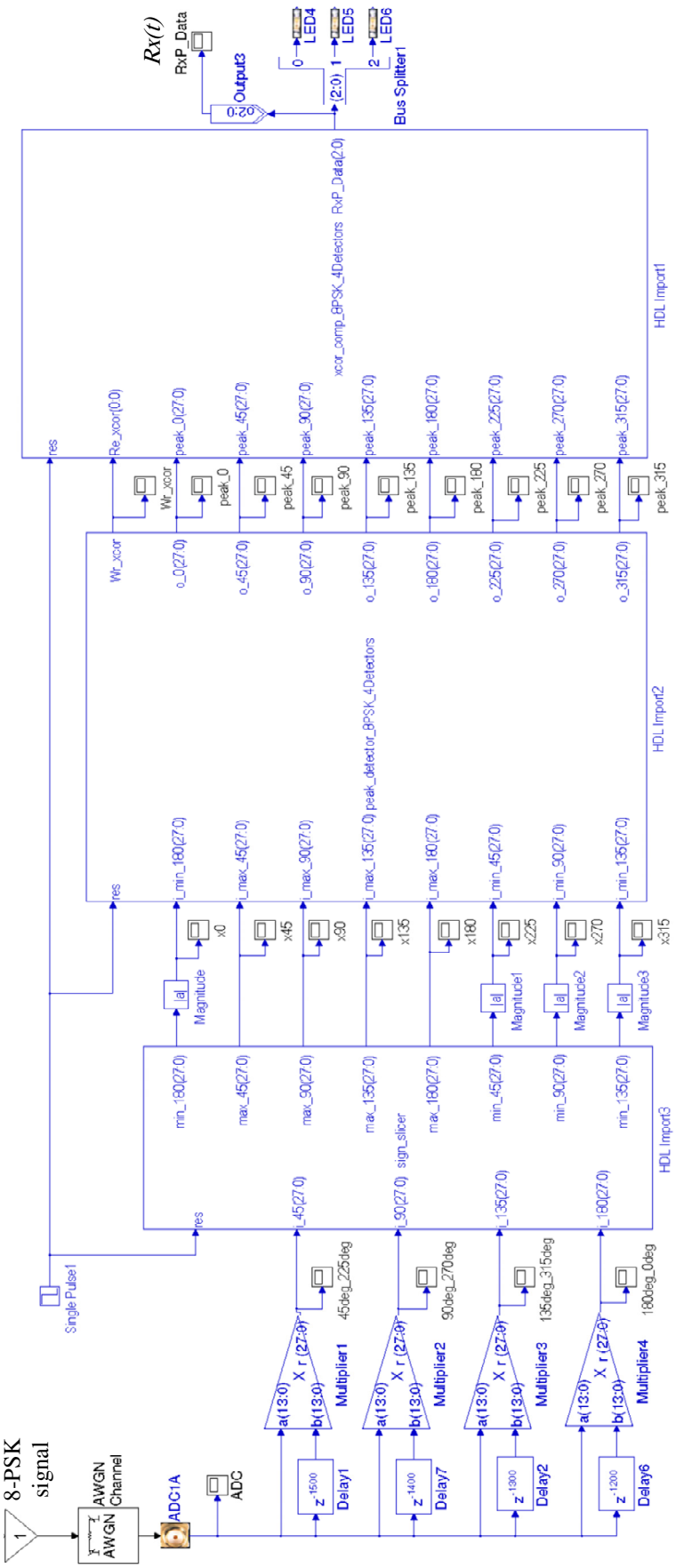

Figure 4.27: Matlab-Simulink and Altera-DSP Builder Implementation of 8-PSK receiver using cross-correlation approach

The 8-PSK receiver design is sampled at 16 kHz for simulation in Matlab and 50 MHz for practical experimentations. Therefore, the samples of a complete cycle of 20 Hz are 800. The 8 angles are sampled equally and separated by 100 samples. Table 4.5 shows the angles, their associated samples and complementary samples.

Angle (Degree)	Samples	Complementary samples
0^o	0	800
45^o	100	700
90^o	200	600
135^o	300	500
180^o	400	400
225^o	500	300
270^o	600	200
315^o	700	100

Table 4.5: Angles, samples and complement samples

Figure 4.28 shows an example of the four cross correlation detectors shown in figure 4.27 which is the 45^o where the received signal is directly cross correlated with the complemented angle. It can be noticed that the complement angle is 700 samples but an extra 800 samples were added to allow enough time for the highest cross correlated point to be detected as what the practical examination showed in the presence of noise.

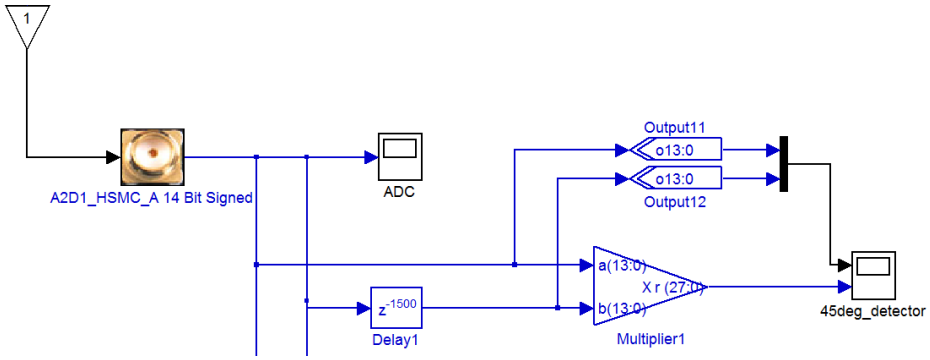

Figure 4.28: The correlator of 45^o angle

The top trace in figure 4.29 shows the 2 inputs to the detector of figure 4.28 which is the received signal (yellow) and the complement angle of 45^o (magenta) that lags the received signal. The bottom trace of figure 4.29 shows the cross correlated version of the received signal (yellow) and its delayed version by the complement angle of 45^o (magenta).

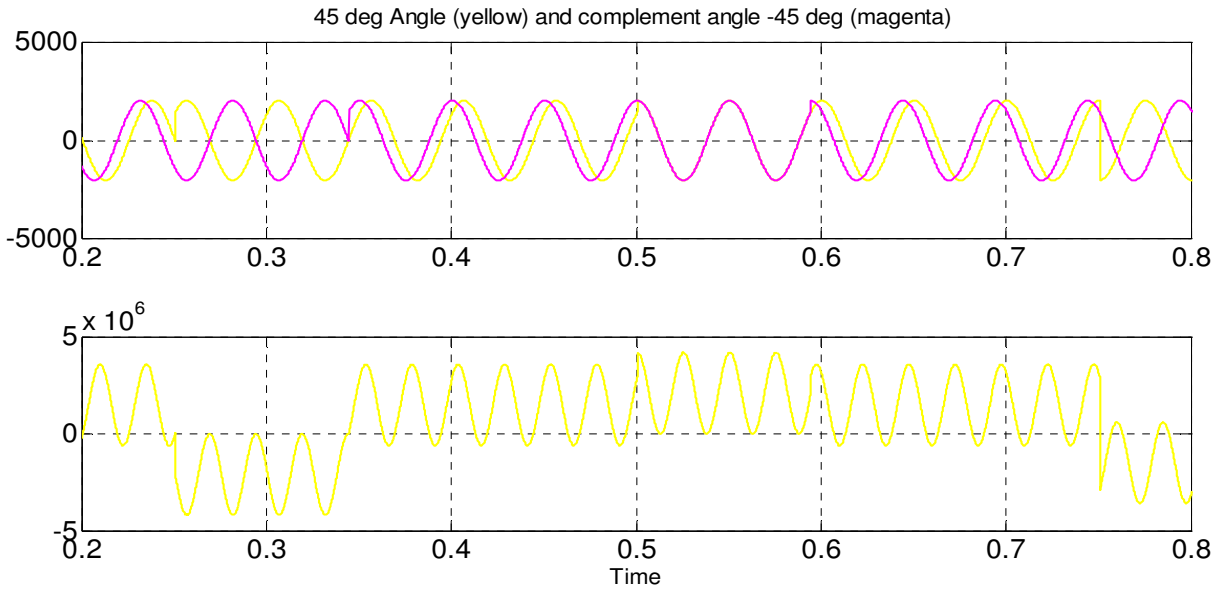

Figure 4.29: The input and output of the 45^o angle detector

The 8-PSK transmitter keyed the angles 225^o and 45^o at 0.25s and 0.5s respectively. It can be seen in the top trace of figure 4.29 that there are phase transitions as per the transmitted angles. In addition, the lowest cross correlated points are located at 0.25s when the received

signals are 180^o out of phase with the complement angle and it can be noticed that the highest cross correlated points are located at 0.5s when the received signals are in-phase with the complement angle.

Lowest= $\cos(\omega_c t + 225^o)\cos(\omega_c t + 315^o)$

$$= \frac{1}{2}[\cos(2\omega_c t) + \cos(180^o)]$$

$$= \frac{1}{2}[\cos(2\omega_c t) - 1]$$

Highest= $\cos(\omega_c t + 45^o)\cos(\omega_c t + 315^o)$

$$= \frac{1}{2}[\cos(2\omega_c t) + \cos(0^o)]$$

$$= \frac{1}{2}[\cos(2\omega_c t) + 1]$$

It can be concluded that each cross correlation detector results in antipodal points when the corresponding angles are detected or otherwise the cross correlated points are below the level of 0^o indicating no data transmission. However, the output of each detector can be separated into two halves; positive and negative using sign_slicer.vhd code shown in Appendix I.2 and summarised in flowchart 4.4.

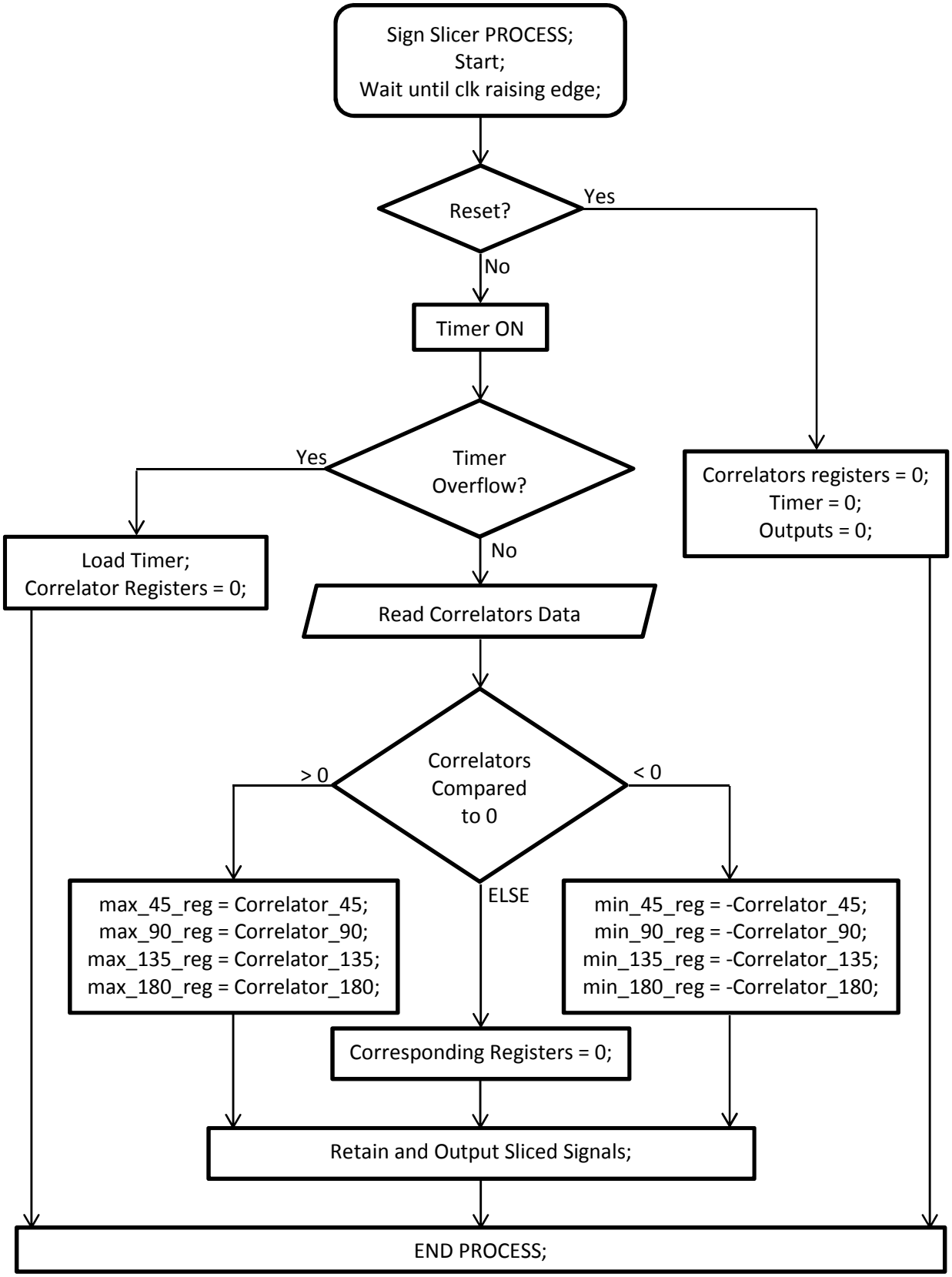

Flowchart 4.4: sign_slicer VHDL process

The positive part indicates the detected in-phase angle and the negative part indicates the detected 180^o out of phase which is 45^o and 225^o respectively in this example. The absolute value of the negative part is to be taken as shown in figure 4.30 using Magnitude function. Therefore, the output of the sign_slicer.vhd code separates the signals of 4 detectors to 8 angles.

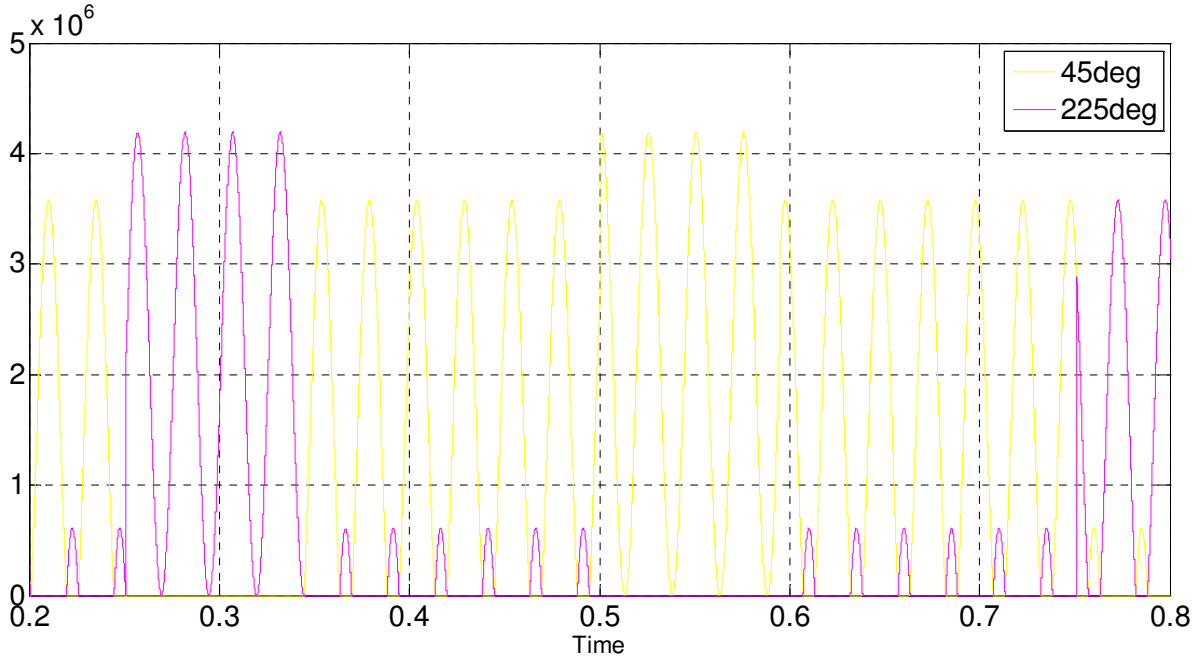

Figure 4.30: Cross correlated signals are separated; 45^o (yellow) and 225^o (magenta)

Figure 4.31 shows the cross correlated signals of the 4 detectors where the absolute value of the negative parts were taken. The correlated signals show that the time taken to reach the highest peaks is equal to the half time of twice the carrier frequency which is 12.5 ms (200 samples).

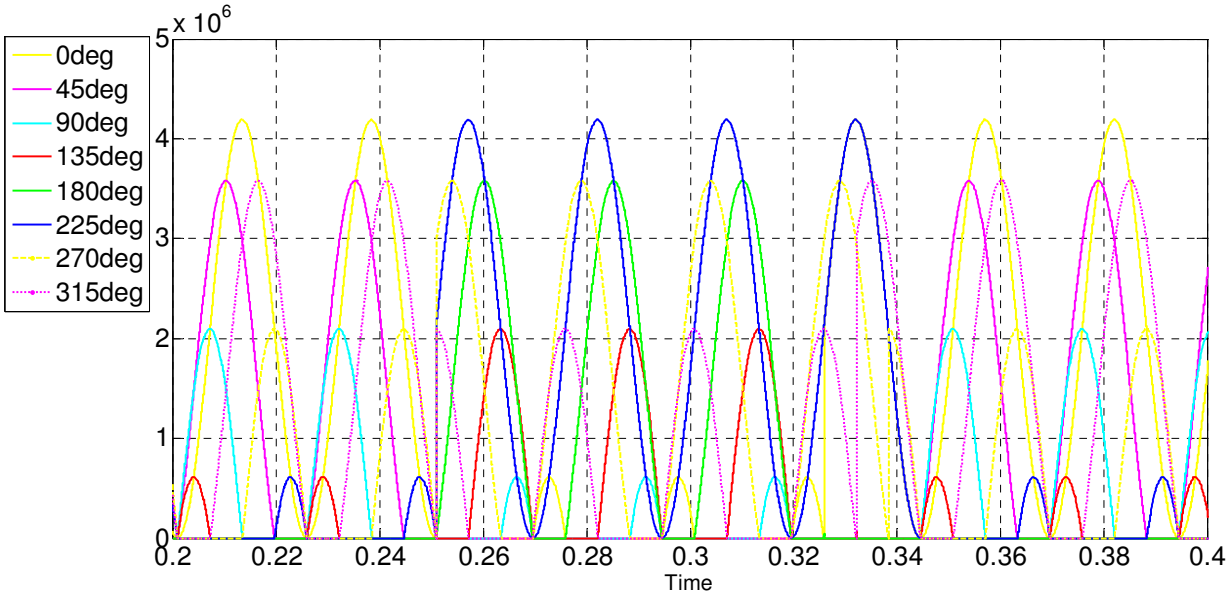

Figure 4.31: Correlated - Separated, 0^o (yellow), 45^o (magenta), 90^o (cyan), 135^o (Red), 180^o (Green), 225^o (Blue), 270^o (yellow), 315^o (magenta)

A peak detector was designed using peak_detector_8PSK_4Detectors.vhd code shown in Appendix I.3 and summarised in flowchart 4.5 to detect the highest peaks of the correlated signals shown in figure 4.31. Simulation experimentations showed that it is best to output the detected peaks every $\frac{3}{8}$ the carrier cycle time (300 samples) which is $\frac{3}{4}$ the correlated signals (18.75 mS) but practical experimentations showed 500 samples due to phase response of the filter preceding the ADC input.

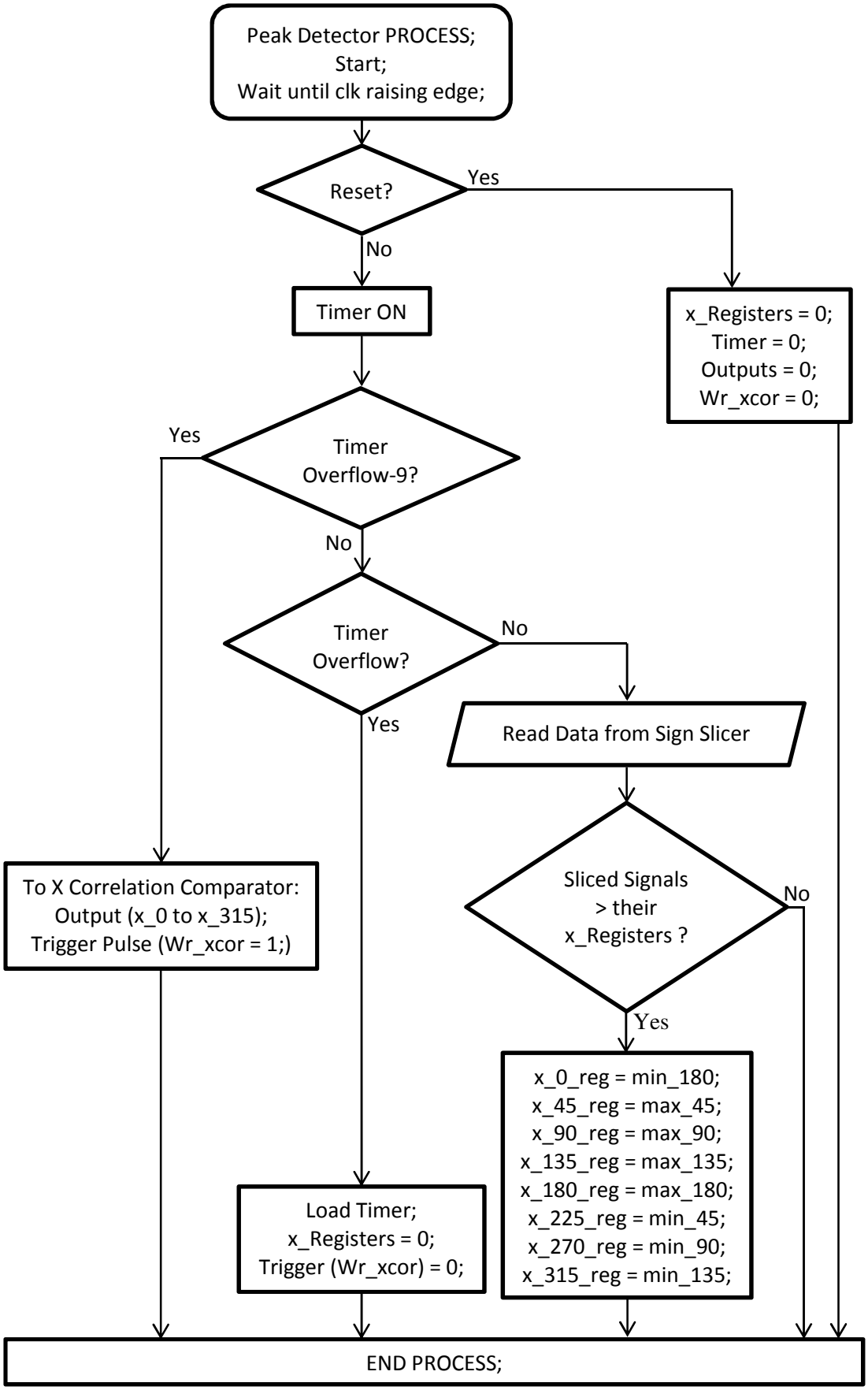

Flowchart 4.5: peak_detector VHDL process

The peaks were detected only if the input is greater than the registered previous value. At the same, a timer within peak_detector_8PSK_4Detectors.vhd counts down and eventually outputs the updated peaks when it overflows as shown in figure 4.32. *The detected peaks were slightly delayed by the author in figure 4.32 to better explain the idea but practically there should be no delay for direct comparison of angles and data outputting.*

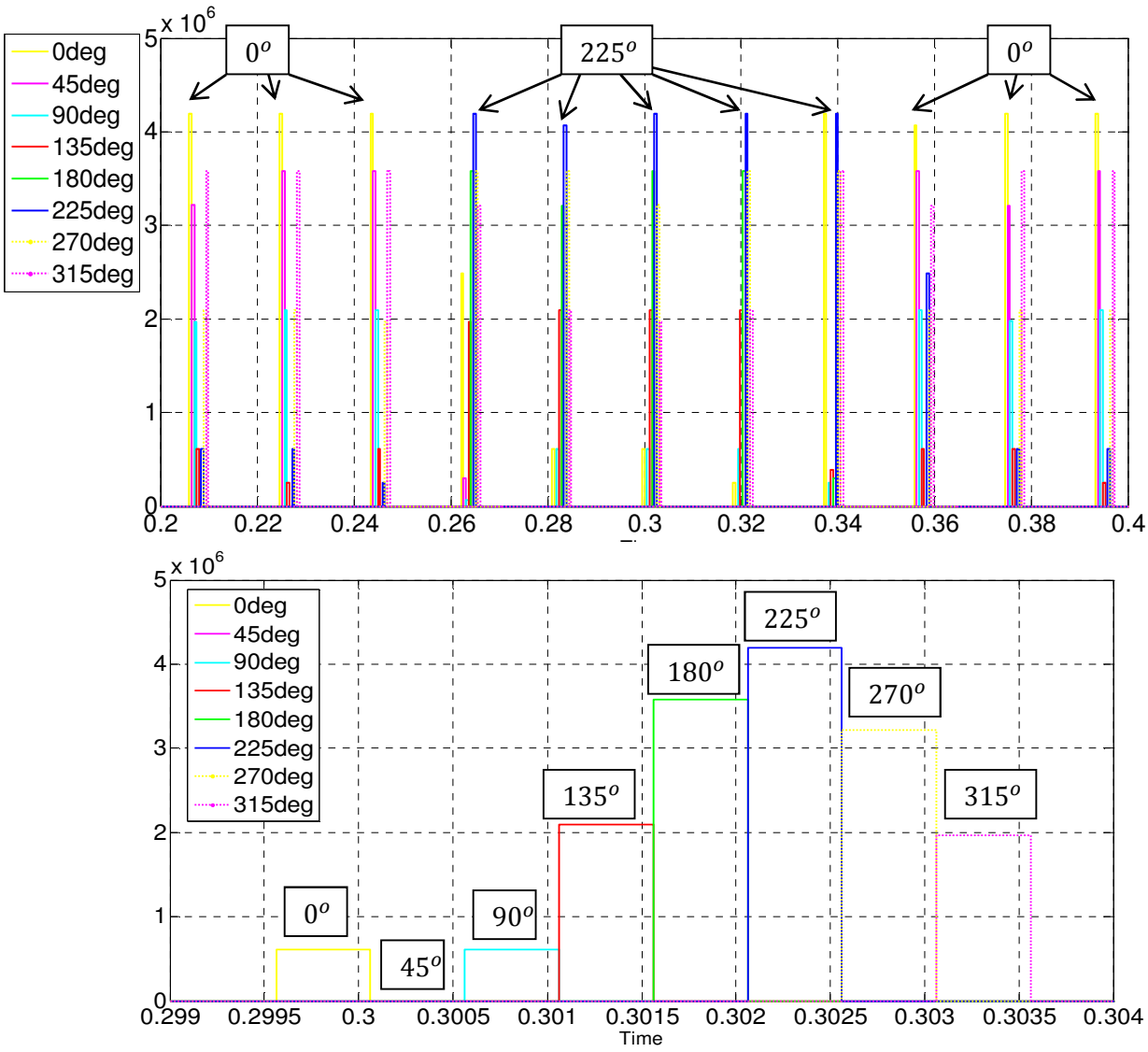

Figure 4.32: Detected Peaks where 225^o is dominant and 45^o is the weakest

It can be concluded that the 0^o angle is the reference to the received angles where the highest cross correlated point in figure 4.32 reflects the detected angle. This can be supported by double checking the opposite angle, 45^o in this case. Another example is shown in figure 4.33 when 45^o is detected.

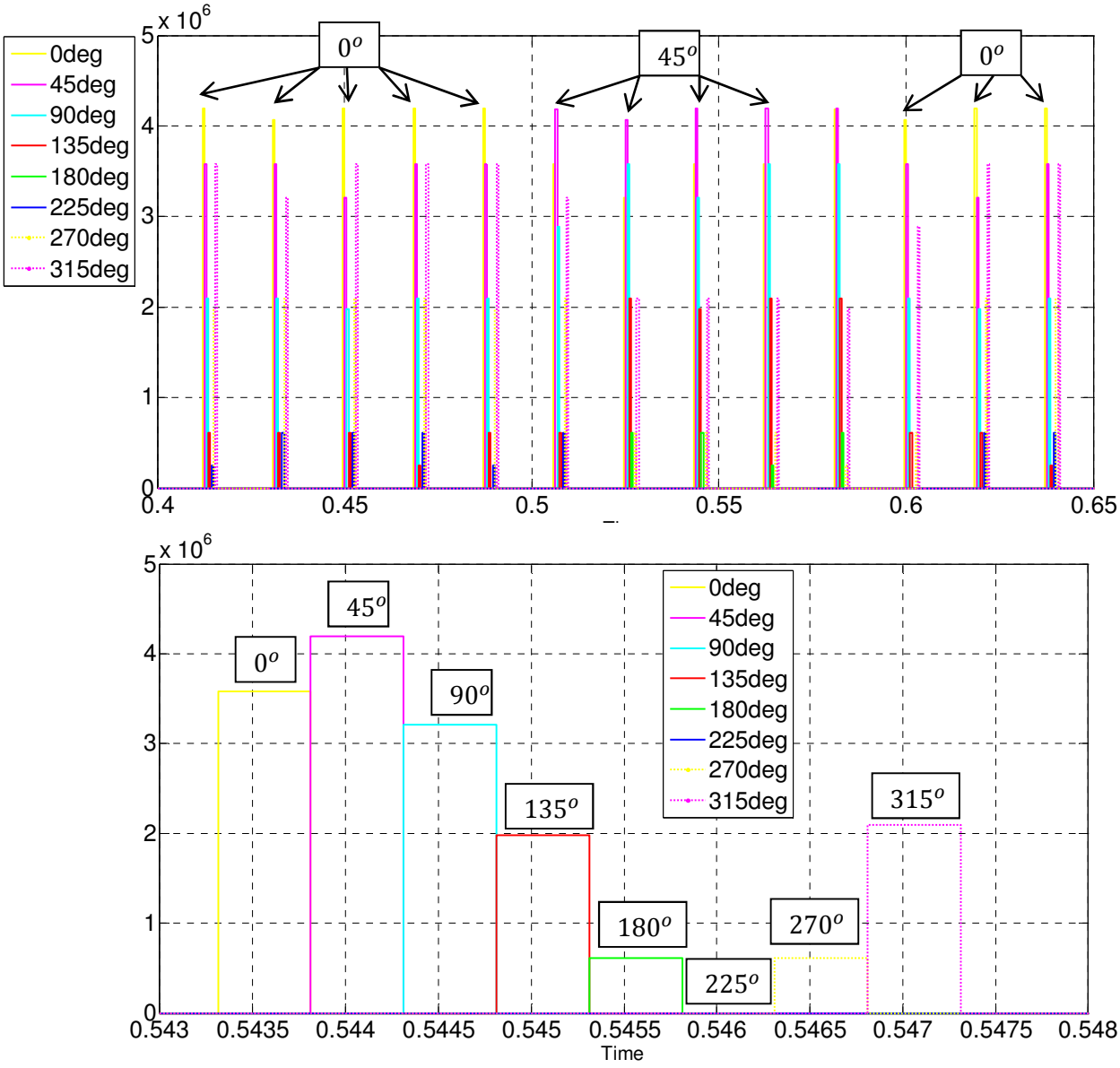

Figure 4.33: Detected Peaks where 45^o is dominant and 225^o is the weakest

Figure 4.33 proves the idea of double checking the opposite angle of the highest cross correlated point angle to minimise the probability of error. Now, these 8 points could be compared using the Cross Correlation Comparator (xcor_comp_8PSK_Gray.vhd) code shown in Appendix I.4 and summarised in flowchart 4.6. This code compares the points in figure 4.32 and 4.33 every time when it is triggered by peak_detector_8PSK_4Detectors.vhd code at the time of outputting the highest peaks. Since the transmitter is sending the data at rate of 0.25 s, the xcor_comp_8PSK_Gray.vhd is updated regulary almost every 0.25 s.

A direct comparison of the transmitted and recovered data by xcor_comp_8PSK_Gray.vhd is shown in figure 4.34. A delayed version of the transmitted data was displayed on figure 4.34 for the comparison. The receiver missed two symbols at startup and then fully recovered the data.

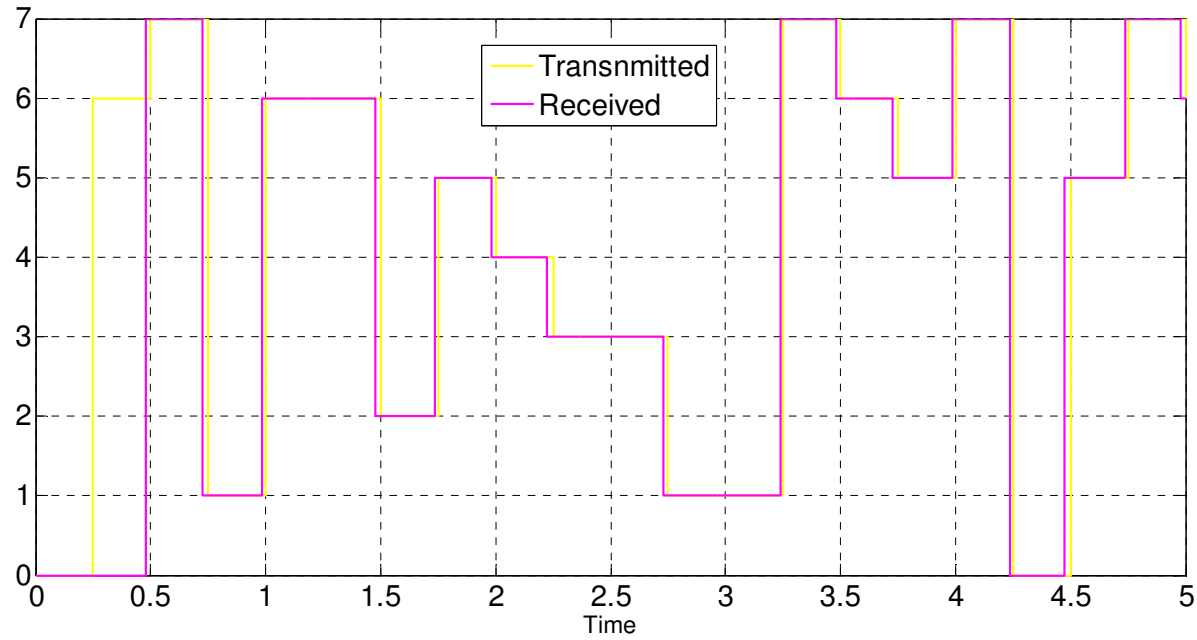

Figure 4.34: Comparison of the 8-PSK transmitted and received data over 5 s

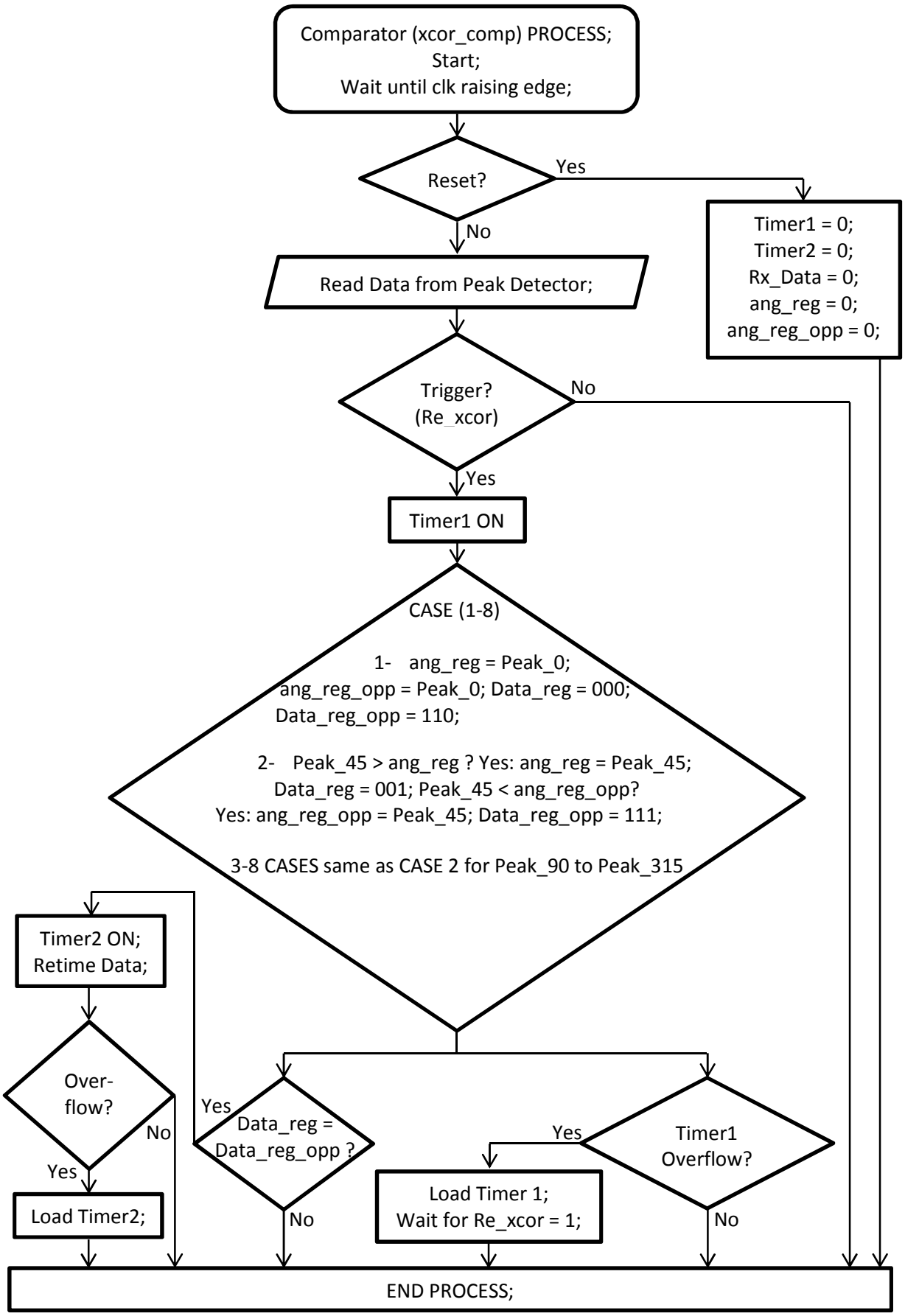

Flowchart 4.6: Cross Correlation Comparator VHDL process

4.2.3 Performance of cross correlation in 8-PSK detection

Additive White Gaussian Noise (AWGN) Channel of the Communication Toolbox in Simulink was used as shown in figure 4.35 to introduce limitless noise across the 8-PSK transmitter-receiver channel as shown in figure 4.36. The ROHDE & SCHWARZ Noise generator was used in the laboratory to add the noise to the 8-PSK signal. Amplifiers were used to balance the 8-PSK to noise ratio. Simulink was used to present the noise in time domain in this section.

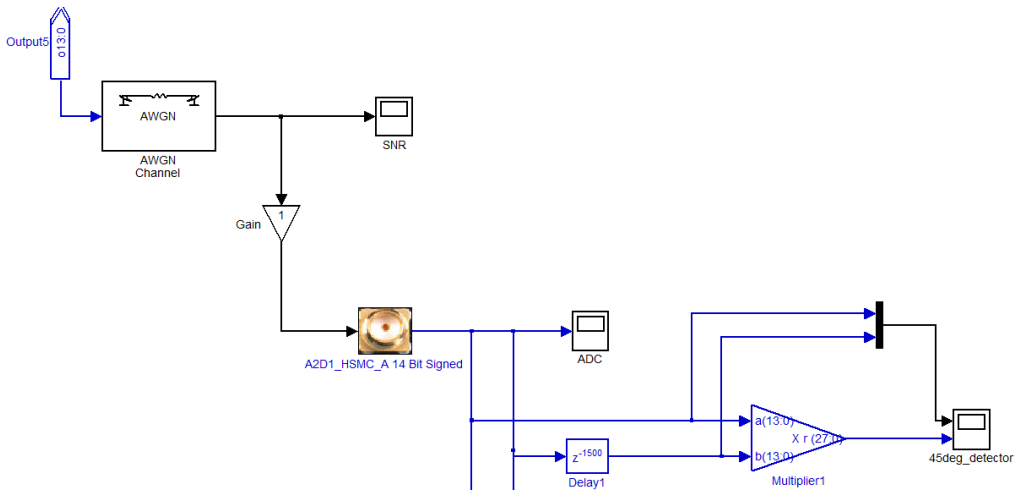

Figure 4.35: The 8-PSK correlator of 45^o in the presence of AWGN

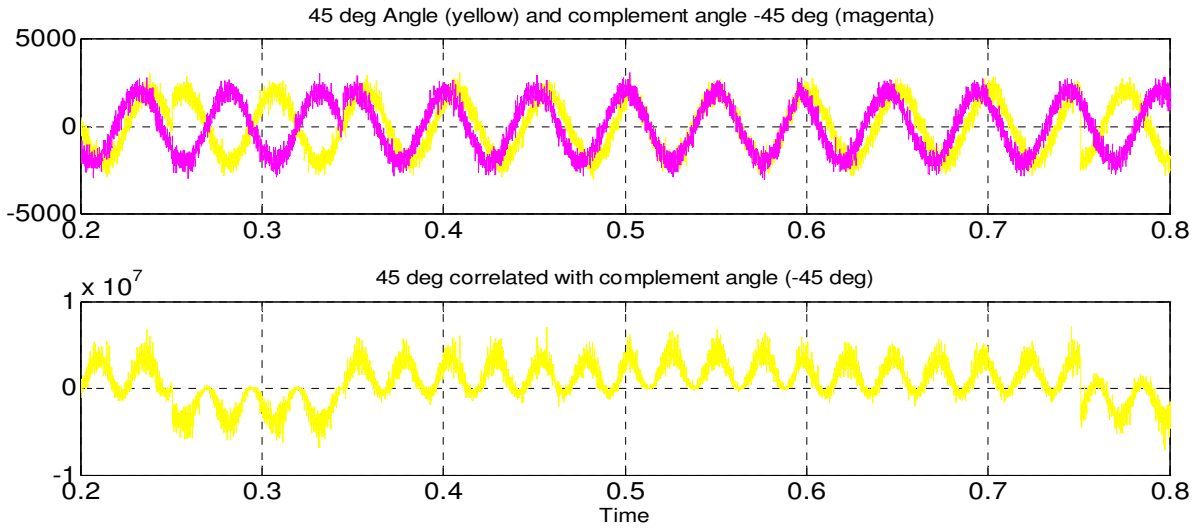

Figure 4.36: The input and output of the 45^o angle detector in presence of AWGN

Figure 4.37 shows the correlated and sliced signals of figure 4.36 in the presence of AWGN. The spikes of the AWGN are clearly digitised and confirmed the noise in (78), presented and observed in section 4.2.2. The output of all correlators and sign slicer are shown in figure 4.38.

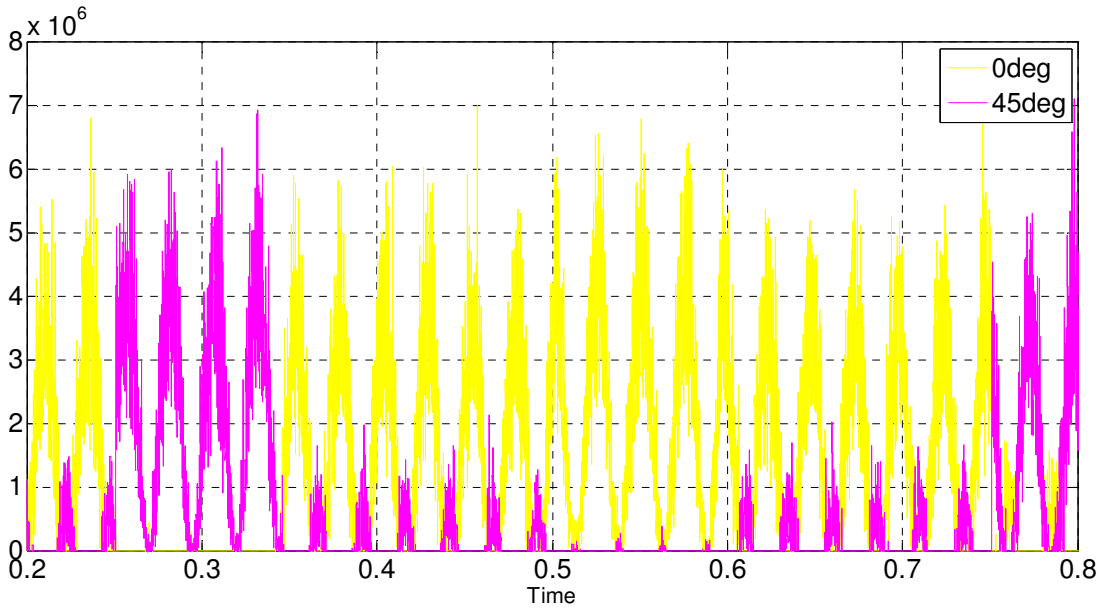

Figure 4.37: Cross correlated and separated signals of 45^o (yellow) and 225^o (magenta) in the presence of AWGN

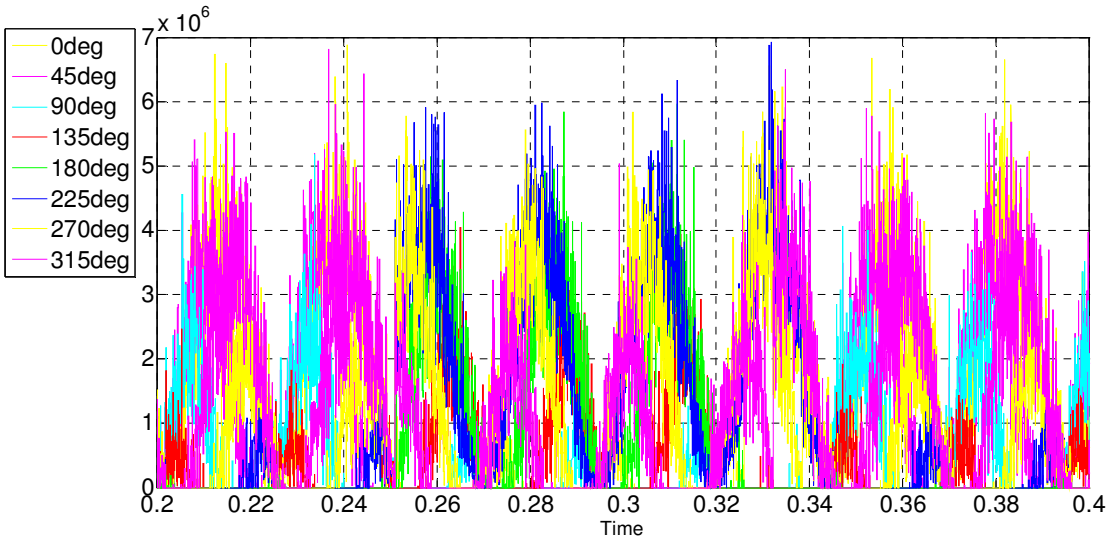

Figure 4.38: 8-PSK Correlated - Separated, all angles in the presence of AWGN

Figure 4.39 shows a zoomed-in version of figure 4.38 where all correlated signals are contaminated with AWGN. It can be seen that the blue (225^0) trace is dominant among all traces where the green (180^0) and yellow (270^0) traces are just close to the blue trace. This confirmed that the highest cross correlated point is within the bounded area of the detected angle shown in figure 4.13.

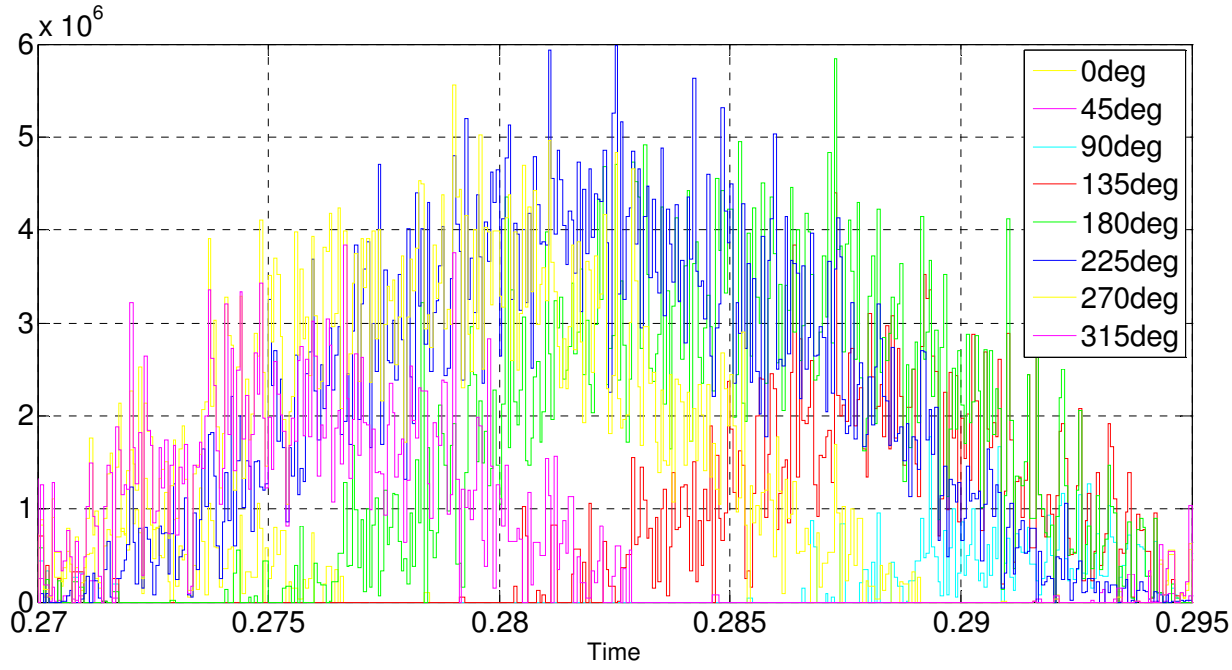

Figure 4.39: Zoomed-in of figure 4.38, all angles in the presence of 10dB AWGN

The peak_detector VHDL code observed the peaks of figure 4.38 every half the carrier cycle as presented in figure 4.40. The influence of the AWGN is apparent on the peaks of the cross correlated signal. Figure 4.40 (bottom) shows a zoomed-in version of (top), where the observed peaks by the peak_detector can be compared by naked eye. This is evident by using the "Cross Correlation Comparator" code by checking the opposite angle, 45^0 in this case. The *Comparator* compares the highest (detected angle) to the minimum (opposite angle) peaks, retimes any new data and eventually outputs the received data.

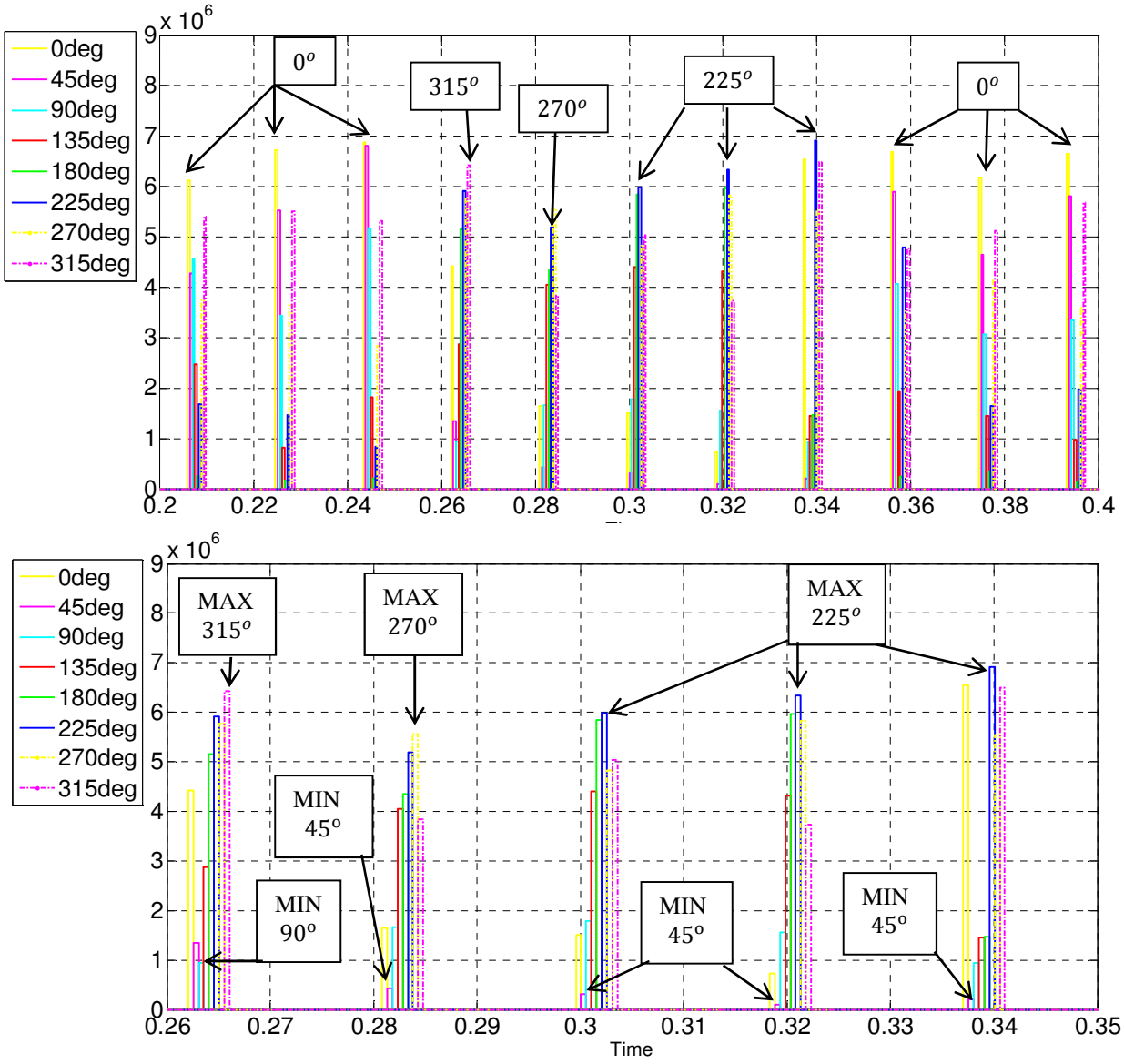

Figure 4.40: Detected Peaks where 225^o is dominant and 45^o is the weakest at 10 dB

Figure 4.41 shows an error detected at 10dB SNR. The error was found at 180^0. Figure 4.42 analyses the detected peaks. There is 180^0 twice, but the peak of the opposite angle was susceptible to noise as well as the 180^0 was. So, the AWGN misled the Comparator to output 000_2.

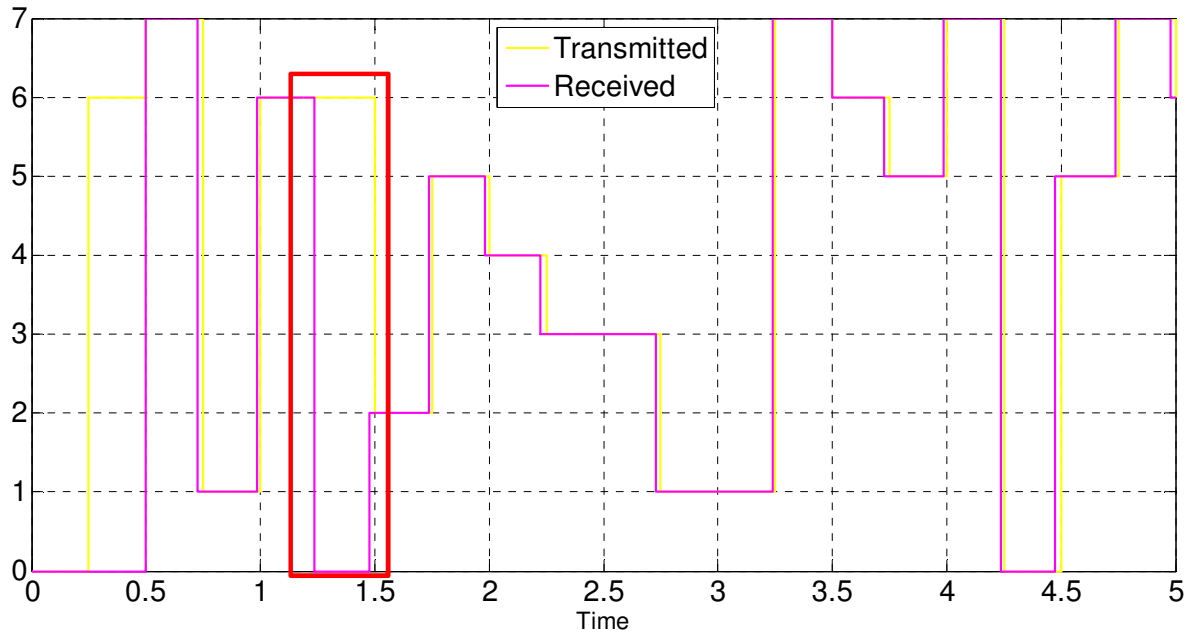

Figure 4.41: 8-PSK transmitted versus received data at 10 dB, detected an error

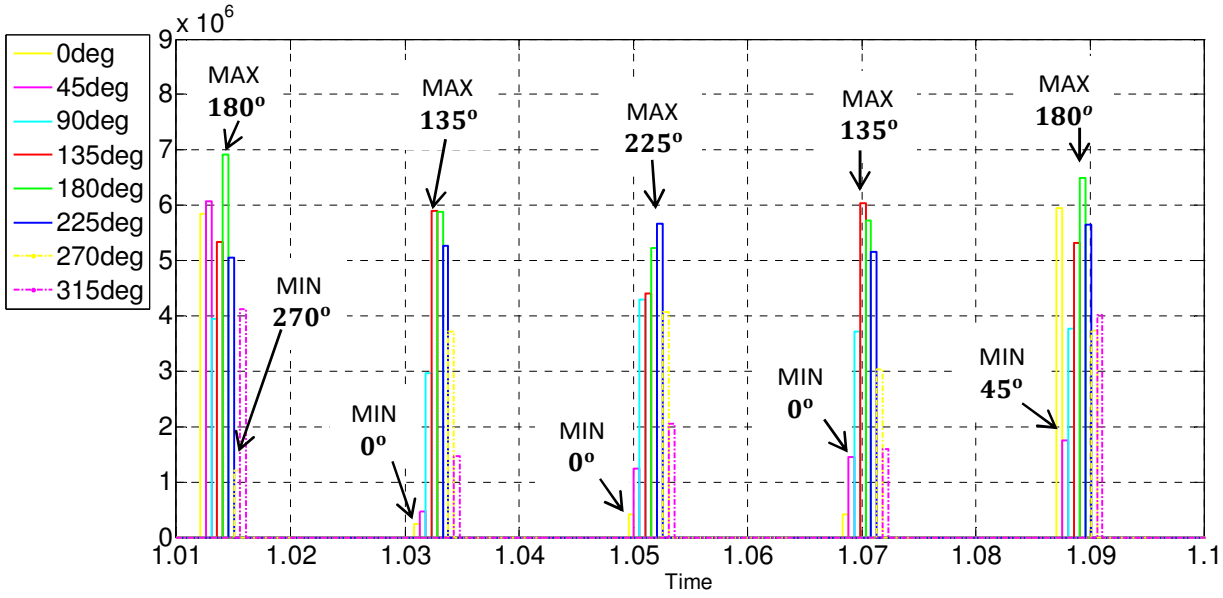

Figure 4.42: Detected Error of 180^o (Green) angle at 10 dB

Practical implementations of the link were conducted to introduce noise across the 8-PSK transmitter-receiver channel using ROHDE & SCHWARZ Noise Generator over a range of 0-25dB. Figure 4.43 shows SNR for a limitless noise across the channel where the 8-PSK signal is floating on the noise floor.

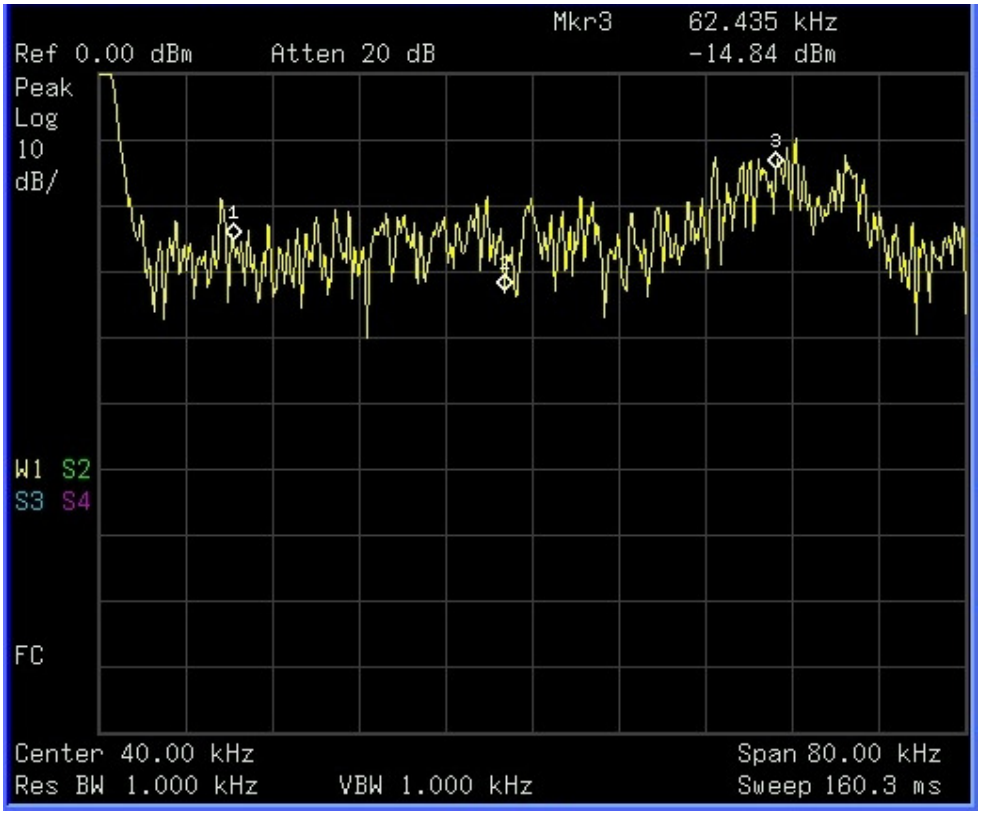

Figure 4.43: 8-PSK spectrum floating on the noise floor

A VHDL code based error calculator computed the differences between the transmitted and received symbols/bits. Figure 4.44 shows the performance of the 8-PSK demodulator with no error coding using cross-correlation. Tests were performed 4 times: Carrier-to-Noise-Ratio (CNR); Bit-to-Noise-Ratio (EbNR); Symbol-to-Noise-Ratio (EsNR); and limitless noise.

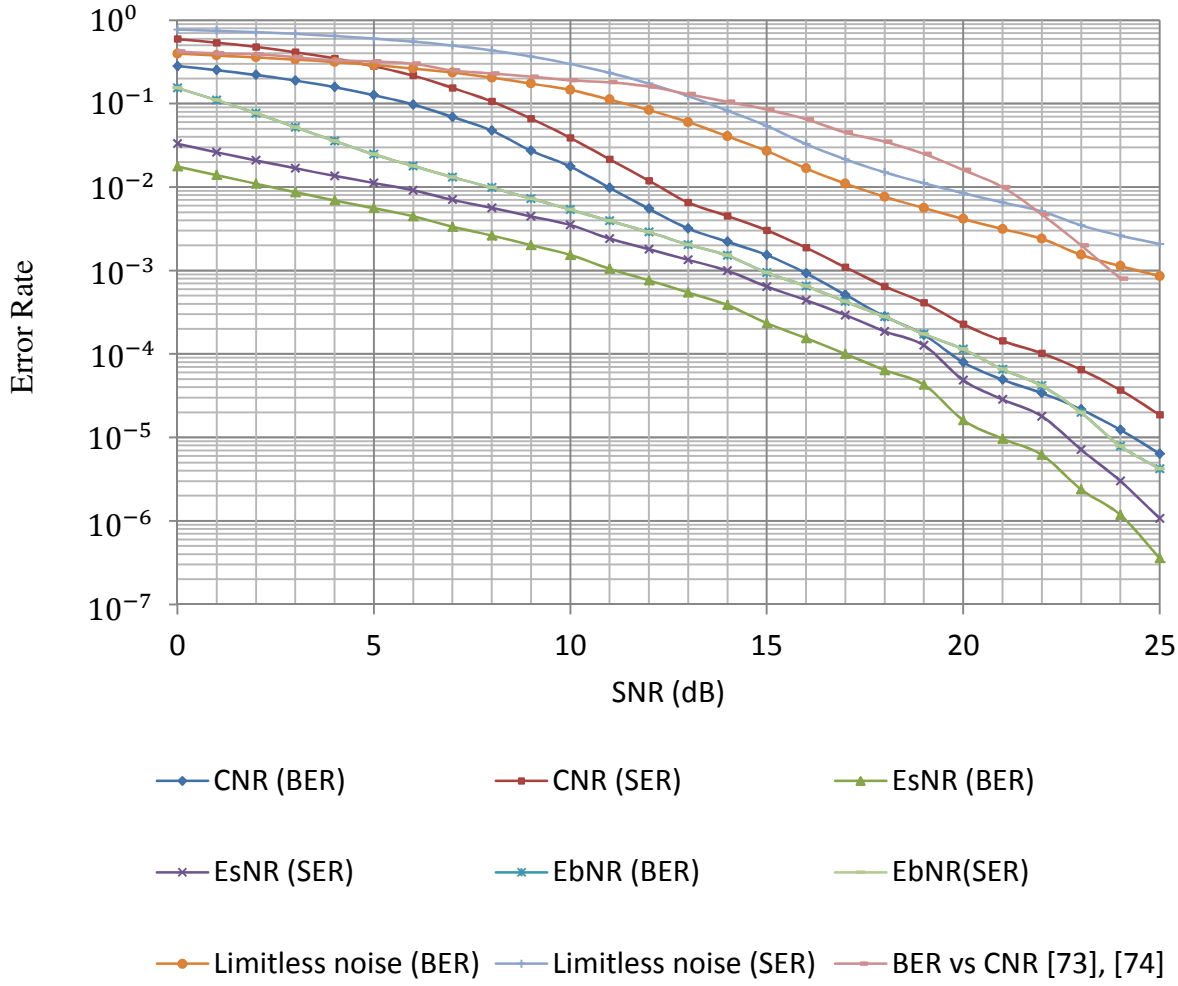

Figure 4.44: Performance of 8-PSK using cross correlation versus Monte Carlo simulations by [73] and [74]

4.3 Comments on PSK transmitter/receiver

An Altera CYCLONE III EP3C120F780C7N based DSP development board was used to implement the test rig shown in flowchart 4.3. An Altera Quartus II analysis showed that the system utilises only 2% out of 119,088 Total Logic Elements, less than 1% out of 4 Mb Total Memory Bits and 1% out of 576 Embedded Multiplier 9-bit Elements. In contrast to the system of [75] that utilises 800 LUTs, the system presented in this chapter utilises 678 LUTs. In addition, this system used no filters compared to the conventional demodulation technique of [75], that uses a set of Finite Impulse Response (FIR) LPFs to get rid of the carrier components at the output of the correlators. This technique yields cost reduction of applications that use 8-PSK scheme, particularly ELF Data Transmission Link.

The optimum error rate is 10^{-5} that provides maximum performance for 16-bit and lower resolutions. However, the presented system achieves 10^{-5} error rate at least 21 dB above noise level as shown in figure 4.44. As discussed in section 4.2.2, the system requires pre-filtering units to keep CNR with respect to phase response at a reasonable level and the highest cross correlated points within the bounded area of the detected angle.

References [73] and [74] implemented a Hierarchical 8-PSK constellation and used Monte Carlo algorithms to analyse the BER over a range of CNR 0-24dB with an assumption of perfect carrier recovery and ability of tracking phase fluctuations. A direct comparison of the error rate in this work shows in figure 4.44 that the Monte Carlo analysis of [73] and [74] delivers a maximum 8×10^{-4} BER at 24dB of CNR whereas the cross-correlation scheme delivers the same BER with only 16dB of CNR. In addition, the performance of the cross-correlation scheme is still better than [73] and [74] for limitless noise across the channel. The use of error coding should enhance the performance further.

Reference [76] designed a receiver on FPGA to comply with the IESS 308/310 Satellite Communication Standards based on PSK modulation scheme. The 8-PSK scheme in these standards requires 6dB, EbNR to attain lock to the carrier. In contrast, cross-correlation does not require carrier recovery and can deliver a maximum 9×10^{-3} BER at lower than 6dB compared to [76] that requires at least 6dB to attain lock.

IEEE 802.11b-1999, 802.11g-2003 and IEEE 802.15.4 standards [1] use adaptive systems to compensate the error rate at low SNR by switching between DPSK, BPSK and QPSK. Applications of these standards include WCDMA, HSDPA, WiMAX and WLAN broadband wireless access technologies. This leads the author of the thesis to propose an adaptive system, in parallel with error coding, to use cross-correlation at low SNR and back to normal operation at high SNR for the Satellite and Broadband standards.

5. Quadrature Amplitude Modulation (QAM) transmitter/receiver

Chapter 4 discussed the use of cross-correlation to demodulate 8-PSK signal compared to the schemes that use carrier recovery as part of extracting the phase data. It was concluded in the previous chapter that the cross correlation provides better immunity at low SNR. This chapter is intended to combine Binary ASK (BASK) and 8-PSK to form 16-QAM. As a result, 4-bits are transmitted per symbol. This would enhance the capacity of the ELF link without increasing the bandwidth.

The baud rate of simulating the link in Simulink is still *4 symbols/s* at 20 Hz carrier. On the other hand, it is *12.5 k.symbols/s* at 62.5 kHz carrier for the practical experimentations due to the practical issues of the FPGA development board discussed previously in chapter 4. The sampling frequency of the simulation and practical experimentations were 16 kHz and 50 MHz respectively. The concept of the cross-correlation theory and implementations used in chapter 4 will be applied again in this chapter to extract the phase modulated data (8-PSK). The VHDL codes and the 8-PSK receiver of chapter 4 will be modified in this chapter to include the detection of the BASK data that is in the form of AM signal. In this chapter, the BASK data is referred as AM data.

5.1 Theory

Star and Square QAM techniques are widely used to transmit *m*-bit symbols via a 2^M signal point constellation, distributed on a complex plane [33]-[35], [72]. The higher the value of *M*, the more highly bandwidth efficient modulation scheme can be designed [33]-[35], [42]. The 16-QAM is one of the standard modulation schemes in OFDM [3] applications such as DVB-T and HIPERLAN [4].

5.1.1 Star 16-QAM

The Star 16-QAM has two amplitude levels that are two circles around the origin as shown in figure 5.1. The outer ring is 3 times greater than the inner ring. It is considered as two 8-PSK with different amplitude level [72]. The 8-PSK and 16-QAM occupies the same bandwidth shown in figure 4.2 since they share the same symbol rate of *4 symbols/s*.

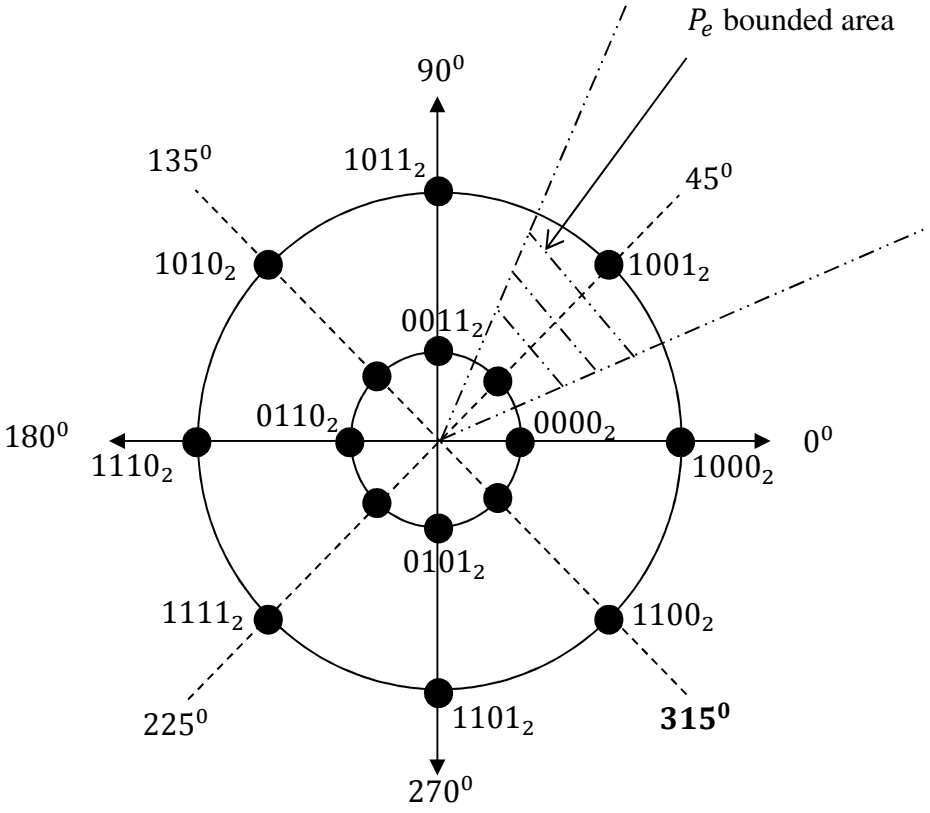

Figure 5.1: Star 16-QAM Gray coding constellation

The Star 16-QAM can be modulated using the 8-PSK modulator discussed in section 4.1.3, chapter 4. The data source is divided 4 *bit/symbol* (a_n, b_n, c_n, d_n). The b_n, c_n, d_n data modulate the 8-PSK signal as discussed previously (phase mapper) and a_n modulate the BASK signal using Voltage-Controlled-Amplifier (VCA) or a Multiplexer (MUX) to multiplex the amplitude level of the 8-PSK signal. This results in a Star 16-QAM signal as will be seen and discussed later in section 5.2.1. The BASK data should be differentially encoded on the carrier. The phase data (b_n, c_n, d_n) of 16-QAM is tabulated in table 4.2. The transmitted 16-QAM signal can be represented the same as QPSK in equation (65), rewritten as (79).

$$S_{QAM}(t) = A\ \cos(\omega_c t + \theta_t) \tag{79}$$

The amplitude *A* in (79) represents the BASK data whereas θ_t represents the 8-PSK data. In contrast to PSK schemes, the amplitude *A* is a constant and the θ_t represents the transmitter phase data. The transmitted 16-QAM signal is suppressed carrier where half the power is concentrated in the carrier and the other half is QAM modulated data. Demodulation of 16-QAM is crucial where 2 vectors have to be tracked, phase and amplitude. The phase can be tracked using complex number, Costas loop or digital PLL and *ATAN* function using DSP processor as discussed in chapter 4. The amplitude can be tracked easily in the case of Star 16-QAM by comparing the absolute values of a current sample with a full carrier cycle to differentially decode the BASK data. Section 5.1.3 is concerned about 16-QAM receiver issues.

5.1.2 Square 16-QAM

The Square 16-QAM has three amplitude levels compared to Star 16-QAM. The constellation points are distributed on 3 circles of the signal plane as shown in figure 5.2. The points are separated in uniform square arrays [33]. The distance between all points is equal. This optimises the transmission over Gaussian channel [72] compared to Star 16-QAM. The Square and Star QAM occupies the same bandwidth for the same transmission rate.

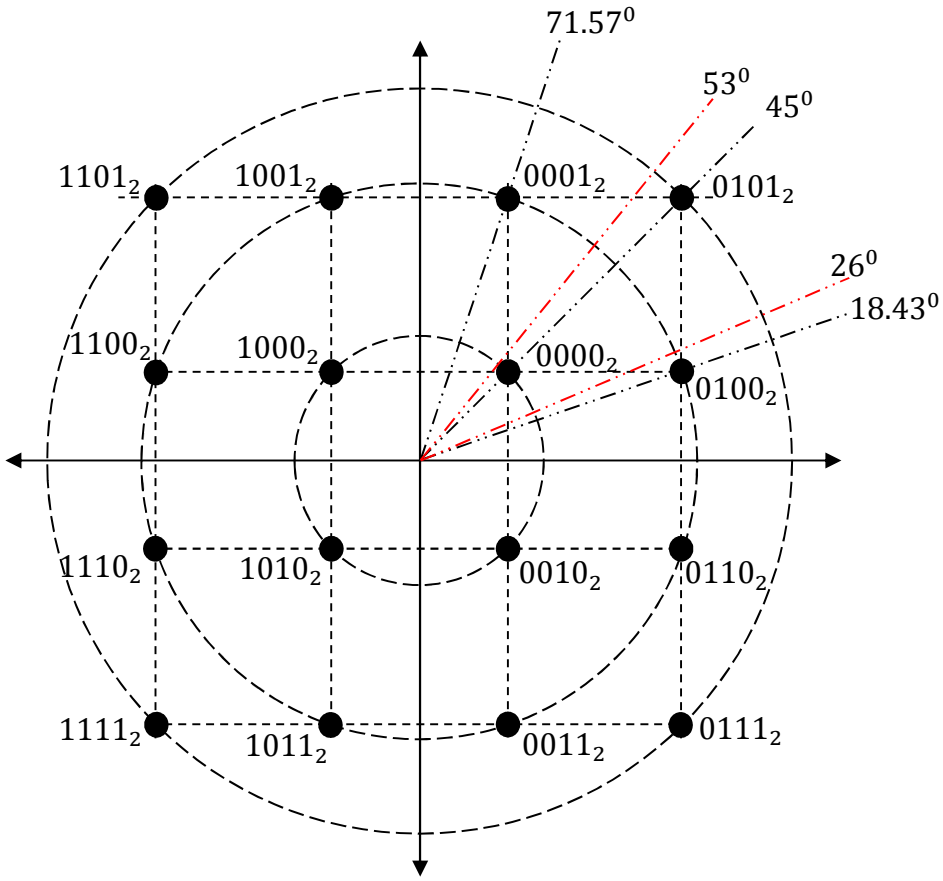

Figure 5.2: Square 16-QAM Gray coding constellation

The Square 16-QAM can be modulated in the same way of QPSK discussed in section 4.1.2, chapter 4 using in-phase and quadrature carriers. The data source is divided to 4 *bit/symbol* (a_n, b_n, c_n, d_n) to represent the 16 constellation points shown in figure 5.2. A demultiplexer splits the data to Even and Odd NRZ parts as shown in table 5.1. The Odd part controls the

amplitude level of the in-phase carrier. Similarly, the Even part controls the amplitude level of the quadrature carrier.

$x_i(t)$, (4-bit)		NRZ data		Transmitted carrier, $S_{QAM}(t) = A\ \cos(\omega_c t + \theta_t)$
ODD	EVEN	a_1	a_2	
00	00	+1	+1	$\cos(\omega_c t) + \sin(\omega_c t) = 1.41\ \cos(\omega_c t + 45^0)$
00	01	+1	+3	$\cos(\omega_c t) + 3\sin(\omega_c t) = 3.16\ \cos(\omega_c t + 71.56^0)$
00	10	+1	-1	$\cos(\omega_c t) - \sin(\omega_c t) = 1.41\ \cos(\omega_c t - 45^0)$
00	11	+1	-3	$\cos(\omega_c t) - 3\sin(\omega_c t) = 3.16\ \cos(\omega_c t - 71.56^0)$
01	00	+3	+1	$3\cos(\omega_c t) + \sin(\omega_c t) = 3.16\ \cos(\omega_c t + 18.43^0)$
01	01	+3	+3	$3\cos(\omega_c t) + 3\sin(\omega_c t) = 4.24\ \cos(\omega_c t + 45^0)$
01	10	+3	-1	$3\cos(\omega_c t) - \sin(\omega_c t) = 3.16\ \cos(\omega_c t - 18.43^0)$
01	11	+3	-3	$3\cos(\omega_c t) - 3\sin(\omega_c t) = 4.24\ \cos(\omega_c t - 45^0)$
10	00	-1	+1	$-\cos(\omega_c t) + \sin(\omega_c t) = 1.41\ \cos(\omega_c t + 135^0)$
10	01	-1	+3	$-\cos(\omega_c t) + 3\sin(\omega_c t) = 3.16\ \cos(\omega_c t + 108.43^0)$
10	10	-1	-1	$-\cos(\omega_c t) - \sin(\omega_c t) = 1.41\ \cos(\omega_c t - 135^0)$
10	11	-1	-3	$-\cos(\omega_c t) - 3\sin(\omega_c t) = 3.16\ \cos(\omega_c t - 108.43^0)$
11	00	-3	+1	$-3\cos(\omega_c t) + \sin(\omega_c t) = 3.16\ \cos(\omega_c t + 161.57^0)$
11	01	-3	+3	$-3\cos(\omega_c t) + 3\sin(\omega_c t) = 4.24\ \cos(\omega_c t + 135^0)$
11	10	-3	-1	$-3\cos(\omega_c t) - \sin(\omega_c t) = 3.16\ \cos(\omega_c t - 161.57^0)$
11	11	-3	-3	$-3\cos(\omega_c t) - 3\sin(\omega_c t) = 4.24\ \cos(\omega_c t - 135^0)$

Table 5.1: Properties of Square 16-QAM modulated carrier

Figure 5.3 shows the Square 16-QAM transmitter where equation (79) formulates the output of the transmitter. Table 5.1 shows that the transmitted carrier output represents 4 *bit/symbol*.

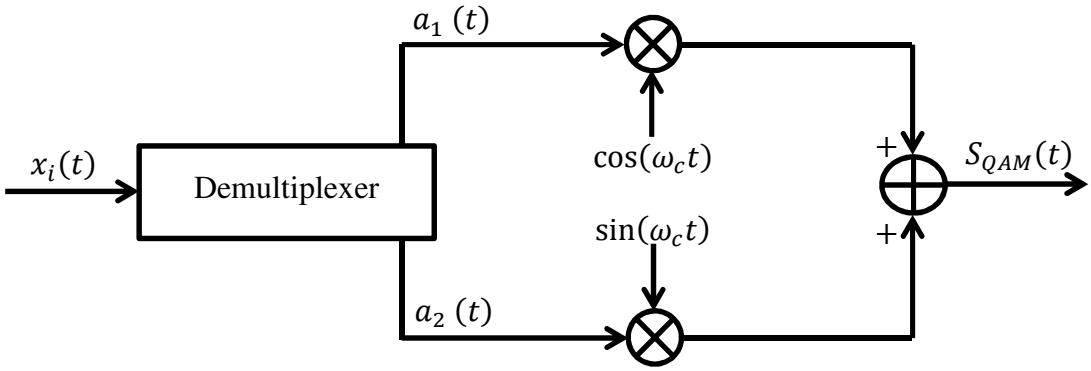

Figure 5.3: Square 16-QAM transmitter

The transmitted Square 16-QAM signal is a suppressed carrier. The mean power transmitted by Square QAM is slightly larger than the Star QAM [68]. Unlike Star 16-QAM, the *A* of equation (79) in the Square 16-QAM cannot be tracked separately from θ_t where the symbols are not stack on each other on the circles. However, the symbols are strictly dependent on *A* and θ_t. This requires phase knowledge which in practice must be estimated. The phase can be tracked using complex number, Costas loop or digital PLL and *ATAN* function using DSP processor as discussed in chapter 4. The fading channel makes the Square 16-QAM unable to keep a track of phase and the PLL locks to a false quadrant [40], [72]. It also suffers from false lock positions at 26^0 and 53^0 as shown in figure 5.2. Section 5.1.3 is concerned about 16-QAM receiver issues. The performance of Square 16-QAM ($P_{e_{16-QAM}}$) over Gaussian is derived in Appendix J as equation (80):

$$P_{e_{16-QAM}} = 3Q\left(\sqrt{\frac{E_S}{5N_0}}\right) - 2.25\left(Q\left(\sqrt{\frac{E_S}{5N_0}}\right)\right)^2$$

$$= \frac{3}{2}erfc\left(\sqrt{\frac{E_S}{10N_0}}\right) - 2.25\left(\frac{1}{2}erfc\left(\sqrt{\frac{E_S}{10N_0}}\right)\right)^2 \qquad (80)$$

5.1.3 16-QAM receiver

Chapter 4 showed that carrier recovery is not efficient as exact phase cannot be guaranteed or maintained and, with DSP processors, the carrier recovery requires LUTs to slice and scale the phases. Mainly, system integrators use *ATAN* function in parallel with digital PLL to detect the phase changes [37], [39], [40], [43]. Consequently, high implementation resources are needed to perform such an operation.

In general, Square 16-QAM requires coherent detection which requires phase knowledge where the phase noise causes the constellation points to rotate, and so absolute phase reference must be maintained or estimated [34], [35], [38]-[40], [42]-[44], [72], [77]. However, Square QAM requires AGC and carrier recovery for coherent detection [34], [42], [44], [72]. Figure 5.4 shows a typical Square 16-QAM receiver. The carrier recovery unit recovers the carrier to in-phase and quadrature components. The matched filters remove the carrier components and output the baseband signal. An LUT de-maps baseband signal and combine the decoded data to 4-bit.

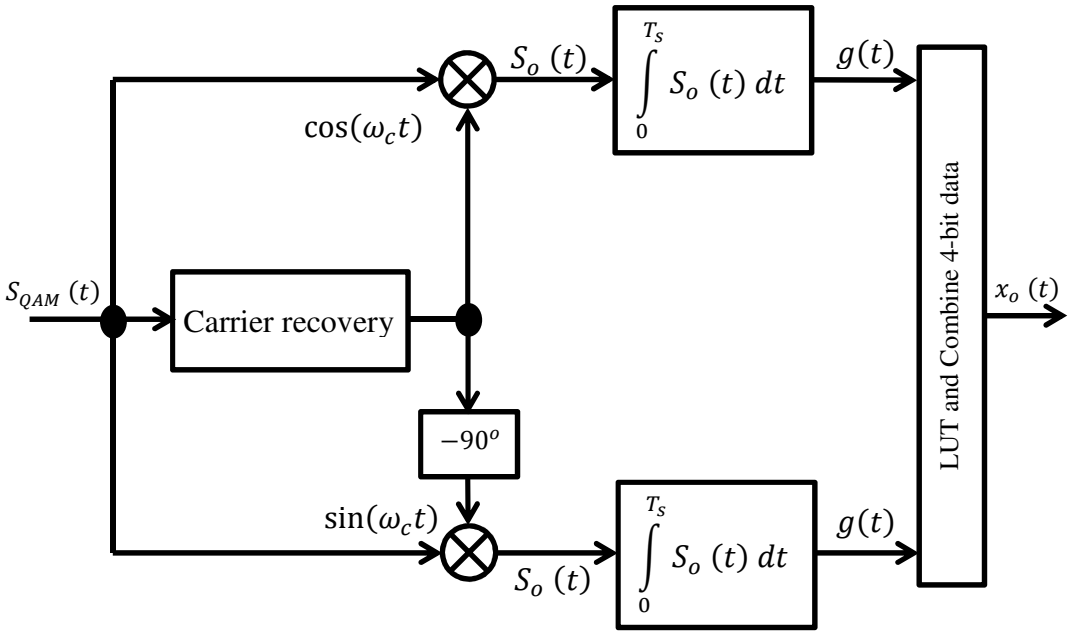

Figure 5.4: Square 16-QAM receiver

The coherent detection is severely affected by multipath fading, mainly because of carrier recovery issues in a fast-fading environment [34], [42], [44], [72] where the PLL locks onto a different quadrant than that required [34], [40], [44], [72]. The AGC has to react fast to follow the fades and maintain high accuracy for amplitude information to be correctly decoded [34], [42], [72]. This issue is minor in detecting Star 16-QAM signal compared to Square 16-QAM [34].

The Star 16-QAM can be demodulated using the 8-PSK receiver discussed in chapter 4, section 4.1.3 by adding an AM detector. This can be done by comparing the absolute values of a current sample with a full carrier cycle to differentially decode the BASK data (a_n). Section 5.2.2 is concerned about implementations of Star 16-QAM receiver.

5.1.4 Performance of Star and Square 16-QAM

The error performance of any digital communication system is fundamentally related to the distance between points in the signal space diagram [34], [72]. The 16-QAM has a noise bandwidth that is relatively smaller than that of the 8-PSK or lower PSK schemes although the error distance between the two points is smaller in 8-PSK [34], [72]. The distance between all constellation points in Square 16-QAM is equal which in return optimises the transmission over Gaussian channel [72] compared to Star 16-QAM. On the other hand, the use of Star QAM reduces the effects of Rayleigh fading [34], [72] compared to Square QAM. Moreover, the Star QAM does not experience false lock positions and the transmitted mean power is relatively smaller compared to the Square QAM [68]. In addition, the author of [35] found that Star QAM has the property that PAPR is less than that for Square QAM. Also, [35] has found that the coded Star 16-QAM symbol error performance is better than that of square 16-QAM. For these reasons, Star 16-QAM was chosen and implemented in this chapter, section 5.2. To the author's knowledge, there is a lack of literature discussing the probability of error performance of Star 16-QAM. This is left for further work. The performance of Square 16-QAM is presented in figure 5.5 using equation (80). It requires 20dB to deliver 10^{-5} error rate.

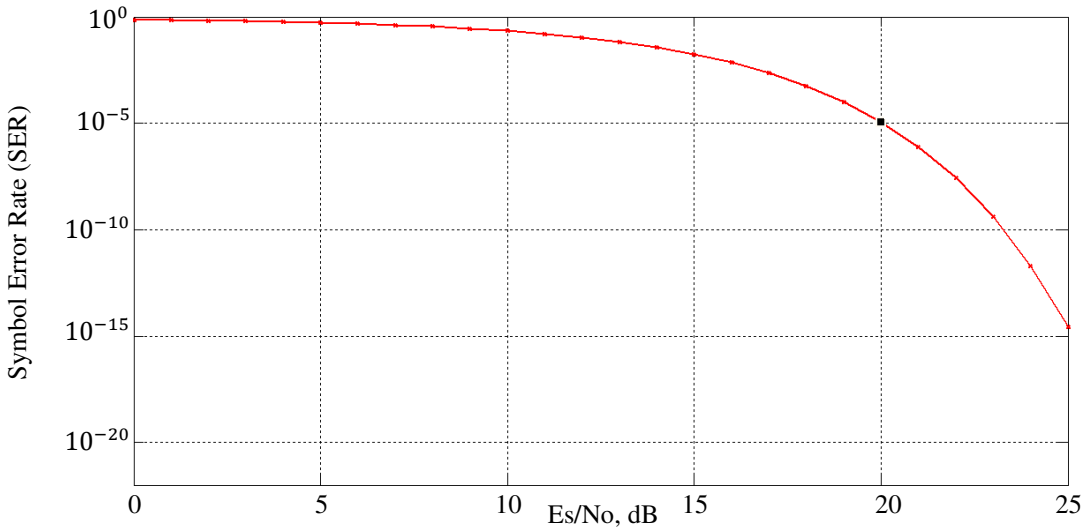

Figure 5.5: Performance of Square 16-QAM modulation

5.2 Implementation of 16-QAM link

5.2.1 Star 16-QAM Transmitter

The Star 16-QAM transmitter was designed and implemented as shown in figure 5.6 by adopting a MUX to the 8-PSK transmitter shown in figure 4.20 to amplitude modulate the 8-PSK output by a factor of 3. The constellation points of Star 16-QAM is shown in figure 5.1. The Matlab-Simulink, Altera DSP Builder and Quartus II, and an Altera CYCLONE III EP3C120F780C7N based DSP development board were used to develop the 16-QAM link. However, an NCO [71] was used with the same parameters applied in chapter 4, section 4.2.1, where the phase and amplitude precision are 12-bit. These parameters fit with the 14-bit DAC resolution. The data source is divided to 4 bit/symbol where the 3 Least Significant Bits (LSB) $b_{n,}c_n, d_n$ modulates the 8-PSK signal separated at 45^0, as indicated in table 4.3. The Most Significant Bit (MSB) a_n modulates the amplitude of 8-PSK signal by a factor of 3. The symbols are distributed equally around the circle as show in figure 5.1. Gray coding was used to minimise the bit error at the presence of noise. The data are mapped to the amplitude and phase of the carrier at the speed of symbol rate using VHDL entity entitled QAM_mapper shown in Appendix I.5 and summarised in flowchart 5.1. The AM data is differentially encoded at the transmitter side. The receiver, peak_detector_QAM specifically check the absolute values of current samples to a full delayed carrier cycle, whichever is twice greater than the other one, then a logic 1_2 is detected.

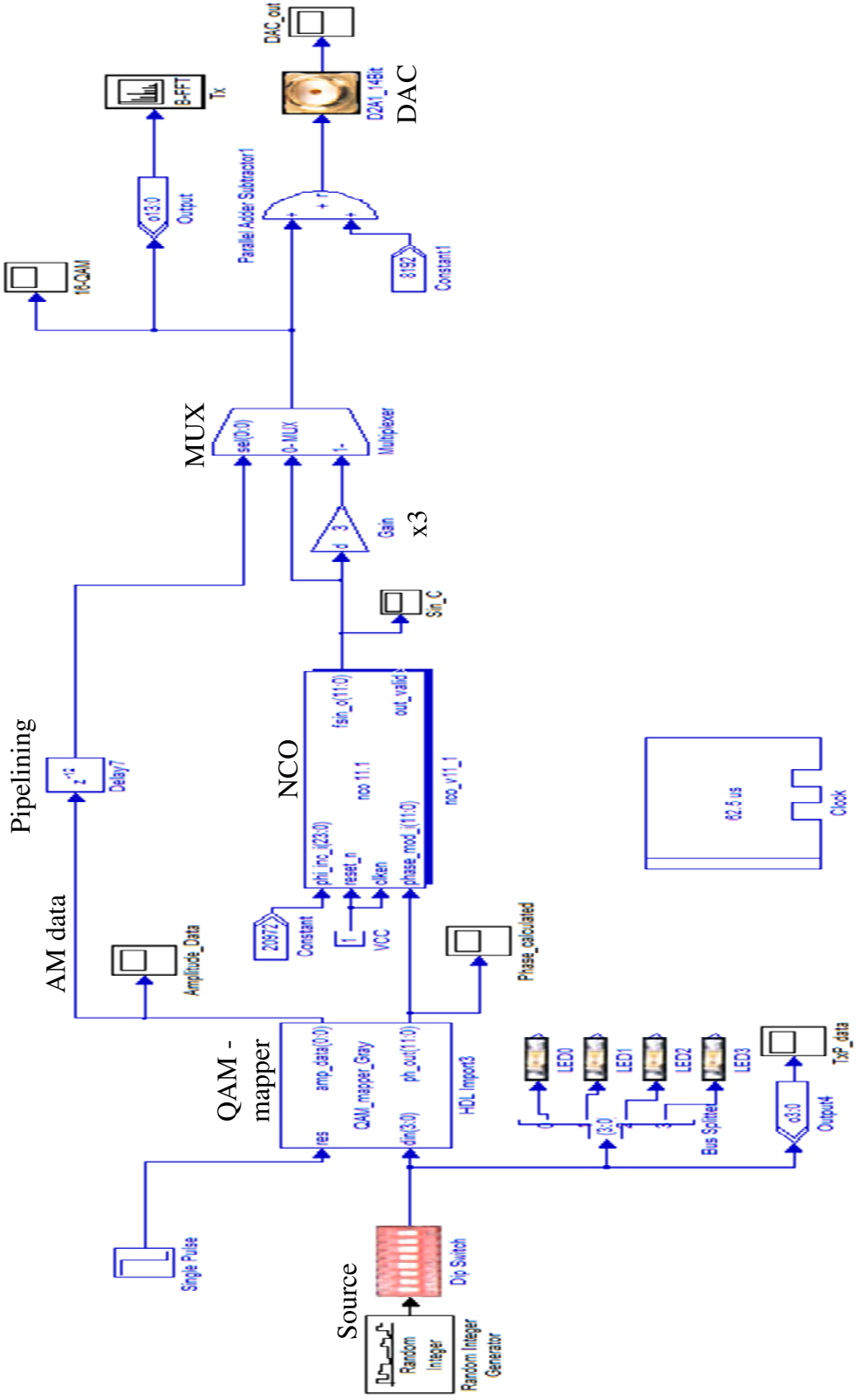

Figure 5.6: 16-QAM transmitter design using Altera Builder and Simulink

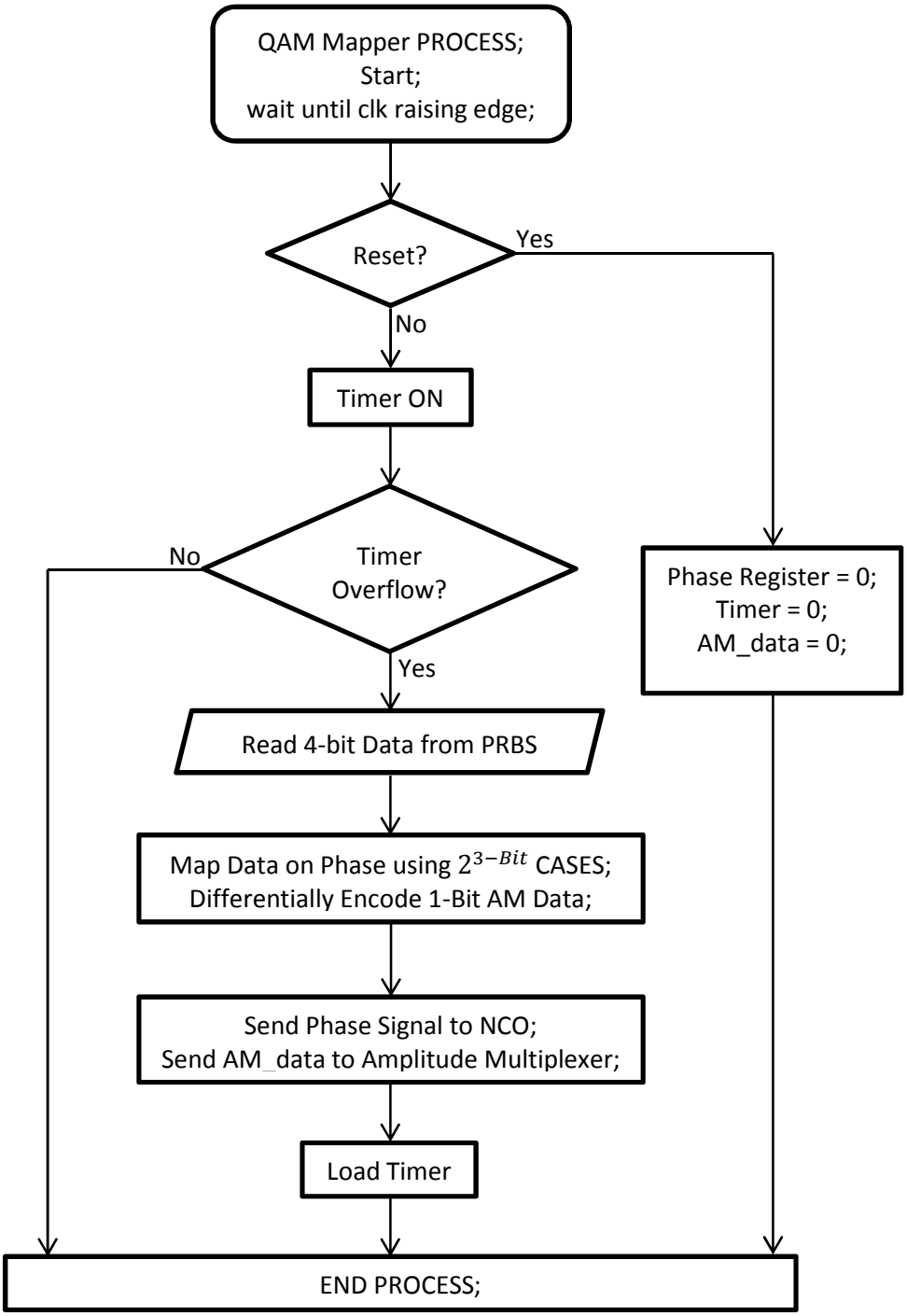

Flowchart 5.1: QAM_mapper VHDL process

The NCO [71] output two's complement numbers while the 14-bit DAC is unsigned. An adder was used to add the output of the MUX with a constant number to remove the two's complement. The design can be tested using; Random Integer Generator for Simulink, PRBS or DIP switches to control the VHDL code on the FPGA chip [58]-[62], [71].

The transmitter shown in figure 5.6 was sourced using Random Integer Generator; 0000_2 to 1111_2 with respect to the phase constellation points shown in figure 4.13 of the 8-PSK while the amplitude data was differentially encoded. Figure 5.7 shows the 16-QAM transmitter output. The amplitude (a_n) and phase (b_n, c_n, d_n) data of the 16-QAM shown in figure 5.7 was altered by 270^0, 135^0, 270^0, 135^0 and 270^0 using 0101_2, 1010_2, 0101_2, 1010_2 and 0101_2 respectively.

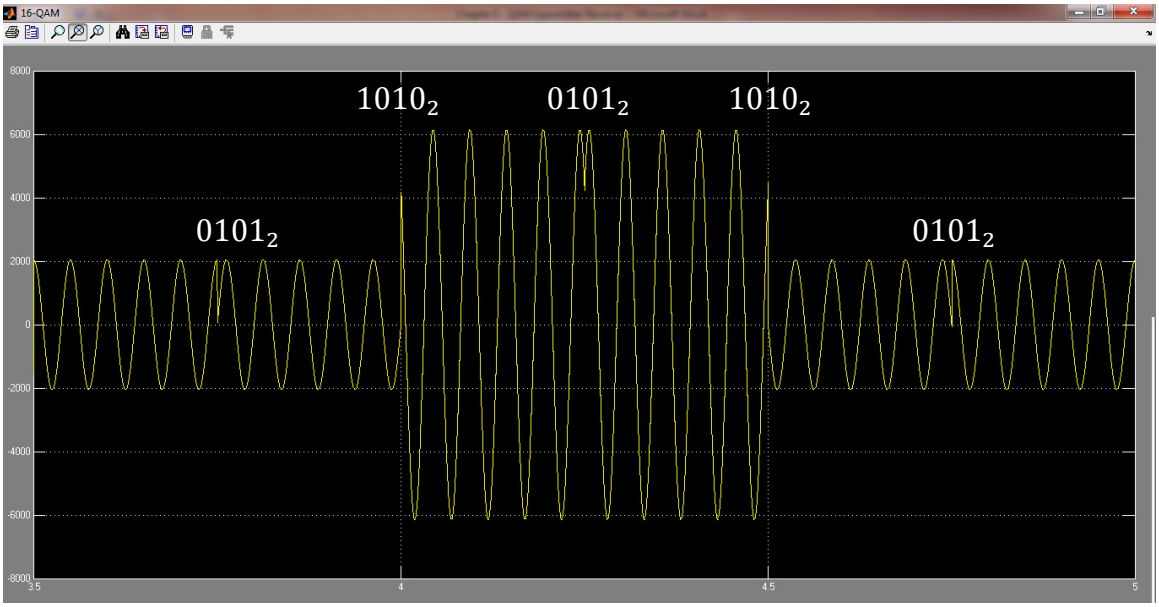

Figure 5.7: Simulink results of the 16-QAM transmitter

The 16-QAM transmitter was fully designed using Altera DSP Builder. The generated system was downloaded on the FPGA. The laboratory test rig is shown in figure 4.22. As discussed earlier, due to the practical issue of the development board, the sampling and carrier frequencies were changed to be 50MHz and 62.5 kHz respectively. Flowchart 5.2 summarises the 16-QAM transmitter VHDL process behaviour.

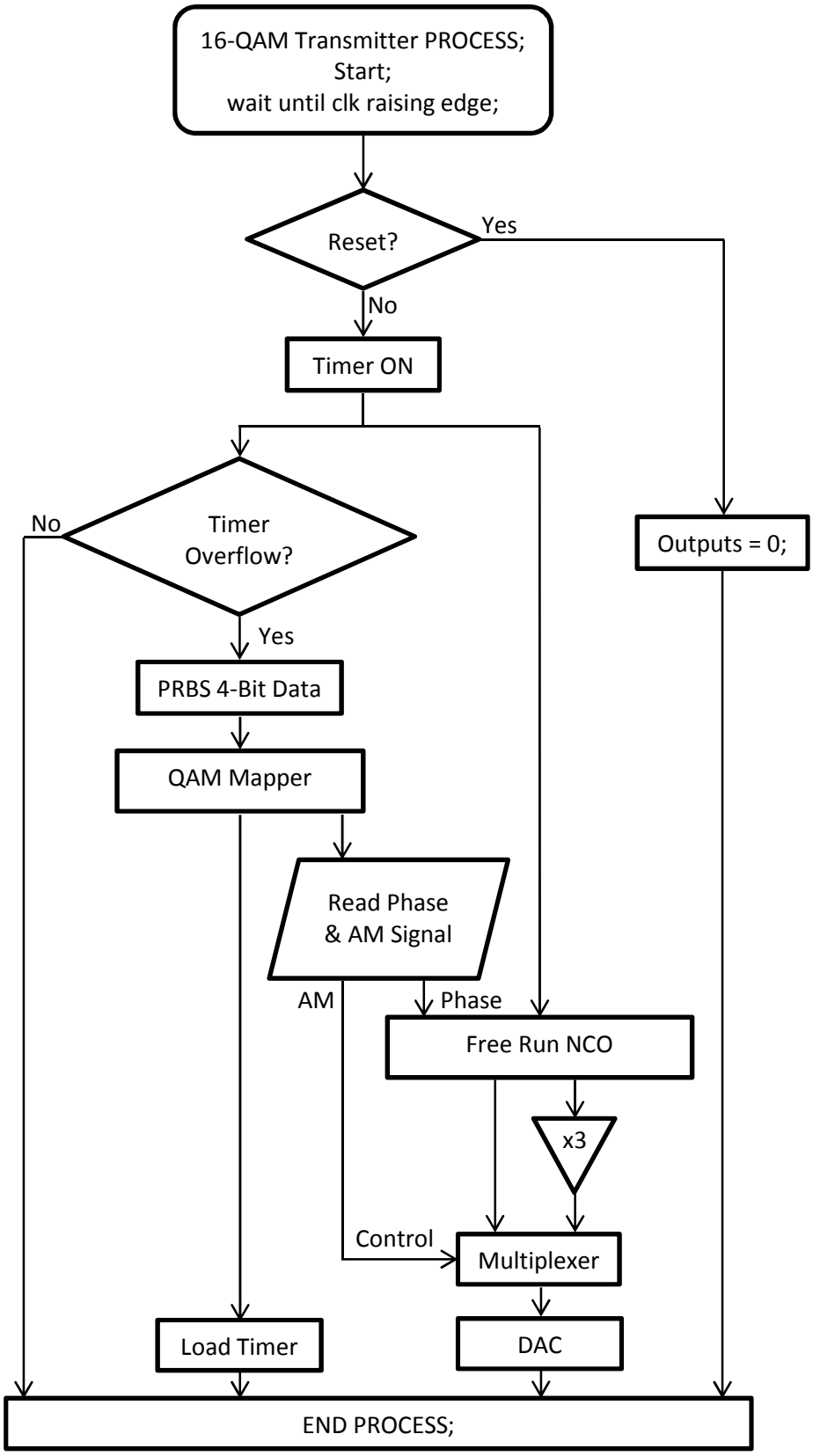

Flowchart 5.2: 16-QAM transmitter VHDL process

Figure 5.8 shows 16-QAM signal at 62.5 kHz carrier using Cyclone III FPGA DSP development board. A PRBS was sourcing QAM_mapper. The data and angles were (0100_2, 1000_2, 1001_2, 1011_2, 1001_2, 0000_2); and (315^0, 0^0, 45^0, 90^0, 45^0, 0^0) respectively. Clearly, the HPF of the DAC unit is affecting the phase and amplitude of the 16-QAM signal. This would in return affect the receiver as will be seen later.

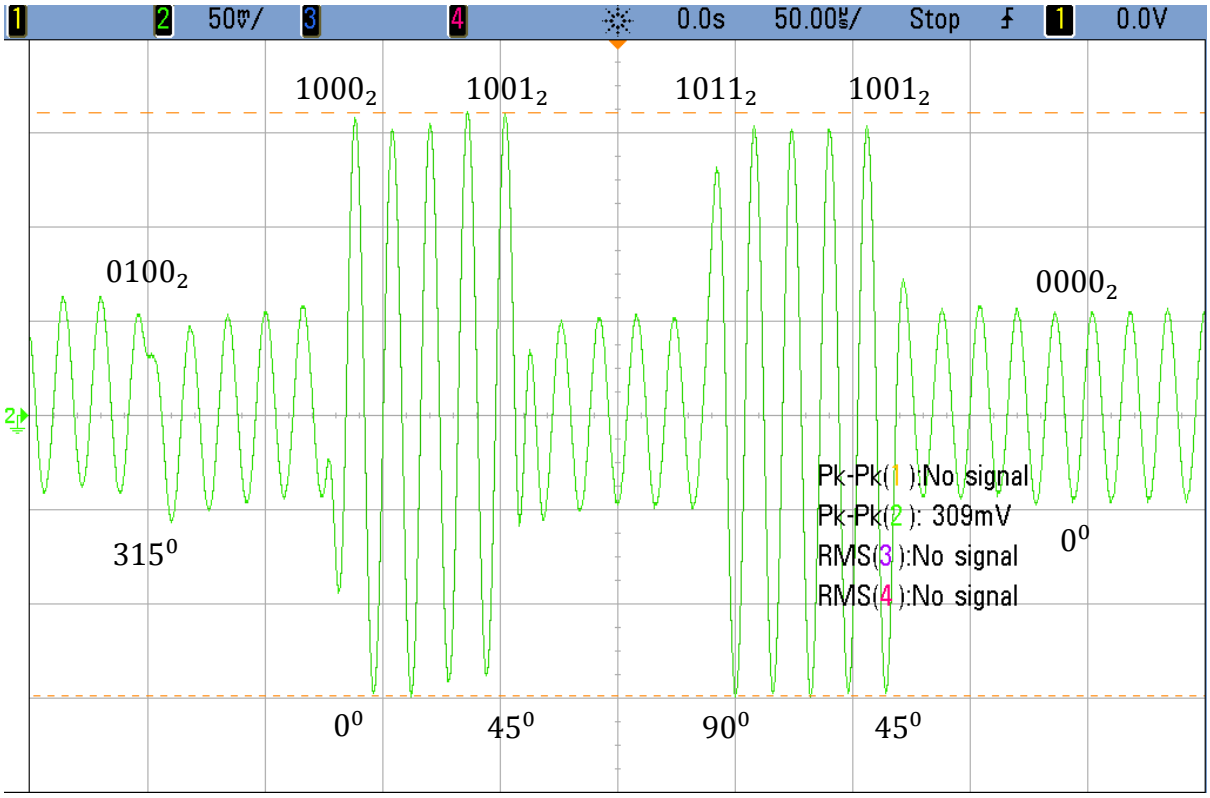

Figure 5.8: 16-QAM signal using Cyclone III FPGA DSP development board

5.2.2 Star 16-QAM Receiver

Chapter 4 discussed the phase detection of PSK signal and showed the disadvantages of Costas loop, Complex number and *ATAN* approaches where $n_{nb}(t)$ deviates the recovered carrier as proven in (72). It also showed that the 8-PSK signal can be demodulated using cross-correlation to replace all approaches of carrier recovery. The same principle and theory will be applied in this chapter to demodulate 16-QAM signal shown in figure 5.7 and 5.8. The 16-QAM is amplitude and phase data dependent compared to 8-PSK. The performance of the cross-correlation approach was derived in (78), chapter 4, section 4.2.2, when a $n_{nb}(t)$ presences across the transmitter-receiver channel. This also applies to 16-QAM receiver. However, the 16-QAM receiver will still suffer from $x(t), x(t-T_c)$, $y(t)$ and $y(t-T_c)$ amplitude noise in (77) that deflects and rotates the constellation points away from the origin. This requires an AGC and pre-filtering units keep SNR at reasonable level and the highest cross correlated points within the bounded area of the detected point shown in figure 5.1 over the symbol period.

The 16-QAM receiver shown in figure 5.9 is similar to the 8-PSK receiver shown in figure 4.26 and summarised in flowchart 4.3. This flowchart is modified to be 16-QAM receiver flowchart 5.3. The differences are; AM detector to demodulate BASK data; and MUXs to multiplex/amplify the amplitude signal by a factor of 3 to balance the amplitudes across all correlators to maximise the precision of cross-correlation. The MUXs were controlled using AM_timer VHDL entity over 1 carrier cycle, shown in Appendix I.6 and summarised in flowchart 5.4. The use of them was very good practice in the laboratory site compared to Matlab-Simulink. The simulation results in this chapter are without AM_timer.

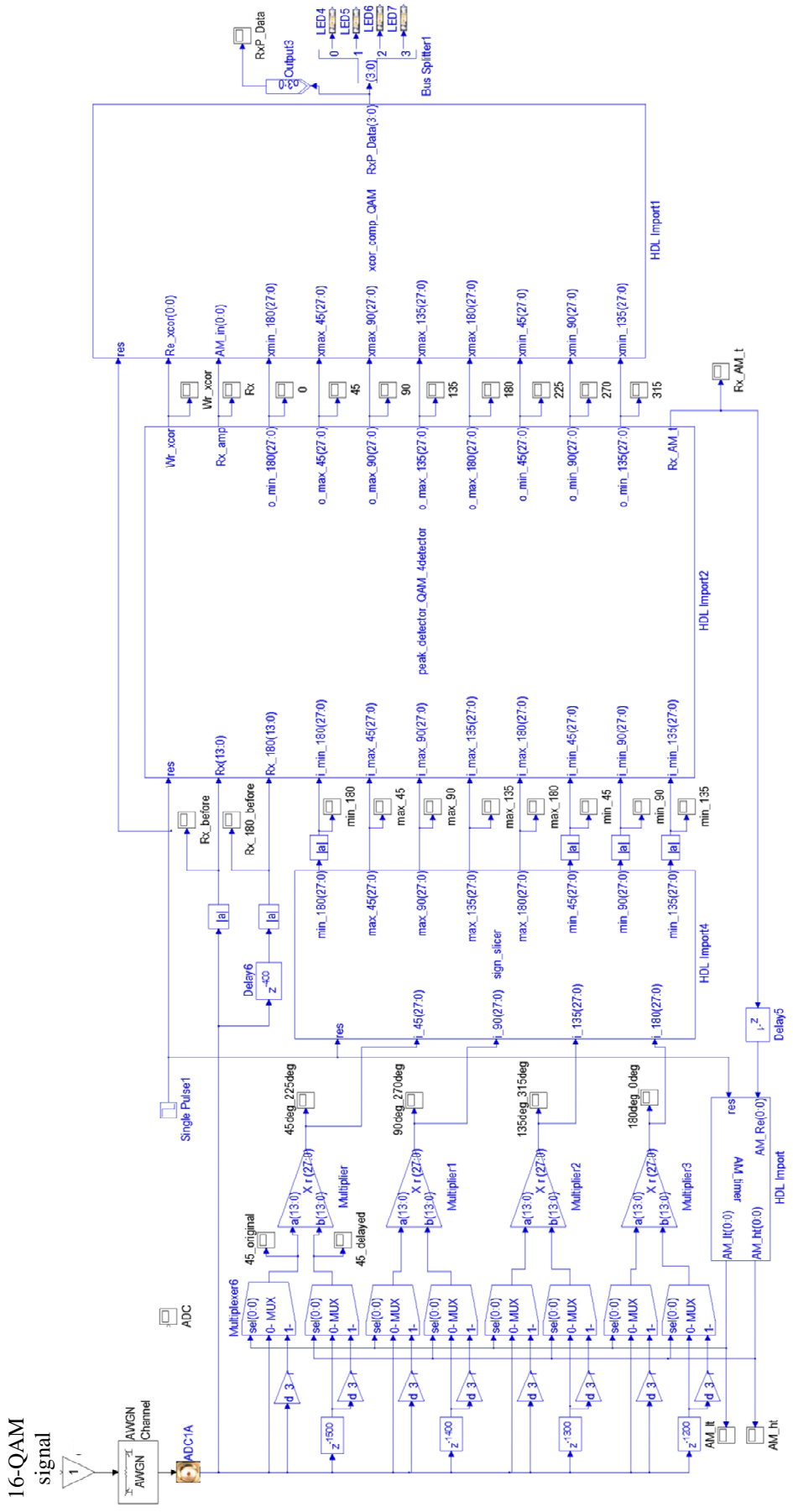

Figure 5.9: Matlab-Simulink and Altera-DSP Builder Implementation of 16-QAM receiver using cross-correlation approach

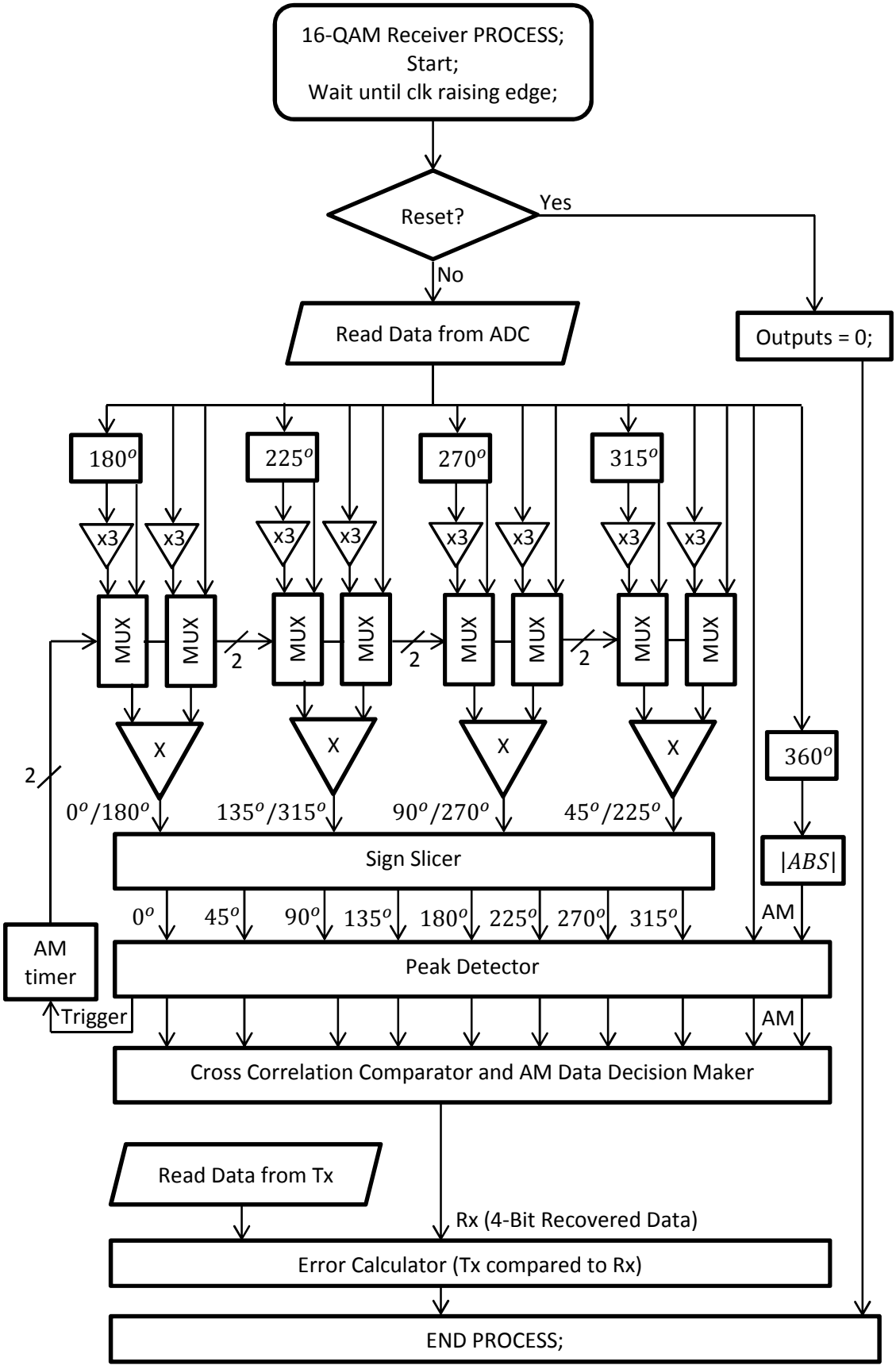

Flowchart 5.3: 16-QAM receiver VHDL process using cross-correlation

The general operation of the 16-QAM receiver is four detectors cross correlating the carrier by the complement transmitted angles to detect 8 separate phase angles and a timer to update and compare the cross correlated angles every half carrier cycle interval for instant observations. The cross correlated signals are separated into 2 parts and then the absolute value of both parts are obtained with the highest absolute value identifying the received data phase angle. In addition, the received signal is delayed 360^0 to compare it with current samples. These two signals are now differentially decoded by peak_detector_QAM VHDL code, summarised in flowchart 5.5. The peak_detector_QAM triggers the AM_timer once an AM signal is present. The AM_timer fed back a pulse width over a carrier cycle which multiplies the amplitude by a factor of 3. This balances the amplitudes input of the correlators which in return maximise the precision of cross-correlation.

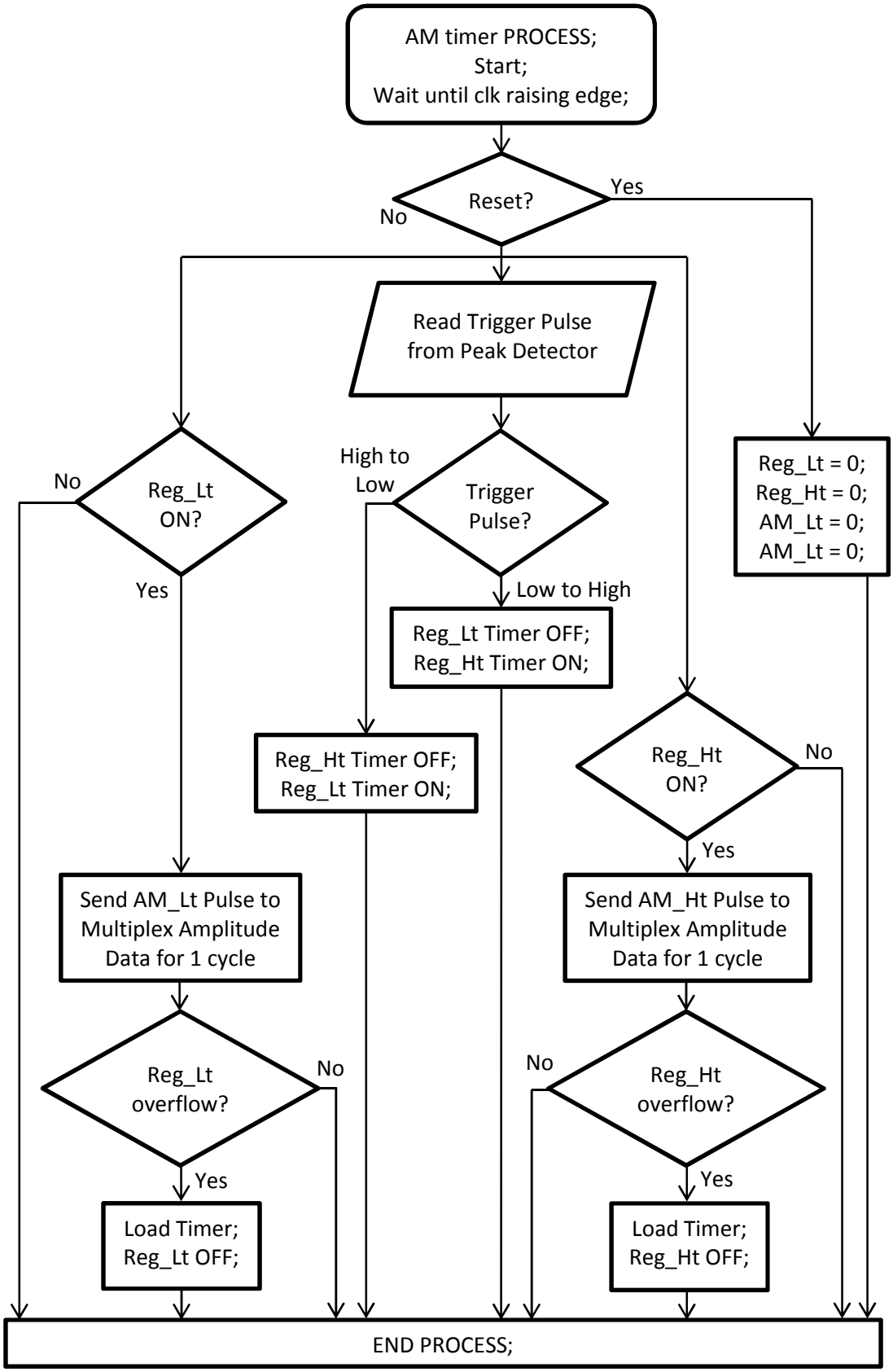

Flowchart 5.4: AM_timer VHDL process

Figure 5.10 shows a phase correlator of the 16-QAM correlators. The MUXs are controlled by AM_timer to control either the current or delayed samples. Table 4.5 shows the angles, their associated samples and complementary samples. Extra 800 samples (1 carrier cycle) were added to allow an enough time for the highest cross correlated point to be detected as what the practical examination showed at the presence of noise.

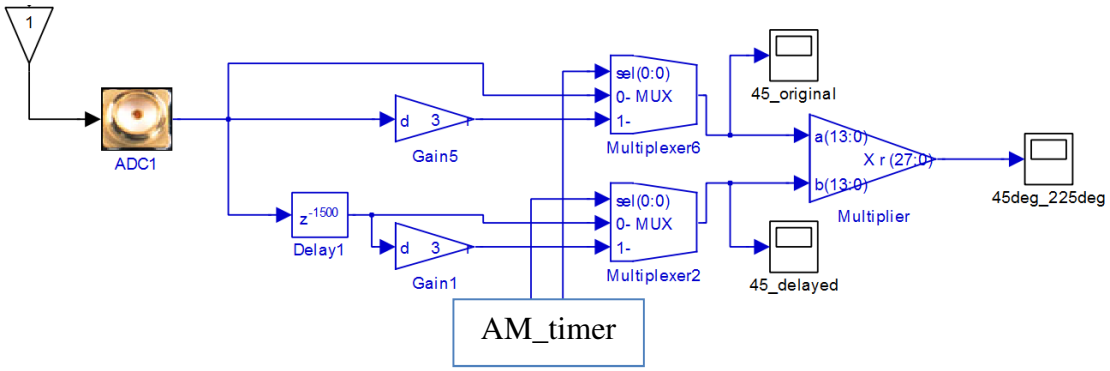

Figure 5.10: The correlator of 45^0 angle of 16-QAM receiver

Figure 5.11 shows output of the 16-QAM correlators. The phases were clearly sliced even at the presence of AM signal. This is apparent on the highest and lowest peaks as will be seen later.

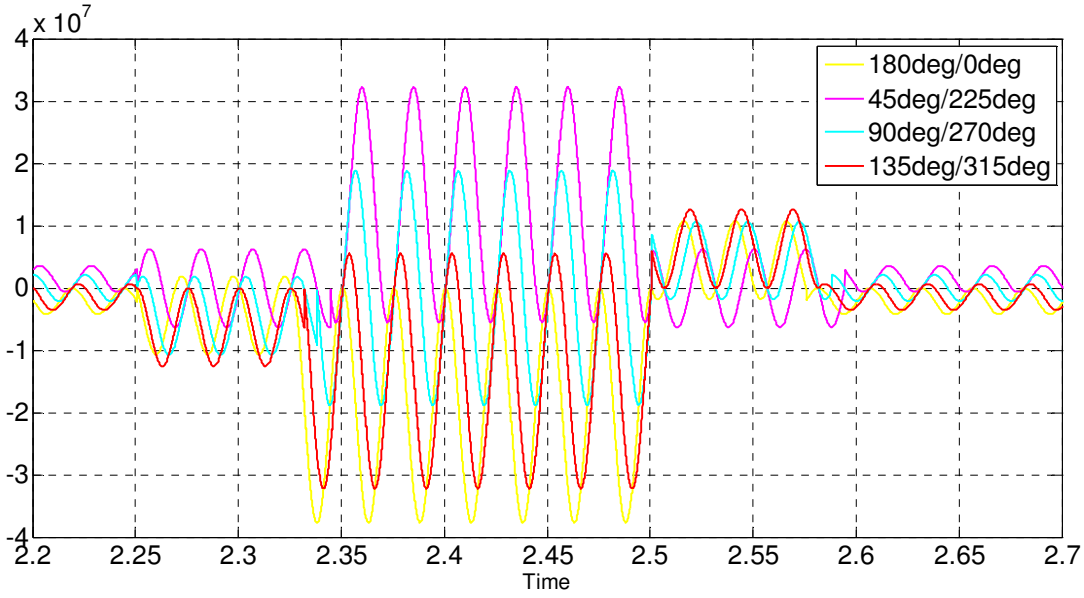

Figure 5.11: The 16-QAM correlators' outputs; $0^0/180^0$ (Yellow), $45^0/225^0$ (Magenta), $90^0/270^0$ (Cyan), $135^0/315^0$ (Red)

The correlated signals in figure 5.11 are now separated using the same sign_slicer used for the 8-PSK shown in flowchart 4.4. The absolute values of the negative parts were taken as shown in figure 5.12.

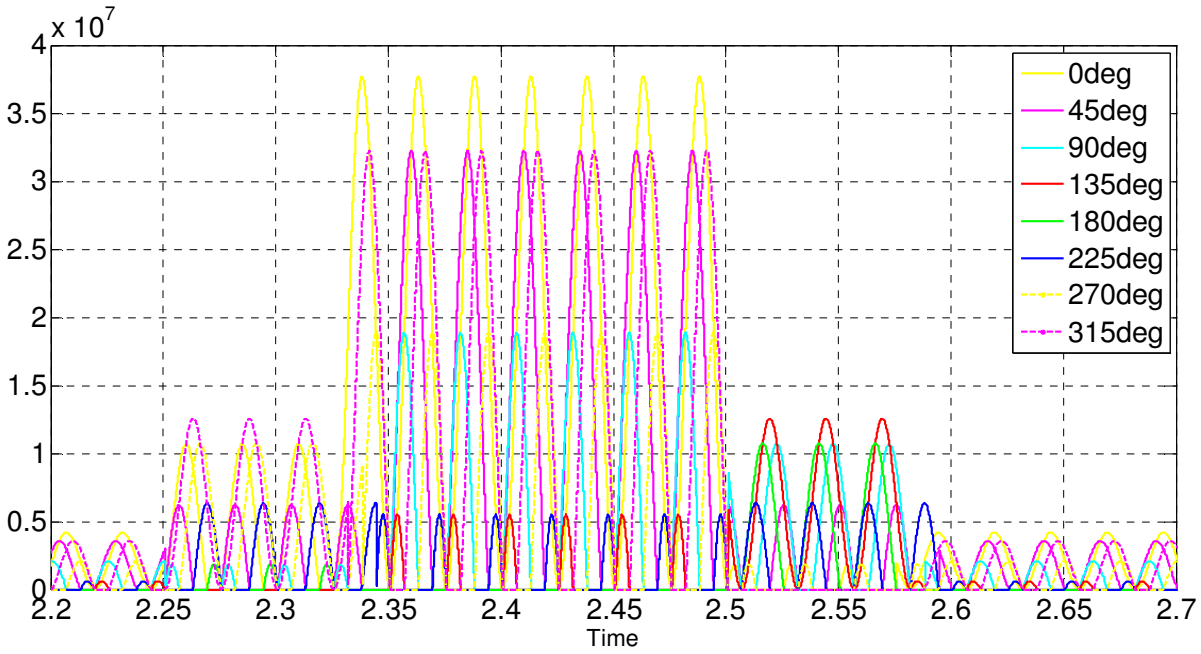

Figure 5.12: Correlated - Separated, 0^o (yellow), 45^o (magenta), 90^o (cyan), 135^o (Red), 180^o (Green), 225^o (Blue), 270^o (yellow), 315^o (magenta)

The peak_detector of the 8-PSK system is modified in this chapter. The peak_detector_ QAM VHDL code is shown in the Appendix I.7 and the behaviour is summarised in flowchart 5.5. It observes the AM and phase peaks separately. The phase peaks are observed over half the carrier cycle while the AM peaks are observed over quarter the carrier cycle whenever the current sample is greater than the previous sample. Any AM transitions would trigger the AM_timer and also indicates $a_n = 1_2$. The phase peaks are updated whenever the current sample is greater than the previous sample over half the carrier cycle. Once the phase timer overflowed, the highest detected phase peaks, AM data and a trigger pulse (Wr_xcor) of 8 samples are sent to the Cross Correlation Comparator (xcor_comp_QAM) shown in Appendix I.8 and summarised in flowchart 5.6.

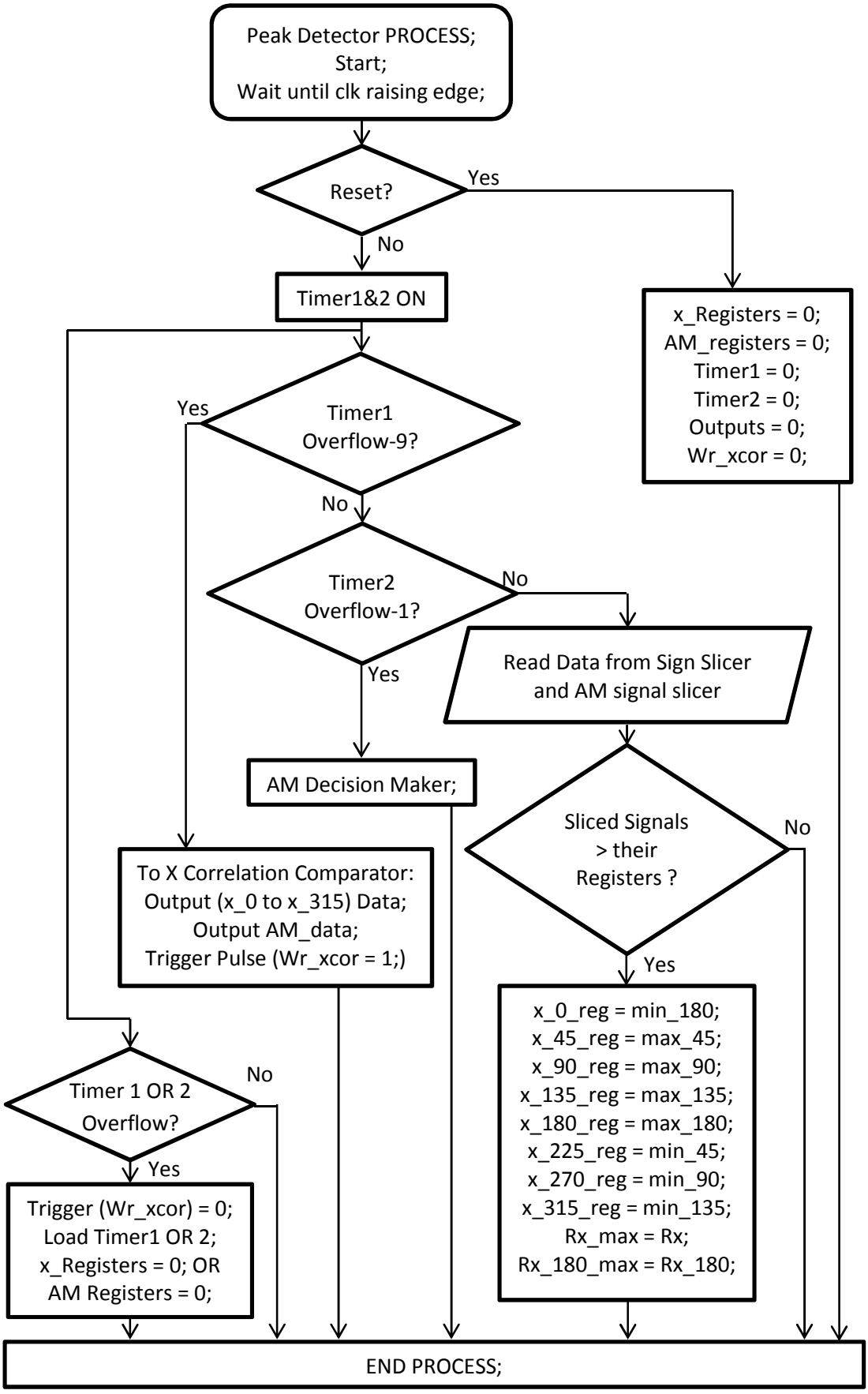

Flowchart 5.5: peak_detector_QAM VHDL process

Figure 5.13 shows the detect peaks of 16-QAM correlated in figure 5.11 and sliced in figure 5.12. The 16-QAM peaks are not consistent compared to the 8-PSK shown in figure 4.32. *The detected peaks were slightly delayed by the author in figure 5.13 to better explain the idea but practically there should be no delay for direct comparison of angles and data outputting.*

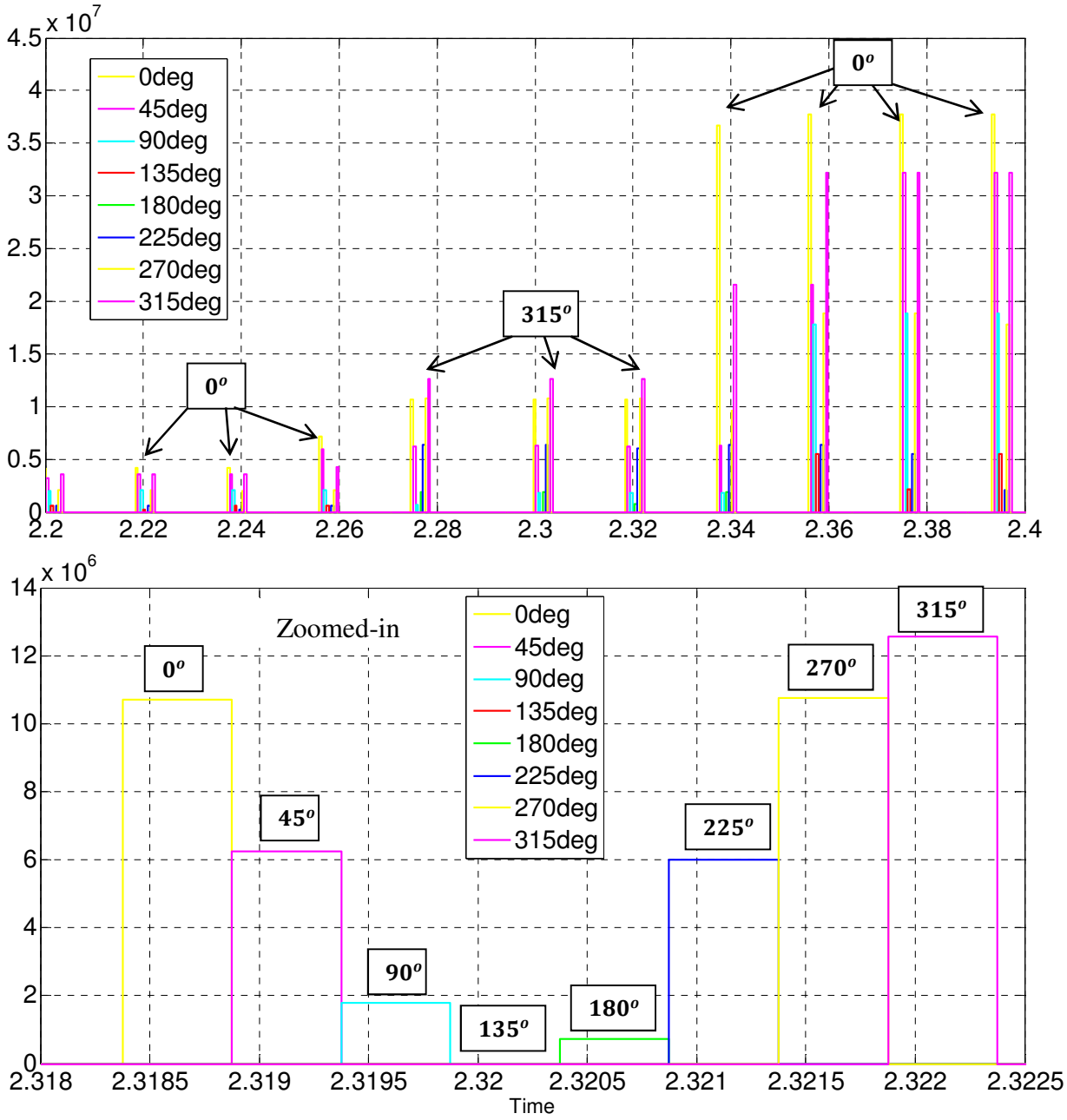

Figure 5.13: Detected peaks, where 315^0 is dominant and 135^0 is the weakest

As discussed previously, the highest peak in figrure 5.13 indicates the detected angle, 315^0. This is evident by checking the minimum peak shown in figure 5.13 which is the opposite angle, 135^0. Another example is shown in figure 5.14 when 0^0 is detected. It is apparent in figrue 5.14 that the 16-QAM peak detector has detected a leakage of the 45^0 angle caused by the delayed complement angle of the correlator. However such a leakage is cancelled out when compared by the Cross Correlation Comparator as the opposite angle is not confirmed.

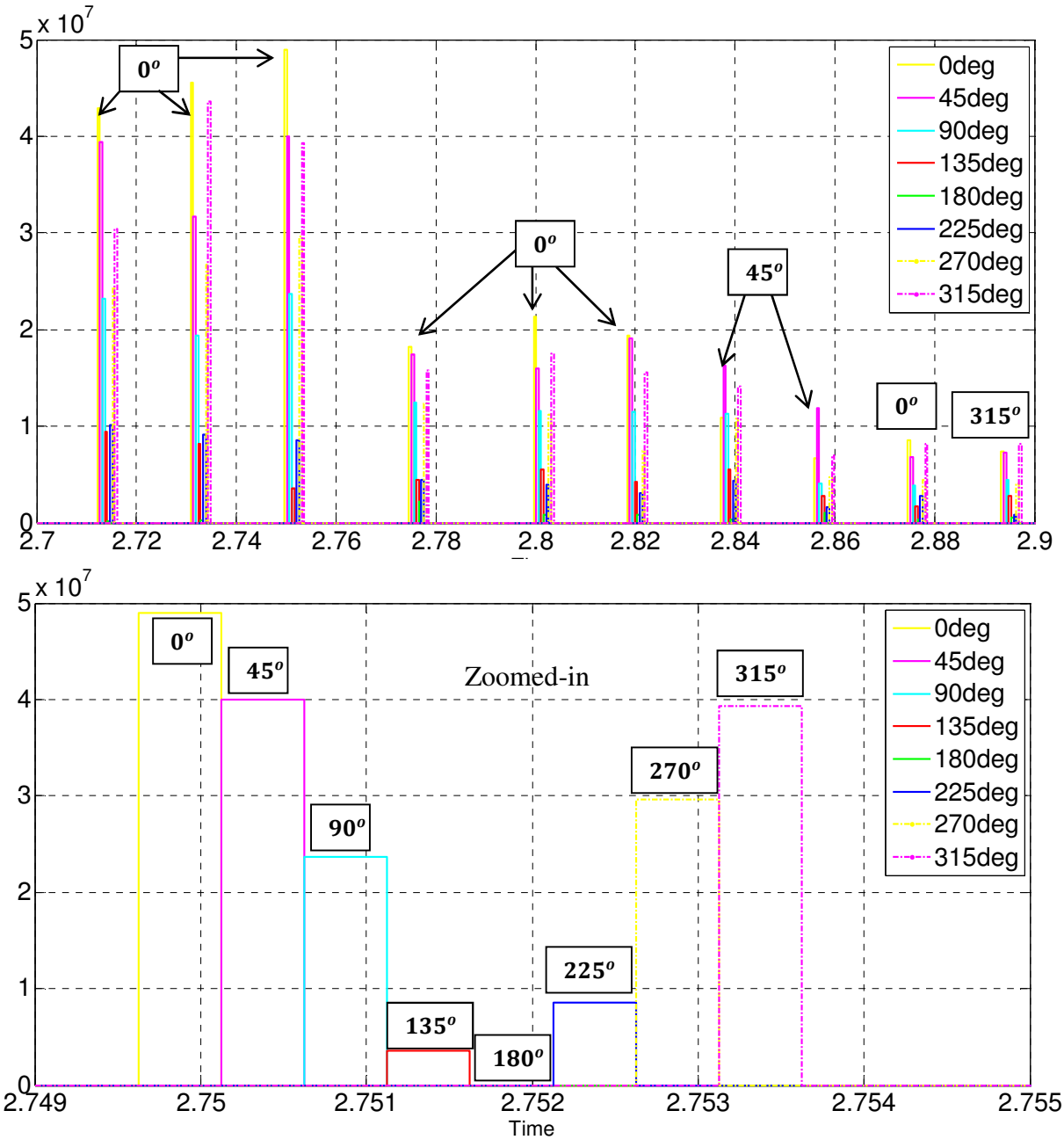

Figure 5.14: Detected peaks, where 0^0 is dominant and 180^0 is the weakest

Now, these 8 points could be compared using the Cross Correlatin Comparator (xcor_comp_QAM) code shown in Appendix I and summarised in flowchart 5.6. This code compares the points in figure 5.13 and 5.14 and combine the BASK data with 8-PSK data every time when it is triggered by (Wr_xcor) of the peak_detector_QAM code at the time of outputting the highest peaks. Since the transmitter is sending the data at rate of 0.25 s, the xcor_comp_QAM is updated regulary almost every 0.25 s.

A direct comparison of the transmitted and recovered data by xcor_comp_QAM is shown in figure 5.15. A delayed version of the transmitted data was displayed on figure 5.15 for the comparison. The receiver missed two symols at startup and then fully recovered the data.

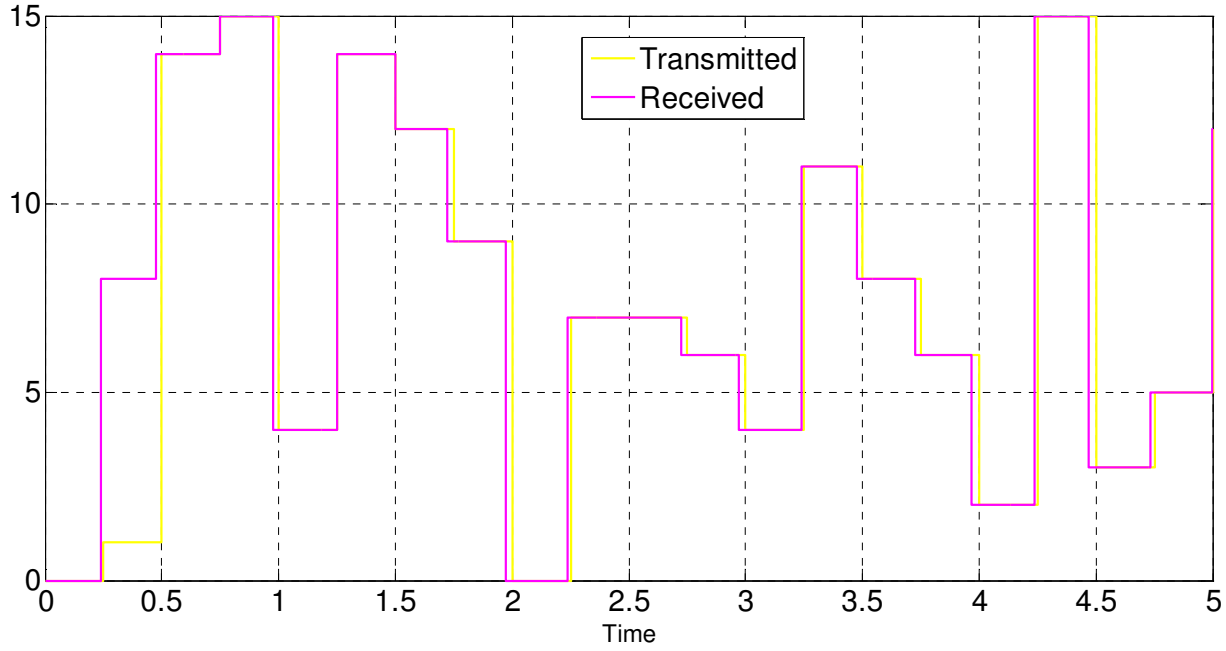

Figure 5.15: Comparison of the 16-QAM transmitted (yellow) and received (magenta) data over 5 s

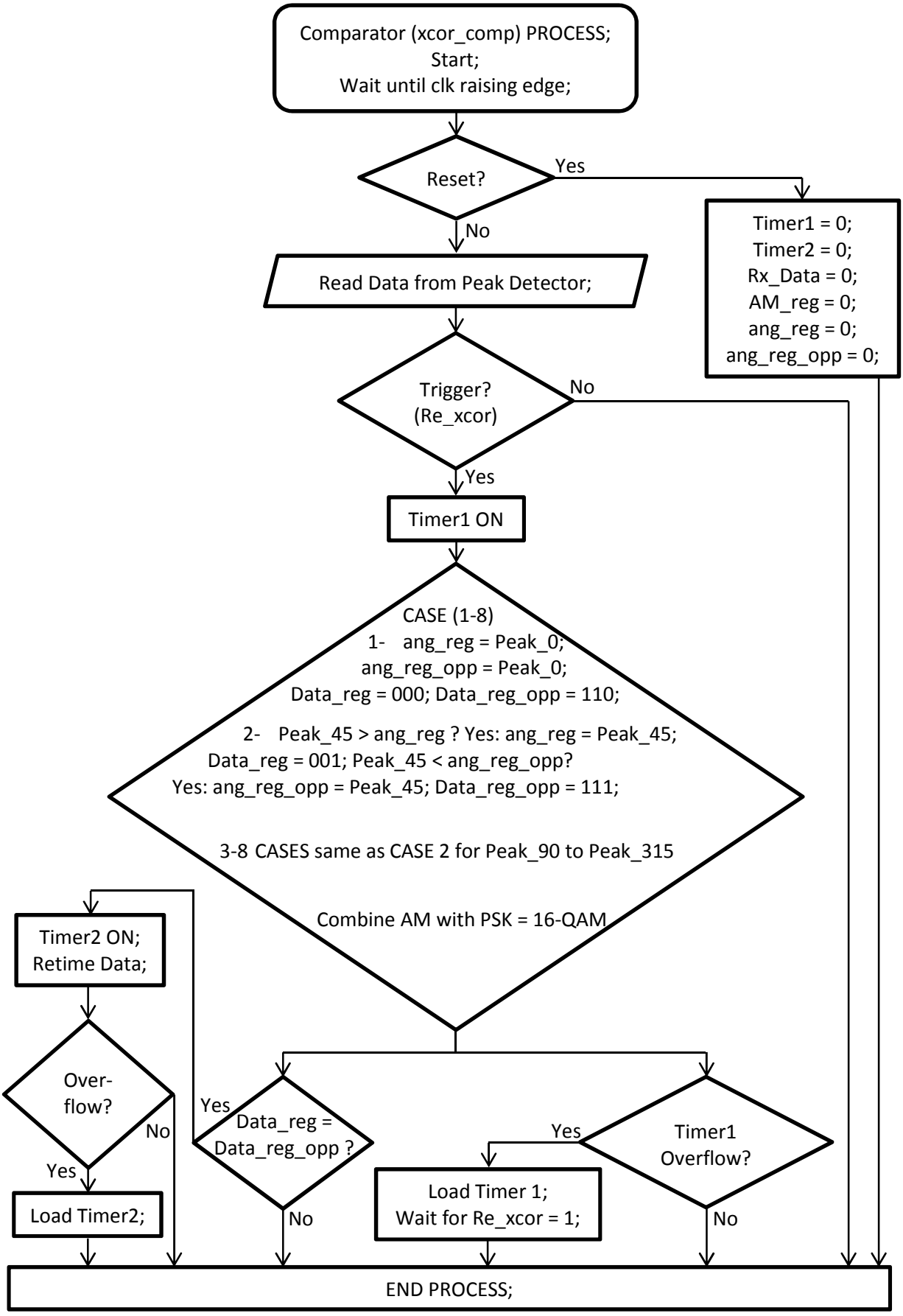

Flowchart 5.6: 16-QAM Cross Correlation Comparator VHDL process

5.2.3 Performance of cross correlation in Star 16-QAM detection

AWGN Channel of the Communication Toolbox in Simulink was used as shwon in figure 5.16 to introduce limitless noise across the 16-QAM transmitter-receiver channel as shown in figure 5.17. The link was successfully simulated in Matlab-Simulink at the presence of AWGN. The 16-QAM transmitter-receiver was also successfully implemented on FPGA in the laboratory.

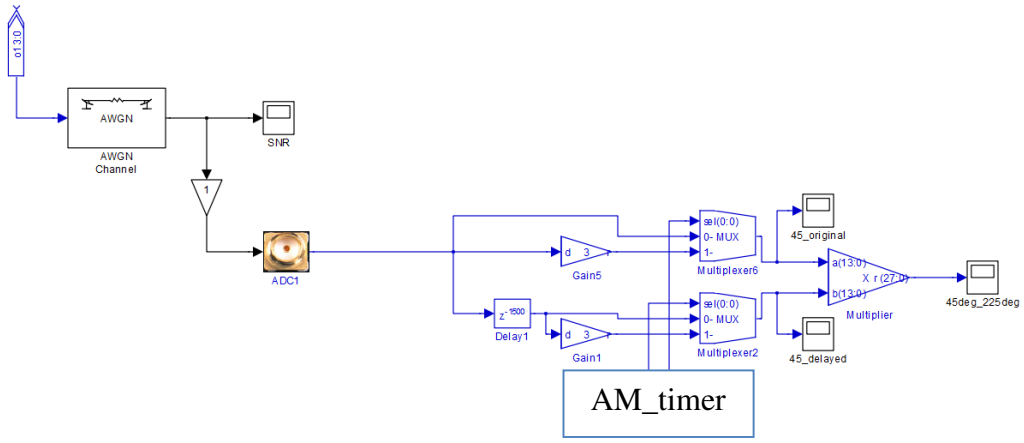

Figure 5.16: The 16-QAM correlator of 45^{o} in the presence of AWGN

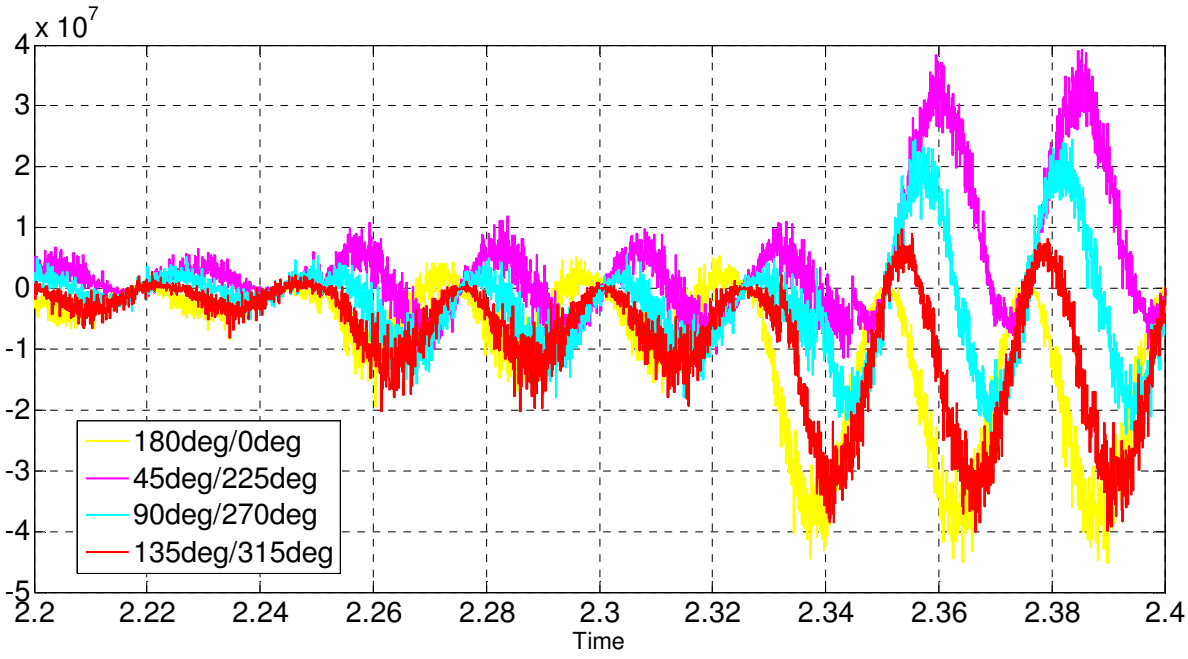

Figure 5.17: The 16-QAM correlators' outputs in the presence of AWGN

Figure 5.18 shows all the correlated – separated signals of the 16-QAM signal at the presence of AWGN. The noise is similarly digitised and confirmed the noise in (78), presented and observed in chapter 4, section 4.2.2. The zoomed-in area in figure 5.18 shows that the magenta (315^o) trace is dominant among all traces where the magenta (315^o) and green (45^o) are just close to the 315^o trace. This confirms that the cross correlated point is within the bounded area of the detected angle shown in figure 5.1.

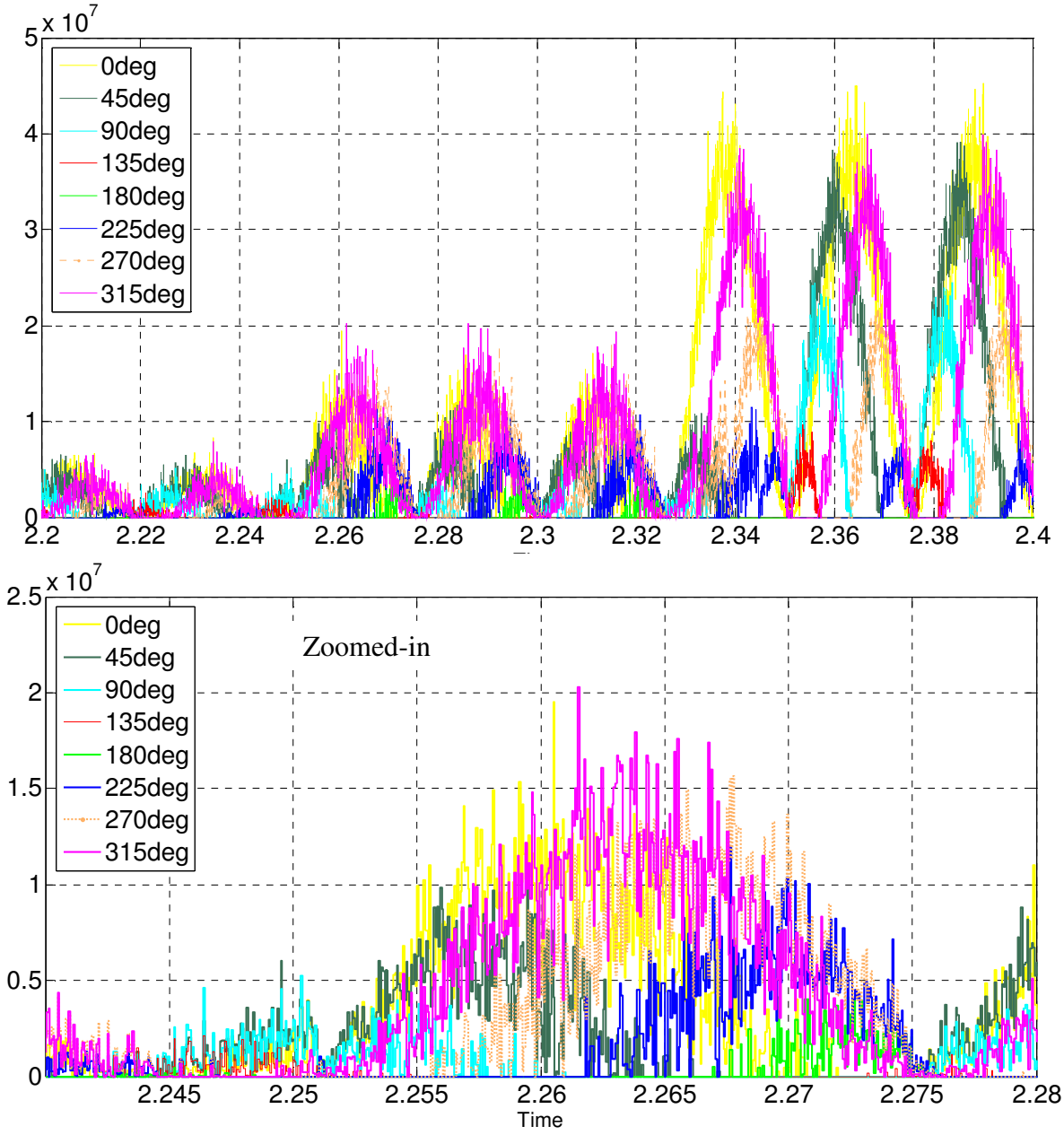

Figure 5.18: 16-QAM Correlated - Separated, all angles in the presence of 15dB AWGN

The peak_detector_QAM VHDL code observed the peaks of figure 5.18 every half the carrier cycle as presented in figure 5.19. Clearly, the AWGN affected the peaks of the cross correlated points. A close-up to the peaks detected is shown in figure 5.19 (bottom) where the *Comparator* compares the highest (detected angle) to the minimum (opposite angle) peaks, retimes any new data and eventually outputs the received data. The new angle is 315^0 (maximum) and evident by the opposite angle 135^0 (minimum). The peaks on the far right are ignored by the *Comparator* as the angle (maximum) and its opposite (minimum) are not valid.

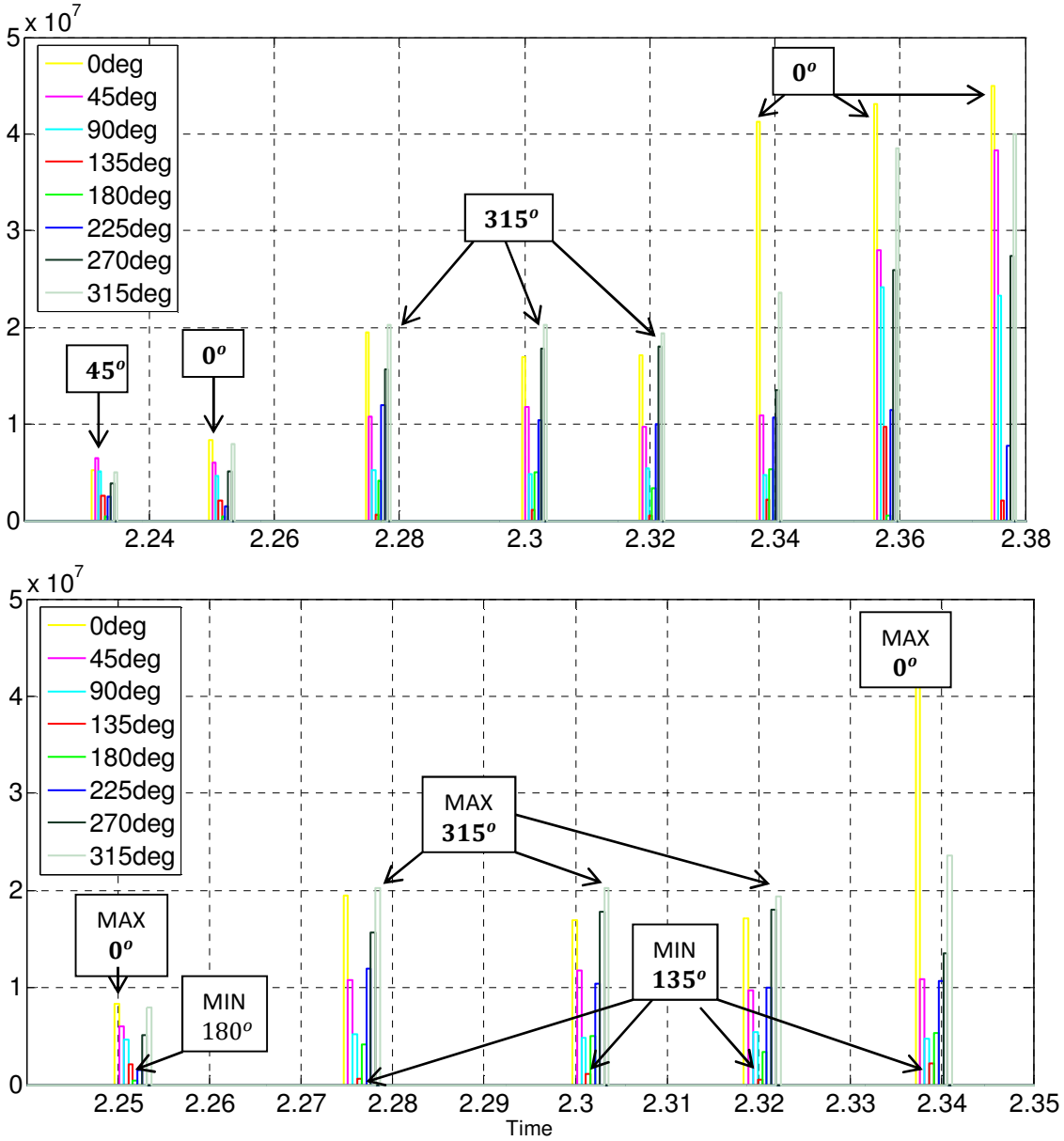

Figure 5.19: Detected Peaks where 315^o is dominant and 135^o is the weakest at 15 dB

Figure 5.20 shows an error detected at 12dB SNR. The error was found at 135^0. Figure 5.21 analyses the detected peaks where 135^0 was detected twice and 315^0 was just detected before 135^0 as well due to the AWGN. This is unavoidable and misleads the *Comparator*. This confirms the need of pre-filtering and AGC units to keep CNR at reasonable level.

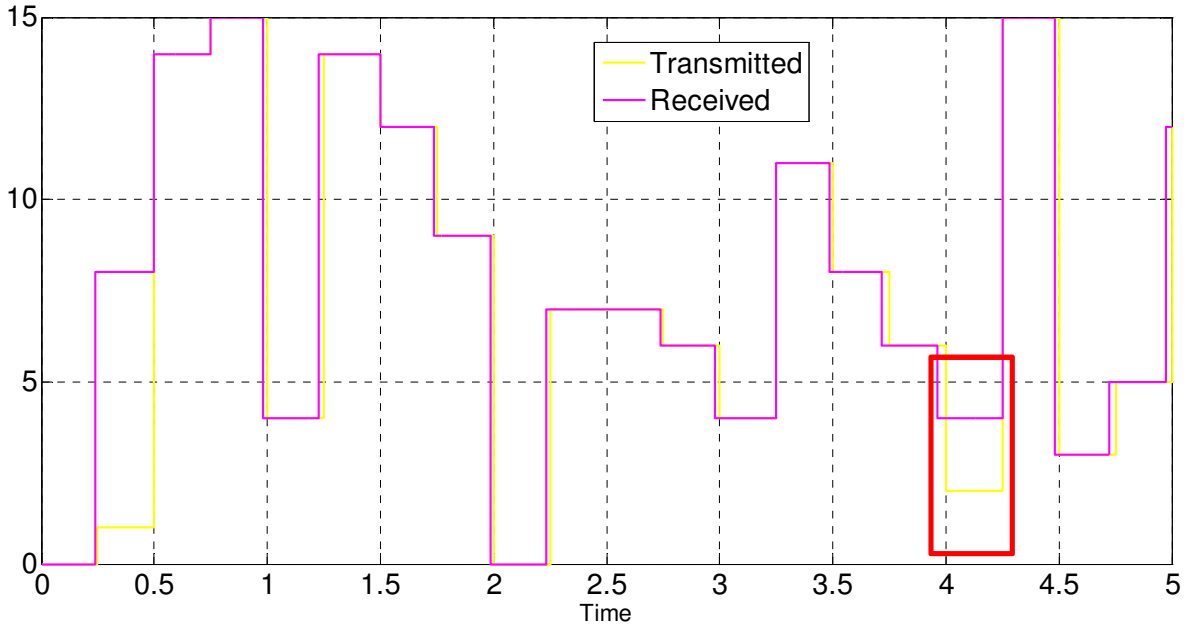

Figure 5.20: 16-QAM transmitted (yellow) versus received (magenta) data at 12 dB, detected an error

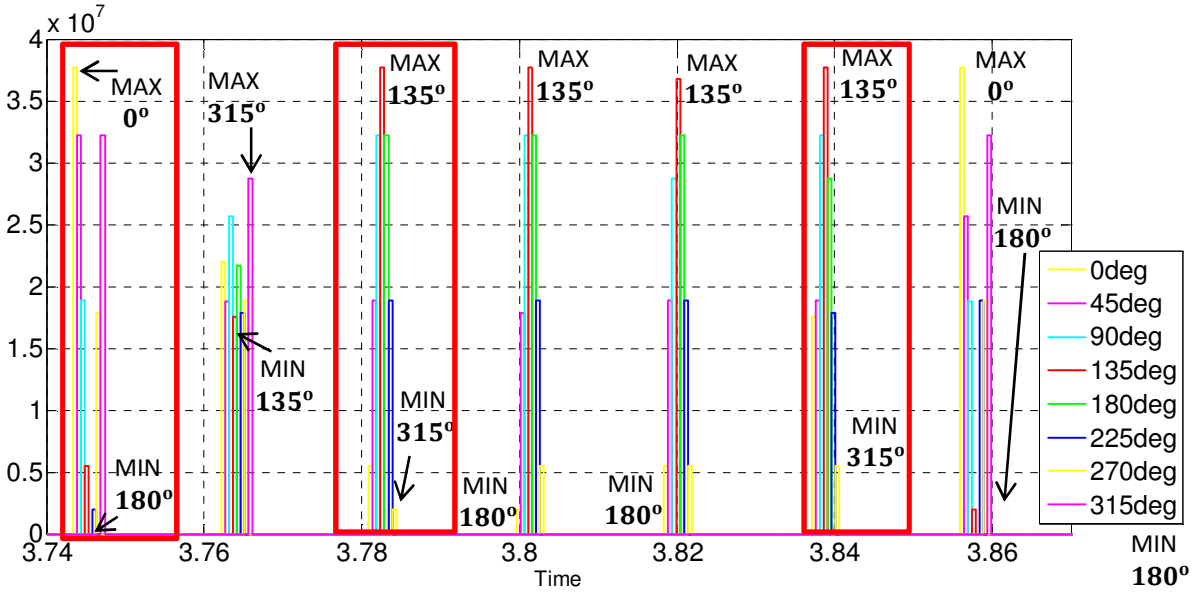

Figure 5.21: Detected Error of 135^o (red) angle at 12 dB

Flowchart 5.7 shows the behaviour of 16-QAM *Error Calculator* to compute the differences between the transmitted and received symbols/bits. The VHDL code shown in Appendix I.9, counts the total symbols/bits and computes the differences separately. At the end, the code computes the symbol and bit error.

The concept of using cross correlation to demodulate the 16-QAM signal was proven in Matlab-Simulink and in the laboratory using practical implementations of FPGA. However, the practical implementation needs to be optimised as the HPF of the DAC unit affects the phase and amplitude of the 16-QAM transmitter as shown in figure 5.8. In addition, the 14-bit ADC input is limited to 512 mV while the laboratory is rich in 50 Hz ambient noise that can be easily measured with Oscilloscope. Table 5.2 summarises the transmission attempts over 1s to fix the practical issues by varying the window size of the AM and Peak detector. In fact when the AM detector, detects BASK data, it empties the correlators registers to record the new peaks as the 16-QAM signal goes from high to low otherwise the peak_detector_QAM would not be able to update the registers. Hence, wrong data are detected. Thus, table 5.2 shows the best time for Peak Detector is 250 samples plus 200 samples for the AM detection (450 samples in total) compared to the 8-PSK that require 500 samples. The optimisation of the practical implementaion is left as further work due to the time limitation of the research.

MUXs are enabled, total symbols = 12,500 symbols, total bits = 50,000 bits						
Peak Detector timer	249	299	349	399	449	499
AM_timer	199	199	399	199	549	299
Bit_error	295	370	261	386	795	790
Symbol_error	267	294	226	224	511	483
MUXs are disabled, total symbols = 12,500 symbols, total bits = 50,000 bits						
Peak Detector timer	249	299	349	399	449	499
AM_timer	299	349	399	499	549	549
Bit_error	517	526	212	452	769	949
Symbol_error	383	369	202	331	460	624

Table 5.2: A summary of varying the AM and Peak detectors windows to cope with the practical issues

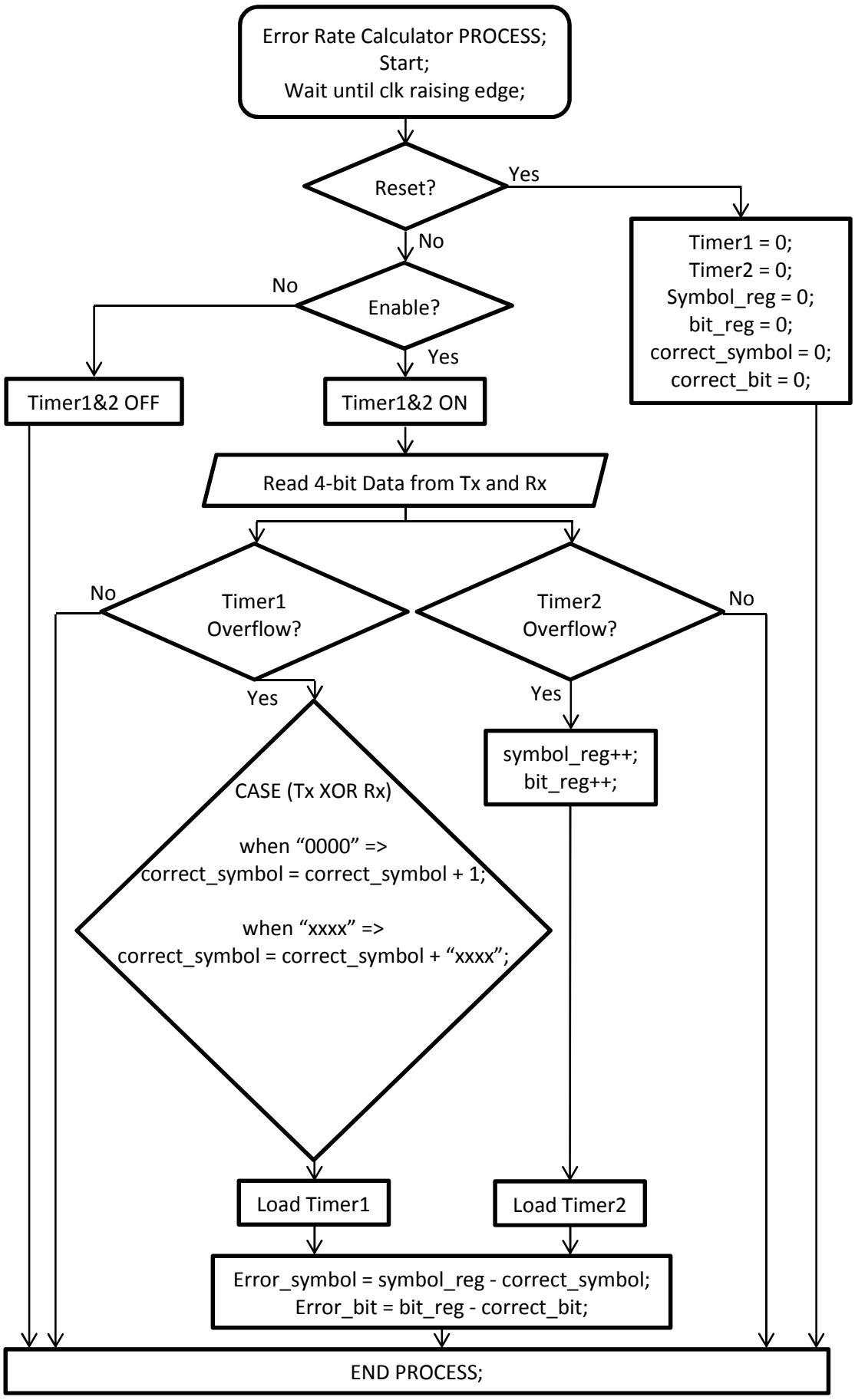

Flowchart 5.7: 16-QAM Error calculator VHDL process

5.3 Comments on QAM transmitter/receiver

The constellation points of Square QAM optimise the transmission over Gaussian channel compared to Star QAM [72]. The Square QAM requires AGC and carrier recovery for coherent detection [34], [42], [44], [72]. The carrier recovery is severely affected by the fading channel [34], [40], [42], [44], [72]. In contrast, Star QAM reduces the effects of Rayleigh fading [34], [72]. The AGC in Square QAM has to maintain stability fast enough to decode the AM data [34], [42], [72]. The symbols in Square QAM are strictly dependent on *A* and θ_t. On the other hand, the amplitude can be tracked easily in the case of Star 16-QAM to decode the BASK data separately from the phase data θ_t. The Star QAM does not experience false lock positions and the transmitted mean power is relatively smaller compared to the Square QAM [68]. In addition, it has the property that PAPR is less than that for Square QAM [35]. For this reason, Star 16-QAM is preferred to Square QAM in OFDM systems to keep the effects of PAPR low [4]. Moreover, the coded Star 16-QAM symbol error rate is better than that of Square 16-QAM [35].

An Altera CYCLONE III EP3C120F780C7N based DSP development board was used to develop the 16-QAM link for the same transmission rate of the 8-PSK in chapter 4, hence the same bandwidth. The authors of [39] implemented a carrier recovery system for Square 16-QAM and the authors of [43] implemented Square 16-QAM receiver based on FPGA using the *ATAN* function and digital PLL. Hence, a direct comparison of the number of FPGA system resources, to these works is given in table 5.3. Clearly, the proposed demodulation scheme significantly reduced the number of Embedded Multipliers to demodulate 16-QAM compared to [39], [43]. In addition, the prototyped scheme does not need carrier recovery and uses only 4 Embedded Multipliers compared to [39] that uses 8 Embedded Multipliers just to extract the carrier prior demodulation.

Type of resources	Resources used by carrier recovery [39]	Resources used by Square 16-QAM receiver [43]	Resources used by Star 16-QAM [thesis author]
Embedded Multipliers	8	48	4
LUTs	Not presented by [39]	4674	1858

Table 5.3 16-QAM Implementation Resources Requirements

The concept of using cross correlation to demodulate the 16-QAM signal was proven by using Matlab-Simulink and practical implementations of FPGA. The cross correlation has been used for the first time in the Star 16-QAM demodulator system, replacing the *ATAN* function and DPLL to detect the phase change on the received signal. This yields a significant reduction in terms of complexity and the silicon required to integrate the Star 16-QAM receiver onto an IC. The reduced complexity of the receiver leads to a reduced number of resources required, for the design, and thus power consumption of the system. This technique will yield cost reduction in products using 16-QAM demodulators, namely broadband internet and Digital TV. The 16-QAM is one of the standard modulation schemes in OFDM [3] applications such as DVB-T, and HIPERLAN [2], [4]. The 16-QAM is widely used in WCDMA, HSDPA, WiMAX, WLAN, ADSL and HDSL broadband technologies [1], [2].

The practical implementations need to be optimised to perform the probability of error tests over the proposed scheme. The use of error coding should improve the performance. The receiver should be Electromagnetic Compatibility (EMC) shielded as the laboratory site is rich in 50 Hz noise.

6. Discussion and further work

Chapter 2 has reviewed the use of ground as transmission medium, current uses of ELF band in communication, digital modulation techniques and multi-carrier communication systems. Chapters 3, 4 and 5 have investigated ASK, PSK and 16-QAM digital communication schemes in detail. This chapter discusses the issues and applications related to the use of ground as transmission medium, ELF band and multi-carrier (i.e. OFDM) communication systems in implementing a complete ELF Transmission Data Link based on the facts presented in the literature review and the implementations of the digital modulation schemes in chapters 3, 4 and 5.

Briefly, the analysis in chapter 3 and 5 showed that the BASK data can be easily tracked by comparing the absolute values of the current sample with a delayed full carrier cycle. In addition, the analysis in chapters 4 and 5 showed that demodulating phase data is generally performed using carrier recovery. Consequently, this inspired the need for a novel and simpler function than the carrier recovery, which is where the concept of cross correlation to detect the phase changes was investigated in chapter 4. As it does not extract the carrier for demodulation purposes; the proposed detection scheme offers improved phase detection performance as well as superior resistance to AWGN compared to a carrier recovery scheme operating at low SNR. Patent literature review showed that there is no such patent or known prior art related to the presented system design in chapters 4 and 5. The previous methods require high system resources in terms of IC silicon area to implement the 8-PSK and 16-QAM receiver using the ‘tan’ function, complex mathematical operations and thus IC resources that consume more system power. The author of this thesis concluded that demodulation of phase data can also be undertaken using the cross correlation function that need maximum 4 multipliers, which requires significantly less multipliers than carrier

recovery units, thus IC resources. The reduced complexity of the receiver leads to a reduced number of resources required, for the design, and thus power consumptions of the system. To the author's knowledge, cross correlation was used, for the first time in the 16-QAM demodulator system. This technique will yield cost reduction in products using 8-PSK and 16-QAM demodulators, namely broadband internet and Digital TV.

6.1 OFDM design

With reference to chapters 3, 4 and 5; a single carrier of 20 Hz is capable of sending *4 symbols/s*; 4 bps, 8 bps, 12 bps and 16 bps using BPSK, QPSK, 8-PSK and 16-QAM respectively where the bandwidth will be twice the symbol rate for all techniques. So, if the minimum ELF subcarrier frequency used in OFDM system shown in figure 2.18 is 20 Hz and the maximum ELF subcarrier frequency is 280 Hz, then there will be a large delay caused by the large number of cycles per symbol in 280 Hz that may shut down the receiver. Thus, using OFDM system in ELF band will limit the number of sub-carriers per channel. However, a possible OFDM channel can be made up of 8 subcarriers spaced at 4 Hz where the minimum subcarrier of this channel is 16 Hz and maximum subcarrier is 44 Hz as shown in figure 6.1 to avoid the noise effects of 50 Hz of the power feed cables. Each subcarrier is capable of sending 4 symbols/s and 16 bps in total whereas the whole channel is capable of sending 8 $subcarriers \times 16\ bps = 128\ bps$ in total.

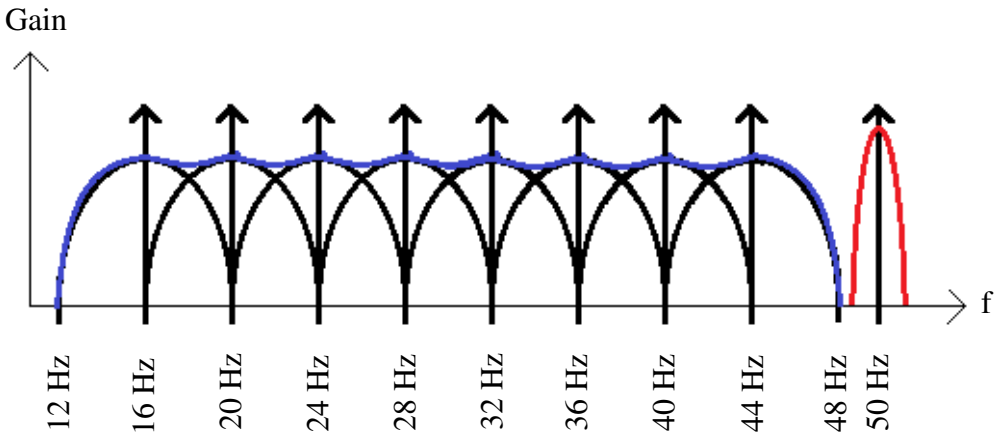

Figure 6.1: Possible ELF – OFDM channel lower than 50 Hz

Similarly, another possible OFDM channel can be made up of 13 subcarriers spaced at 18 Hz where the minimum ELF subcarrier of this channel is 72 Hz and maximum ELF subcarrier is 288 Hz as shown in figure 6.2 to avoid the noise effects of 50 Hz of the power feed cables. Each subcarrier is capable of sending 18 symbols/s and 72 bps in total whereas the whole channel is capable of sending 13 $subcarriers \times 72\ bps = 936\ bps$ in total.

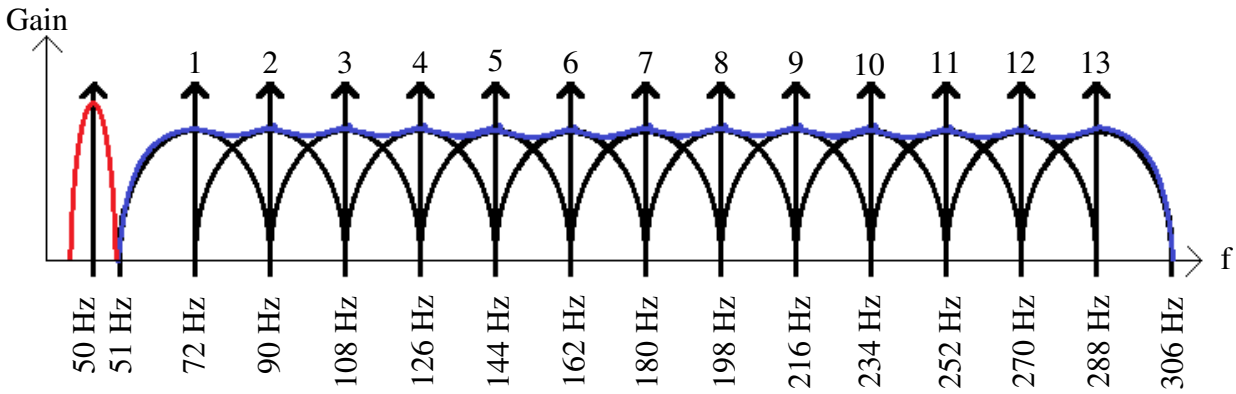

Figure 6.2: ELF – OFDM channel higher than 50 Hz

The first and second ELF – OFDM channels have a speed of 128 bps and 936 bps respectively. Each channel could be divided to two halves for FDD transceiver communication where the speed will consequently be halved. Alternatively, both channels can be used in one FDD transceiver communication link so that one channel is faster than the other. This scenario is useful for admin and user transceivers remote control so that the admin is always faster than the user.

Another scenario is to use the two channels to achieve 1,064 bps OFDM throughput of transmission in parallel with TDMA as in Walkie Talkie radio. This way, a user engages the channel and the others wait for the channel to be freed.

6.2 CDMA in ELF

SC-CDMA allows multiple access but significantly make the usable data speed much slower than what it is expected with QAM system. However, MC-CDMA using OFDM would allow multiple access within the ELF channel but the drawbacks are the speed of the link and the limited bandwidth. This needs a further investigation of coding scheme that suit the ELF data link.

6.3 Noise in ELF band

Noise is a major problem when transmitting/receiving data through wireless channels. Shot noise is generated by the random flow of charge carriers in semiconductors and thermal noise occuring in resistive components due to the thermal agitation of electrons in resistors [78], [79]. Another type of noise is called flicker (pink or 1/f) noise. It is inversely proportional to the frequency being used and expected to affect the ELF link at such low frequencies [66], [67], [78], [79]. Flicker noise usually occurs in Metal-Oxide Semiconductor Field-Effect Transistor (MOSFET) systems but Junction Field-Effect Transistor (JFET) and Bipolar systems have less 1/f noise than the MOSFET [66], [67], [78], [79]. It is envisaged that JFET systems [66], [67] should be used in the ELF link to keep the 1/f noise low. In addition, the 50Hz radiation of the power feed cables underground requires very narrowband notch filter to attenuate it for better SNR.

6.4 Ground antenna

The literature review showed that Mr. Stubblefield and cave radios use the inductive field between the earth electrodes to communicate through the ground itself. Simple calculations of useable antenna size could explain and confirm the idea of inductive communication. The calculation of any physical size of useable antenna is based on the wavelength, speed of light and carrier frequency [80].

For instance,

$f_c = 20\ Hz$, carrier frequency

$C = 300\ \times 10^6\ m.s^{-1}$, speed of light

$\lambda = \frac{C}{f_c}$, wavelength [80]

$$\therefore\ \lambda = \frac{300\ \times\ 10^6\ m.s^{-1}}{20\ Hz} = 15{,}000\ km$$

The wavelength λ size is longer than the diameter of earth planet that is 12,752 km [81]. There are several types of antennas such as dipole, folded dipole and monopole antennas [80], [82], [83]. Each one has its own characteristics such as the impedance, bandwidth, length, etc [80], [82], [83]. Dipole antenna is widely used in analogue TV reception and requires half the wavelength 7,500 km [80], [82], [83]. Moreover, folded dipole antenna is widely used in top roof TV aerial and requires full wave length 15,000 km [80], [82], [83]. Also, monopole is widely used in TV broadcasting tower antennas and requires quarter of the wavelength 3,750 km [80], [82], [83]. In addition, loading coil [80], [82], [83] is widely used in handheld radio systems and can be used to reduce the length of the antenna to less than quarter the wavelength if used in series with the monopole lead. Clearly, all the types of the

discussed antennas require large area to implement an antenna for just one transceiver even if a loading coil is used. So, this justifies the purpose of using the ground itself as transmission medium and confirms the use of induction in between the earth electrodes to communicate underground. Therefore, a high conductive material, earth electrode is essential to enhance the transmission and reception of signals. The Stubblefield's, Molefone and HeyPhone systems used steel rods [13], [17]-[19] that has a conductivity [84] of $\gamma = 0.9 \times 10^7\ \Omega^{-1}m^{-1}$ but various materials have a better conductivity [83]-[86] compared to steel such as silver, copper and aluminium as shown in table 6.1.

Material	Conductivity ($\Omega^{-1}m^{-1}$)	Proportion to steel (%)
Silver	6.17×10^7	685.6
Copper	5.8×10^7	644.4
Gold	4.10×10^7	455.6
Aluminum	3.82×10^7	424.4
steel	0.9×10^7	100
Stainless Steel	0.11×10^7	12.2

Table 6.1: Conductivity of materials compared with steel [83]-[86]

Table 6.1 shows that the silver, copper and gold have the best conductivity ever. Silver and gold are really expensive compared to copper where copper is widely used in electrical earthing systems of buildings [28], [29]. Aluminium is cheaper than copper in which can be

used in ELF communication link instead of steel to provide an almost 4 times better conductivity as indicated in table 6.1.

Therefore, the antenna of the ELF communication link was designed using a high conductive aluminium round solid bar, round tube and square plate as shown in figure 6.3. The designed antenna is expected to reference the transmitted signals to the ground via the round tube [57].

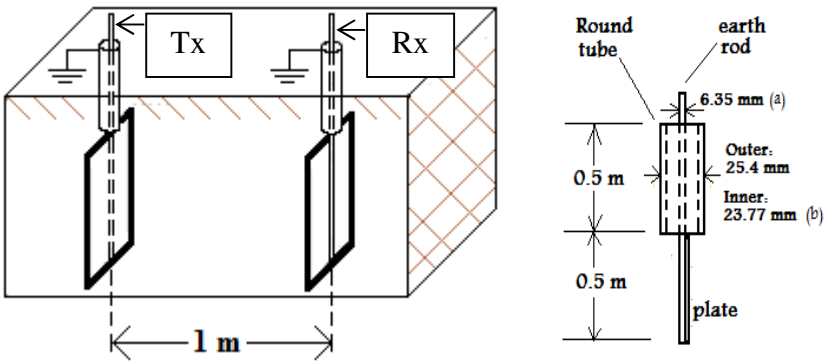

Figure 6.3: Cross section area of the transmission medium and antenna [57]

Figure 6.3 shows a cross-section-area of the prototype environment design which can be used in parallel with real environment to classify the propagation characteristics per meter by applying various simulations events across the region of antenna like vibration, raising the conductivity using water and clay, and wrapping electrical cables in order to simulate the noise of the feed cables buried below the level of the ground. Initial tests can be conducted using DC and sine wave signals to test the conductivity of the ground and eventually compare it to the prototype design results. Thereafter, the transmission distance is to be measured and repeaters can be used to regenerate the signal for long transmission distance. The propagation characteristics test is left as further work due to the time limitation of the research.

6.5 Applications

As discussed previously in chapter 2, section 2.5.2 that the use of ELF band and ground as transmission medium in civil applications is negligible. A generic communication link was suggested in section 2.5.1 based on the use of 16-QAM and OFDM to enhance the transmission rate at low frequencies which could replace RF in some applications.

More importantly, cave radios such as Molefone, HeyPhone and System Nicola still use 87 kHz that is part of LF band for subterranean communication [17]-[21]. These cave radios have achieved a transmission distance of 800m using earth rods with features like text messaging [17]-[21]. So, with reference to the US navy's observations [23]-[26] (the lower the frequency being transmitted the deeper it penetrates seawater) and the observations of the reporters [9], [13], [15] who tested a good quality of voice transmission of Stubblefield' system using steel rods stuck 1 mile apart into the ground without using communication repeaters in between, a novel ELF data transmission link can be developed based on the these criteria and circumstances to achieve long transmission distances at low power compared to Stubblefield's system, Molefone, HeyPhone and System Nicola. In fact ELF is slower than LF but with help of QAM and OFDM techniques as discussed previously, the transmission rate can be enhanced at such low frequencies and replace the use of SSB in cave radios. A flexible digital data communication system such the envisaged ELF link compared to voice transmission of Molefone and HeyPhone could provide the flexibility of implementing various features such as text, voice and video messaging. A new scheme similar to Radio Data System (RDS) can also be embedded to the ELF link to broadcast time, weather forecast, special announcement related to safety, etc of rural tourist areas.

So far, the 16-QAM transmitter/receiver was implemented. The priorities for the future work involves the design and simulation of ELF Data Transmission link discussed in this thesis based on OFDM technique using MATLAB and Altera DSP Builder and, design, build and implement a prototype and a real antenna environment to investigate the propagation characteristics. In addition, the noise is to be discussed for better SNR. After that, repeaters may be used to test the transmission distances.

7. Conclusion

This thesis has investigated the practical implementations of BASK, 8-PSK and 16-QAM using 20 Hz carrier and a data rate of *4 symbols/s* from context to practice. A cross-correlation function was used for the first time to detect the phase modulated data. This thesis has described the theoretical aspects of adopting the ELF band and the ground itself as transmission medium in a communication link based on OFDM scheme. The cross correlations would have potential impacts on the development of ELF link using OFDM scheme that would require significantly less resources compared to recent OFDM systems.

It was found that the ground can be used as a transmission medium using buried earth rods where ELF signals propagate for long distances without regeneration compared to RF. The use of buried earth rods in ELF band greatly improves the transmission range compared to loop antenna. Rocky soil and the radiation of the power feed cables degrade the SNR. OFDM enhances the transmission rate of a given bandwidth and offers high spectral efficiency but suffers from high PAPR in which requires highly linear amplifiers. In contrast, the spread spectrum allows multiple access but significantly reduces the speed of the usable data.

The 16-QAM and OFDM were chosen for the ELF Transmission Data Link to enhance the transmission capacity at such low frequencies and reduce the multi-path interference. Transceivers can be designed using FDD form especially for the remote control applications. This link could replace the complexity of and reduce the power needed for an RF link in some applications such as sensing and broadcasting the weather of mountain areas, a remote control and telemetry of oil wells valves and motors, power substations and train tracks located in countryside.

Literature showed that demodulating phase data is generally performed using carrier recovery. An original, novel and simpler function than the carrier recovery was implemented to detect the phase modulated data in 8-PSK and Star 16-QAM schemes. Patent literature review showed that there is no such patent or known prior art related to the presented system design in this thesis. The 8-PSK and 16-QAM are widely used in WCDMA, HSDPA, WiMAX and WLAN broadband wireless access technologies. The HDSPA, WiMAX and WLAN are part of the 3GPP WCDMA, IEEE 802.16 and IEEE 802.11 standards respectively. The 16-QAM is one of the standard modulation schemes in OFDMs' applications such as DVB-T and HIPERLAN.

The matched filter is the best binary digital communication detector. On the other hand, it experiences difficulties when long strings of 0's are sent in which the carrier needs to be resynchronised with BASK scheme. The BASK performs better at higher frequencies. The performance of non-coherent to coherent detectors is mostly 0.78dB.

The use of cross-correlation in this thesis to demodulate phase data, removed the need for LPF to get rid of the carrier components at the output of the correlators. This technique yields cost reduction of applications that use 8-PSK scheme. As it does not extract the carrier for demodulation purposes; the presented detection scheme offers improved phase detection performance as well as superior resistance to AWGN compared to a carrier recovery scheme operating at low SNR. Some standard applications such the IESS 308/310 Satellite Communication require at least 6dB to attain lock for data recovery. In addition, IEEE 802.11b-1999, IEEE 802.11g-2003 and IEEE 802.15.4 standards use adaptive systems to compensate the error rate at low SNR by switching between DPSK, BPSK and QPSK. This leads the author of this thesis to propose an adaptive system, in parallel with error coding

schemes, to use cross-correlation at low SNR and back to normal operation at high SNR for the Satellite and Broadband standards.

The constellation points of Square QAM optimise the transmission over Gaussian channel compared to Star QAM. In contrast, Star QAM reduces the effects of Rayleigh fading where carrier recovery is severely affected by fading channel. The transmitted mean power by Star QAM is relatively small compared to the Square QAM. The Star 16-QAM is preferred to Square QAM in OFDM systems to keep the effects of PAPR low. The use of error coding schemes enhances the Star 16-QAM performance compared to Square 16-QAM. The cross correlation has been used for the first time in the Star 16-QAM demodulator system, replacing the *ATAN* function and DPLL to detect the phase change on the received signal. The FPGA implementations resources of the Embedded Multipliers and LUTs, of the 16-QAM link compared to recent systems were cut by 91.67% and 60.25% respectively. The presented system will yield cost reduction in products using 16-QAM demodulators, namely Broadband internet and Digital TV.

It was found that using OFDM in ELF band limits the sub-carriers per channel. The author envisaged two OFDM channels in the ELF band with respect to the 50Hz radiation of power feed cables. One channel is lower than 50Hz and handles at least 128 bps. Another channel is higher than 50Hz and handles 936 bps. As a whole, the channels could handle at least 1 kbps. Each channel could be halved or both channels could be used in FDD transceivers for remote control applications. Another scenario is to use the envisaged OFDM channels in parallel with TDMA so that one use engages the channels and another waits for the channel to be freed. MC-CDMA needs a further investigation of coding scheme that suit the ELF data link to maximise the speed of usable data.

There are two major noise sources in the ELF band, namely flicker noise (1/f) and 50Hz radiation of power feed cables underground. It is envisaged that JFET systems should be used in the ELF link to keep the 1/f noise low. In addition, the 50Hz radiation requires very narrowband notch filter to attenuate it for better SNR.

It was found that the communication underground through the ground itself is done using the induction between the earth electrodes. So, a high conductive material earth electrode is essential to enhance the transmission and reception of signals. Aluminium is not the best but cheap and has very good conductivity compared to other materials and resists corrosion. The ground antenna of the ELF communication link was designed and built using high conductive aluminium.

In contrast to the existing technologies such as Molefone and HeyPhone; various features could be embedded to the ELF link such as text, voice and video messaging for subterranean and rural areas communication where RF requires complex receiver in these areas. A new protocol similar to RDS could also be embedded to the ELF link to broadcast time, weather forecast, special announcement related to safety, etc of rural tourist areas.

The priorities for future work involve the design and simulation of ELF Data Transmission link discussed in this thesis based on OFDM scheme. Furthermore, to build and implement a prototype and a real antenna environment to investigate the propagation characteristics.

8. References

[1] Esmailzadeh, R. (2006). Broadband wireless communications business: an introduction to the costs and benefits of new technologies. West Sussex: John Wiley.

[2] Bruin, R. and Smits, J. (1999). 'Digital transmission'. *In*: Digital video broadcasting: technology, standards and regulations. Boston, Mass: Artech House, pp. 167-201.

[3] de Lucena, A. M. P., Mota, J. C. M. and Cavalcante, C. C. (2008). 'Optimum detection of non-orthogonal QAM signals with spectral overlapping'. *Communications, IET,* 3, (2) pp. 249-256.

[4] Abdullah, K., Mahmoud, S. S., and Hussain, Z. M. (2009). 'Performance analysis of an optimal Circular 16-QAM for wavelet based OFDM systems' *International Journal of Communications, Network and System Sciences,* 2, pp. 836-844. Available at: http://dx.doi.org/10.4236/ijcns.2009.29097

[5] BBC. (2013). Michael Faraday (1791-1867). [Online]. London: BBC. Available at: http://www.bbc.co.uk/history/historic_figures/faraday_michael.shtml [Accessed 22nd July 2013]

[6] Garratt, G. R. M. (1994). The early history of radio: from Faraday to Marconi. London: Institution of Electrical Engineers in association with the Science Museum.

[7] Hart, M. H. (1992). The 100: a ranking of the most influential persons in history. New York: Citadel Press.

[8] Sarkar, T. K., et al. (2006). History of wireless. Chichester: John Wiley.

[9] Clifford, M. (1985). 'The early days of radio'. Radio Electronics, 57, (11) pp: 60-62.

[10] Sibley, M. (1996). Introduction to electromagnetism. London: Arnold.

[11] Coe, L. (2006). "They called it wireless". *In*: Wireless radio: a brief history. London: McFarland & Co. pp. 3-14.

[12] Fahie, J. J. (2011). A history of wireless telegraphy: including some bare-wire proposals for subaqueous telegraphs. London: Cambridge University Press.

[13] Lochte, B. (2001). Kentucky farmer invents wireless telephone! But was it radio? Facts and folklore about Nathan Stubblefield. Murray KY: All about wireless.

[14] Lee, T. H. (2004). "A nonlinear history of radio". *In*: The design of CMOS radio-frequency integrated circuits. Cambridge: Cambridge University Press. pp. 1-39.

[15] Hoffer, T. (1972). 'Nathan B. Stubblefield and his wireless'. *Journal of Broadcasting and Electronic Media*, 15 (3) pp. 317-327.

[16] Freeman, R.L. (2005). Fundamentals of telecommunications. West Sussex: John Wiley. pp. 90.

[17] Bedford, M. (2010). 'Cave radio – fifty years of development'. *Mountain Rescue Magazine*, July 2010, pp. 18-19. [online] Available at: < http://www.mountain.rescue.org.uk/assets/files/The%20Oracle/Underground%20Rescue/CaveRadio.pdf > [Accessed 15th March 2012]

[18] Bedford, M. (2001). 'Introducing the HeyPhone'. *C&C,* Autumn/Winter 200, pp. 15-17. [online]. Available at: < http://bcra.org.uk/creg/heyphone/pdf/cavesandcaving-autwin-2001.pdf > [Accessed 15th March 2012]

[19] Bedford, M. (2002). 'The 'HeyPhone' to the Rescue'. *RadCom*. January 2002, pp. 16-18. [online]. Available at: < http://bcra.org.uk/creg/heyphone/pdf/radcom-january-2002.pdf > [Accessed 15th March 2012]

[20] Bedford, M. (2001). 'The HeyPhone Story'. *Descent*. Oct/Nov, 162, pp.32-33 [online] Available at: < http://bcra.org.uk/creg/heyphone/pdf/descent-octnov-2001.pdf > [Accessed 15th March 2012]

[21] Bedford, M. (2000). 'Introducing a new cave radio for rescue use'. *Cave Radio & Electronics Group*. September, 41, pp.3 [online] Available at: < http://bcra.org.uk/creg/heyphone/pdf/cregj-september-2000.pdf > [Accessed 15th March 2012]

[22] Frater, M. and Ryan, M.J. (2003). Communications and information systems. Canberra: Argos Press. pp. 18-19.

[23] The United States Navy. (2001). Extremely Low Frequency transmitter site: Clam Lake, Wisconsin, *US Navy Fact File*, June 28, 2001 [Online]. Available at: < http://www.fas.org/nuke/guide/usa/c3i/fs_clam_lake_elf2003.pdf > [Accessed 30th AUG 2009].

[24] Sueker, Keith H. (2005). Power electronics design a practitioner's guide. Burlington: Newnes. Pp 221-222.

[25] Aldridge, B. (February 2001). ELF history: Extreme Low Frequency communication [Online] by *Pacific Life Research Centre-United States*. Available at: < http://www.plrc.org/docs/941005B.pdf > [Accessed 4th September 2008]

[26] National Research Council Staff. (1997). Evaluation of the U. S. Navy's Extremely-Low-Frequency submarine communications ecological monitoring program. Washington, DC, USA: National Academies Press, 1997. p 13. < http://site.ebrary.com/lib/uoh/Doc?id=10055127&ppg=27 > [Accessed 27th March 2008]

[27] Betz, H. D., Schumann, U. and Laroche, P. (2008). Lightning: Principles, instruments and applications: Review of modern lightning research. Dordrecht: Springer. Pp 347-378.

[28] Preve, C. (2006). Protection of electrical networks. London: ISTE. Pp 53-54.

[29] Rigby, B. (2005). Design of electrical services for buildings. 4th Ed. London: Spon Press. Pp 137-139.

[30] Federal Communications Commission office of engineering and technology, Policy and rules division. (2010). FCC online table of frequency allocations. [Online]. USA: Federal Register, 2010. Available at: < http://www.fcc.gov/oet/spectrum/table/fcctable.pdf > [Accessed 3rd May 2011]

[31] Lax, S. (1997). Digital signals. *In*: Lax, S. (1997) Beyond the horizon : communication technologies: past, present and future. Luton: University of Luton Press. Pp. 51-62.

[32] Hanes, D. and Salgueiro, G. (2008). How modems work. *In*: Hanes, D. and Salgueiro, G. (2008). Fax, modem, and text for IP telephony. London: Cisco; Pearson Education, Pp. 5-51.

[33] Roden, M. S. (1996). Digital modulation. *In*: Roden, M. S. (1996). Analog and digital communication systems. London: Prentice-Hall International Inc, pp. 470-523

[34] Qatawneh, I. A. Z. (1997). The use of Orthogonal Frequency Division Multiplex (OFDM) techniques in mobile broadband applications. PhD thesis, University of Huddersfield-UK.

[35] Rice, F., Rice, M. and Cowley, B. (2003) 'A new bound and algorithm for Star 16-QAM carrier phase estimation'. *IEEE Transactions on Communications,* 51, (2) pp. 161-165.

[36] Lax, S. (1997). Data communications and the internet. *In*: Lax, S. (1997). Beyond the horizon : communication technologies: past, present and future. Luton : University of Luton Press, Pp. 93-106.

[37] Balasubramanian, P., Aravindakshan, P. M., Parameswaran, K. and Agrawal, V. K. (2004). 'A simple scheme for PSK demodulation'. *Microprocessors and Microsystems*. [Online]. 28(7), pp. 351-355. Available: http://dx.doi.org/10.1016/j.micpro.2003.08.002

[38] D'Andrea, A. N. and Luise, M. (1996). 'Optimization of symbol timing recovery for QAM data demodulators'. *IEEE Transactions on Communications,* 44, (3) pp. 399-406.

[39] Dick, C., Harris, F. and Rice, M. (2004). 'FPGA implementation of carrier synchronization for QAM receivers'. *The Journal Of VLSI Signal Processing,* 36, (1) pp. 57-71.

[40] Metref, A., Le Guennec, D. and Palicot, J. (2007). 'Optimized decision-directed carrier recovery loop for 16-QAM constellations'. Paper presented to the *Global Telecommunications Conference, 2007. GLOBECOM '07. IEEE, 26-30 Nov. 2007.* Washington, DC. Pp. 3112-3117.

[41] Toeda, T., Okuizumi, R. and Muraguchi, M. (2009). 'Demodulation of 16-QAM signals using RF direct orthogonal phase under-sampling technique'. Paper presented to the *Microwave Conference, 2009. APMC 2009. 7-10 Dec. 2009*. Asia Pacific. Pp. 508-511.

[42] Wang, X. H., Qiu, X. Z., Lambrecht, P., Vandewege, J. De Meyer, K. And Trog, W. (1996). 'Burst-mode 16 QAM receiver for upstream transmission over CATV networks'. Paper presented to the *IEEE 39th Midwest symposium on Circuits and Systems,* 3, pp 1260-1263.

[43] Xuan-Thang Vu., Nguyen Anh Duc. and Trinh Anh Vu. (2010). '16-QAM transmitter and receiver design based on FPGA'. Paper presented to the *Electronic Design, Test and Applications, 2008. DELTA 2008. 4th IEEE International Symposium on. 13-15 Jan. 2010*. Ho Chi Minh City. Pp. 95-98.

[44] Young-Ok Park. and Jee-Hwan Ahn. (1997). 'A new carrier recovery method for 16-QAM signal'. Paper presented to the *IEEE International Conference on Personal Wireless Communications ICPWC'97*, *17-19 Dec 1997.* Mumbai , India.. Pp. 194-197.

[45] Croft, T., Davison, R. and, Hargreaves, M. (2001). Engineering mathematics: a foundation for electronic, electrical, communications, and systems engineers. 3rd Ed. Harlow: Prentice Hall.

[46] Stroud, K. A. and Booth, D. J. (2007). Engineering mathematics. 6th Ed. New York: Industrial Press.

[47] Fazel, K. & Kaiser, S. (2008). Multi-Carrier and Spread Spectrum systems: From OFDM and MC-CDMA to LTE and WiMAX. 2nd Ed. West Sussex: John Wiley.

[48] Hanzo, L., Munster, M., Choi, B.J. & Keller, T. (2003). OFDM and MC-CDMA for broadband multi-user communications, WLANs, and Broadcasting. England: John Wiley. Pp. 7-9.

[49] Hurst, J. A. (2000). Introduction. *In*: An investigation into methods for the correction of frequency offset in OFDM systems. PhD thesis, University of Huddersfield-UK. Pp. 1-4.

[50] Kumar, V., Panda, G. and Sahu, P. K. (2009). 'DHT based 4 QAM OFDM baseband system and channel estimation' *International Journal of Recent Trends in Engineering,* 2, (5) pp. 80-84.

[51] Saunders, R.S. (1999). Antennas and propagation for wireless communication systems. New York: J. Wiley. P.p78.

[52] Prasad, R. (1996). CDMA for wireless personal communications. Boston: Artech House.

[53] Harte, L., Hoenig, M., McLaughlin, D. & K.Kta, R. (1999). History of CDMA. *In*: CDMA IS-95 for Cellular and PCS technology, economics and services. New York: McGraw-Hill Telecommunications.

[54] Plass, S., Dammann, A., Kaiser, S. and Fazel, K. (2007). Multi-Carrier Spread Spectrum 2007. London: Springer.

[55] Nassar, C.R., Natarajan, B., Wu, Z., Wiegandt, D., Zekavat, S.A. & Shattil, S. (2001). Overview of Multi-Carrier technologies. *In*: Multi-Carrier technologies for wireless communication. Hingham, MA, USA: Kluwer Academic Publishers, pp. 5-38.

[56] Mensing, C. (2008). *History of the Multi-Carrier Spread Spectrum workshop* [Online]. Available at: < http://www.kn-s.dlr.de/mcss2007/history.php > [Accessed 12th September 2009].

[57] Alaiwi, A., Sibley, M., Mather, P. and Holmes, V. (2009). 'Extremely low frequency based communication link'. Presented to the *Computing and Engineering Annual Researchers' Conference 2009: CEARC'09, December 2009*. Huddersfield: University of Huddersfield, pp. 105-110. Available at: < http://eprints.hud.ac.uk/6870/1/18_A_Alaiwi.pdf > [Accessed 20th August 2010]

[58] Altera. (2010). *Cyclone III FPGA development kit*. [Online] Available at: < http://www.altera.com/products/devkits/altera/kit-cyc3.html > [Accessed 16th May 2012]

[59] Altera. (2009). *The MathWorks and Altera DSP collaboration* [Online]. Available at :< http://www.altera.com/products/ip/altera/t-alt-matlab.html > [Accessed 16th May 2012]

[60] Altera. (2009). *DSP Builder* [Online]. Available at: < http://www.altera.com/products/software/products/dsp/dsp-builder.html > [Accessed 16th May 2012]

[61] Altera. (2009). *DSP Builder/Simulink* [Online]. Available at: < http://www.altera.com/technology/dsp/dsp-builder/dsp-simulink.html > [Accessed 16th May 2012]

[62] The MathWorks. (2009). *Altera DSP Builder and HDL Coder* [Online]. Available at: < http://www.mathworks.co.uk/fpga-design/simulink-with-altera-dsp-builder.html > [Accessed 16th May 2012]

[63] Ash, D. L. (2002). A comparison between OOK/ASK and FSK modulation techniques for radio links. *RF Monolithics, Inc.*, Dallas, Texas. [Online] Available at: < http://www.rfm.com/products/apnotes/ookvsfsk.pdf > [Accessed 24th May 2012]

[64] Singh, K. (2003). Engineering Mathematics through applications. Basingstoke: Palgrave Macmillan.

[65] Smith, S. W. (1997). Continuous signal processing. *In*: Smith, S. W. (1997) The scientist and engineer's guide to digital signal processing. San Diego-Calif: California Technical Publishing, pp. 243-260.

[66] Hiatt, C. F., van der Ziel, A. and van Viet, K. M. (1975). 'Generation-recombination noise produced in the channel of JFETs'. *IEEE Transactions on Electronic Devices*, ED-22, pp. 614-616.

[67] Klaassen, F. M. and Robinson, J. R. (1970). 'Anomalous noise behaviour of the Junction Gate Field Effect Transistor at low temperatures'. *IEEE Transactions on Electronic Devices*, ED-17, pp. 852-857.

[68] Proakis, J. G. (1995). Digital communications. New York: McGraw-Hill.

[69] Proakis, J. G. and Salehi, M. (1994). Communication systems engineering. Englewood Cliffs: Prentice Hall.

[70] Lindsey, W. C. and Simon, M. K. (1973). Telecommunication systems engineering. Englewood Cliffs: Prentice-Hall.

[71] Altera. (2009). *NCO MegaCore function user guide*. [Online] Available at: < http://www.altera.com/support/design-support-resources/spt-index-guide.html > [Accessed 20th August 2010]

[72] Webb, W. T., Hanzo, L. and Steele, R. (1991). 'Bandwidth efficient QAM schemes for Rayleigh fading channels'. Presented to the *IEE Proceeding-I Communications Speech and Vision,* 33(3), pp. 169-175. Available at: http://dx.doi.org/10.1049/ip-i-2.1991.0023

[73] Vitthaladevuni, P. K. and Alouini, M. S. (2005). 'Effect of imperfect phase and timing synchronization on the bit-error rate performance of PSK modulations'. *IEEE Transactions on Communications*. 53(7), pp. 1096-1099. Available at: http://dx.doi.org/10.1109/TCOMM.2005.851616

[74] Vitthaladevuni, P. K. and Alouini, M. S. (2003). 'Exact BER computation of generalized hierarchical PSK constellations'. *IEEE Transactions on Communications,* 51(12), pp. 2030-2037. Available at: http://dx.doi.org/10.1109/TCOMM.2003.820748

[75] Arun Kumar, K. A. (2012). 'FPGA implementation of PSK modems using partial re-configuration for SDR and CR applications'. Presented to the *Proc. INDICON 2012, Annual IEEE*. Kochi, pp. 205-209. Available at: http://dx.doi.org/10.1109/INDCON.2012.6420616

[76] Velkuru, V. K. and Samant, A. (2011). 'A design for software defined M-PSK radio on FPGA for low SNRs and symbol rates upto 10MS/s'. Presented to the *Proc. ICSIPA 2011, IEEE*. Kuala Lumpur, pp. 574-578. Available: http://dx.doi.org/10.1109/ICSIPA.2011.6144169

[77] Lin, H., Wang, X., Lu, J. and Yahagi, T. (2001). 'Adaptive detection using self-organizing map in 16 QAM system'. Presented to the *Info-tech and Info-net, 2001. Proceedings. ICII 2001 - Beijing. 2001 International Conferences on*, 3, pp. 698-703.

[78] Horowitz, P. and Hill, W. (1994). The art of electronics. 2nd ed. Cambridge: Cambridge University Press.

[79] Storey, N. (1998). Electronics: A system approach. Reading: Addison-Wesley. pp. 314.

[80] Gosling, W. (1998). Radio antennas and propagation. Oxford: Newnes.

[81] Navarra, J. G. (1980). Earth, space and time: an introduction to earth science. Chichester: Wiley.

[82] Kraus, J. D. and Marhefka, R. J. (2003). Antennas: for all applications. 3rd Ed. London: McGraw-Hill.

[83] Macnamara, T. (2010). Introduction to antenna placement and installation. Oxford: Wiley.

[84] Illston, J. M. and Domone, P. L. J. (2001). Electrical and thermal conductivity. *In*: Illston, J. M. and Domone, P. L. J., eds. Construction materials their nature and behaviour. London: Spon.

[85] Griffiths, D. J. (2008). Introduction to electrodynamics. London: Pearson.

[86] Serway, R. A. (1998). Principles of physics. London: Saunders College Pub.

9. Bibliography

[1] Rowe, H. E. (1974). 'Extremely Low Frequency (ELF) communication to submarines'. *IEEE Transactions on Communications*, 22(4), pp. 371-385.

[2] Chu, T. (1974). 'The radiation of Extremely Low Frequency (ELF) waves' *IEEE Transactions on Communications*, 22(4), pp. 386-388.

[3] Wolf, S., Davis, J. and Nisenoff, M. (1974). 'Superconducting Extremely Low Frequency (ELF) magnetic field sensors for submarine communications' *IEEE Transactions on Communications*, 22(4), pp. 549-554.

[4] Wei, R. (2011) 'Differential encoding by a look-up table for Quadrature-Amplitude Modulation' *IEEE Transactions on Communications,* 59(1)*,* pp. 84-94.

[5] Camatel, S. and Ferrero, V. (2006). 'Homodyne coherent detection of ASK and PSK signals performed by a subcarrier optical phase-locked loop'. *IEEE Photonics Technology Letters*. 18(1), pp. 142-144.

[6] Linn, Y. (2005). 'A robust phase detection structure for M-PSK: Theoretical derivations, simulation results, and system identification analysis'. Presented to the *Proc. CCECE'05, IEEE.* Saskatoon, Sask, pp. 869 - 883. Available at: http://dx.doi.org/10.1109/CCECE.2005.1557117

[7] Pike, J. (2004). *Extremely Low Frequency communications program* [Online]. Available at: < http://www.fas.org/nuke/guide/usa/c3i/elf.htm > [Accessed on 21st Mar 2008]

[8] Linnartz, Professor Jean-Paul. (2006). *OFDM and MC-CDMA* [Online] Available at: <http://ofdm.linnartz.net> [Accessed 12th September 2009]

[9] Lawrey, E. (1997). The suitability of OFDM as a modulation technique for wireless telecommunications, with a CDMA comparison. Bachelor Thesis, University of James Cook-Australia. pp. 29-32.

[10] CDMA Certification Forum. (2007). *History and milestones of CDMA* [Online]. Available at: < http://globalccf.org/cdma_resources/history.html > [Accessed 12th September 2009].

[11] Cataldo, A., Benedetto, E. D. and Cannazza, G. (2011). Broadband reflectometry for enhanced diagnostics and monitoring applications. Heidelberg: Springer.

[12] Furuta, K. and Ishikawa, J. (2009). Anti-personnel landmine detection for humanitarian demining: the current situation and future direction for Japanese research and development. London: Springer.

[13] Millman, J. and Grabel, A. (1987). Microelectronics. London: McGraw-Hill.

Cross Correlation at the presence of 0 degree angle

Delayed (B2)		Shifted (B1)		Cos(wt+B1)*Cos(wt-B2) simplified		Cross Correlated
Angle (Degree)	Angle (Radian)	Angle (Degree)	Angle (Radian)	Cos(2wt+B1-B2)	cos(B1+B2)	0.5*[Cos(2wt+B1-B2)+Cos(B1+B2)]
0	0.000	0	0.000	1.000	1.000	1.000
-45	5.498	0	0.000	1.000	0.707	0.854
-90	4.712	0	0.000	1.000	0.000	0.500
-135	3.927	0	0.000	1.000	-0.707	0.146
-180	3.142	0	0.000	1.000	-1.000	0.000
-225	2.356	0	0.000	1.000	-0.707	0.146
-270	1.571	0	0.000	1.000	0.000	0.500
-315	0.785	0	0.000	1.000	0.707	0.854

Cross Correlation at the presence of 45 degree angle

Delayed (B2)		Shifted (B1)		Cos(wt+B1)*Cos(wt-B2) simplified		Cross Correlated
Angle (Degree)	Angle (Radian)	Angle (Degree)	Angle (Radian)	Cos(2wt+B1-B2)	cos(B1+B2)	0.5*[Cos(2wt+B1-B2)+Cos(B1+B2)]
0	0.000	45	0.785	1.000	0.707	0.854
-45	5.498	45	0.785	1.000	1.000	1.000
-90	4.712	45	0.785	1.000	0.707	0.853
-135	3.927	45	0.785	1.000	0.000	0.500
-180	3.142	45	0.785	1.000	-0.707	0.146
-225	2.356	45	0.785	1.000	-1.000	0.000
-270	1.571	45	0.785	1.000	-0.707	0.147
-315	0.785	45	0.785	1.000	0.000	0.500

Cross Correlation at the presence of 90 degree angle						
Delayed (B2)		Shifted (B1)		Cos(wt+B1)*Cos(wt-B2) simplified		Cross Correlated
Angle (Degree)	Angle (Radian)	Angle (Degree)	Angle (Radian)	Cos(2wt+B1-B2)	cos(B1+B2)	0.5*[Cos(2wt+B1-B2)+Cos(B1+B2)]
0	0.000	90	1.571	1.000	0.000	0.500
-45	5.498	90	1.571	1.000	0.707	0.853
-90	4.712	90	1.571	1.000	1.000	1.000
-135	3.927	90	1.571	1.000	0.707	0.854
-180	3.142	90	1.571	1.000	0.000	0.500
-225	2.356	90	1.571	1.000	-0.707	0.147
-270	1.571	90	1.571	1.000	-1.000	0.000
-315	0.785	90	1.571	1.000	-0.707	0.146

Cross Correlation at the presence of 135 degree angle						
Delayed (B2)		Shifted (B1)		Cos(wt+B1)*Cos(wt-B2) simplified		Cross Correlated
Angle (Degree)	Angle (Radian)	Angle (Degree)	Angle (Radian)	Cos(2wt+B1-B2)	cos(B1+B2)	0.5*[Cos(2wt+B1-B2)+Cos(B1+B2)]
0	0.000	135	2.356	1.000	-0.707	0.147
-45	5.498	135	2.356	1.000	0.000	0.500
-90	4.712	135	2.356	1.000	0.707	0.854
-135	3.927	135	2.356	1.000	1.000	1.000
-180	3.142	135	2.356	1.000	0.707	0.853
-225	2.356	135	2.356	1.000	0.000	0.500
-270	1.571	135	2.356	1.000	-0.707	0.146
-315	0.785	135	2.356	1.000	-1.000	0.000

Cross Correlation at the presence of 180 degree angle

Delayed (B2)		Shifted (B1)		Cos(wt+B1)*Cos(wt-B2) simplified		Cross Correlated
Angle (Degree)	Angle (Radian)	Angle (Degree)	Angle (Radian)	Cos(2wt+B1-B2)	cos(B1+B2)	0.5*[Cos(2wt+B1-B2)+Cos(B1+B2)]
0	0.000	180	3.142	1.000	-1.000	0.000
-45	5.498	180	3.142	1.000	-0.707	0.146
-90	4.712	180	3.142	1.000	0.000	0.500
-135	3.927	180	3.142	1.000	0.707	0.853
-180	3.142	180	3.142	1.000	1.000	1.000
-225	2.356	180	3.142	1.000	0.707	0.854
-270	1.571	180	3.142	1.000	0.000	0.500
-315	0.785	180	3.142	1.000	-0.707	0.147

Cross Correlation at the presence of 225 degree angle

Delayed (B2)		Shifted (B1)		Cos(wt+B1)*Cos(wt-B2) simplified		Cross Correlated
Angle (Degree)	Angle (Radian)	Angle (Degree)	Angle (Radian)	Cos(2wt+B1-B2)	cos(B1+B2)	0.5*[Cos(2wt+B1-B2)+Cos(B1+B2)]
0	0.000	225	3.927	1.000	-0.707	0.146
-45	5.498	225	3.927	1.000	-1.000	0.000
-90	4.712	225	3.927	1.000	-0.707	0.146
-135	3.927	225	3.927	1.000	0.000	0.500
-180	3.142	225	3.927	1.000	0.707	0.854
-225	2.356	225	3.927	1.000	1.000	1.000
-270	1.571	225	3.927	1.000	0.707	0.854
-315	0.785	225	3.927	1.000	0.000	0.500

Cross Correlation at the presence of 270 degree angle						
Delayed (B2)		Shifted (B1)		Cos(wt+B1)*Cos(wt-B2) simplified		Cross Correlated
Angle (Degree)	Angle (Radian)	Angle (Degree)	Angle (Radian)	Cos(2wt+B1-B2)	cos(B1+B2)	0.5*[Cos(2wt+B1-B2)+Cos(B1+B2)]
0	0.000	270	4.712	1.000	0.000	0.500
-45	5.498	270	4.712	1.000	-0.707	0.146
-90	4.712	270	4.712	1.000	-1.000	0.000
-135	3.927	270	4.712	1.000	-0.707	0.147
-180	3.142	270	4.712	1.000	0.000	0.500
-225	2.356	270	4.712	1.000	0.707	0.854
-270	1.571	270	4.712	1.000	1.000	1.000
-315	0.785	270	4.712	1.000	0.707	0.853

Cross Correlation at the presence of 315 degree angle						
Delayed (B2)		Shifted (B1)		Cos(wt+B1)*Cos(wt-B2) simplified		Cross Correlated
Angle (Degree)	Angle (Radian)	Angle (Degree)	Angle (Radian)	Cos(2wt+B1-B2)	cos(B1+B2)	0.5*[Cos(2wt+B1-B2)+Cos(B1+B2)]
0	0.000	315	5.498	1.000	0.707	0.854
-45	5.498	315	5.498	1.000	0.000	0.500
-90	4.712	315	5.498	1.000	-0.707	0.147
-135	3.927	315	5.498	1.000	-1.000	0.000
-180	3.142	315	5.498	1.000	-0.707	0.146
-225	2.356	315	5.498	1.000	0.000	0.500
-270	1.571	315	5.498	1.000	0.707	0.853
-315	0.785	315	5.498	1.000	1.000	1.000

Cross Correlation at the presence of 0 degree angle

Delayed (B2)		Shifted (B1)		Cos(wt+B1)*Cos(wt-B2) simplified		Cross Correlated
Angle (Degree)	Angle (Radian)	Angle (Degree)	Angle (Radian)	Cos(2wt+B1-B2)	cos(B1+B2)	0.5*[Cos(2wt+B1-B2)+Cos(B1+B2)]
-180	-3.142	0	0.000	1.000	-1.000	0.000
-45	-0.785	0	0.000	1.000	0.707	0.854
-90	-1.571	0	0.000	1.000	0.000	0.500
-135	-2.356	0	0.000	1.000	-0.707	0.146
-180	-3.142	0	0.000	1.000	-1.000	0.000
-135	-2.356	0	0.000	1.000	-0.707	0.146
-90	-1.571	0	0.000	1.000	0.000	0.500
-45	-0.785	0	0.000	1.000	0.707	0.854

Cross Correlation at the presence of 45 degree angle

Delayed (B2)		Shifted (B1)		Cos(wt+B1)*Cos(wt-B2) simplified		Cross Correlated
Angle (Degree)	Angle (Radian)	Angle (Degree)	Angle (Radian)	Cos(2wt+B1-B2)	cos(B1+B2)	0.5*[Cos(2wt+B1-B2)+Cos(B1+B2)]
-180	-3.142	45	0.785	1.000	-0.707	0.146
-45	-0.785	45	0.785	1.000	1.000	1.000
-90	-1.571	45	0.785	1.000	0.707	0.853
-135	-2.356	45	0.785	1.000	0.000	0.500
-180	3.142	45	0.785	1.000	-0.707	0.146
-135	-2.356	45	0.785	1.000	0.000	0.500
-90	-1.571	45	0.785	1.000	0.707	0.853
-45	-0.785	45	0.785	1.000	1.000	1.000

Cross Correlation at the presence of 90 degree angle

Delayed (B2)		Shifted (B1)		Cos(wt+B1)*Cos(wt-B2) simplified		Cross Correlated
Angle (Degree)	Angle (Radian)	Angle (Degree)	Angle (Radian)	Cos(2wt+B1-B2)	cos(B1+B2)	0.5*[Cos(2wt+B1-B2)+Cos(B1+B2)]
-180	-3.142	90	1.571	1.000	0.000	0.500
-45	-0.785	90	1.571	1.000	0.707	0.853
-90	-1.571	90	1.571	1.000	1.000	1.000
-135	-2.356	90	1.571	1.000	0.707	0.854
-180	3.142	90	1.571	1.000	0.000	0.500
-135	-2.356	90	1.571	1.000	0.707	0.854
-90	-1.571	90	1.571	1.000	1.000	1.000
-45	-0.785	90	1.571	1.000	0.707	0.853

Cross Correlation at the presence of 135 degree angle

Delayed (B2)		Shifted (B1)		Cos(wt+B1)*Cos(wt-B2) simplified		Cross Correlated
Angle (Degree)	Angle (Radian)	Angle (Degree)	Angle (Radian)	Cos(2wt+B1-B2)	cos(B1+B2)	0.5*[Cos(2wt+B1-B2)+Cos(B1+B2)]
-180	-3.142	135	2.356	1.000	0.707	0.853
-45	-0.785	135	2.356	1.000	0.000	0.500
-90	-1.571	135	2.356	1.000	0.707	0.854
-135	-2.356	135	2.356	1.000	1.000	1.000
-180	3.142	135	2.356	1.000	0.707	0.853
-135	-2.356	135	2.356	1.000	1.000	1.000
-90	-1.571	135	2.356	1.000	0.707	0.854
-45	-0.785	135	2.356	1.000	0.000	0.500

Cross Correlation at the presence of 180 degree angle						
Delayed (B2)		Shifted (B1)		Cos(wt+B1)*Cos(wt-B2) simplified		Cross Correlated
Angle (Degree)	Angle (Radian)	Angle (Degree)	Angle (Radian)	Cos(2wt+B1-B2)	cos(B1+B2)	0.5*[Cos(2wt+B1-B2)+Cos(B1+B2)]
-180	-3.142	180	3.142	1.000	1.000	1.000
-45	-0.785	180	3.142	1.000	-0.707	0.146
-90	-1.571	180	3.142	1.000	0.000	0.500
-135	-2.356	180	3.142	1.000	0.707	0.853
-180	3.142	180	3.142	1.000	1.000	1.000
-135	-2.356	180	3.142	1.000	0.707	0.853
-90	-1.571	180	3.142	1.000	0.000	0.500
-45	-0.785	180	3.142	1.000	-0.707	0.146

Cross Correlation at the presence of 225 degree angle						
Delayed (B2)		Shifted (B1)		Cos(wt+B1)*Cos(wt-B2) simplified		Cross Correlated
Angle (Degree)	Angle (Radian)	Angle (Degree)	Angle (Radian)	Cos(2wt+B1-B2)	cos(B1+B2)	0.5*[Cos(2wt+B1-B2)+Cos(B1+B2)]
-180	-3.142	225	3.927	1.000	0.707	0.854
-45	-0.785	225	3.927	1.000	-1.000	0.000
-90	-1.571	225	3.927	1.000	-0.707	0.146
-135	-2.356	225	3.927	1.000	0.000	0.500
-180	3.142	225	3.927	1.000	0.707	0.854
-135	-2.356	225	3.927	1.000	0.000	0.500
-90	-1.571	225	3.927	1.000	-0.707	0.146
-45	-0.785	225	3.927	1.000	-1.000	0.000

Cross Correlation at the presence of 270 degree angle						
Delayed (B2)		Shifted (B1)		Cos(wt+B1)*Cos(wt-B2) simplified		Cross Correlated
Angle (Degree)	Angle (Radian)	Angle (Degree)	Angle (Radian)	Cos(2wt+B1-B2)	cos(B1+B2)	0.5*[Cos(2wt+B1-B2)+Cos(B1+B2)]
-180	-3.142	270	4.712	1.000	0.000	0.500
-45	-0.785	270	4.712	1.000	-0.707	0.146
-90	-1.571	270	4.712	1.000	-1.000	0.000
-135	-2.356	270	4.712	1.000	-0.707	0.147
-180	3.142	270	4.712	1.000	0.000	0.500
-135	-2.356	270	4.712	1.000	-0.707	0.147
-90	-1.571	270	4.712	1.000	-1.000	0.000
-45	-0.785	270	4.712	1.000	-0.707	0.146

Cross Correlation at the presence of 315 degree angle						
Delayed (B2)		Shifted (B1)		Cos(wt+B1)*Cos(wt-B2) simplified		Cross Correlated
Angle (Degree)	Angle (Radian)	Angle (Degree)	Angle (Radian)	Cos(2wt+B1-B2)	cos(B1+B2)	0.5*[Cos(2wt+B1-B2)+Cos(B1+B2)]
-180	-3.142	315	5.498	1.000	-0.707	0.146
-45	-0.785	315	5.498	1.000	0.000	0.500
-90	-1.571	315	5.498	1.000	-0.707	0.147
-135	-2.356	315	5.498	1.000	-1.000	0.000
-180	3.142	315	5.498	1.000	-0.707	0.146
-135	-2.356	315	5.498	1.000	-1.000	0.000
-90	-1.571	315	5.498	1.000	-0.707	0.147
-45	-0.785	315	5.498	1.000	0.000	0.500

Cross Correlation at the presence of 0 degree angle

Delayed (B2)		Shifted (B1)		Cos(wt+B1)*Cos(wt-B2), simplified, filtered carrier (wt)		Cross Correlated
Angle (Degree)	Angle (Radian)	Angle (Degree)	Angle (Radian)	Cos(2wt+B1-B2)	cos(B1+B2)	0.5*[Cos(2wt+B1-B2)+Cos(B1+B2)]
-180	-3.142	0	0.000	0.000	-1.000	-0.500
-45	-0.785	0	0.000	0.000	0.707	0.354
-90	-1.571	0	0.000	0.000	0.000	0.000
-135	-2.356	0	0.000	0.000	-0.707	-0.354
-180	-3.142	0	0.000	0.000	-1.000	-0.500
-135	-2.356	0	0.000	0.000	-0.707	-0.354
-90	-1.571	0	0.000	0.000	0.000	0.000
-45	-0.785	0	0.000	0.000	0.707	0.354

Cross Correlation at the presence of 45 degree angle

Delayed (B2)		Shifted (B1)		Cos(wt+B1)*Cos(wt-B2), simplified, filtered carrier (wt)		Cross Correlated
Angle (Degree)	Angle (Radian)	Angle (Degree)	Angle (Radian)	Cos(2wt+B1-B2)	cos(B1+B2)	0.5*[Cos(2wt+B1-B2)+Cos(B1+B2)]
-180	-3.142	45	0.785	0.000	-0.707	-0.354
-45	-0.785	45	0.785	0.000	1.000	0.500
-90	-1.571	45	0.785	0.000	0.707	0.353
-135	-2.356	45	0.785	0.000	0.000	0.000
-180	3.142	45	0.785	0.000	-0.707	-0.354
-135	-2.356	45	0.785	0.000	0.000	0.000
-90	-1.571	45	0.785	0.000	0.707	0.353
-45	-0.785	45	0.785	0.000	1.000	0.500

Cross Correlation at the presence of 90 degree angle

Delayed (B2)		Shifted (B1)		Cos(wt+B1)*Cos(wt-B2), simplified, filtered carrier (wt)		Cross Correlated
Angle (Degree)	Angle (Radian)	Angle (Degree)	Angle (Radian)	Cos(2wt+B1-B2)	cos(B1+B2)	0.5*[Cos(2wt+B1-B2)+Cos(B1+B2)]
-180	-3.142	90	1.571	0.000	0.000	0.000
-45	-0.785	90	1.571	0.000	0.707	0.353
-90	-1.571	90	1.571	0.000	1.000	0.500
-135	-2.356	90	1.571	0.000	0.707	0.354
-180	3.142	90	1.571	0.000	0.000	0.000
-135	-2.356	90	1.571	0.000	0.707	0.354
-90	-1.571	90	1.571	0.000	1.000	0.500
-45	-0.785	90	1.571	0.000	0.707	0.353

Cross Correlation at the presence of 135 degree angle

Delayed (B2)		Shifted (B1)		Cos(wt+B1)*Cos(wt-B2), simplified, filtered carrier (wt)		Cross Correlated
Angle (Degree)	Angle (Radian)	Angle (Degree)	Angle (Radian)	Cos(2wt+B1-B2)	cos(B1+B2)	0.5*[Cos(2wt+B1-B2)+Cos(B1+B2)]
-180	-3.142	135	2.356	0.000	0.707	0.353
-45	-0.785	135	2.356	0.000	0.000	0.000
-90	-1.571	135	2.356	0.000	0.707	0.354
-135	-2.356	135	2.356	0.000	1.000	0.500
-180	3.142	135	2.356	0.000	0.707	0.353
-135	-2.356	135	2.356	0.000	1.000	0.500
-90	-1.571	135	2.356	0.000	0.707	0.354
-45	-0.785	135	2.356	0.000	0.000	0.000

Cross Correlation at the presence of 180 degree angle

Delayed (B2)		Shifted (B1)		Cos(wt+B1)*Cos(wt-B2), simplified, filtered carrier (wt)		Cross Correlated
Angle (Degree)	Angle (Radian)	Angle (Degree)	Angle (Radian)	Cos(2wt+B1-B2)	cos(B1+B2)	0.5*[Cos(2wt+B1-B2)+Cos(B1+B2)]
-180	-3.142	180	3.142	0.000	1.000	0.500
-45	-0.785	180	3.142	0.000	-0.707	-0.354
-90	-1.571	180	3.142	0.000	0.000	0.000
-135	-2.356	180	3.142	0.000	0.707	0.353
-180	3.142	180	3.142	0.000	1.000	0.500
-135	-2.356	180	3.142	0.000	0.707	0.353
-90	-1.571	180	3.142	0.000	0.000	0.000
-45	-0.785	180	3.142	0.000	-0.707	-0.354

Cross Correlation at the presence of 225 degree angle

Delayed (B2)		Shifted (B1)		Cos(wt+B1)*Cos(wt-B2), simplified, filtered carrier (wt)		Cross Correlated
Angle (Degree)	Angle (Radian)	Angle (Degree)	Angle (Radian)	Cos(2wt+B1-B2)	cos(B1+B2)	0.5*[Cos(2wt+B1-B2)+Cos(B1+B2)]
-180	-3.142	225	3.927	0.000	0.707	0.354
-45	-0.785	225	3.927	0.000	-1.000	-0.500
-90	-1.571	225	3.927	0.000	-0.707	-0.354
-135	-2.356	225	3.927	0.000	0.000	0.000
-180	3.142	225	3.927	0.000	0.707	0.354
-135	-2.356	225	3.927	0.000	0.000	0.000
-90	-1.571	225	3.927	0.000	-0.707	-0.354
-45	-0.785	225	3.927	0.000	-1.000	-0.500

Cross Correlation at the presence of 270 degree angle						
Delayed (B2)		Shifted (B1)		Cos(wt+B1)*Cos(wt-B2), simplified, filtered carrier (wt)		Cross Correlated
Angle (Degree)	Angle (Radian)	Angle (Degree)	Angle (Radian)	Cos(2wt+B1-B2)	cos(B1+B2)	0.5*[Cos(2wt+B1-B2)+Cos(B1+B2)]
-180	-3.142	270	4.712	0.000	0.000	0.000
-45	-0.785	270	4.712	0.000	-0.707	-0.354
-90	-1.571	270	4.712	0.000	-1.000	-0.500
-135	-2.356	270	4.712	0.000	-0.707	-0.353
-180	3.142	270	4.712	0.000	0.000	0.000
-135	-2.356	270	4.712	0.000	-0.707	-0.353
-90	-1.571	270	4.712	0.000	-1.000	-0.500
-45	-0.785	270	4.712	0.000	-0.707	-0.354

Cross Correlation at the presence of 315 degree angle						
Delayed (B2)		Shifted (B1)		Cos(wt+B1)*Cos(wt-B2), simplified, filtered carrier (wt)		Cross Correlated
Angle (Degree)	Angle (Radian)	Angle (Degree)	Angle (Radian)	Cos(2wt+B1-B2)	cos(B1+B2)	0.5*[Cos(2wt+B1-B2)+Cos(B1+B2)]
-180	-3.142	315	5.498	0.000	-0.707	-0.354
-45	-0.785	315	5.498	0.000	0.000	0.000
-90	-1.571	315	5.498	0.000	-0.707	-0.353
-135	-2.356	315	5.498	0.000	-1.000	-0.500
-180	3.142	315	5.498	0.000	-0.707	-0.354
-135	-2.356	315	5.498	0.000	-1.000	-0.500
-90	-1.571	315	5.498	0.000	-0.707	-0.353
-45	-0.785	315	5.498	0.000	0.000	0.000

$$\operatorname{erf}(x) = \frac{2}{\sqrt{\pi}}\int_0^x e^{-u^2}du$$

x	erf (x)	erfc (x)	x	erf (x)	erfc (x)
0	0	1	0.05	0.056	0.944
0.10	0.112	0.888	0.15	0.168	0.832
0.20	0.223	0.777	0.25	0.276	0.724
0.30	0.329	0.671	0.35	0.379	0.621
0.40	0.428	0.572	0.45	0.475	0.525
0.50	0.521	0.479	0.55	0.563	0.437
0.60	0.604	0.396	0.65	0.642	0.358
0.70	0.678	0.322	0.75	0.711	0.289
0.80	0.742	0.258	0.85	0.771	0.229
0.90	0.797	0.203	0.95	0.821	0.179
1.00	0.843	0.157	1.05	0.862	0.138
1.10	0.880	0.120	1.15	0.896	0.104
1.20	0.910	0.0901	1.25	0.923	0.0768
1.30	0.934	0.0659	1.35	0.944	0.0564
1.40	0.952	0.0481	1.45	0.960	0.0400
1.50	0.966	0.0338	1.55	0.972	0.0284
1.60	0.976	0.0238	1.65	0.980	0.0199
1.70	0.984	0.0156	1.75	0.987	0.0128
1.80	0.989	0.0105	1.85	0.991	8.53×10^{-3}
1.90	0.993	6.91×10^{-3}	1.95	0.994	5.57×10^{-3}
2.00	0.995	4.59×10^{-3}	2.05	0.996	3.68×10^{-3}
2.10	0.997	2.98×10^{-3}	2.15	0.998	2.33×10^{-3}
2.20	0.998	1.84×10^{-3}	2.25	0.999	1.44×10^{-3}
2.30	0.999	1.13×10^{-3}	2.35	0.999	8.80×10^{-4}
2.40	0.999	6.82×10^{-4}	2.45	0.999	5.26×10^{-4}
2.50	1.000	4.03×10^{-4}	2.55	1.000	3.08×10^{-4}
2.60	1.000	2.34×10^{-4}	2.65	1.000	1.77×10^{-4}
2.70	1.000	1.33×10^{-4}	2.80	1.000	7.46×10^{-5}
2.90	1.000	4.09×10^{-5}	3.00	1.000	2.20×10^{-5}
3.10	1.000	1.16×10^{-5}	3.20	1.000	6.00×10^{-6}
3.30	1.000	3.06×10^{-6}	3.40	1.000	1.52×10^{-6}
3.50	1.000	7.43×10^{-7}	3.60	1.000	3.56×10^{-7}
3.70	1.000	1.67×10^{-7}	3.80	1.000	7.70×10^{-8}

x	erf (x)	erfc (x)	x	erf (x)	erfc (x)
3.90	1.000	3.48×10^{-8}	4.00	1.000	1.54×10^{-8}
4.10	1.000	6.70×10^{-9}	4.20	1.000	2.86×10^{-9}
4.30	1.000	1.19×10^{-9}	4.40	1.000	4.89×10^{-10}
4.50	1.000	1.97×10^{-10}	4.60	1.000	7.75×10^{-11}
4.70	1.000	3.00×10^{-11}	4.80	1.000	1.14×10^{-11}
4.90	1.000	4.22×10^{-12}	5.00	1.000	1.54×10^{-12}

f (Hz)	A (V)	No (watt/Hz)	S (watt)	N (watt)	SNR	SNR (dB)	Rb (bps)	Eo	Pe (Incoh.)	x (Coherent)	Pe (Coh.)	x dB	ΔdB
20	1.414E-04	5.00E-10	1.000E-08	1.00E-08	1.000E+00	0	4	1.250E-09	1.43E-01	1.118033989	0.09705	1.18	1.18
20	1.587E-04	5.00E-10	1.259E-08	1.00E-08	1.259E+00	1	4	1.574E-09	1.04E-01	1.254454768	0.0768	1.76	0.76
20	1.780E-04	5.00E-10	1.585E-08	1.00E-08	1.585E+00	2	4	1.981E-09	6.90E-02	1.4075214	0.0481	2.73	0.73
20	1.998E-04	5.00E-10	1.995E-08	1.00E-08	1.995E+00	3	4	2.494E-09	4.13E-02	1.579264985	0.0261	3.73	0.73
20	2.241E-04	5.00E-10	2.512E-08	1.00E-08	2.512E+00	4	4	3.140E-09	2.16E-02	1.771964458	0.01165	4.78	0.78
20	2.515E-04	5.00E-10	3.162E-08	1.00E-08	3.162E+00	5	4	3.953E-09	9.60E-03	1.988176822	5.08E-03	5.65	0.65
20	2.822E-04	5.00E-10	3.981E-08	1.00E-08	3.981E+00	6	4	4.976E-09	3.45E-03	2.230771085	1.64E-03	6.60	0.60
20	3.166E-04	5.00E-10	5.012E-08	1.00E-08	5.012E+00	7	4	6.265E-09	9.51E-04	2.502966324	4.03E-04	7.56	0.56
20	3.552E-04	5.00E-10	6.310E-08	1.00E-08	6.310E+00	8	4	7.887E-09	1.88E-04	2.808374406	7.46E-05	8.48	0.48
20	3.986E-04	5.00E-10	7.943E-08	1.00E-08	7.943E+00	9	4	9.929E-09	2.44E-05	3.15104791	8.80E-06	9.42	0.42
20	4.472E-04	5.00E-10	1.000E-07	1.00E-08	1.000E+01	10	4	1.250E-08	1.86E-06	3.535533906	5.50E-07	10.40	0.40
20	5.018E-04	5.00E-10	1.259E-07	1.00E-08	1.259E+01	11	4	1.574E-08	7.32E-08	3.966934288	2.51E-08	11.29	0.29
20	5.630E-04	5.00E-10	1.585E-07	1.00E-08	1.585E+01	12	4	1.981E-08	1.24E-09	4.450973478	3.43E-10	12.27	0.27
20	6.317E-04	5.00E-10	1.995E-07	1.00E-08	1.995E+01	13	4	2.494E-08	7.37E-12	4.994074382	2.88E-12	13.16	0.16
20	7.088E-04	5.00E-10	2.512E-07	1.00E-08	2.512E+01	14	4	3.140E-08	1.16E-14	5.603443619	1.54E-12	13.26	-0.74

f (Hz)	A (V)	No (watt/Hz)	S (watt)	N (watt)	SNR	SNR (dB)	Rb (bps)	Eo	Pe (Incoh.)	x (Coherent)	Pe (Coh.)	x dB	ΔdB
288	5.367E-04	5.00E-10	1.440E-07	1.44E-07	1.000E+00	0	18	4.000E-09	9.16E-03	2	4.59E-03	0.69	0.69
288	6.021E-04	5.00E-10	1.813E-07	1.44E-07	1.259E+00	1	18	5.036E-09	3.25E-03	2.244036909	1.44E-03	1.65	0.65
288	6.756E-04	5.00E-10	2.282E-07	1.44E-07	1.585E+00	2	18	6.340E-09	8.83E-04	2.517850824	4.03E-04	2.51	0.51
288	7.580E-04	5.00E-10	2.873E-07	1.44E-07	1.995E+00	3	18	7.981E-09	1.71E-04	2.825075089	7.46E-05	3.43	0.43
288	8.505E-04	5.00E-10	3.617E-07	1.44E-07	2.512E+00	4	18	1.005E-08	2.16E-05	3.169786385	1.16E-05	4.26	0.26
288	9.543E-04	5.00E-10	4.554E-07	1.44E-07	3.162E+00	5	18	1.265E-08	1.61E-06	3.55655882	5.50E-07	5.35	0.35
288	1.071E-03	5.00E-10	5.733E-07	1.44E-07	3.981E+00	6	18	1.592E-08	6.07E-08	3.99052463	1.54E-08	6.36	0.36
288	1.201E-03	5.00E-10	7.217E-07	1.44E-07	5.012E+00	7	18	2.005E-08	9.83E-10	4.477442277	3.43E-10	7.22	0.22
288	1.348E-03	5.00E-10	9.086E-07	1.44E-07	6.310E+00	8	18	2.524E-08	5.47E-12	5.023772863	1.54E-12	8.21	0.21

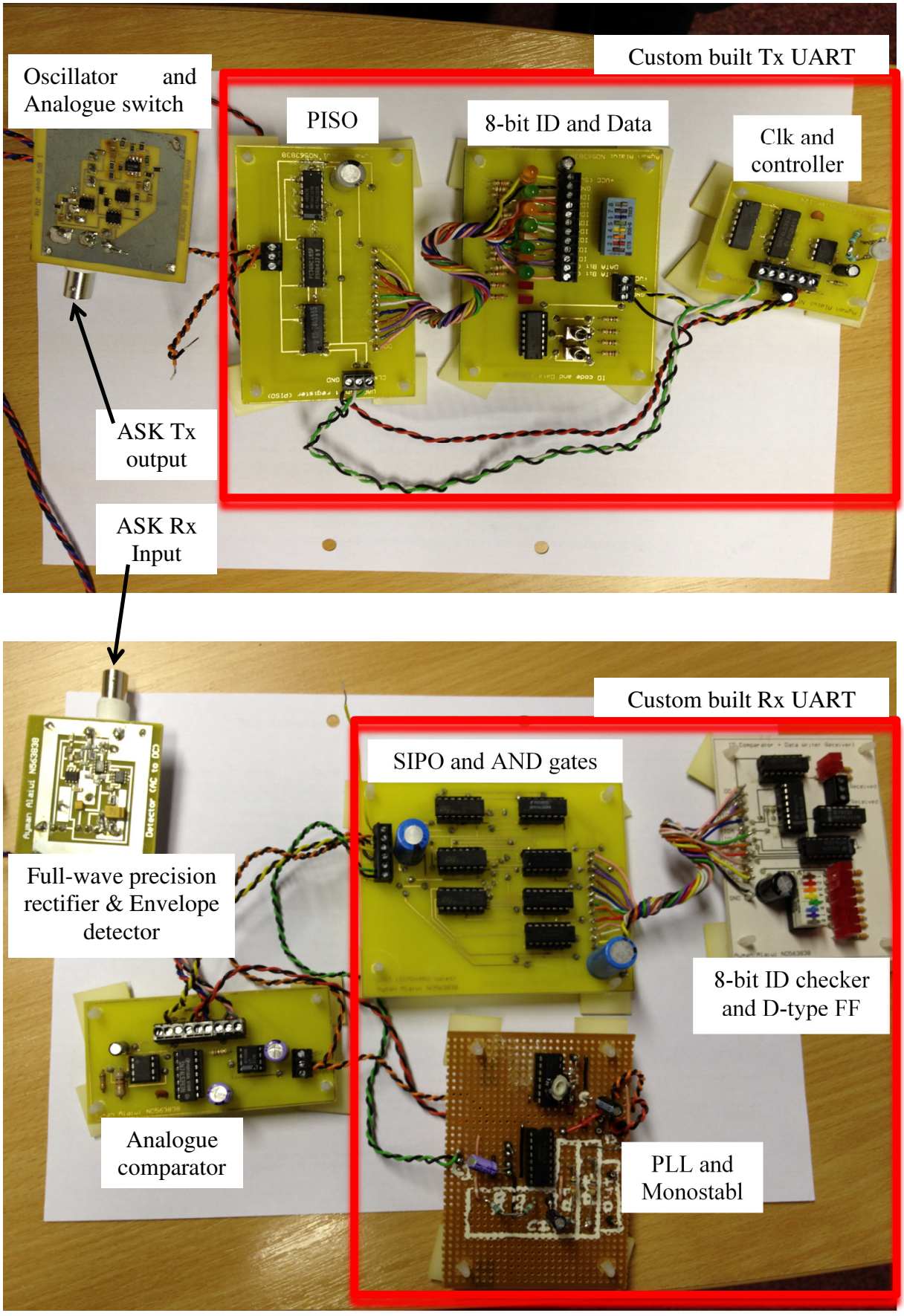
Oscillator and Analogue switch
Custom built Tx UART
PISO
8-bit ID and Data
Clk and controller
ASK Tx output
ASK Rx Input
Custom built Rx UART
SIPO and AND gates
Full-wave precision rectifier & Envelope detector
8-bit ID checker and D-type FF
Analogue comparator
PLL and Monostabl

x	Q (x)	x	Q (x)
0	0.500	0.05	0.480
0.10	0.460	0.15	0.440
0.20	0.421	0.25	0.401
0.30	0.382	0.35	0.363
0.40	0.345	0.45	0.326
0.50	0.309	0.55	0.291
0.60	0.274	0.65	0.258
0.70	0.242	0.75	0.227
0.80	0.212	0.85	0.198
0.90	0.184	0.95	0.171
1.00	0.159	1.05	0.147
1.10	0.136	1.15	0.125
1.20	0.115	1.25	0.106
1.30	0.097	1.35	0.089
1.40	0.081	1.45	0.074
1.50	0.067	1.55	0.061
1.60	0.055	1.65	0.049
1.70	0.045	1.75	0.04
1.80	0.036	1.85	0.032
1.90	0.029	1.95	0.026
2.00	0.023	2.05	0.020
2.10	0.018	2.15	0.016
2.20	0.014	2.25	0.012
2.30	0.011	2.35	0.009
2.40	0.008	2.45	0.007
2.50	0.006	2.55	0.005
2.60	0.005	2.65	0.004
2.70	0.003	2.75	0.003
2.80	0.003	2.85	0.002
2.90	0.002	2.95	0.002
3.00	0.001	3.05	0.001
3.10	9×10^{-4}	3.15	8×10^{-4}
3.20	7×10^{-4}	3.25	6×10^{-4}
3.30	6×10^{-4}	3.35	5×10^{-4}
3.40	4×10^{-4}	3.45	3×10^{-4}
3.50	3×10^{-4}	3.55	3×10^{-4}

```
% Matlab code for comparing the symbol error rate of Non-Coherent ASK,
Coherent ASK, BPSK, DPSK, QPSK, 8-PSK, Square 16-QAM, Star 16-QAM and My
16-QAM modulation
clear
M = 8;
Es_N0_dB = [0:25]; % multiple Es/N0 values
theorySer_CASK = 0.5*erfc(sqrt((10.^(Es_N0_dB/10))/2)); % Coherent ASK
theorySer_IASK = 0.5*exp(-(10.^(Es_N0_dB/10))/2);       % Noncoherent ASK
theorySer_BPSK = 0.5*erfc(sqrt(10.^(Es_N0_dB/10)));     % BPSK
theorySer_DPSK = 0.5*exp(-10.^(Es_N0_dB/10));           % DPSK
(Noncoherent)
theorySer_QPSK = 0.5*erfc(sqrt(10.^(Es_N0_dB/10))*sin(2*pi/M)); % QPSK
theorySer_8PSK = 0.5*erfc(sqrt(10.^(Es_N0_dB/10))*sin(pi/M));   % 8-PSK
theorySer_sq16QAM = 3/2*erfc(sqrt(0.1*10.^(Es_N0_dB/10)))-
9/4*((0.5*erfc(sqrt(0.1*10.^(Es_N0_dB/10))))).^2; % Square 16-QAM
close all
figure
semilogy(Es_N0_dB,theorySer_CASK,'bd-','LineWidth',2);
hold on
semilogy(Es_N0_dB,theorySer_IASK,'gs-','LineWidth',2);
hold on
semilogy(Es_N0_dB,theorySer_BPSK,'rd-','LineWidth',2);
hold on
semilogy(Es_N0_dB,theorySer_DPSK,'cp-','LineWidth',2);
hold on
semilogy(Es_N0_dB,theorySer_QPSK,'m--','LineWidth',2);
hold on
semilogy(Es_N0_dB,theorySer_8PSK,'ko-','LineWidth',2);
hold on
semilogy(Es_N0_dB,theorySer_sq16QAM,'rx-','LineWidth',2);
axis([0 25 10^-15 1])
grid on
legend('Coherent ASK', 'Noncoherent ASK', 'BPSK', 'DPSK (Noncoherent)',
'QPSK', '8-PSK', 'Square 16-QAM');
xlabel('Es/No, dB')
ylabel('Symbol Error Rate (SER)')
title('Pe for Coherent ASK, Noncoherent ASK, BPSK, DPSK, QPSK, 8PSK and
Square 16-QAM modulation');
```

```
1 library IEEE;
2 use IEEE.std_logic_1164 .all;
3 use IEEE.STD_LOGIC_UNSIGNED .all;
4
5 ENTITY phase_mapper IS
6 PORT (res : IN STD_LOGIC;
7 clk : IN STD_LOGIC;
8 din : IN std_logic_vector (2 downto 0); -- modulating data
9 ph_out : OUT std_logic_vector (11 downto 0):= (OTHERS => '0'));-- phase
output to NCO input
10 END phase_mapper ;
11
12 ARCHITECTURE behaviour OF phase_mapper IS
13
14 SIGNAL reg : STD_LOGIC_VECTOR (11 downto 0):= (OTHERS => '0'); --
Register to choose
the phase every 1/data_rate
15 SIGNAL cal_ph : std_logic_vector (12 downto 0):= (OTHERS => '0'); --
Phase register
16
17 BEGIN
18
19 PROCESS
20
21 BEGIN
22
23 WAIT UNTIL RISING_EDGE (clk);
24
25 IF res = '1' THEN reg (11 downto 0) <= (OTHERS => '0'); cal_ph<= (OTHERS
=> '0'); --
System reset
26
27 ELSE
28
29 reg (11 downto 0) <= reg (11 downto 0) - "000000000001" ; -- Count down
from
1/data_rate to 0
30
31 IF reg = "000000000000" THEN reg (11 downto 0) <= "111110011111" ; --
Choose the
corresponding phase and reset reg to 3999 (250 ms)
32
33 -- According to modulating data, shift the phase by:
34 CASE din (2 downto 0) IS
35 WHEN"001" => cal_ph(12 downto 0)<= cal_ph(11 downto 0)+"0001000000000"
;-- 45
degree
36 WHEN"010" => cal_ph(12 downto 0)<= cal_ph(11 downto 0)+"0010000000000"
;-- 90
degree
37 WHEN"011" => cal_ph(12 downto 0)<= cal_ph(11 downto 0)+"0011000000000"
;--
135 degree
38 WHEN"100" => cal_ph(12 downto 0)<= cal_ph(11 downto 0)+"0100000000000"
;--
180 degree
39 WHEN"101" => cal_ph(12 downto 0)<= cal_ph(11 downto 0)+"0101000000000"
;--
225 degree
40 WHEN"110" => cal_ph(12 downto 0)<= cal_ph(11 downto 0)+"0110000000000"
;--
270 degree
41 WHEN"111" => cal_ph(12 downto 0)<= cal_ph(11 downto 0)+"0111000000000"
;--
315 degree
42 WHEN OTHERS => cal_ph(11 downto 0)<= cal_ph(11 downto 0); -- Doesn't
shift
the phase
43 END CASE;
```

```
44
45 END IF;
46
47 ph_out(11 downto 0) <= cal_ph(11 downto 0); -- Send the new phase to NCO
(Phase
modulator)
48
49 END IF;
50
51 END PROCESS;
52
53 END behaviour;
```

```
1 library IEEE;
2 use IEEE.std_logic_1164 .all;
3 use IEEE.STD_LOGIC_SIGNED .all;
4
5 ENTITY sign_slicer IS
6 PORT (res : IN STD_LOGIC; -- Reset input
7 clk : IN STD_LOGIC; -- Clock
8
9 -- Pre-calculated cross correlation inputs
10 i_45 : IN STD_LOGIC_VECTOR (27 DOWNTO 0);
11 i_90 : IN STD_LOGIC_VECTOR (27 DOWNTO 0);
12 i_135 : IN STD_LOGIC_VECTOR (27 DOWNTO 0);
13 i_180 : IN STD_LOGIC_VECTOR (27 DOWNTO 0);
14
15 -- Highest of min and max points of cross correlation output
16 min_180 : OUT STD_LOGIC_VECTOR (27 DOWNTO 0):= (OTHERS => '0');
17 max_45 : OUT STD_LOGIC_VECTOR (27 DOWNTO 0):= (OTHERS => '0');
18 max_90 : OUT STD_LOGIC_VECTOR (27 DOWNTO 0):= (OTHERS => '0');
19 max_135 : OUT STD_LOGIC_VECTOR (27 DOWNTO 0):= (OTHERS => '0');
20 max_180 : OUT STD_LOGIC_VECTOR (27 DOWNTO 0):= (OTHERS => '0');
21 min_45 : OUT STD_LOGIC_VECTOR (27 DOWNTO 0):= (OTHERS => '0');
22 min_90 : OUT STD_LOGIC_VECTOR (27 DOWNTO 0):= (OTHERS => '0');
23 min_135 : OUT STD_LOGIC_VECTOR (27 DOWNTO 0):= (OTHERS => '0'));
24
25 END sign_slicer;
26
27 ARCHITECTURE bhv OF sign_slicer IS
28
29 SIGNAL x_peak_t_0 : INTEGER RANGE 0 TO 1; -- peak time of twice fc
30 SIGNAL x_peak_t_45 : INTEGER RANGE 0 TO 199; -- peak time of twice fc
31 SIGNAL x_peak_t_90 : INTEGER RANGE 0 TO 199; -- peak time of twice fc
32 SIGNAL x_peak_t_135 : INTEGER RANGE 0 TO 199; -- peak time of twice fc
33 SIGNAL min_180_reg : STD_LOGIC_VECTOR (27 DOWNTO 0) := (OTHERS => '0');
34 SIGNAL min_135_reg : STD_LOGIC_VECTOR (27 DOWNTO 0) := (OTHERS => '0');
35 SIGNAL min_90_reg : STD_LOGIC_VECTOR (27 DOWNTO 0) := (OTHERS => '0');
36 SIGNAL min_45_reg : STD_LOGIC_VECTOR (27 DOWNTO 0) := (OTHERS => '0');
37 SIGNAL max_180_reg : STD_LOGIC_VECTOR (27 DOWNTO 0) := (OTHERS => '0');
38 SIGNAL max_135_reg : STD_LOGIC_VECTOR (27 DOWNTO 0) := (OTHERS => '0');
39 SIGNAL max_90_reg : STD_LOGIC_VECTOR (27 DOWNTO 0) := (OTHERS => '0');
40 SIGNAL max_45_reg : STD_LOGIC_VECTOR (27 DOWNTO 0) := (OTHERS => '0');
41
42 BEGIN
43
44 PROCESS
45
46 BEGIN
47
48 WAIT UNTIL RISING_EDGE (clk);
49
50 IF res = '1' THEN -- System master reset --
51
52 x_peak_t_0 <= 1; -- Set to 199
53 x_peak_t_45 <= 199; -- Set to 199
54 x_peak_t_90 <= 199; -- Set to 199
55 x_peak_t_135 <= 199; -- Set to 199
56
57 min_45 (27 DOWNTO 0) <= (OTHERS => '0');
58 max_45 (27 DOWNTO 0) <= (OTHERS => '0');
59 min_90 (27 DOWNTO 0) <= (OTHERS => '0');
60 max_90 (27 DOWNTO 0) <= (OTHERS => '0');
61 min_135 (27 DOWNTO 0) <= (OTHERS => '0');
62 max_135 (27 DOWNTO 0) <= (OTHERS => '0');
63 min_180 (27 DOWNTO 0) <= (OTHERS => '0');
64 max_180 (27 DOWNTO 0) <= (OTHERS => '0');
65
66 min_45_reg (27 DOWNTO 0) <= (OTHERS => '0');
67 max_45_reg (27 DOWNTO 0) <= (OTHERS => '0');
68 min_90_reg (27 DOWNTO 0) <= (OTHERS => '0');
69 max_90_reg (27 DOWNTO 0) <= (OTHERS => '0');
```

```
70 min_135_reg (27 DOWNTO 0) <= (OTHERS => '0');
71 max_135_reg (27 DOWNTO 0) <= (OTHERS => '0');
72 min_180_reg (27 DOWNTO 0) <= (OTHERS => '0');
73 max_180_reg (27 DOWNTO 0) <= (OTHERS => '0');
74
75 ELSE
76
77 x_peak_t_0 <= x_peak_t_0 - 1; -- count down for the highest point
78
79 -------- Timing x0------------
80 IF x_peak_t_0 = 0 THEN
81
82 x_peak_t_0 <= 1;
83
84 min_45_reg (27 DOWNTO 0) <= (OTHERS => '0');
85 max_45_reg (27 DOWNTO 0) <= (OTHERS => '0');
86 min_90_reg (27 DOWNTO 0) <= (OTHERS => '0');
87 max_90_reg (27 DOWNTO 0) <= (OTHERS => '0');
88 min_135_reg (27 DOWNTO 0) <= (OTHERS => '0');
89 max_135_reg (27 DOWNTO 0) <= (OTHERS => '0');
90 min_180_reg (27 DOWNTO 0) <= (OTHERS => '0');
91 max_180_reg (27 DOWNTO 0) <= (OTHERS => '0');
92
93 END IF;
94
95
96 ------------- Find the highest cross correlation points ----------------
97
98 IF i_45 > "0" THEN max_45_reg <= i_45; END IF;
99 IF i_45 < "0" THEN min_45_reg <= i_45; END IF;
100
101 IF i_90 > "0" THEN max_90_reg <= i_90; END IF;
102 IF i_90 < "0" THEN min_90_reg <= i_90; END IF;
103
104 IF i_135 > "0" THEN max_135_reg <= i_135; END IF;
105 IF i_135 < "0" THEN min_135_reg <= i_135; END IF;
106
107 IF i_180 > "0" THEN max_180_reg <= i_180; END IF;
108 IF i_180 < "0" THEN min_180_reg <= i_180; END IF;
109
110 END IF;
111
112 min_45 <= min_45_reg;
113 max_45 <= max_45_reg;
114 min_90 <= min_90_reg;
115 max_90 <= max_90_reg;
116 min_135 <= min_135_reg;
117 max_135 <= max_135_reg;
118 min_180 <= min_180_reg;
119 max_180 <= max_180_reg;
120
121 END PROCESS;
122 END bhv;
```

```
1 library IEEE;
2 use IEEE.std_logic_1164 .all;
3 use IEEE.STD_LOGIC_SIGNED .all;
4
5 ENTITY peak_detector_8PSK_4Detectors IS
6 GENERIC (peak_t : STD_LOGIC_VECTOR := "00011000111" ); -- 199
7 PORT (res : IN STD_LOGIC; -- Reset input
8 clk : IN STD_LOGIC; -- Clock
9
10 -- Pre-calculated cross correlation inputs
11 i_min_180 : IN STD_LOGIC_VECTOR (27 DOWNTO 0);
12 i_max_45 : IN STD_LOGIC_VECTOR (27 DOWNTO 0);
13 i_max_90 : IN STD_LOGIC_VECTOR (27 DOWNTO 0);
14 i_max_135 : IN STD_LOGIC_VECTOR (27 DOWNTO 0);
15 i_max_180 : IN STD_LOGIC_VECTOR (27 DOWNTO 0);
16 i_min_45 : IN STD_LOGIC_VECTOR (27 DOWNTO 0);
17 i_min_90 : IN STD_LOGIC_VECTOR (27 DOWNTO 0);
18 i_min_135 : IN STD_LOGIC_VECTOR (27 DOWNTO 0);
19
20 -- Cross Correlation result ready for comparison
21 Wr_xcor : OUT STD_LOGIC;
22
23 -- Highest of min and max points of cross correlation output
24 o_0 : OUT STD_LOGIC_VECTOR (27 DOWNTO 0):= (OTHERS => '0');
25 o_45 : OUT STD_LOGIC_VECTOR (27 DOWNTO 0):= (OTHERS => '0');
26 o_90 : OUT STD_LOGIC_VECTOR (27 DOWNTO 0):= (OTHERS => '0');
27 o_135 : OUT STD_LOGIC_VECTOR (27 DOWNTO 0):= (OTHERS => '0');
28 o_180 : OUT STD_LOGIC_VECTOR (27 DOWNTO 0):= (OTHERS => '0');
29 o_225 : OUT STD_LOGIC_VECTOR (27 DOWNTO 0):= (OTHERS => '0');
30 o_270 : OUT STD_LOGIC_VECTOR (27 DOWNTO 0):= (OTHERS => '0');
31 o_315 : OUT STD_LOGIC_VECTOR (27 DOWNTO 0):= (OTHERS => '0'));
32
33 END peak_detector_8PSK_4Detectors ;
34
35 ARCHITECTURE bhv OF peak_detector_8PSK_4Detectors IS
36
37 SIGNAL reg : STD_LOGIC_VECTOR (10 DOWNTO 0); -- counter of cross
correlation
38
39 --------- Registers of max and min of cross correlation -------------
40 SIGNAL x_0_reg : STD_LOGIC_VECTOR (27 DOWNTO 0);
41 SIGNAL x_45_reg : STD_LOGIC_VECTOR (27 DOWNTO 0);
42 SIGNAL x_90_reg : STD_LOGIC_VECTOR (27 DOWNTO 0);
43 SIGNAL x_135_reg : STD_LOGIC_VECTOR (27 DOWNTO 0);
44 SIGNAL x_180_reg : STD_LOGIC_VECTOR (27 DOWNTO 0);
45 SIGNAL x_225_reg : STD_LOGIC_VECTOR (27 DOWNTO 0);
46 SIGNAL x_270_reg : STD_LOGIC_VECTOR (27 DOWNTO 0);
47 SIGNAL x_315_reg : STD_LOGIC_VECTOR (27 DOWNTO 0);
48
49 BEGIN
50
51 PROCESS
52
53 BEGIN
54
55 WAIT UNTIL RISING_EDGE (clk);
56
57 IF res = '1' THEN -- System master reset --
58
59 reg <= "00100101011" ; -- 299 -- "00100101011"; -- Set to 299
60
61 x_0_reg (27 DOWNTO 0) <= (OTHERS => '0');
62 x_45_reg (27 DOWNTO 0) <= (OTHERS => '0');
63 x_90_reg (27 DOWNTO 0) <= (OTHERS => '0');
64 x_135_reg (27 DOWNTO 0) <= (OTHERS => '0');
65 x_180_reg (27 DOWNTO 0) <= (OTHERS => '0');
66 x_225_reg (27 DOWNTO 0) <= (OTHERS => '0');
67 x_270_reg (27 DOWNTO 0) <= (OTHERS => '0');
68 x_315_reg (27 DOWNTO 0) <= (OTHERS => '0');
```

```
69
70 o_0 (27 DOWNTO 0) <= (OTHERS => '0');
71 o_45 (27 DOWNTO 0) <= (OTHERS => '0');
72 o_90 (27 DOWNTO 0) <= (OTHERS => '0');
73 o_135 (27 DOWNTO 0) <= (OTHERS => '0');
74 o_180 (27 DOWNTO 0) <= (OTHERS => '0');
75 o_225 (27 DOWNTO 0) <= (OTHERS => '0');
76 o_270 (27 DOWNTO 0) <= (OTHERS => '0');
77 o_315 (27 DOWNTO 0) <= (OTHERS => '0');
78
79 Wr_xcor <= '0';
80
81 ELSE
82
83 ------------ Find the highest cross correlation points ---------------
84
85 IF i_min_180 > x_0_reg THEN x_0_reg <= i_min_180; reg <= peak_t; END IF;
86 IF i_max_45 > x_45_reg THEN x_45_reg <= i_max_45; END IF;
87 IF i_max_90 > x_90_reg THEN x_90_reg <= i_max_90; END IF;
88 IF i_max_135 > x_135_reg THEN x_135_reg <= i_max_135; END IF;
89 IF i_max_180 > x_180_reg THEN x_180_reg <= i_max_180; END IF;
90 IF i_min_45 > x_225_reg THEN x_225_reg <= i_min_45; END IF;
91 IF i_min_90 > x_270_reg THEN x_270_reg <= i_min_90; END IF;
92 IF i_min_135 > x_315_reg THEN x_315_reg <= i_min_135; END IF;
93
94 reg (10 DOWNTO 0) <= reg (10 DOWNTO 0) - "00000000001" ; -- count down
for the cross correlation
95
96 IF reg = "00000001000" THEN -- hold min and max point for 8 samples
97
98 o_0 <= x_0_reg;
99 o_45 <= x_45_reg;
100 o_90 <= x_90_reg;
101 o_135 <= x_135_reg;
102 o_180 <= x_180_reg;
103 o_225 <= x_225_reg;
104 o_270 <= x_270_reg;
105 o_315 <= x_315_reg;
106
107 Wr_xcor <= '1';
108
109 -- Reset the registers after holding the max and min
110 -- of the cross correlation calculated above
111 ELSIF reg = "00000000000" THEN reg <= "00100101011" ; -- 299 --
"00100101011"; --  299 -- "00011111001"; -- 249 --"00110001111"; -- 399 --
peak_t; -- 199 "01001010111"; -- Set to 599
112
113 o_0 <= (OTHERS => '0');
114 x_0_reg <= (OTHERS => '0');
115 o_45 <= (OTHERS => '0');
116 x_45_reg <= (OTHERS => '0');
117 o_90 <= (OTHERS => '0');
118 x_90_reg <= (OTHERS => '0');
119 o_135 <= (OTHERS => '0');
120 x_135_reg <= (OTHERS => '0');
121 o_180 <= (OTHERS => '0');
122 x_180_reg <= (OTHERS => '0');
123 o_225 <= (OTHERS => '0');
124 x_225_reg <= (OTHERS => '0');
125 o_270 <= (OTHERS => '0');
126 x_270_reg <= (OTHERS => '0');
127 o_315 <= (OTHERS => '0');
128 x_315_reg <= (OTHERS => '0');
129
130 Wr_xcor <= '0';
131
132 END IF;
133 ------------------- End of cross correlation -------------------------
-
```

```
134
135 END IF;
136
137 END PROCESS;
138
139 END bhv;
```

```
1 library IEEE;
2 use IEEE.std_logic_1164 .all;
3 use IEEE.STD_LOGIC_SIGNED .all;
4
5 ENTITY xcor_comp_8PSK_Gray IS
6 GENERIC (angle_t : INTEGER := 3199);
7 PORT (res : IN STD_LOGIC; -- Reset input
8 clk : IN STD_LOGIC; -- Clock
9
10 -- Cross Correlation result ready for comparison
11 Re_xcor : IN STD_LOGIC_VECTOR (0 DOWNTO 0);
12
13 -- Highest of min and max points of cross correlation input
14 peak_0 : IN STD_LOGIC_VECTOR (27 DOWNTO 0);
15 peak_45 : IN STD_LOGIC_VECTOR (27 DOWNTO 0);
16 peak_90 : IN STD_LOGIC_VECTOR (27 DOWNTO 0);
17 peak_135 : IN STD_LOGIC_VECTOR (27 DOWNTO 0);
18 peak_180 : IN STD_LOGIC_VECTOR (27 DOWNTO 0);
19 peak_225 : IN STD_LOGIC_VECTOR (27 DOWNTO 0);
20 peak_270 : IN STD_LOGIC_VECTOR (27 DOWNTO 0);
21 peak_315 : IN STD_LOGIC_VECTOR (27 DOWNTO 0);
22
23 -- Phase data decided by the comparator
24 RxP_Data : OUT STD_LOGIC_VECTOR (2 DOWNTO 0):= (OTHERS => '0');
25 RxP_Data2 : OUT STD_LOGIC_VECTOR (2 DOWNTO 0):= (OTHERS => '0');
26 RxP_Data3 : OUT STD_LOGIC_VECTOR (2 DOWNTO 0):= (OTHERS => '0');
27 RxP_Data4 : OUT STD_LOGIC_VECTOR (2 DOWNTO 0):= (OTHERS => '0'));
28
29 END xcor_comp_8PSK_Gray ;
30
31 ARCHITECTURE bhv OF xcor_comp_8PSK_Gray IS
32
33 -- counter for the comparator of 8 angles
34 SIGNAL reg : INTEGER range 0 to 8;
35
36 -- Counter to detect the highest cross correlated point
37 SIGNAL reg2 : INTEGER range 0 to 3999;
38
39 --------- Registers of received phase data ----------
40 SIGNAL RxP_reg : STD_LOGIC_VECTOR (3 DOWNTO 0) := (OTHERS => '0');
41 SIGNAL RxP_reg_opp : STD_LOGIC_VECTOR (3 DOWNTO 0) := (OTHERS => '0');
42 SIGNAL RxP_reg2 : STD_LOGIC_VECTOR (3 DOWNTO 0):= (OTHERS => '0');
43 SIGNAL RxP_reg3 : STD_LOGIC_VECTOR (3 DOWNTO 0):= (OTHERS => '0');
44
45 --------- Register of an angle for the comparator ----------
46 SIGNAL ang_reg : STD_LOGIC_VECTOR (27 downto 0) := (OTHERS => '0');
47 SIGNAL ang_reg_opp : STD_LOGIC_VECTOR (27 downto 0) := (OTHERS => '0');
48
49
50 BEGIN
51
52 PROCESS
53
54 BEGIN
55
56 WAIT UNTIL RISING_EDGE (clk);
57
58 IF res = '1' THEN -- System master reset --
59
60 reg <= 0;
61
62 reg2 <= 0;
63
64 ELSE
65
66 IF Re_xcor = "1" THEN reg <= reg - 1; END IF;
67
68 CASE reg IS
69
```

```
70 WHEN 8 => ang_reg (27 downto 0) <= peak_0; RxP_reg <= "0000";
ang_reg_opp (27
downto 0) <= peak_0; RxP_reg_opp <= "0110";
71
72 WHEN 7 => IF peak_45 (27 downto 0)> ang_reg (27 downto 0) THEN
73 ang_reg (27 downto 0) <= peak_45 (27 downto 0);
74 RxP_reg <= "0001"; END IF;
75
76 IF peak_45 (27 downto 0)< ang_reg_opp (27 downto 0) THEN
77 ang_reg_opp (27 downto 0) <= peak_45 (27 downto 0); RxP_reg_opp
<= "0111";
78 END IF;
79
80 WHEN 6 => IF peak_90 (27 downto 0)> ang_reg (27 downto 0) THEN
81 ang_reg (27 downto 0) <= peak_90 (27 downto 0); RxP_reg <= "0011"; END
IF;
82
83 IF peak_90 (27 downto 0)< ang_reg_opp (27 downto 0) THEN
84 ang_reg_opp (27 downto 0) <= peak_90 (27 downto 0); RxP_reg_opp
<= "0101";
85 END IF;
86
87 WHEN 5 => IF peak_135 (27 downto 0) > ang_reg (27 downto 0) THEN
88 ang_reg (27 downto 0) <= peak_135 (27 downto 0); RxP_reg <= "0010"; END
IF;
89
90 IF peak_135 (27 downto 0)< ang_reg_opp (27 downto 0) THEN
91 ang_reg_opp (27 downto 0) <= peak_135 (27 downto 0); RxP_reg_opp
<= "0100";
92 END IF;
93
94 WHEN 4 => IF peak_180 (27 downto 0) > ang_reg (27 downto 0) THEN
95 ang_reg (27 downto 0) <= peak_180 (27 downto 0); RxP_reg <= "0110"; END
IF;
96
97 IF peak_180 (27 downto 0)< ang_reg_opp (27 downto 0) THEN
98 ang_reg_opp (27 downto 0) <= peak_180 (27 downto 0); RxP_reg_opp
<= "0000";
99 END IF;
100
101 WHEN 3 => IF peak_225 (27 downto 0) > ang_reg (27 downto 0) THEN
102 ang_reg (27 downto 0) <= peak_225 (27 downto 0); RxP_reg <= "0111"; END
IF;
103
104 IF peak_225 (27 downto 0)< ang_reg_opp (27 downto 0) THEN
105 ang_reg_opp (27 downto 0) <= peak_225 (27 downto 0); RxP_reg_opp
<= "0001";
106 END IF;
107
108 WHEN 2 => IF peak_270 (27 downto 0) > ang_reg (27 downto 0) THEN
109 ang_reg (27 downto 0) <= peak_270 (27 downto 0); RxP_reg <= "0101"; END
IF;
110
111 IF peak_270 (27 downto 0)< ang_reg_opp (27 downto 0) THEN
112 ang_reg_opp (27 downto 0) <= peak_270 (27 downto 0); RxP_reg_opp
<= "0011";
113 END IF;
114
115 WHEN 1 => IF peak_315 (27 downto 0) > ang_reg (27 downto 0) THEN
116 ang_reg (27 downto 0) <= peak_315 (27 downto 0); RxP_reg <= "0100"; END
IF;
117
118 IF peak_315 (27 downto 0)< ang_reg_opp (27 downto 0) THEN
119 ang_reg_opp (27 downto 0) <= peak_315 (27 downto 0); RxP_reg_opp
<= "0010";
120 END IF;
121
122 WHEN 0 => IF RxP_reg = RxP_reg_opp THEN RxP_reg2 (2 downto 0) <=
RxP_reg ( 2
```

```
downto 0); RxP_Data4 (2 downto 0) <= RxP_reg ( 2 downto 0);
123 ELSIF RxP_reg2 = RxP_reg THEN RxP_reg2 (2 downto 0) <= RxP_reg ( 2
downto 0); RxP_Data4 (2 downto 0) <= RxP_reg ( 2 downto 0); END IF;
124 --ELSE RxP_reg2 (2 downto 0) <= RxP_reg_opp ( 2 downto 0); END IF;
125
126 --RxP_reg2 (2 downto 0) <= RxP_reg (2 downto 0);
127 IF Re_xcor <= "1" THEN reg <= 0; ELSE reg <= 8; END IF;
128
129 WHEN OTHERS => reg <= 0;
130
131 END CASE;
132
133
134 RxP_Data2 (2 downto 0) <= RxP_reg (2 downto 0); -- Output test point
135 RxP_Data3 (2 downto 0) <= RxP_reg_opp (2 downto 0); -- Output test
point
136 --RxP_Data4 (2 downto 0) <= RxP_reg (2 downto 0); -- Output test point
137
138
139 reg2 <= reg2 - 1;
140
141 IF RxP_reg2 > RxP_reg3 THEN
142
143 reg2 <= angle_t;
144
145 RxP_reg3 <= RxP_reg2;
146
147 END IF;
148
149 IF reg2 = 8 THEN
150
151 RxP_Data (2 downto 0) <= RxP_reg3 (2 downto 0);
152
153 ELSIF reg2 = 0 THEN
154
155 reg2 <= 3999;
156
157 RxP_reg2 (3 downto 0) <= (OTHERS => '0');
158
159 RxP_reg3 (3 downto 0) <= (OTHERS => '0');
160
161 END IF;
162 END IF;
163 END PROCESS;
164 END bhv;
```

```
1 library IEEE;
2 use IEEE.std_logic_1164 .all;
3 use IEEE.STD_LOGIC_SIGNED .all;
4
5 ENTITY QAM_mapper IS
6 PORT (res : IN STD_LOGIC;
7 clk : IN STD_LOGIC;
8 din : IN std_logic_vector (3 downto 0); -- modulating data
9 amp_data : OUT std_logic_vector (0 downto 0):= (OTHERS => '0'); --
Amplitude
data
10 ph_out : OUT std_logic_vector (11 downto 0):= (OTHERS => '0'));-- phase
output to NCO input
11 END QAM_mapper;
12
13 ARCHITECTURE behaviour OF QAM_mapper IS
14
15 SIGNAL reg : INTEGER range 0 to 3999; -- Register to choose the phase
every 1/data_rate
16 SIGNAL amp_reg: std_logic_vector (0 downto 0):= (OTHERS => '0'); -- AM
register
17 SIGNAL cal_ph : std_logic_vector (12 downto 0):= (OTHERS => '0'); --
Phase register
18
19 BEGIN
20
21 PROCESS
22
23 BEGIN
24
25 WAIT UNTIL RISING_EDGE (clk);
26
27 IF res = '1' THEN reg <= 0; amp_reg <= (OTHERS => '0'); cal_ph<= (OTHERS
=> '0'); --
System reset
28
29 ELSE
30
31 reg <= reg - 1; -- Count down from 1/data_rate to 0
32
33 IF reg = 0 THEN reg <= 3999; -- Choose the corresponding phase and reset
reg to 249
34 -- According to modulating data, shift the phase by:
35 CASE din (2 downto 0) IS
36 WHEN"001" => cal_ph(12 downto 0)<= cal_ph(11 downto 0)+"0001000000000"
;-- 45
degree
37 WHEN"011" => cal_ph(12 downto 0)<= cal_ph(11 downto 0)+"0010000000000"
;-- 90
degree
38 WHEN"010" => cal_ph(12 downto 0)<= cal_ph(11 downto 0)+"0011000000000"
;--
135 degree
39 WHEN"110" => cal_ph(12 downto 0)<= cal_ph(11 downto 0)+"0100000000000"
;--
180 degree
40 WHEN"111" => cal_ph(12 downto 0)<= cal_ph(11 downto 0)+"0101000000000"
;--
225 degree
41 WHEN"101" => cal_ph(12 downto 0)<= cal_ph(11 downto 0)+"0110000000000"
;--
270 degree
42 WHEN"100" => cal_ph(12 downto 0)<= cal_ph(11 downto 0)+"0111000000000"
;--
315 degree
43 WHEN OTHERS => cal_ph(11 downto 0)<= cal_ph(11 downto 0); -- Doesn't
shift
the phase
44 END CASE;
```

```
45
46 If din(3) = '1' THEN -- Differentially encode the AM data
47
48 amp_reg (0) <= amp_reg (0) XOR '1';
49
50 END IF;
51
52 END IF;
53
54 amp_data(0) <= amp_reg (0); -- Amplitude data to AM modulator
55 ph_out(11 downto 0) <= cal_ph(11 downto 0); -- Send the new phase to NCO
(Phase modulator)
56
57 END IF;
58
59 END PROCESS;
60
61 END behaviour;
```

```
1 library IEEE;
2 use IEEE.std_logic_1164 .all;
3 use IEEE.STD_LOGIC_SIGNED .all;
4
5 ENTITY AM_timer IS
6 PORT (res : IN STD_LOGIC; -- Reset input
7 clk : IN STD_LOGIC; -- Clock
8
9 AM_Re : IN STD_LOGIC_VECTOR (0 DOWNTO 0); -- AM received
10
11 AM_lt : OUT STD_LOGIC_VECTOR (0 DOWNTO 0):= (OTHERS => '0'); --
Amplifiers
controller
12 AM_ht : OUT STD_LOGIC_VECTOR (0 DOWNTO 0):= (OTHERS => '0')); --
Amplifiers
controller
13
14 END AM_timer;
15
16 ARCHITECTURE bhv OF AM_timer IS
17
18 SIGNAL reg_ht : INTEGER range 0 to 799; -- Time of activating the
amplifiers when AM
goes high
19 SIGNAL reg_lt : INTEGER range 0 to 799; -- Time of activating the
amplifiers when AM
goes low
20 SIGNAL reg_h : INTEGER range 0 to 1;
21 SIGNAL reg_l : INTEGER range 0 to 1;
22
23 BEGIN
24
25 PROCESS
26
27 BEGIN
28
29 WAIT UNTIL RISING_EDGE (clk);
30
31 IF res = '1' THEN reg_h <= 0; reg_l <= 0; reg_ht <= 799; reg_lt <= 799;
-- System
master reset --
32
33 ELSE
34
35 ----- Control the Amplifiers when AM goes high -----
36
37 IF AM_Re = "1" AND reg_h = 0 THEN reg_ht <= reg_ht - 1; -- At present of
AM
count down 50ms
38 ELSIF AM_Re = "0" THEN reg_ht <= 799; reg_h <= 0; END IF; -- Otherwise
reset
39
40 IF reg_ht > 1 AND reg_ht < 799 THEN AM_ht <= "1"; -- Activate the
amplifiers for 50ms
41 ELSIF reg_ht = 0 THEN AM_ht <= "0"; reg_h <= 1; END IF; -- Reset the
amplifiers
42
43
44 ----- Control the Amplifiers when AM goes low -----
45
46 IF AM_Re = "0" AND reg_l = 0 THEN reg_lt <= reg_lt - 1; -- When AM goes
low
count down 50ms
47 ELSIF AM_Re = "1" THEN reg_lt <= 799; reg_l <= 0; END IF; -- Otherwise
reset
48
49 IF reg_lt > 1 AND reg_lt < 799 THEN AM_lt <= "1"; -- Activate the
amplifiers for 50ms
```

```
50 ELSIF reg_lt = 0 THEN AM_lt <= "0"; reg_l <= 1; END IF; -- Reset the
amplifiers
51
52 END IF;
53
54 END PROCESS;
55
56 END bhv;
```

```
1 library IEEE;
2 use IEEE.std_logic_1164 .all;
3 use IEEE.STD_LOGIC_UNSIGNED .all;
4
5 ENTITY peak_detector_QAM IS
6 GENERIC (peak_t : STD_LOGIC_VECTOR := "0011000111" ); -- 199 The best
choice
is 199 as I tried 249 and 299
7 PORT (res : IN STD_LOGIC; -- Reset input
8 clk : IN STD_LOGIC; -- Clock
9
10 -- Absolute value of actual and delayed 180deg Received signal
11 Rx : IN STD_LOGIC_VECTOR (13 DOWNTO 0);
12 Rx_180: IN STD_LOGIC_VECTOR (13 DOWNTO 0);
13
14 -- Pre-calculated cross correlation inputs
15 i_min_180 : IN STD_LOGIC_VECTOR (27 DOWNTO 0); -- 0
16 i_max_45 : IN STD_LOGIC_VECTOR (27 DOWNTO 0); -- 45
17 i_max_90 : IN STD_LOGIC_VECTOR (27 DOWNTO 0); -- 90
18 i_max_135 : IN STD_LOGIC_VECTOR (27 DOWNTO 0); -- 135
19 i_max_180 : IN STD_LOGIC_VECTOR (27 DOWNTO 0); -- 180
20 i_min_45 : IN STD_LOGIC_VECTOR (27 DOWNTO 0); -- 225
21 i_min_90 : IN STD_LOGIC_VECTOR (27 DOWNTO 0); -- 270
22 i_min_135 : IN STD_LOGIC_VECTOR (27 DOWNTO 0); -- 315
23
24 -- Cross Correlation result ready for comparison
25 Wr_xcor : OUT STD_LOGIC;
26
27 -- AM detected output to the multiplexer of amplifier
28 Rx_amp : OUT STD_LOGIC;
29
30 -- Highest of min and max points of cross correlation output
31 o_min_180 : OUT STD_LOGIC_VECTOR (27 DOWNTO 0):= (OTHERS => '0'); -- 0
32 o_max_45 : OUT STD_LOGIC_VECTOR (27 DOWNTO 0):= (OTHERS => '0'); -- 45
33 o_max_90 : OUT STD_LOGIC_VECTOR (27 DOWNTO 0):= (OTHERS => '0'); -- 90
34 o_max_135 : OUT STD_LOGIC_VECTOR (27 DOWNTO 0):= (OTHERS => '0'); -- 135
35 o_max_180 : OUT STD_LOGIC_VECTOR (27 DOWNTO 0):= (OTHERS => '0'); -- 180
36 o_min_45 : OUT STD_LOGIC_VECTOR (27 DOWNTO 0):= (OTHERS => '0'); -- 225
37 o_min_90 : OUT STD_LOGIC_VECTOR (27 DOWNTO 0):= (OTHERS => '0'); -- 270
38 o_min_135 : OUT STD_LOGIC_VECTOR (27 DOWNTO 0):= (OTHERS => '0'); -- 315
39
40 -- Timing the AM data to balance the amplitude weight of x correlation
41 Rx_AM_t : OUT STD_LOGIC);
42
43 END peak_detector_QAM ;
44
45 ARCHITECTURE bhv OF peak_detector_QAM IS
46
47 SIGNAL reg : STD_LOGIC_VECTOR (9 DOWNTO 0); -- counter of cross
correlation
48 SIGNAL reg2 : STD_LOGIC_VECTOR (7 DOWNTO 0); -- counter of AM detection
49
50 SIGNAL AM : STD_LOGIC_VECTOR (1 DOWNTO 0);
51
52 --------- Registers of AM singal changes ----------
53 SIGNAL Rx_max : STD_LOGIC_VECTOR (15 DOWNTO 0);
54 SIGNAL Rx_180_max : STD_LOGIC_VECTOR (15 DOWNTO 0);
55
56 --------- Registers of max and min of cross correlation -------------
57 SIGNAL max_45_reg : STD_LOGIC_VECTOR (27 DOWNTO 0);
58 SIGNAL min_45_reg : STD_LOGIC_VECTOR (27 DOWNTO 0);
59 SIGNAL max_90_reg : STD_LOGIC_VECTOR (27 DOWNTO 0);
60 SIGNAL min_90_reg : STD_LOGIC_VECTOR (27 DOWNTO 0);
61 SIGNAL max_135_reg : STD_LOGIC_VECTOR (27 DOWNTO 0);
62 SIGNAL min_135_reg : STD_LOGIC_VECTOR (27 DOWNTO 0);
63 SIGNAL max_180_reg : STD_LOGIC_VECTOR (27 DOWNTO 0);
64 SIGNAL min_180_reg : STD_LOGIC_VECTOR (27 DOWNTO 0);
65
66 BEGIN
```

```
67
68 PROCESS
69
70 BEGIN
71
72 WAIT UNTIL RISING_EDGE (clk);
73
74 IF res = '1' THEN -- System master reset --
75
76 reg <= "0100101011" ; -- Set to 299
77 reg2 <= (OTHERS => '0');
78
79 Rx_max (15 DOWNTO 0) <= (OTHERS => '0');
80 Rx_180_max (15 DOWNTO 0) <= (OTHERS => '0');
81
82 min_45_reg (27 DOWNTO 0) <= (OTHERS => '0');
83 max_45_reg (27 DOWNTO 0) <= (OTHERS => '0');
84 min_90_reg (27 DOWNTO 0) <= (OTHERS => '0');
85 max_90_reg (27 DOWNTO 0) <= (OTHERS => '0');
86 min_135_reg (27 DOWNTO 0) <= (OTHERS => '0');
87 max_135_reg (27 DOWNTO 0) <= (OTHERS => '0');
88 min_180_reg (27 DOWNTO 0) <= (OTHERS => '0');
89 max_180_reg (27 DOWNTO 0) <= (OTHERS => '0');
90
91 o_min_45 (27 DOWNTO 0) <= (OTHERS => '0');
92 o_max_45 (27 DOWNTO 0) <= (OTHERS => '0');
93 o_min_90 (27 DOWNTO 0) <= (OTHERS => '0');
94 o_max_90 (27 DOWNTO 0) <= (OTHERS => '0');
95 o_min_135 (27 DOWNTO 0) <= (OTHERS => '0');
96 o_max_135 (27 DOWNTO 0) <= (OTHERS => '0');
97 o_min_180 (27 DOWNTO 0) <= (OTHERS => '0');
98 o_max_180 (27 DOWNTO 0) <= (OTHERS => '0');
99
100 Rx_AM_t <= '0';
101
102 Rx_amp <= '0';
103
104 Wr_xcor <= '0';
105
106 ELSE
107
108 ------------- Find the highest cross correlation points ---------------
-
109
110 IF i_min_180 > min_180_reg THEN min_180_reg <= i_min_180; reg <=
peak_t; END IF;
111
112 IF i_max_45 > max_45_reg THEN max_45_reg <= i_max_45; END IF;
113 IF i_max_90 > max_90_reg THEN max_90_reg <= i_max_90; END IF;
114 IF i_max_135 > max_135_reg THEN max_135_reg <= i_max_135; END IF;
115 IF i_max_180 > max_180_reg THEN max_180_reg <= i_max_180; END IF; --reg
<= peak_t;
END IF;
116
117 IF i_min_45 > min_45_reg THEN min_45_reg <= i_min_45; END IF;
118 IF i_min_90 > min_90_reg THEN min_90_reg <= i_min_90; END IF;
119 IF i_min_135 > min_135_reg THEN min_135_reg <= i_min_135; END IF;
120
121 reg (9 DOWNTO 0) <= reg (9 DOWNTO 0) - "0000000001" ; -- count down for
the cross
correlation
122
123 IF reg = "0000001000" THEN -- hold min and max point for 1000 samples
124
125 o_min_45 <= min_45_reg;
126 o_max_45 <= max_45_reg;
127 o_min_90 <= min_90_reg;
128 o_max_90 <= max_90_reg;
129 o_min_135 <= min_135_reg;
```

```
130 o_max_135 <= max_135_reg;
131 o_min_180 <= min_180_reg;
132 o_max_180 <= max_180_reg;
133
134 Wr_xcor <= '1';
135
136 -- Reset the registers after holding the max and min
137 -- of the cross correlation calculated above
138 ELSIF reg = "0000000000" THEN reg <= "0100101011" ; -- 299 The best
choice is 299
as I tried 199, 249, 399 and 599
139
140 o_min_45 <= (OTHERS => '0');
141 min_45_reg <= (OTHERS => '0');
142 o_max_45 <= (OTHERS => '0');
143 max_45_reg <= (OTHERS => '0');
144 o_min_90 <= (OTHERS => '0');
145 min_90_reg <= (OTHERS => '0');
146 o_max_90 <= (OTHERS => '0');
147 max_90_reg <= (OTHERS => '0');
148 o_min_135 <= (OTHERS => '0');
149 min_135_reg <= (OTHERS => '0');
150 o_max_135 <= (OTHERS => '0');
151 max_135_reg <= (OTHERS => '0');
152 o_min_180 <= (OTHERS => '0');
153 min_180_reg <= (OTHERS => '0');
154 o_max_180 <= (OTHERS => '0');
155 max_180_reg <= (OTHERS => '0');
156
157 Rx_amp <= '0';
158
159 Wr_xcor <= '0';
160
161 AM <= "10";
162
163 ELSIF AM = "00" OR AM = "01" THEN
164
165 reg <= peak_t;
166
167 o_min_45 <= (OTHERS => '0');
168 --min_45_reg <= (OTHERS => '0'); It was better to disable the reset of
registers only
169 o_max_45 <= (OTHERS => '0');
170 --max_45_reg <= (OTHERS => '0');
171 o_min_90 <= (OTHERS => '0');
172 --min_90_reg <= (OTHERS => '0');
173 o_max_90 <= (OTHERS => '0');
174 --max_90_reg <= (OTHERS => '0');
175 o_min_135 <= (OTHERS => '0');
176 --min_135_reg <= (OTHERS => '0');
177 o_max_135 <= (OTHERS => '0');
178 --max_135_reg <= (OTHERS => '0');
179 o_min_180 <= (OTHERS => '0');
180 --min_180_reg <= (OTHERS => '0');
181 o_max_180 <= (OTHERS => '0');
182 --max_180_reg <= (OTHERS => '0');
183
184 Wr_xcor <= '0';
185
186 AM <= "10";
187
188 END IF;
189 ------------------- End of cross correlation ------------------------
-
190
191
192 ------------------- Find the changes in AM signal --------------------
194 IF Rx > Rx_max THEN Rx_max <= "00"&Rx; END IF;
195 IF Rx_180 > Rx_180_max THEN Rx_180_max <= "00"&Rx_180; END IF;
```

```
196
197 reg2 <= reg2 - "00000001"; -- count down for the AM signals
198
199 IF reg2 = "00000001" THEN
200
201 IF Rx_max > (Rx_180_max + Rx_180_max) THEN
202
203 Rx_amp <= '1';
204
205 Rx_AM_t <= '1';
206
207 AM <= "01";
208
209 ELSIF Rx_180_max > (Rx_max + Rx_max) THEN
210
211 Rx_amp <= '1';
212
213 Rx_AM_t <= '0';
214
215 AM <= "00";
216
217 END IF;
218
219 ELSIF reg2 <= "00000000" THEN reg2 <= "11000111"; -- Then reg2 = 199
220
221 Rx_max (15 DOWNTO 0) <= (OTHERS => '0');
222 Rx_180_max (15 DOWNTO 0) <= (OTHERS => '0');
223
224 END IF;
225 ------------------------ End of AM detection --------------------------
-
226
227 END IF;
228
229 END PROCESS;
230
231 END bhv;
```

```
1 library IEEE;
2 use IEEE.std_logic_1164 .all;
3 use IEEE.STD_LOGIC_SIGNED .all;
4
5 ENTITY xcor_comp_QAM IS
6 GENERIC (angle_t : INTEGER := 3199);
7 PORT (res : IN STD_LOGIC; -- Reset input
8 clk : IN STD_LOGIC; -- Clock
9
10 -- Cross Correlation result ready for comparison
11 Re_xcor : IN STD_LOGIC_VECTOR (0 DOWNTO 0);
12
13 AM_in : IN std_logic_vector (0 downto 0);
14
15 -- Highest of min and max points of cross correlation input
16 xmin_180 : IN STD_LOGIC_VECTOR (27 DOWNTO 0); -- 0
17 xmax_45 : IN STD_LOGIC_VECTOR (27 DOWNTO 0); -- 45
18 xmax_90 : IN STD_LOGIC_VECTOR (27 DOWNTO 0); -- 90
19 xmax_135 : IN STD_LOGIC_VECTOR (27 DOWNTO 0); -- 135
20 xmax_180 : IN STD_LOGIC_VECTOR (27 DOWNTO 0); -- 180
21 xmin_45 : IN STD_LOGIC_VECTOR (27 DOWNTO 0); -- 225
22 xmin_90 : IN STD_LOGIC_VECTOR (27 DOWNTO 0); -- 270
23 xmin_135 : IN STD_LOGIC_VECTOR (27 DOWNTO 0); -- 315
24
25 -- Phase data decided by the comparator
26 RxP_Data : OUT STD_LOGIC_VECTOR (3 DOWNTO 0):= (OTHERS => '0');
27 RxP_Data2 : OUT STD_LOGIC_VECTOR (3 DOWNTO 0):= (OTHERS => '0');
28 RxP_Data3 : OUT STD_LOGIC_VECTOR (3 DOWNTO 0):= (OTHERS => '0');
29 RxP_Data4 : OUT STD_LOGIC_VECTOR (3 DOWNTO 0):= (OTHERS => '0'));
30 END xcor_comp_QAM ;
31
32 ARCHITECTURE bhv OF xcor_comp_QAM IS
33
34 -- counter for the comparator of 8 angles
35 SIGNAL reg : INTEGER range 0 to 8;
36
37 -- Counter to detect the highest cross correlated point
38 SIGNAL reg2 : INTEGER range 0 to 3999;
39
40 SIGNAL AM_reg : std_logic_vector (0 downto 0) := (OTHERS => '0');
41
42 --------- Registers of received phase data ----------
43 SIGNAL RxP_reg : STD_LOGIC_VECTOR (4 DOWNTO 0) := (OTHERS =>
'0');
44 SIGNAL RxP_reg_opp: STD_LOGIC_VECTOR (4 DOWNTO 0) := (OTHERS =>
'0');
45 SIGNAL RxP_reg2 : STD_LOGIC_VECTOR (4 DOWNTO 0):= (OTHERS =>
'0');
46 SIGNAL RxP_reg3 : STD_LOGIC_VECTOR (4 DOWNTO 0):= (OTHERS =>
'0');
47
48 --------- Register of an angle for the comparator ----------
49 SIGNAL ang_reg : STD_LOGIC_VECTOR (27 downto 0) := (OTHERS =>
'0');
50 SIGNAL ang_reg_opp: STD_LOGIC_VECTOR (27 downto 0) := (OTHERS =>
'0');
51
52
53 BEGIN
54
55 PROCESS
56
57 BEGIN
```

```
58
59 WAIT UNTIL RISING_EDGE (clk);
60
61 IF res = '1' THEN -- System master reset --
62
63 reg <= 0;
64
65 reg2 <= 0;
67 AM_reg <= ( OTHERS => '0');
68
69 ELSE
70
71 IF Re_xcor = "1" THEN reg <= reg - 1; END IF;
72
73 CASE reg IS
74
75 WHEN 8 => ang_reg (27 downto 0) <= xmin_180; RxP_reg <= "00000";
ang_reg_opp (27
downto 0) <= xmin_180; RxP_reg_opp <="00110";
76
77 WHEN 7 => IF xmax_45 (27 downto 0)> ang_reg (27 downto 0) THEN
78 ang_reg (27 downto 0) <= xmax_45 (27 downto 0);
79 RxP_reg <= "00001";
80 END IF;
81
82 IF xmax_45 (27 downto 0) < ang_reg_opp (27 downto 0) THEN
83 ang_reg_opp (27 downto 0) <= xmax_45 (27 downto 0); RxP_reg_opp
<=
"00111";
84 END IF;
85
86 IF AM_in (0) = '1' THEN AM_reg (0) <= AM_in (0);
87 ELSE AM_reg <= ( OTHERS => '0'); END IF;
88
89 WHEN 6 => IF xmax_90 (27 downto 0)> ang_reg (27 downto 0) THEN
90 ang_reg (27 downto 0) <= xmax_90 (27 downto 0); RxP_reg <=
"00011"; END
IF;
91
92 IF xmax_90 (27 downto 0) < ang_reg_opp (27 downto 0) THEN
93 ang_reg_opp (27 downto 0) <= xmax_90 (27 downto 0); RxP_reg_opp
<=
"00101";
94 END IF;
95
96 WHEN 5 => IF xmax_135 (27 downto 0) > ang_reg (27 downto 0) THEN
97 ang_reg (27 downto 0) <= xmax_135 (27 downto 0); RxP_reg <=
"00010"; END
IF;
98
99 IF xmax_135 (27 downto 0) < ang_reg_opp (27 downto 0) THEN
100 ang_reg_opp (27 downto 0) <= xmax_135 (27 downto 0); RxP_reg_opp
<=
"00100";
101 END IF;
102
103 WHEN 4 => IF xmax_180 (27 downto 0) > ang_reg (27 downto 0) THEN
104 ang_reg (27 downto 0) <= xmax_180 (27 downto 0); RxP_reg <=
"00110"; END
IF;
105
106 IF xmax_180 (27 downto 0) < ang_reg_opp (27 downto 0) THEN
```

```
107 ang_reg_opp (27 downto 0) <= xmax_180 (27 downto 0); RxP_reg_opp
<=
"00000";
108 END IF;
109
110 WHEN 3 => IF xmin_45 (27 downto 0) > ang_reg (27 downto 0) THEN
111 ang_reg (27 downto 0) <= xmin_45 (27 downto 0); RxP_reg <=
"00111"; END
IF;
112
113 IF xmin_45 (27 downto 0) < ang_reg_opp (27 downto 0) THEN
114 ang_reg_opp (27 downto 0) <= xmin_45 (27 downto 0); RxP_reg_opp
<=
"00001";
115 END IF;
116
117 WHEN 2 => IF xmin_90 (27 downto 0) > ang_reg (27 downto 0) THEN
118 ang_reg (27 downto 0) <= xmin_90 (27 downto 0); RxP_reg <=
"00101"; END
IF;
119
120 IF xmin_90 (27 downto 0) < ang_reg_opp (27 downto 0) THEN
121 ang_reg_opp (27 downto 0) <= xmin_90 (27 downto 0); RxP_reg_opp
<=
"00011";
122 END IF;
123
124 WHEN 1 => IF xmin_135 (27 downto 0) > ang_reg (27 downto 0) THEN
125 ang_reg (27 downto 0) <= xmin_135 (27 downto 0); RxP_reg <=
"00100"; END
IF;
126
127 IF xmin_135 (27 downto 0) < ang_reg_opp (27 downto 0) THEN
128 ang_reg_opp (27 downto 0) <= xmin_135 (27 downto 0); RxP_reg_opp
<=
"00010";
129 END IF;
130
131 WHEN 0 => IF RxP_reg = RxP_reg_opp THEN RxP_reg2 (2 downto 0) <=
RxP_reg (2
downto 0); RxP_reg2 (3) <= AM_reg(0); RxP_Data4 (2 downto 0) <=
RxP_reg (2 downto 0);
RxP_Data4 (3) <= AM_reg(0);
132 ELSIF RxP_reg2 = RxP_reg THEN RxP_reg2 (2 downto 0) <= RxP_reg
(2
downto 0); RxP_Data4 (2 downto 0) <= RxP_reg (2 downto 0); RxP_Data4
(3) <= AM_reg(0);
END IF;
133 RxP_reg2 (3) <= AM_reg(0);
134
135 IF Re_xcor <= "1" THEN reg <= 0; ELSE reg <= 8; AM_reg (0) <=
AM_in (0);
END IF;
136
137 WHEN OTHERS => reg <= 0;
138
139 END CASE;
140
141 RxP_Data2 (2 downto 0) <= RxP_reg (2 downto 0);
142 RxP_Data3 (2 downto 0) <= RxP_reg_opp (2 downto 0);
143
144 reg2 <= reg2 - 1;
145
```

```
146 IF RxP_reg2 > RxP_reg3 THEN
147
148 reg2 <= angle_t;
149
150 RxP_reg3 <= RxP_reg2;
151
152 END IF;
153
154 IF reg2 = 8 THEN
155
156 RxP_Data (3 downto 0) <= RxP_reg3 (3 downto 0);
157
158 ELSIF reg2 = 0 THEN
159
160 reg2 <= 3999;
161
162 RxP_reg2 (4 downto 0) <= (OTHERS => '0');
163
164 RxP_reg3 (4 downto 0) <= (OTHERS => '0');
165
166 END IF;
167
168 END IF;
169
170 END PROCESS;
171
172 END bhv;
```

```
1 library IEEE;
2 use IEEE.std_logic_1164 .all;
3 use IEEE.STD_LOGIC_UNSIGNED .all;
4
5 ENTITY error_rate_4bit IS
6 PORT (res, en : IN STD_LOGIC; -- Reset
7 clk : IN STD_LOGIC; -- Clock
8 Tx : IN std_logic_vector (3 downto 0); -- transmitted data
9 Rx : IN std_logic_vector (3 downto 0); -- received data
10 bit_error : OUT std_logic_vector (50 downto 0):= (OTHERS => '0');
--
total # of correct symbols
11 symbol_error : OUT std_logic_vector (50 downto 0):= (OTHERS =>
'0'));--
total # of error symbols
12 END error_rate_4bit ;
13
14 ARCHITECTURE behaviour OF error_rate_4bit IS
15
16 --SIGNAL reg : STD_LOGIC_VECTOR (11 downto 0):= (OTHERS => '0');
-- counter
17 SIGNAL reg : INTEGER RANGE 0 to 3999;
18 SIGNAL reg2 : INTEGER RANGE 0 to 3999;
19 SIGNAL correct_reg: std_logic_vector (50 downto 0):= (OTHERS =>
'0'); -- total # of
correct symbols register
20 SIGNAL symbol_reg : std_logic_vector (50 downto 0):= (OTHERS =>
'0'); -- total # of
error symbols register
21 SIGNAL c_bit_reg : std_logic_vector (50 downto 0):= (OTHERS =>
'0'); -- total # of
error bits register
22 SIGNAL bit_reg : std_logic_vector (50 downto 0):= (OTHERS =>
'0'); -- total # of bits
register
23
24 SIGNAL XOR_reg : std_logic_vector (3 downto 0):= (OTHERS => '0');
-- total # of error
symbols register
25
26 BEGIN
27
28 PROCESS
29
30 BEGIN
31
32 WAIT UNTIL RISING_EDGE (clk);
33
34 -- System reset
35 IF res = '1' THEN
36
37 --reg (11 downto 0) <= (OTHERS => '0');
38 reg <= 0;
39 reg2 <= 0;
40 correct_reg <= (OTHERS => '0');
41 symbol_reg <= (OTHERS => '0');
42 bit_reg <= (OTHERS => '0');
43 c_bit_reg <= (OTHERS => '0');
44 XOR_reg <= (OTHERS => '0');
45
46 ELSE
47
48 reg <= reg - 1; -- Count down from 1/data_rate to 0
```

```
49
50 reg2 <= reg2 - 1; -- Count down from 1/data_rate to 0
51
52 IF reg = 0 THEN reg <= 3999; END IF; -- Reset register
53
54 IF reg2 = 0 THEN reg2 <= 3999; END IF; -- Reset register
55
56 IF reg2 = 1 AND en = '1' THEN
57
58 symbol_reg <= symbol_reg + "0000000001" ; -- Symbols Error
counter
59 bit_reg <= bit_reg + "0000000100" ; -- Bits Error counter
60
61 END IF;
62
63 IF reg = 1000 AND en = '1' THEN
64
65 CASE (Rx XOR Tx) IS
66
67 WHEN "0001" => c_bit_reg <= c_bit_reg + "0000000011" ; --reg <=
3999;
68 WHEN "0010" => c_bit_reg <= c_bit_reg + "0000000011" ; --reg <=
3999;
69 WHEN "0100" => c_bit_reg <= c_bit_reg + "0000000011" ; --reg <=
3999;
70 WHEN "1000" => c_bit_reg <= c_bit_reg + "0000000011" ; --reg <=
3999;
71
72 WHEN "0011" => c_bit_reg <= c_bit_reg + "0000000010" ; --reg <=
3999;
73 WHEN "0110" => c_bit_reg <= c_bit_reg + "0000000010" ; --reg <=
3999;
74 WHEN "1100" => c_bit_reg <= c_bit_reg + "0000000010" ; --reg <=
3999;
75 WHEN "1010" => c_bit_reg <= c_bit_reg + "0000000010" ; --reg <=
3999;
76 WHEN "1001" => c_bit_reg <= c_bit_reg + "0000000010" ; --reg <=
3999;
77 WHEN "0101" => c_bit_reg <= c_bit_reg + "0000000010" ; --reg <=
3999;
78
79 WHEN "0111" => c_bit_reg <= c_bit_reg + "0000000001" ; --reg <=
3999;
80 WHEN "1110" => c_bit_reg <= c_bit_reg + "0000000001" ; --reg <=
3999;
81 WHEN "1011" => c_bit_reg <= c_bit_reg + "0000000001" ; --reg <=
3999;
82 WHEN "1101" => c_bit_reg <= c_bit_reg + "0000000001" ; --reg <=
3999;
83
84 WHEN "1111" => c_bit_reg <= c_bit_reg; --reg <= 3999;
85
86 WHEN OTHERS => XOR_reg <= "0000"; correct_reg <= correct_reg +
"0000000001" ;
c_bit_reg <= c_bit_reg + "0000000100" ;
87
88 END CASE;
89
90 --IF (Tx = Rx) THEN
91
92 -- correct_reg <= correct_reg + "0000000001"; c_bit_reg <=
c_bit_reg +
"0000000100"; --reg <= 3800; -- Correct symobls counter
```

```
93
94 -- XOR_reg <= "0000";
95
96 --END IF;
97
98 --ELSIF Rx > Tx OR Rx < Tx THEN
99
100 -- reg <= 3199;
101 -- XOR_reg <= Tx XOR Rx;
102
103 END IF;
104
105 END IF;
106
107 bit_error <= bit_reg - c_bit_reg; -- Output # of error bits
108 symbol_error <= symbol_reg - correct_reg; -- Output # of error
symbols
109
110 END PROCESS;
111
112 END behaviour;
```

```
1 library IEEE;
2 use IEEE.std_logic_1164 .all;
3 use IEEE.STD_LOGIC_UNSIGNED .all;
4
5 ENTITY error_rate_3bit IS
6 PORT (res, en : IN STD_LOGIC; -- Reset
7 clk : IN STD_LOGIC; -- Clock
8 Tx : IN std_logic_vector (2 downto 0); -- transmitted data
9 Rx : IN std_logic_vector (2 downto 0); -- received data
10 bit_error : OUT std_logic_vector (50 downto 0):= (OTHERS => '0'); --
total # of correct symbols
11 symbol_error : OUT std_logic_vector (50 downto 0):= (OTHERS => '0'));--
total # of error symbols
12 END error_rate_3bit ;
13
14 ARCHITECTURE behaviour OF error_rate_3bit IS
15
16 --SIGNAL reg : STD_LOGIC_VECTOR (11 downto 0):= (OTHERS => '0'); --
counter
17 SIGNAL reg : INTEGER RANGE 0 to 3999;
18 SIGNAL reg2 : INTEGER RANGE 0 to 3999;
19 SIGNAL correct_reg: std_logic_vector (50 downto 0):= (OTHERS => '0'); --
total # of
correct symbols register
20 SIGNAL symbol_reg : std_logic_vector (50 downto 0):= (OTHERS => '0'); --
total # of
error symbols register
21 SIGNAL c_bit_reg : std_logic_vector (50 downto 0):= (OTHERS => '0'); --
total # of
error bits register
22 SIGNAL bit_reg : std_logic_vector (50 downto 0):= (OTHERS => '0'); --
total # of bits
register
23
24 BEGIN
25
26 PROCESS
27
28 BEGIN
29
30 WAIT UNTIL RISING_EDGE (clk);
31
32 -- System reset
33 IF res = '1' THEN
34
35 --reg (11 downto 0) <= (OTHERS => '0');
36 reg <= 0;
37 reg2 <= 0;
38 correct_reg <= (OTHERS => '0');
39 symbol_reg <= (OTHERS => '0');
40 bit_reg <= (OTHERS => '0');
41 c_bit_reg <= (OTHERS => '0');
42
43 ELSE
44
45 reg <= reg - 1; -- Count down from 1/data_rate to 0
46
47 reg2 <= reg2 - 1; -- Count down from 1/data_rate to 0
48
49 IF reg = 0 THEN reg <= 3999; END IF; -- Reset register
50
51 IF reg2 = 0 THEN reg2 <= 3999; END IF; -- Reset register
52
53 IF reg2 = 1 AND en = '1' THEN
54
55 symbol_reg <= symbol_reg + "0000000001" ; -- Symbols Error counter
56 bit_reg <= bit_reg + "0000000011" ; -- Bits Error counter
57
58 END IF;
```

```
59
60 IF reg = 1000 AND en = '1' THEN
61
62 CASE (Rx XOR Tx) IS
63
64 WHEN "001" => c_bit_reg <= c_bit_reg + "0000000010" ; --reg <= 0;
65 WHEN "010" => c_bit_reg <= c_bit_reg + "0000000010" ; --reg <= 0;
66 WHEN "100" => c_bit_reg <= c_bit_reg + "0000000010" ; --reg <= 0;
67
68 WHEN "011" => c_bit_reg <= c_bit_reg + "0000000001" ; --reg <= 0;
69 WHEN "101" => c_bit_reg <= c_bit_reg + "0000000001" ; --reg <= 0;
70 WHEN "110" => c_bit_reg <= c_bit_reg + "0000000001" ; --reg <= 0;
71
72 WHEN "111" => c_bit_reg <= c_bit_reg; --reg <= 0;
73
74 WHEN OTHERS => correct_reg <= correct_reg + "0000000001" ; c_bit_reg <=
c_bit_reg + "0000000011" ; -- Correct symobls counter
75
76 END CASE;
77
78 --ELSIF Rx > Tx OR Rx < Tx THEN
79
80 --reg <= 3500;
81
82 END IF;
83
84 END IF;
85
86 bit_error <= bit_reg - c_bit_reg; -- Output # of error bits
87 symbol_error <= symbol_reg - correct_reg; -- Output # of error symbols
88
89 END PROCESS;
90
91 END behaviour;
```

```
1 --The code produces PRBS data of 8-Bit length and give an output of 4-Bit
2 --a time as (a,b,c,d) to use them as input to 16-QAM (2^4-QAM)
transmitter
3
4 library IEEE;
5 use IEEE.std_logic_1164 .all;
6 use IEEE.std_LOGIC_UNSIGNED .all;
7
8 ENTITY PRBS3bit IS
9 PORT (clk, res, enable : IN STD_LOGIC; --clock
10 dout : OUT STD_LOGIC_VECTOR (2 downto 0) := (OTHERS => '0')); --
Out register
11 END PRBS3bit;
12
13 ARCHITECTURE bhv OF PRBS3bit IS
14 SIGNAL reg8 : STD_LOGIC_VECTOR (7 downto 0) := (OTHERS => '0'); --PRBS
register
15 SIGNAL reg : INTEGER range 0 to 3999;
16
17 BEGIN
20
21 PROCESS
22 BEGIN
23
24 WAIT UNTIL RISING_EDGE (clk);
25
26 IF (res='1') THEN
27
28 reg8 <= (OTHERS => '0'); -- Reset the PRBS shift register
29
30 reg <= 0;
31
32 ELSE
33
34 reg <= reg - 1;
35
36 IF reg = 1 THEN
37
38 reg8 (7 downto 0) <= reg8 (6 downto 0) & reg8 (7);--shifting the PRBS
data
39
40 reg8 (7) <= reg8 (6) XOR reg8 (5) XOR reg8 (4); -- Making random data
for PRBS
41
42 IF reg8 = "0" THEN reg8 (0) <= '1'; END IF;
43
44 ELSIF reg = 0 THEN
45
46 reg <= 3999;
47
48 END IF;
49
50 END IF;
51
52 END PROCESS;
53
54 dout(2 downto 0) <= reg8 (2 downto 0) AND enable&enable&enable; --The
output to be
fed to the 8-PSK transmitter
55
56 END bhv;
```

```
1 --The code produces PRBS data of 8-Bit length and give an output of 4-Bit
2 --a time as (a,b,c,d) to use them as input to 16-QAM (2^4-QAM)
transmitter
3
4 library IEEE;
5 use IEEE.std_logic_1164 .all;
6 use IEEE.std_LOGIC_UNSIGNED .all;
7
8 ENTITY PRBS4bit IS
9 PORT (clk, res, enable : IN STD_LOGIC; --clock
10 dout : OUT STD_LOGIC_VECTOR (3 downto 0) := (OTHERS => '0')); --
Out register
11 END PRBS4bit;
12
13 ARCHITECTURE bhv OF PRBS4bit IS
14 SIGNAL reg8 : STD_LOGIC_VECTOR (7 downto 0) := (OTHERS => '0'); --PRBS
register
15 SIGNAL reg : INTEGER range 0 to 3999;
16
17 BEGIN
18
19
20
21 PROCESS
22 BEGIN
23
24 WAIT UNTIL RISING_EDGE (clk);
25
26 IF (res='1') THEN
27
28 reg8 <= (OTHERS => '0'); -- Reset the PRBS shift register
29
30 reg <= 0;
31
32 ELSE
33
34 reg <= reg - 1;
35
36 IF reg = 1 THEN
37
38 reg8 (7 downto 0) <= reg8 (6 downto 0) & reg8 (7);--shifting the PRBS
data
39
40 reg8 (7) <= reg8 (6) XOR reg8 (5) XOR reg8 (4); -- Making random data
for PRBS
41
42 IF reg8 = "0" THEN reg8 (0) <= '1'; END IF;
43
44 ELSIF reg = 0 THEN
45
46 reg <= 3999;
47
48 END IF;
49
50 END IF;
51
52 END PROCESS;
53
54 dout(3 downto 0) <= reg8 (3 downto 0) AND enable&enable&enable&enable; -
-The output to be fed to the 16-QAM transmitter
56 END bhv;
```

To analyse the SER of Square 16-QAM, the constellation points are bounded in the blue, green and red squares shown in figure J.1. The distance between all points is clearly shown in figure J.1. Chapter 4, section 4.1.1 discussed the use of *erfc* and *Q* functions to analyse the performance of a digital communication link using the distance between the constellation points. Equation (51) of the *Q* function is rewritten below, where *m* is the mean value of density equal to 0, σ is the standard deviation of density (see equation 49) and *x* is the distance of a point from the origin of constellation point.

$$P_e = Q\left(\frac{x-m}{\sigma}\right)$$

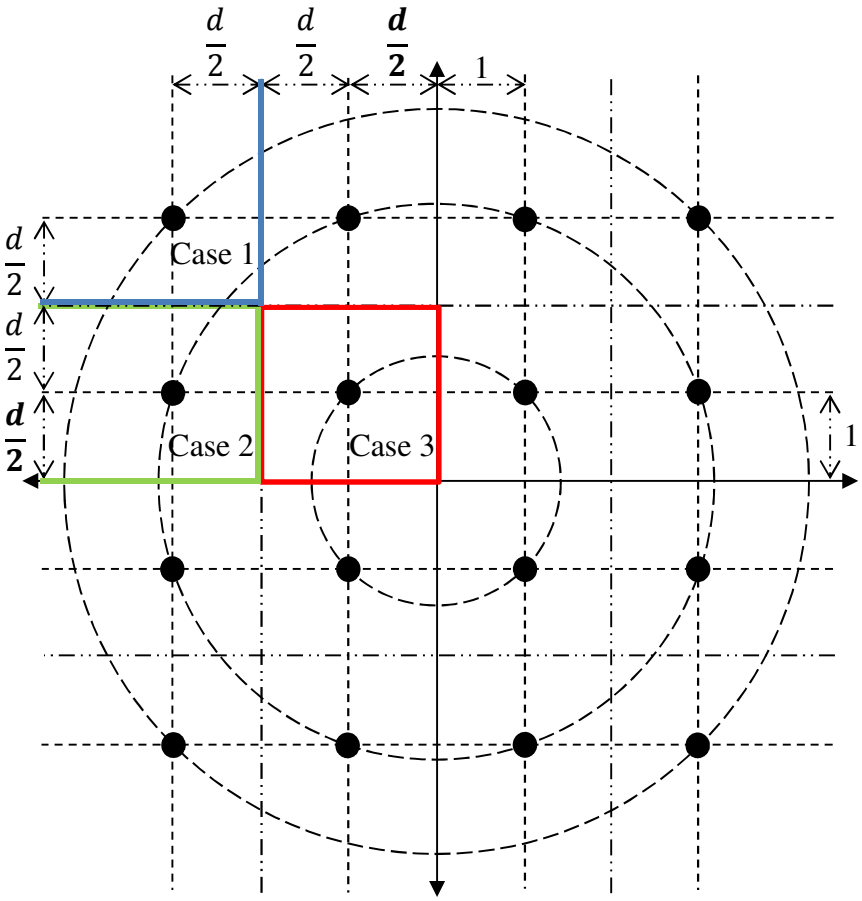

Figure J.1: Geometry of Square 16-QAM constellation

The analysis covers 3 cases of the constellation points with respect to n_x and n_y noise directions. Each case represents a set of points (J.1, J.2, and J.3). The individual probability of error of all cases, are added at the end with respect to their proportions out of 16 points as shown in (J.4). In addition, the Energy of a single point in all cases is calculated in (J.5, J.6, and J.7). Then, the Average Energy of Square 16-QAM constellation points, is calculated in (J.8) with respect to their proportions out of 16 points. The Average Energy is now used to formulate the resultant probability of error as equation (J.9). The equivalent form of *Q* to *erfc* function is used to find the probability of error using *erfc* function as equation (J.10).

- Case 1: Probability of error of the point shown right hand side (RHS)

$$P_{[c]} = \Pr\left\{n_x < \frac{d}{2}\ AND\ n_y < \frac{d}{2}\right\}$$

(Probability of correct ($P_{[c]}$))

$$= \Pr\left\{n_x < \frac{d}{2}\right\}.\Pr\left\{n_y < \frac{d}{2}\right\}$$

$$= \left(1 - Q\left(\frac{d}{2\sigma}\right)\right).\left(1 - Q\left(\frac{d}{2\sigma}\right)\right)$$

$$= \left(1 - Q\left(\frac{d}{2\sigma}\right)\right)^2$$

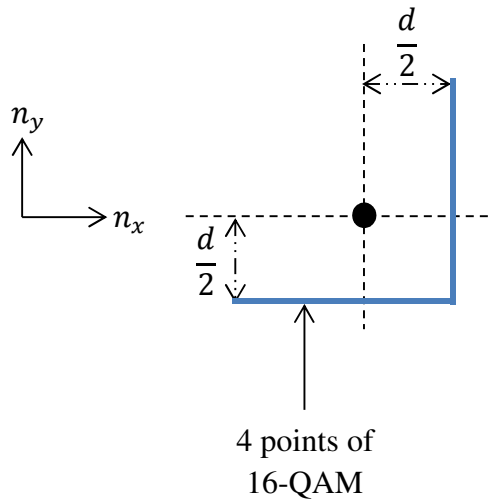

$$P_{e_1} = 1 - P_{[c]}$$

$$= 1 - \left(1 - Q\left(\frac{d}{2\sigma}\right)\right)^2$$

$$P_{e_1} = 2\,Q\left(\frac{d}{2\sigma}\right) - \left(Q\left(\frac{d}{2\sigma}\right)\right)^2 \qquad \text{(J.1)}$$

- Case 2: Probability of error of the point shown RHS

$$P_{[c]} = \Pr\left\{n_x < \frac{d}{2}\right\}.\Pr\left\{-\frac{d}{2} < n_y < \frac{d}{2}\right\}$$

$$= \left(1 - Q\left(\frac{d}{2\sigma}\right)\right)\left(1 - 2Q\left(\frac{d}{2\sigma}\right)\right)$$

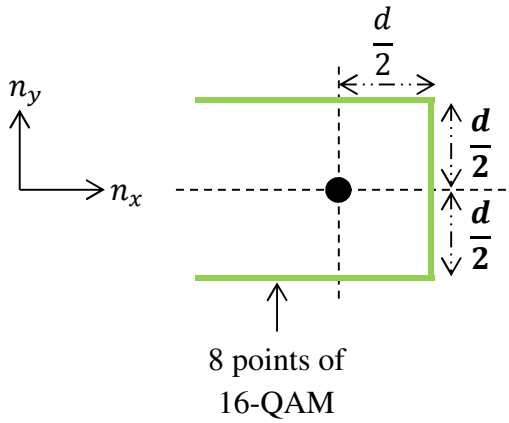

$$P_{e_2} = 1 - P_{[c]}$$

$$= 1 - \left(1 - Q\left(\frac{d}{2\sigma}\right)\right).\left(1 - 2Q\left(\frac{d}{2\sigma}\right)\right)$$

$$P_{e_2} = 3\,Q\left(\frac{d}{2\sigma}\right) - 2\left(Q\left(\frac{d}{2\sigma}\right)\right)^2 \qquad \text{(J.2)}$$

- Case 3: Probability of error of the point shown RHS

$$P_{[c]} = \Pr\left\{-\frac{d}{2} < n_x < \frac{d}{2}\right\}.\Pr\left\{-\frac{d}{2} < n_y < \frac{d}{2}\right\}$$

$$= \left(1 - 2Q\left(\frac{d}{2\sigma}\right)\right)\left(1 - 2Q\left(\frac{d}{2\sigma}\right)\right)$$

$$= \left(1 - 2Q\left(\frac{d}{2\sigma}\right)\right)^2$$

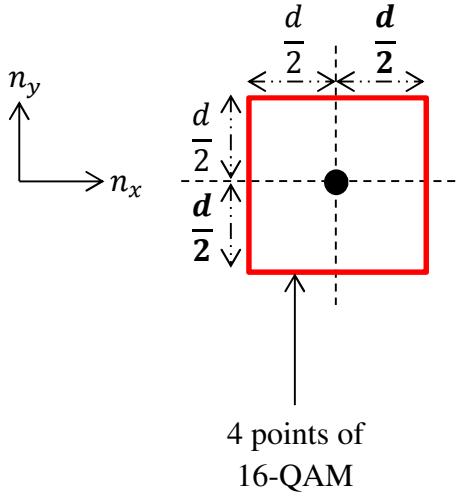

$$P_{e_3} = 1 - P_{[c]}$$

$$= 1 - \left(1 - 2Q\left(\frac{d}{2\sigma}\right)\right)^2$$

$$P_{e_3} = 4Q\left(\frac{d}{2\sigma}\right) - 4\left(Q\left(\frac{d}{2\sigma}\right)\right)^2 \qquad \text{(J.3)}$$

Calculating the total probability of error:

$$P_{e_t} = \frac{4}{16}P_{e_1} + \frac{8}{16}P_{e_2} + \frac{4}{16}P_{e_3}$$

$$= \frac{1}{4}\left[2\,Q\left(\frac{d}{2\sigma}\right) - \left(Q\left(\frac{d}{2\sigma}\right)\right)^2\right]$$

$$+ \frac{1}{4}\left[6\,Q\left(\frac{d}{2\sigma}\right) - 4\left(Q\left(\frac{d}{2\sigma}\right)\right)^2\right]$$

$$+ \frac{1}{4}\left[4Q\left(\frac{d}{2\sigma}\right) - 4\left(Q\left(\frac{d}{2\sigma}\right)\right)^2\right]$$

$$= \frac{1}{4}\left[12\,Q\left(\frac{d}{2\sigma}\right) - 9\left(Q\left(\frac{d}{2\sigma}\right)\right)^2\right]$$

$$= 3\,Q\left(\frac{d}{2\sigma}\right) - 2.25\left(Q\left(\frac{d}{2\sigma}\right)\right)^2 \qquad \text{(J.4)}$$

The Energy of a single point is given by:

$$E_1 = 2\left(\frac{d}{2}\right)^2 \qquad \text{(J.5)}$$

$$E_2 = \left(\frac{3d}{2}\right)^2 + \left(\frac{d}{2}\right)^2 \qquad \text{(J.6)}$$

$$E_3 = 2\left(\frac{3d}{2}\right)^2 \qquad \text{(J.7)}$$

The Average Energy of Square 16-QAM points:

$$E_s = \frac{4}{16}\left[2\left(\frac{d}{2}\right)^2\right] + \frac{8}{16}\left[\left(\frac{3d}{2}\right)^2 + \left(\frac{d}{2}\right)^2\right] + \frac{4}{16}\left[2\left(\frac{3d}{2}\right)^2\right]$$

$$= \frac{1}{4}\left[\frac{d^2}{2}\right] + \frac{1}{4}[5d^2] + \frac{1}{4}\left[\frac{9d^2}{2}\right]$$

$$= \frac{5}{2}d^2$$

$$\therefore d = \sqrt{\frac{2}{5}E_s} \qquad \text{(J.8)}$$

Now, replacing *d* with its equivalent in equation (J.8),

$$P_e = 3\,Q\left(\sqrt{\frac{E_s}{5N_0}}\right) - 2.25\left(Q\left(\sqrt{\frac{E_s}{5N_0}}\right)\right)^2 \qquad \text{(J.9)}$$

Rewrite (J.9) using *erfc*,

$$P_e = \frac{3}{2}\,erfc\left(\sqrt{\frac{E_s}{10N_0}}\right) - 2.25\left(\frac{1}{2}erfc\left(\sqrt{\frac{E_s}{10N_0}}\right)\right)^2 \qquad \text{(J.10)}$$

EXTREMELY LOW FREQUENCY BASED A COMMUNICATION LINK

A. Alaiwi[1], M. Sibley[1], P. Mather[1] and V. Holmes[1]
[1] University of Huddersfield, Queensgate, Huddersfield HD1 3DH, UK

ABSTRACT

The paper discusses the literature review and the possibility of using the ground itself as transmission medium for various users' transceivers and an administrator transceiver using Multi-Carrier-Direct Sequence-Code Division Multiple Access (MC-DS-CDMA), Orthogonal Frequency Division Multiplexing (OFDM),16-Quadrature Amplitude Modulation (QAM), Frequency Division Duplex (FDD) and Extremely Low Frequency (ELF) band for the applications of Oil Well Telemetry, remote control of power substations or any system that its responding time is not critical.

Keywords Extremely Low Frequency, Multi-Carrier Code Division Multiple Access, Multi-Carrier Direct Sequence Code Division Multiple Access, Orthogonal Frequency Division Multiplexing, Frequency Division Duplex

1 INTRODUCTION

ELF is the band of 0 up to 300 Hz is allocated by the Federal Communications Commission (FCC) for general purposes free of charge. The idea of using the ground as transmission medium goes back to the beginning of 20th century when Mr. Nathan Stubblefield used it to transmit the human voice through the ground itself. In addition, the United States (U.S.) and Russian navies use the ELF frequencies to communicate with their submerged submarines operated at frequency lower than 100 Hz. Moreover, the electricity all over the world almost operated at either 50 or 60 Hz. The advantage of using ELF in communications comparing to Radio Frequencies (RF) is that the ELF capable to propagate for long distances at low power without regeneration.

2 LITERATRUE REVIEW

The literature review shows the history of using the ELF band and the ground itself as transmission medium. It also discusses the possibility of using multi-carrier modulation techniques for multiple access and enhancing the transmission rate at such low frequencies.

2.1 TRANSMISSION MEDIUM

The farmer Mr. Nathan Beverly Stubblefield (1860-1928) was the first person to broadcast the human voice using his telephone system that attached to earth rods in 1900 and on the new year's day of 1902 Stubblefield and his son demonstrated this system to the people in Kentucky-USA. In March 1902, he successfully showed to scientists and quite people how easy he could communicate from ship to shore using wires dropped from the stern of ship and the receiver at shore connected to ground via earth rod near the Potomac River-USA. Stubblefield experienced problems when he tried his system in Manhattan Island-USA because of the soil was rocky and the bad Signal-to-Noise-Ratio (SNR) caused by 60 Hz of the power cables. Stubblefield's son mentioned that his father did not use radio frequencies with his system. In 1992, Bob Lochte a Professor in the Department of Journalism and Mass Communication at Murray State University, and Larry Albert a TV Engineer with a historical research replicated Stubblefield's system and successfully demonstrated it. This confirmed that Nathan B. Stubblefield used the ELF and VF band (0 up to 3 KHz) to transmit the human voice through the ground [1-3].

2.2 EXTREMELY LOW FREQUENCY

ELF is mostly used by the navies. The U.S. Navy found that the ELF penetrates the sea water comparing to RF signals. However, the lower the frequency being transmitted the deeper it penetrates the seawater. The U.S. Navy radiate the ELF waves using large transmitters facilities between the lower part of the ionosphere layer and the earth's surface as electromagnetic waveguide and part of these waves pass into the ocean and submarines are equipped to receive and decode these waves. Biological and ecological impact studies of using ELF on human and plant were conducted by National Research Council-USA and the American Institute of Biological Science and concluded that there are no serious adverse effects of using ELF band. It is expected that any communication system using the ELF band will suffer from noise caused by the electric feed cables, electric leakage through the earth rods and the lightning strikes that make the electrons in the atmosphere to oscillate between the ionosphere and surface [4-12].

2.3 SINGLE- AND MULTI-CARRIER SYSTEMS

A high spectral efficiency spectrum, maximising the number of users and transmission rate within a frequency band are the most critical design objectives and challenge to improve the reliability and performance of wireless communications systems. Multipath channels degrade the performance of the single carrier modulation technique. However, most of the conventional modulation techniques are sensitive to Intersymbol Interference (ISI) unless the channel symbol rate is small compared to the delay spread of the channel in the multipath environment [13-14, 16-19].

2.3.1 ORTHOGONAL FREQUENCY DIVISION MULTIPLEXING (OFDM)

OFDM offers high spectral efficiency due to the large numbers of sub-carriers that form nearly rectangular frequency spectrum. It can be easily realized using Fast Fourier Transform (FFT). A guard interval (GI) is used in OFDM symbol to reduce the complexity of receiver that avoids ISI and Intercarrier Interference (ICI). But, OFDM suffer from high Peak-to-Average-Power-Ratio (PAPR) that requires high linear amplifiers or otherwise the out-of-band power will be enhanced. In addition, Coded OFDM (COFDM) is the same as OFDM except that Forward Error Correction (FEC) is applied to the signal before transmission to avoid bit errors on subcarriers in deep fade so that the number of subcarriers needed is larger than the number of bits or symbols transmitted simultaneously. This is an advantage at high frequency transmission links such the Digital Audio Broadcasting (DAB), Digital Video Broadcasting (DVB) and Digital Video Broadcasting – Terrestrial (DVB-T) systems used in Europe [13-20].

2.3.2 SINGLE-CARRIER SPREAD SPECTRUM SYSTEMS

Nowadays, the Spread spectrum is rapidly growing technology and widely used in wireless communications to allow multiple access simultaneously and privacy within the same channel whereas the OFDM itself does not. DS-CDMA and Frequency Hopping (FH)-CDMA are the primary types of spread spectrum. The DS-CDMA spread the narrowband channel over a continuous bandwidth by mixing the data with Pseudo-random Noise (PN) code whereas the narrowband signal in the FH-CDMA is hopping over wide bandwidth using the PN code instead of spreading the signals over a continuous bandwidth. The DS-CDMA is preferred on FH-CDMA for long transmission distance due to the interference and multipath signals of the other systems. The DS-CDMA requires accurate power control so that no user masks all the users if its power is too high comparing to the other users at the receiver side. The DS-CDMA offers easy frequency planning, high immunity against interference if a high processing gain is used, flexible data rate adaptation and multiple access. Multiple access interference (MAI) occurs as the number of simultaneously active users increases in which the Single-Carrier (SC)-CDMA limited the number of users according to the processing gain [16-17].

2.3.3 MULTI-CARRIER SPREAD SPECTRUM SYSTEMS

The combination of OFDM and CDMA offers a robust system that is immune to the multipath waves, reduces the ISI and ICI, allows multiple access and privacy. This combination is known as Multi-Carrier (MC)-CDMA that usually uses Walsh Hadamard orthogonal code. MC-CDMA is similar to the

DS-CDMA except that the MC-CDMA performs the spreading code in the frequency domain. MC-CDMA can achieve good BER for N users using standard receiver techniques comparing to SC-DS-CDMA that requires highly complex receiver for the same N users. MC-CDMA better than COFDM in term of multiple access and also it replaces the encoder of COFDM by an NxN matrix to avoid bit errors [13, 16, 20].

MC-DS-CDMA is a descent of MC-CDMA in which both allow the users to share the same bandwidth at the same time using PN code to separate the data of users. The main different is that the MC-CDMA apply the PN code in the frequency domain whereas the MC-DS-CDMA apply it in the time domain as shown in figure (5). However, MC-CDMA can be realized using low complex OFDM operation and offers a flexible system design as the spreading code does not have to be equal to the number or sub-carriers. The MC-DS-CDMA can be realized with or without OFDM in which depends on the number of sub-carriers used as large number sub-carriers can be efficiently realized using OFDM [16].

3 METHODOLOGY

Literally, Mr. Stubblefield managed to transmit the human voice through the ground. The frequency components of the human voice extend from 20 Hz to about 3 KHz [26] in which varying in term of frequency and amplitude. However, the human voice includes the ELF band which is an advantage to adopt this band in a communication link based on multicarrier system such MC-DS-CDMA. Using MC-DS-CDMA with help of OFDM and QAM to transmit the data in parallel form would enhance the transmission rate at such low frequencies; reduce the multi-path interference and maintaining multiple access [21]. Transceivers are to be designed using FDD form to allow 2 ways of transmission simultaneously especially for the remote control applications. FPGA and DSP chips are to be used to design, simulate, build and test the transceivers in laboratory. After that, the propagation characteristics of the transmission medium are to be tested, measured and classified by driving metal spikes into the ground and compared to the prototyped design shown in figure (1). Thereafter, the transmission distance is to be measured and repeaters can be used to regenerate the signal for long transmission distance.

4 EXPERIMENTAL APPARATUS, RESULTS AND DISCUSSIONS

The transceiver design involves the use of Phase Shift Key (PSK) modulation technique. The bandwidth of Binary (B)PSK technique is twice the bit rate $(2R_b)$ where the Quadrature (Q)PSK requires R_b only [21]. QAM is an advanced technique that combines the QPSK and Amplitude Modulation (AM) forms. For example, a 16-QAM can be modulated using In-phase and Quadrature signal where the Quadrature is to be used as a reference (threshold) to a single bit that is Amplitude Modulated on the In-phase signal. However, 3 bits (b_n, c_n, d_n) occupy 8 states on the carrier phase. Initially, they are to be modulated on the phase of 0^0 and once the phase is shifted to 45^0, the data states will be changed to $(b_{n+1}, c_{n+1}, d_{n+})$ at the same time there is a single bit (a_n) of the data is to be modulated on the Amplitude and it can be seen in figure (2) that the Quadrature is shifted with the In-phase by 45^0 to be 135^0. The transceiver compares the absolute value of the In-phase and Quadrature to decide logic [1] is received when the Quadrature value is greater than the In-phase value or otherwise no changes occur to (a_n). 16-QAM enhances the transmission rate of the QPSK twice while occupying a bandwidth of less than that of the QPSK to be $\frac{3R_b}{4}$ [18, 19, 21].

The ELF limits the transmission rate according to lowest frequency in the channel. However, the minimum frequency transmitted should carry at least 4 cycles to represent a single bit in order to reach the receiver in good power. For instance, a single carrier of 20 Hz is capable of sending 5 bps using BPSK, 10 bps using QPSK and 20 bps using 16-QAM. So, using a multi-carrier system will limit the number of sub-carriers in the single channel. However, if the minimum frequency used is 20 Hz and the maximum frequency is 280 Hz there will be a large delay caused by the large number of cycles per bit that may shut down the receiver. Therefore, allocating many channels within the ELF

band is the best way to examine the propagation characteristics of the ELF band and users can share the bandwidth. With aid of spectrum analyzer, the frequency components of the ground itself obtained using the earthing system of the laboratory and founds that there were odd harmonics of 50 Hz and integer harmonics of 60 Hz that will affect the data link. Therefore, 9 channels can be allocated as shown in figure (4) in order to meet these conditions and avoid problems of large delay and each channel is divided into two halves so that the users access the admin receiver via the first half and the admin access the users' receiver via the second half using FDD. In addition, using MC-DS-CDMA will cope in the presence of 50 Hz noise.

The calculation of any physical size of useable antenna is basically depending on the wavelength [27], for instant the 20 Hz requires: $\lambda = \frac{C}{f} = \frac{300\times10^6}{20}$

$Antenna\_size = \frac{15{,}000Km}{2} = 7500Km$ This is bigger than the radius of the earth planet and confirms that the Mr. Nathan Stubblefield managed the transmit the human voice using the induction between the two earth rods. Therefore, a high conductive aluminium round solid bar, round tube and plate are used to design the antenna desired to link the transceivers. The designed antenna shown in figure (1) expected to reference the signals to the ground via the round tube and sends the signals from one to another plate. A prototyped design in parallel with real environment is envisioned to consist of 2 boxes to contain the plates covered by sand as shown in figure (1) and a piece of pipe connecting the boxes together. In this case, various type of simulations can be applied like raising the conductivity using water, clay, etc. In addition, the pipe connecting the boxes can be surrounded by electrical cables in order to simulate the noise of the feed cables buried below the level of the ground. Also, vibration can be easily done on the pipe that will apply vibration on the transmission bath directly.

The solid round bar passing through the round tube shown in figure (1) for a capacitor that may attenuate the signals or form a short circuit but at the same time reference the signals into the ground. The capacitance and reactance calculations of this formation is

The capacitance of this form is $C = \frac{2\pi\varepsilon_0\varepsilon_r}{\ln(\frac{b}{a})} = \frac{2\times\pi\times8.854\times10^{-12}\times5}{\ln(\frac{23.77\times10^{-2}}{6.35\times10^{-3}})} = 42.2pF.m^{-1}$

Reactance at the lowest frequency $X_c = \frac{1}{2\times\pi\times20Hz\times42.2pF\times0.5m} = 377.8M\Omega$

Reactance at the highest frequency $X_c = \frac{1}{2\times\pi\times300Hz\times42.2pF\times0.5m} = 25.1M\Omega$

These figures clarify that referencing the signals to the ground using this form will not attenuate the signals.

Noise is a major problem when transmitting/receiving data through wireless channels. Shot noise is generated by the random flow of charge carriers in semiconductors and thermal noise occurs in resistive components due to the thermal agitation of electrons in resistors. Another type of noise called flicker (pink or 1/f) noise is expected to affect the ELF link at such low frequencies. Flicker noise usually occurs in Metal-Oxide Semiconductor Field-Effect Transistor (MOSFET) systems but Junction Field-Effect Transistor (JFET) and Bipolar systems have less 1/f noise than the MOSFET. It is envisaged that JFET systems will be used to keep the 1/f noise low [22-25].

5 FURTHER WORK

The priorities for the future work involves the design and simulation of ELF Data Transmission link discussed in this paper based on MC-DS-CDMA, OFDM, 16-QAM and FFT using MATLAB that provide powerful functions like QAM, Raised-Cosine Filter, Square-Root-Raised-Cosine filter, coding techniques, channels, graphical representations, etc. After that, the MATLAB codes are to be

converted to VHDL code using ModelSim and DSP Builder provided by Quartus II-Altera in order to download it on Cyclone II FPGA [28]. Burying the antenna designed and the noise is to be discussed for better SNR. Repeaters may be used later to test the transmission distances.

6 CONCLUSION

The possibility of using a communication link over the ELF band has been discussed for multiple access using the literature review based on the history of using the ground as transmission medium, ELF for telecommunications purposes and multi-carrier communications systems. Many problems associated with the receiver were discussed and solutions envisioned to use MC-DS-CDMA to operate the ELF Data Transmission Link.

REFERENCES

[1] Lochte, B. (2001). KENTUCK FARMER INVENTS WIRELESS TELEPHONE! But Was It Radio? FACTS AND FOLKLORE ABOUT NATHAN STUBBLEFIELD. Printed by Innovative Printing and Graphics, Murray KY.

[2] HOFFER, T. (1972) 'NATHAN B. STUBBLEFIELD AND HIS WIRELESS' JOURNAL *OF BROADCASTING AND ELECTRONIC MEDIA*, 15 (3) pp. 317-327

[3] CLIFFORD, M. (1985) 'THE EARLY DAYS OF RADIO' *RADIO ELECTRONICS*, 57, (11) pp: 60-62

[4] Extremely Low Frequency Transmitter Site: Clam Lake, Wisconsin, US Navy Fact File, June 28, 2001 [Online]. Available at: < http://www.fas.org/nuke/guide/usa/c3i/fs_clam_lake_elf2003.pdf > [Accessed 30th AUG 2009].

[5] Aldridge, B. (February 2001). ELF HISTORY: EXTREME LOW FREQUENCY COMMUNICATION [Online] by Pacific Life Research Centre-United States. Available at: < http://www.plrc.org/docs/941005B.pdf > [Accessed 4th September 2008]

[6] National Research Council Staff. (1997) Evaluation of the U. S. Navy's Extremely-Low-Frequency Submarine Communications Ecological Monitoring Program.
Washington, DC, USA: National Academies Press, 1997. p 13.
< http://site.ebrary.com/lib/uoh/Doc?id=10055127&ppg=27 > [Accessed 27th March 2008]

[7] Pike, J. (2004) Extremely Low Frequency Communications Program [Online]. Available at: < http://www.fas.org/nuke/guide/usa/c3i/elf.htm > [Accessed on 21st Mar 2008]

[8] Preve, C. (2006) Protection of Electrical Networks. ISTE: Printed and bounded in Great Britain by Antony Rowe Ltd, Chippenham, Wiltshire. Pp 53-54.

[9] Rigby, B. (2005) Design of Electrical Services for Buildings. 4th Ed. Spon Press: Printed and bounded in Great Britain by TJ International Ltd, Padstow, Cornwall. Pp 137-139.

[10] Frater, M. and Ryan, M.J. (2003) Communications and Information Systems. Argos Press. Pp 18-19.

[11] Sueker, Keith H. (2005) Power Electronics Design A Practitioner's Guide. Newnes: Printed in United States of America. Pp 221-222.

[12] Betz, H.D., Schumann, U. & Laroche, P. (2008) Lightning: Principles, Instruments and Applications: Review of Modern Lightning Research. Springer Netherlands. Pp 347-378.

[13] Linnartz, Professor Jean-Paul. (2006) OFDM and MC-CDMA [Online] Available at: <http://ofdm.linnartz.net> [Accessed 12th September 2009]

[14] Hanzo, L., Munster, M., Choi, B.J. & Keller, T. (2003) OFDM and MC-CDMA for Broadband Multi-User Communications, WLANs, and Broadcasting. England: John Wiley. Pp. 7-9.

[15] Lawrey, E. (1997) The suitability of OFDM as a modulation technique for wireless telecommunications, with a CDMA comparison. PhD thesis, University of James Cook- Australia. Pp. 29-32
[16] Fazel, K. & Kaiser, S. (2008) Fundamentals In: Multi-Carrier and Spread Spectrum Systems: From OFDM and MC-CDMA to LTE and WiMAX. 2nd Ed. West Sussex: John Wiley.

[17] Esmailzadeh, R. (2006) Broadband Wireless Communications Business: An Introduction to the Costs and Benefits of New Technologies. West Sussex: John Wiley.

[18] Qatawneh, I.A.Z. (1997) Introduction to OFDM. In: THE USE OF ORTHOGONAL FREQUENCY DIVISION MULTIPLEX (OFDM) TECHNIQUES IN MOBILE BROADBAND APPLICATIONS. PhD thesis, University of Huddersfield-UK. Pp. 1-11

[19] Hurst, J.A. (2000) Introduction. In: AN INVESTIGATION INTO METHODS FOR THE CORRECTION OF FREQUENCY OFFSET IN OFDM SYSTEMS. PhD thesis, University of Huddersfield-UK. Pp. 1-4

[20] Nassar, C.R., Natarajan, B., Wu, Z., Wiegandt, D., Zekavat, S.A. & Shattil, S. (2001) Overview of Multi-Carrier Technologies. In: Multi-Carrier Technologies for Wireless Communication. Hingham, MA, USA: Kluwer Academic Publishers. Pp. 5-38

[21] Prasad, R. (1996) CDMA FOR WIRELESS PERSONAL COMMUNICATIONS. Artech House Publishers.

[22] Horowitz, P. and Hill, W. (1994) THE ART OF ELECTRONICS. 2nd ed. Printed in USA 1994, Cambridge University Press. Pp.267-281 & P.p.222.

[23] Storey, N. (1998). Electronics: A System Approach. 2nd ed. Printed and bound in Great Britain by Biddles Ltd, Guildford and King's Lynn, Addison Wesley Longman Limited. P.p314.

[24] F.M.Klaassen and J.R.Robinson, "Anomalous Noise Behaviour of the Junction Gate Field Effect Transistor at Low Temperatures", IEEE Transactions. Electronic Devices, ED-17, 852-857 (1970).

[25] C.F. Hiatt, A. van der Ziel and K.M. van Viet, "Generation-Recombination Noise Produced in the Channel of JFETs", IEEE Transactions. Electronic Devices, ED-22, 614-616 (1975).

[26] Freeman, R.L. (2005) Fundamentals of telecommunications. West Sussex, UK: John Wiley. Pp. 90

[27] Gosling, W. (1998) Radio Antennas and Propagation. Oxford: Newnes, 1998. P.p9, 41, 49 and 120.

[28] Altera. (2009) The Mathworks and Altera DSP Builder Collaboration [Online]. Available at: < http://www.altera.com/products/ip/altera/t-alt-matlab.html?GSA_pos=4&WT.oss_r=1&WT.oss=matlab >

Figures

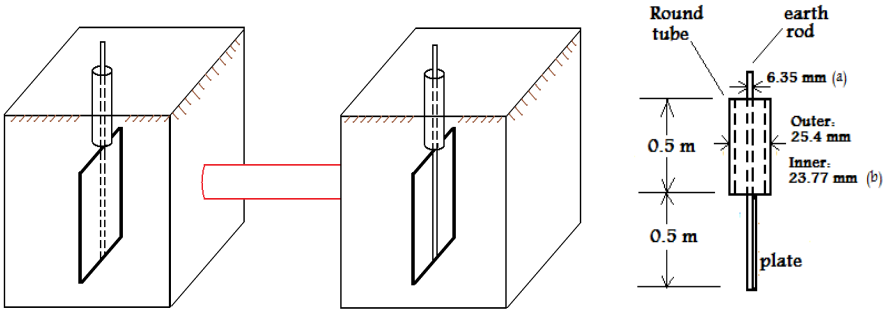

Figure 1: Prototype of the transmission medium

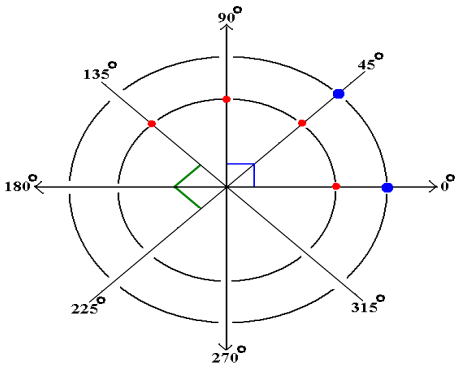

Figure 2: 16-QAM constellation

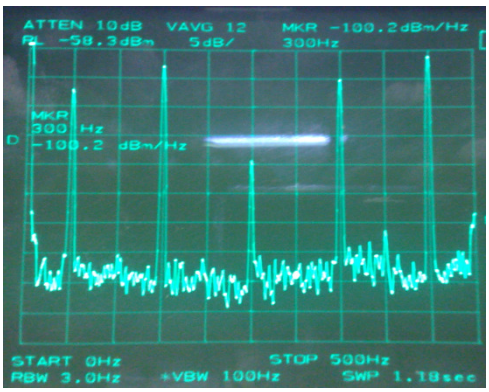

Figure 3: Ground spectrum

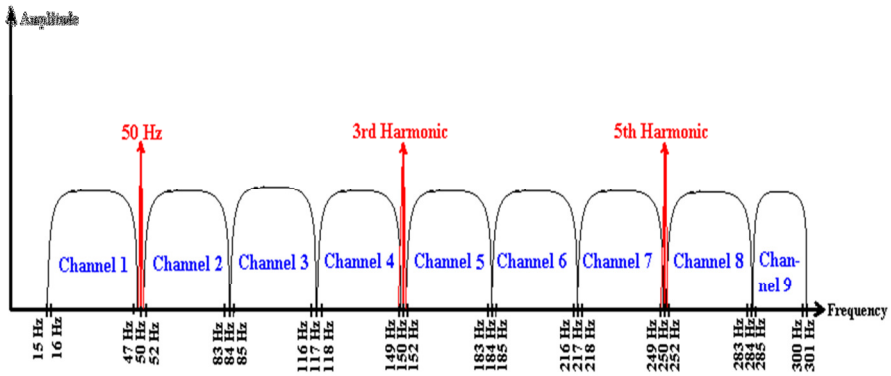

Figure 4: 9 channels allocated in the ELF band

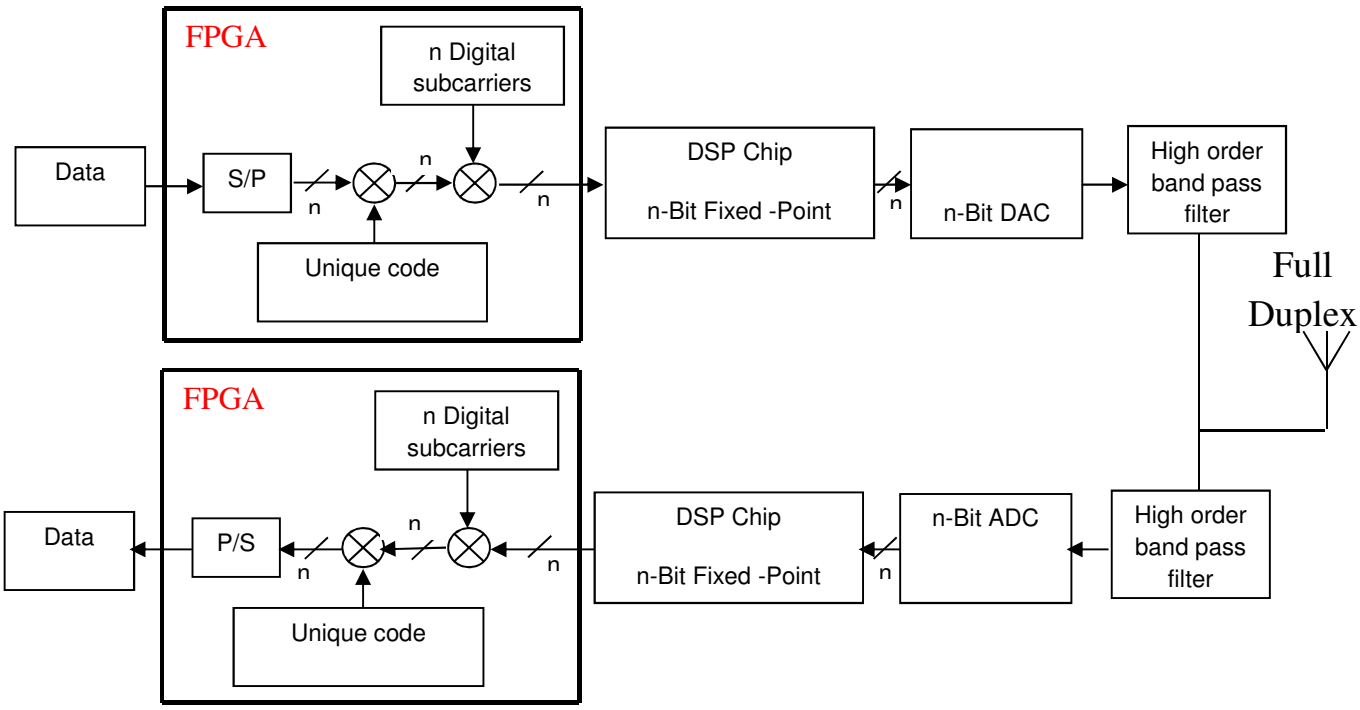

Figure (5) Transceiver design using FPGA, DSP, DAC and ADC chips and filters.

Demonstration of data transmission using an Extremely Low Frequency (ELF) Carrier

A. Alaiwi, M.J.N. Sibley and P. J. Mather
University of Huddersfield, Queensgate, Huddersfield HD1 3DH, UK
E-mail: ayman.alaiwi@hud.ac.uk

ABSTRACT

The use of the extremely low frequency (ELF) band (3-300 Hz) has largely been confined to submerged submarines operated by the United States (US) and Russian navies. Although ELF transmission was first demonstrated in 1900, its application to civilian data transmission has been neglected. This paper describes the design and build of a data link operating with a 21 Hz carrier using amplitude shift keying (ASK) at a data rate of 4 bit/s. 16-quadrature amplitude modulation (16-QAM) and orthogonal frequency division multiplexing (OFDM) would enhance the capacity of the link significantly. Possible applications of this link include remote control of traffic gates, motorway signage, plant equipment, subterranean communication, telemetry, diversions of train tracks, etc.

Keywords – 1/f noise, 16-QAM, ASK, earth electrodes, ELF, OFDM, PLL, subterranean

INTRODUCTION

In 1902, Mr. Nathan Stubblefield [1] became the first person to broadcast the human voice using a baseband telephone system based on buried metal rods. Extremely low frequency (ELF) is allocated by the Federal Communications Commission (FCC) for general purposes as free of charge; however there is currently no commercial use due to the low data rate. In 2001, the British cave rescue council (BCRC) developed a cave radio operating at low frequency (LF) of 87 kHz using single side band (SSB) technique, the HeyPhone [2]. The communication range using HeyPhone cave radio is greatly improved to 800m using earth electrodes compared to loop antennas. The US and Russian navies use frequencies lower than 100 Hz to communicate with submerged submarines [3]. ELF propagates at low power for long distances through the ground without regeneration [1,3]. It is expected that any ELF link will suffer interference from power cables and flicker (1/f) noise. Biological and ecological impact studies of ELF have been conducted by the National Research Council-US and the American Institute of Biological Science. They concluded that there are no serious adverse effects on humans and plants [3].

An ASK system using a nominal 20 Hz carrier, with transmission rate of $\boldsymbol{R_b = 4\ bit/s}$, was chosen to transmit digital data using ELF and ground as transmission medium. This differs from Stubblefield's, BCRC and Naval systems [1-3] with the possibility of enhancing the capacity and speed of the link using 16-QAM and OFDM systems. Possible applications of this link include remote control of traffic gates, motorway signage, plant equipment, subterranean communication, telemetry, diversions of train tracks, etc.

THEORY

For simplicity of design, a 20 Hz carrier ASK transmitter and non-coherent receiver were designed and constructed. Custom-built transmit and receive universal asynchronous receiver/transmitter (UARTs) encoded/decoded 2 bits of data. The generated digital word consists of a start sequence of 1.5 bits, an 8-bit address code, 2 bits of data and a stop sequence of 0.5 bit as can be seen in fig. 1. The word keys a Wien-bridge oscillator using a Single-Pole-Single-Throw (SPST) switch as shown in fig. 2. A band-pass filter (BPF) removes harmonics caused by the carrier switching as shown in fig. 3 and JFET input operational amplifiers minimise 1/f noise [4].

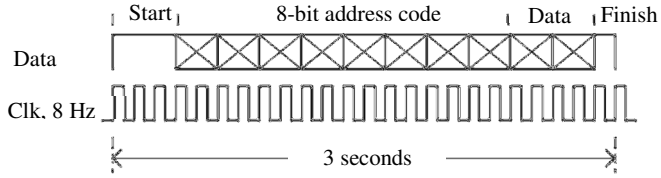

Fig. 1 Digital word generated by the transmit UART.

Fig. 4 shows the non-coherent receiver schematic design. The receive UART removes the start/finish bits and checks the 8 bits of address code before outputting the 2 data bits when the receiver address matches that of the incoming word. Active filters and a full-wave precision rectifier recover the data. The rectifier is followed by a voltage-follower and 2 envelope detectors. The second envelope detector has a time constant 3 times that of the first envelope detector to provide a definite threshold to the comparator. The voltage comparator and phase-locked-loop (PLL) slice and retime the recovered signal.

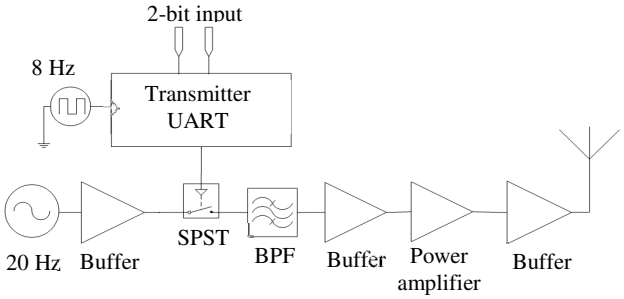

Fig. 2 ASK transmitter design.

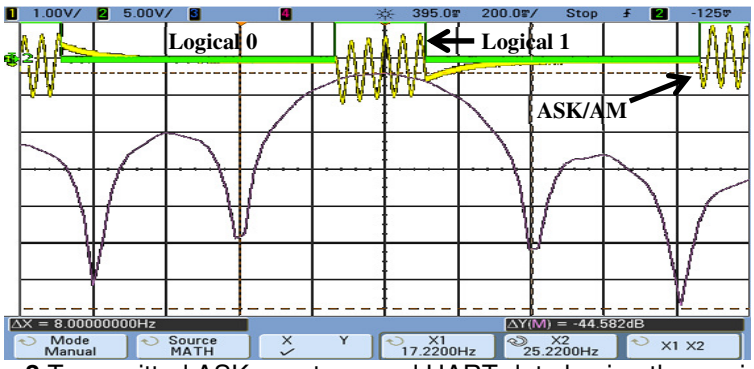

Fig. 3 Transmitted ASK spectrum and UART data keying the carrier.

Fig. 5 shows the performance of the ASK coherent and non-coherent detectors that were estimated using an assumed value of the noise density $N_o = 5 \times 10^{-10}\ watt/Hz$ of the channel and the probability of error, P_e equations [5] in (1) and (2). A is the received amplitude of the carrier. The amplitude A was calculated for various $x\ dB$ values of signal-to-noise-ratio (SNR) using (3) where N is the noise $N = N_o f_c\ watt$ and f_c is the carrier frequency.

$$P_e = \frac{1}{2} erfc\left(\sqrt{\frac{A^2}{8N_o R_b}}\right) \qquad (1)$$

$$P_e = \frac{1}{2}\left[e^{-\frac{A^2 T_b}{8N_o}}\right] = \frac{1}{2}\left[e^{-\frac{A^2}{8N_o R_b}}\right] \quad (2)$$

$$A = \sqrt{10^{\frac{x\,dB}{10}} \times 2N} \quad (3)$$

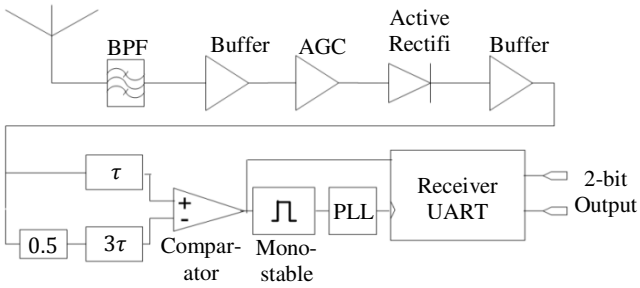

Fig. 4 Non-coherent ASK receiver design

The performance was also estimated at $f_c = 288\,Hz$ in the ELF band to show the difference when subcarriers are used in OFDM system using the same noise level and $R_b = 18\,bit/s$. Fig. 5 shows that the coherent detector performs better than the non-coherent detector. It was found that the higher the carrier frequency being used, the lower the probability of error.

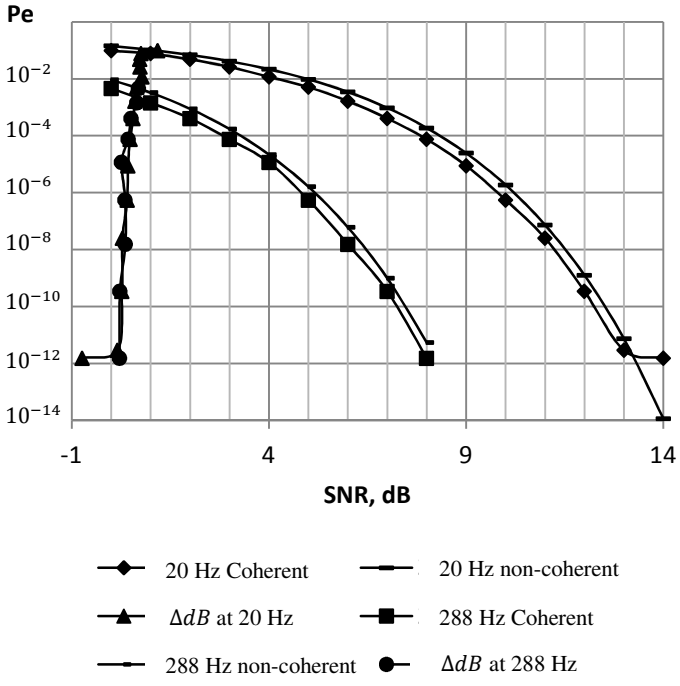

Fig. 5 Performance of ASK detector operating at 20 Hz and 280 Hz.

The difference in SNR for the same amount of P_e of various $x\,dB$ gains were calculated using (4) as well to evaluate the power (ΔdB) needed for non-coherent detector to perform as coherent detector.

$$x\,dB = 10\,\log_{10}\left(\frac{-4R_b \times \ln(2P_e)}{f_c}\right) \qquad (4)$$

Fig. 5 shows that there is a linear (ΔdB) region where non-coherent detector requires less than 1 dB to make significant changes in P_e as in coherent detector. In addition, non-coherent detector of low frequencies performs better than coherent detectors at higher SNRs.

RESULTS AND DISCUSSIONS

The transmitter had a carrier frequency of 21 Hz due to tolerances of components. The analogue switch produced harmonics due to the data clock not being phase locked to the carrier. A third order active BPF with 60 dB/decade roll-off at 17 Hz and 25 Hz cut-off frequencies rejects the harmonics of the carrier, preventing any UART transmitter low frequency harmonics, and reduce flicker noise. In the receiver, a BPF removes any harmonics of 50 Hz harmonics and 1/f noise. The Automatic-Gain-Control (AGC) keeps the data amplitude within specified limits. Transmitted data was successfully received using non-coherent detector.

CONCLUSION AND FURTHER WORK

A low speed data communication link using a 20 Hz carrier with ASK digital modulation technique has been evaluated. The transmitter and receiver were constructed using readily available electronic components and a data rate of 4 bit/s was used. ELF propagates at low power for long distances through the ground without regeneration. The main noise components anticipated in the ground transmission system are 50 Hz of the power feed cables, and 1/f noise. ASK non-coherent detectors require an extra 1 dB to perform better than coherent detector. 8 of 16-QAM subcarriers in OFDM could enhance the capacity of the link significantly to 128 bit/s at such low frequencies. Possible applications of this link include remote control of traffic gates, motorway signage, plant equipment, subterranean communication, telemetry, diversions of train tracks, etc. Work is continuing to enhance the transmission rate of the link. Results will be presented shortly.

REFERENCES

1. Clifford, M.: 'The early days of radio', *Radio Electronics*, 1985, 57, (11), pp. 60-62.

2. Bedford, M.: 'Introducing a New Cave Radio for Rescue Use', *Cave Radio & Electronics Group*. September, 2000, 41, pp.3, http://bcra.org.uk/creg/heyphone/pdf/cregj-september-2000.pdf, Accessed 15th March 2012

3. National Research Council Staff.: 'An evaluation of the U.S. Navy's extremely low frequency communications system ecological monitoring program', Washington-DC: National Academy Press, 1997.

4. Hiatt, C. F., van der Ziel, A. and van Viet, K. M.: 'Generation-Recombination Noise Produced in the Channel of JFETs', *IEEE Transactions on Electron Devices*, 1975, 22, (8), pp. 614-616

5. Roden, M. S.: 'Analog and Digital Communication Systems', London: Prentice-Hall International Inc., 1996.

DRAFT

Improvements to Receivers and Method of Use Thereof

The present invention relates to the improvements of apparatuses which include demodulators.

Although the following description refers to Quadrature Amplitude Modulation (QAM) and Phase Shift Keying (PSK) modulation techniques, the person skilled in the art will appreciate that the present invention could be used for other modulation techniques such as Amplitude Shift Keying (ASK) and other Modulation techniques, such as 64 and/or 256 -Quadrature Amplification Modulation.

Digital modulation is the process of converting a series of data bits to signals that can be transmitted over a communications medium. The modulation can be carried out by altering the magnitude, frequency, or phase of a signal. A combination of phase and amplitude modulation is considered to be the most efficient in terms of wireless communication system capacity, with the 16- QAM technique being is one of the most efficient techniques. The 16-QAM is widely used in Wide-band Code Division Multiple Access (WCDMA), High-Speed Downlink Packet Access (HSDPA), World-wide Inter-operability for Microwave Access (WiMAX) and Wireless Local Area Network (WLAN) broadband wireless access technologies. The HDSPA, WiMAX and WLAN are part of the 3rd Generation Partnership Project (3GPP) WCDMA, Institute of Electrical and Electronics Engineers (IEEE) 802.16 and IEEE 802.11 standards respectively.

Several different forms of PSK are used in the IEEE 802.11b-1999 standard with Differential PSK (DPSK) being used at low data rates and Quadrature PSK (QPSK) being used at 11 Mb/s. The IEEE 802.11g-2003 standard uses Binary PSK (BPSK) and QPSK at faster

transmission speeds. BPSK is also used in the IEEE 802.15.4, or ZigBee, standard. Applications of these standards include Wide-band Code Division Multiple Access (WCDMA), High-Speed Downlink Packet Access (HSDPA), World-wide Inter-operability for Microwave Access (WiMAX) and Wireless Local Area Network (WLAN) broadband wireless access technologies. The HDSPA is part of the 3rd Generation Partnership Project (3GPP) WCDMA.

Applications of 16-QAM includes mobile and fixed broadband internet. In addition, for domestic broadcast applications, 64-QAM and 256-QAM are often used in digital cable television and cable modem applications. In the UK, 16-QAM and 64-QAM are currently used for digital terrestrial television using Digital Video Broadcasting (DVB).

Demodulation of the signal and in particular the phase data is generally performed using a carrier, which is recovered from the received signal, to determine the phase difference between the original and recovered carrier. A complication is that the exact phase and frequency of the carrier have to be recovered to track the abrupt changes of phase caused by data changes. This makes the receiver sensitive to noise and changes in the signal.

The majority of Field Programmable Gate Array manufacturers provide a ‘tan’ operator of trigonometric functions, which is currently used in the demodulation of phase data.

This is a complex mathematic ‘tan’ function to detect the phase changes. This requires carrier signal recovery circuitry and Look-Up-Tables (LUTs) to distinguish phase levels and changes on the received signals. Consequently, large memory blocks are required to perform the demodulation processes which requires significant levels of integrated circuit (IC) resources to be implemented.

It is therefore an aim of the present invention to provide an apparatus that overcomes the abovementioned problems.

It is a further aim of the present invention to provide a method of amplitude demodulation which overcomes the abovementioned problems.

In a first aspect of the invention there is provided a receiver and/or detector apparatus capable of receiving a modulated signal, said apparatus including a demodulator means, wherein said demodulator means uses at least one cross correlation function to demodulate the received signal.

Typically at least one reference signal or carrier component of the modulated signal has been modulated using a phase shift or shift in phase. The degree of phase shift relates to at least one bit of binary data. Further typically the digital modulation techniques that incorporate a shift in phase are Phase Shift Keying (PSK) and Quadrature Amplitude Modulation (QAM).

In one embodiment the modulation technique is a 16-QAM technique. Typically the modulation technique is 16-QAM, Star 16-QAM or Square 16-QAM.

Typically the cross correlation technique is a function wherein there is a measure of similarity between at least two signals or waveforms received by the receiver and/or detector apparatus. Further typically the cross correlation function is used to compare the phases of two or more portions of the received signal.

In one embodiment the apparatus includes at least one detector or receiver means. Typically the apparatus includes a plurality of

detector means, such that different portions of the detected signal can be compared using cross correlation. Further typically the apparatus includes at least two detector means. Preferably four detector means are used to detect eight separate phase angles of a phase modulated signal.

In one embodiment the detector or receiver means are QAM receivers. Typically QAM receivers track at least two vectors. Further typically the receiver tracks phase and amplitude vectors.

In one embodiment the apparatus includes at least one correlator means. Typically the correlator means cross correlates the signals received by the detector means. Thus a measure of similarity between the signals, and/or portions thereof, received by the detector means can be obtained.

In one embodiment the apparatus includes at least one analogue to digital converter (ADC). Typically the ADC quantizes the input signal from the detectors means into the phase angles used for modulation.

In one embodiment the apparatus includes a timer means. Typically the timer means updates and/or compares the cross correlated angles at one or more full cycles, or a fraction of a cycle, of the carrier signal. Further typically at least one timer means is used to update and/or compare the cross-correlated angles every half cycle of the carrier. The timer means provides a reference with regard to the portions of the signal received by the detector means which undergo cross correlation.

In one embodiment the apparatus includes a separator means. Typically the separator means converts the negative cross correlation values obtained by the correlator means into positive values. Thus, as

each detector means detects an in-phase (positive) and an out of phase (negative) signal and/or portion thereof, each detector means and/or correlator means provides two output peaks or values.

In one embodiment the apparatus includes a peak detector means. Typically the peak detector identifies the signals and/or portions thereof that have the largest and/or smallest degree of correlation. As such, peaks from the detector means and/or the correlator means are identified. Furthermore, identification of the peaks allows the symbols and/or data bits assigned to the particular phase angles to be determined.

In one embodiment the peak detector observes the peaks of detected angles and triggers an amplitude modulation timer means if an amplitude modulated signal is detected. Typically the amplitude modulation timer means feeds back a pulse width over a carrier cycle which multiplexes the amplitude. Further typically the multiplex is a factor of 3. This balances the amplitude inputs of the correlator means which in turn maximise the precision of cross-correlation.

In one embodiment a comparator means compares the cross correlated output of the detector means and/or the correlator means. Typically from the comparison of all of the cross correlated outputs the carrier frequency can be determined.

Typically the apparatus is implemented on a field programmable gate array and/or integrated circuit.

In a second aspect of the invention there is provided a method for demodulating at least one modulated signal and/or a portion thereof, said method including the steps of;

- performing cross-correlation of at least a portion of said signal with a further portion of the same.

In one embodiment a plurality of detector means are used to detect a number of separate phase angles.

In one embodiment a timer is used to update and/or compare the cross correlated phase angles at an integer of the cycle of the carrier and/or a fraction of the same. Preferably the timer updates and compares the cross-correlated values every half cycle of the carrier.

In one embodiment the cross correlated signals are separated into at least two parts. Typically the absolute values of both parts are obtained.

In one embodiment the highest absolute value identifies the received data phase angle. Typically the absolute values of separated signals are then recorded and updated every carrier cycle (or fraction thereof) through a peak detector.

This technique reduces circuitry requirements by over 75% in comparison to those utilising the 'tan' function and carrier recovery

Specific embodiments of the invention are now described with reference to the following figures, wheren:

Figure 1 shows a diagram of 8-PSK constellation points;

Figure 2 shows a diagram of the Costas loop

Figure 3 shows a diagram of an 8-PSK receiver using the Costas loop;

Figure 4 shows a diagram of an 8-PSK receiver using complex number demodulation;

Figure 5 shows a diagram of phase demodulation using an ATAN function;

Figure 6 shows a diagram of one embodiment of the invention;

Figure 7 shows a diagram of the effect of narrow band noise on carrier recovery demodulation;

Figure 8 shows the effect of narrow band noise on the cross-correlation approach of the present invention;

Figure 9 shows a schematic of an 8-PSK receiver test rig according to one embodiment of the invention;

Figure 10 is a graph of the input and output of a detector functioning according to one embodiment of the invention;

Figure 11 is a graph showing cross correlated signals according to one embodiment of the invention;

Figure 12 is a graph showing separated cross correlated signals according to one embodiment of the invention;

Figure 13 is a graph showing the detected cross correlated peaks in accordance with one embodiment of the invention;

Figure 14 is a graph of the peaks with added noise;

Figure 15 is a graph comparing the transmitted and received data in accordance with one embodiment of the invention; and

Figure 16 shows a number of plots comparing 8-PSK cross correlation with Monte Carlo simulations.

The present invention discloses a demodulation technique for PSK and/or QAM signals. Instead of using the atan function, the new technique presented here uses the cross-correlation method to demodulate the signals. As will be shown, this novel method of demodulation results in a considerable reduction in circuit complexity and hence less use of available silicon.

Demodulation of PSK signals using cross-correlation techniques

Fig. 1 shows a Phase Shift Keying (PSK) signal with 8 possible positions - 8-PSK. It is a popular form of digital modulation because M-PSK has a much higher spectral efficiency than conventional Intensity Modulation (IM) by a factor $\log_2(M)$. Thus the bandwidth of 8-PSK is three times narrower than standard intensity modulation which makes PSK modulation formats particularly useful in bandwidth limited channels. In addition, PSK has been often used for digital modulation of satellite link because of its good noise resistance

Several different forms of PSK are used in the IEEE 802.11b-1999 standard with Differential PSK (DPSK) being used at low data rates and Quadrature PSK (QPSK) being used at 11 Mb/s. The IEEE 802.11g-2003 standard uses Binary PSK (BPSK) and QPSK at faster transmission speeds. BPSK is also used in the IEEE 802.15.4, or ZigBee, standard. Applications of these standards include Wide-band Code Division Multiple Access (WCDMA), High-Speed Downlink Packet Access (HSDPA), World-wide Inter-operability for Microwave Access (WiMAX) and Wireless Local Area Network (WLAN) broadband wireless access technologies. The HDSPA is part of the 3rd Generation Partnership Project (3GPP) WCDMA.

Demodulation of phase data is generally performed using a carrier, which is recovered from the received signal, to determine the phase

difference between the original and recovered carrier. A complication is that the exact phase and frequency of the carrier have to be recovered to track the abrupt changes of phase caused by data changes. This makes the receiver sensitive to noise and changes in the signal.

This invention is presented as follows: the rest of this section presents various demodulation techniques and methods of carrier recovery as well as presenting the novel method of demodulating M-PSK; section II presents the mathematics of carrier recovery and derives the performance of the proposed technique; section III presents the implementation of the proposed technique and performance results; section IV analyses and discusses the proposed system and results compared to the prior works; and section V summaries the findings and comes up with possible applications.

COSTAS LOOP

The phase detector used in receivers for phase modulated signals must produce a signal proportional to the phase difference between the received signal and the recovered carrier. One way of recovering the carrier is to use a Costas loop as shown in fig. 2. The outputs of the Low Pass Filters (LPFs) are proportional to the cosine and sine of the phase difference, ϕ. When the two output terms are multiplied together, the result deviates the Voltage Controlled Oscillator (VCO) operating at the carrier frequency (ω_c) until the VCO and received frequency are matched and locked. There are some practical problems associated with the Costas loop: a long acquisition time; possibility of a false lock; a 180° phase ambiguity due to the squaring loop; preamble sequence to aid carrier recovery.

Fig. 3 shows an M-PSK coherent detector consisting of 2^M matched filters or correlators. Each correlator is responsible for an angle

where it correlates the received signal $S_i(t)$ with a delayed complement phase (θ_r) of that angle(θ_t). Decisions about the received data, $Rx(t)$, are made by finding the largest magnitude over the symbol period (T_s). Since two pairs of the transmitted angles are opposite each other, as shown in fig. 1, the number of correlators can be reduced to 2^{M-1} as shown in fig. 3 where 8-PSK has been used as an example.

COMPLEX NUMBER DEMODULATOR

Phase (θ_t) data can be demodulated using the complex number approach. The delayed sample undergoes a complex conjugate conversion $\overline{Z_{n-1}}$ and is then multiplied by the received signal Z_n. Fig. 4 shows an 8-PSK demodulator using the technique.

The advantage of this technique is that a simple multiplication function is required. However it requires Real-Imaginary to Complex conversion which needs to be performed using a high specification processor. The sampling frequency has to be a multiple of the M carrier frequency to slice the phase angles equally. In addition, the output of the mixer needs to be interpreted through a complex phase slicer circuitry before outputting the received data. This phase slicer needs continual calibration depending on the peak-to-peak amplitude of the received signal.

ATAN DEMODULATOR

An alternative PSK demodulation technique is to measure the angle between the baseband signal complex envelope and the nearest constellation point using an ATAN computation. The ATAN approach is an advanced version of the Costas loop, using a digital PLL in parallel with the ATAN function as shown in fig. 5. This technique replaces the matched filters of fig. 3. The ATAN function is implemented using a Look-Up Table (LUT) and the whole can be

implemented using Field Programmable Gate Arrays (FPGAs) with Digital Signal Processing (DSP) capabilities. This technique is very useful for higher M-PSK and M-QAM orders as it can be used to reduce the number of implementation resources required to implement 2^{M-1} matched filters.

This technique is similar to the complex number approach in that the output of the ATAN function needs to be interpreted through an LUT phase slicer before outputting the received data. The digital PLL uses a Numerically Controlled Oscillator (NCO) which experiences jitter noise when narrowband noise is added to the received signal. This causes the received constellation to rotate. The noise can be minimised by using high accuracy ATAN computation but a high level of FPGA resources are required to perform such an operation.

PROPOSED ALTERNATIVE SOLUTION

A new approach to the demodulation of phase data of a M-PSK signal using cross-correlation has been developed. As discussed, current technology generally incorporates a complex ATAN function to detect the phase changes of a phase modulated signal. This requires carrier signal recovery circuitry and LUTs to distinguish phase levels and changes in the received signals. However, the dynamic gain at the phase detector inputs has to be linked to an Automatic Gain Control (AGC) circuit to compensate the changes or otherwise the NCO/VCO characteristics will change accordingly. Consequently, large memory blocks are required to perform the demodulation processes which requires complex and large circuits. By contrast, the cross-correlation technique, described here, does not require carrier recovery circuitry or LUTs to detect the phase changes.

Fig. 6 shows a block diagram of the technique as applied to the detection of 8-PSK. Four detectors are used to detect 8 separate

phase angles and a timer is used to update and compare the cross-correlated angles every half cycle of the carrier. The cross correlated signals are separated into 2 parts and then the absolute value of both parts are obtained, with the highest absolute value identifying the received data phase angle. The absolute values of separated signals are then recorded and updated every half carrier cycles through the peak detector.

When compared to conventional schemes such as the Costas loop, the proposed scheme is very simple and requires less hardware for the realization. Also, as the scheme does not extract the carrier for demodulation purposes, this new method is more tolerant of noise. The proposed cross-correlation technique optimises the number of implementation resources required to demodulate the PSK data, compared to the other techniques discussed, by omitting the carrier recovery circuitry, filters and LUTs to slice the phase data.

MATHEMATICAL DERIVATION AND PERFORMANCE
PERFORMANCE OF CARRIER RECOVERY

The performance of the coherent carrier recovery can be tested by introducing narrowband noise $\boldsymbol{n_{nb}(t)}$ on the received data as shown in fig. 7. The added noise deviates the phase of the transmitted angle by $\boldsymbol{\Delta\theta_t}$. Consequently, the recovered carrier phase suffers from the jitter noise $\boldsymbol{\Delta\theta_r}$ of the VCO.

So, the correlated signal,

$$\boldsymbol{S_o(t) = [A\ \cos(\omega_c t + \theta_t + \Delta\theta_t) + n_{nb}(t)][\cos(\omega_c t - \theta_r + \Delta\theta_r)]} \quad (1)$$

Expanding (1) using the quadrature components of $\boldsymbol{n_{nb}(t)}$:

$$\boldsymbol{S_o(t) = \begin{bmatrix} A\ \cos(\omega_c t + \theta_t + \Delta\theta_t) + x(t)\cos(\omega_c t + \theta_t + \Delta\theta_t) \\ -y(t)\sin(\omega_c t + \theta_t + \Delta\theta_t) \end{bmatrix}}$$

$$\boldsymbol{\times [\cos(\omega_c t - \theta_r + \Delta\theta_r)\ ]}$$

$$= [\boldsymbol{A} + \boldsymbol{x}(\boldsymbol{t})]\cos(\boldsymbol{\omega_c t} + \boldsymbol{\theta_t} + \Delta\boldsymbol{\theta_t})\ \cos(\boldsymbol{\omega_c t} - \boldsymbol{\theta_r} + \Delta\boldsymbol{\theta_r})$$

$$- \boldsymbol{y}(\boldsymbol{t})\sin(\boldsymbol{\omega_c t} + \boldsymbol{\theta_t} + \Delta\boldsymbol{\theta_t})\ \cos(\boldsymbol{\omega_c t} - \boldsymbol{\theta_r} + \Delta\boldsymbol{\theta_r})$$

$$\boldsymbol{S_o(t)} = \frac{[A+x(t)]}{2}[\cos(2\boldsymbol{\omega_c t} + \boldsymbol{\theta_t} - \boldsymbol{\theta_r} + \Delta\boldsymbol{\theta_t} + \Delta\boldsymbol{\theta_r}) + \cos(\boldsymbol{\theta_t} + \boldsymbol{\theta_r} + \Delta\boldsymbol{\theta_t} - \Delta\boldsymbol{\theta_r})]$$

$$- \frac{y(t)}{2}[\sin(2\boldsymbol{\omega_c t} + \boldsymbol{\theta_t} - \boldsymbol{\theta_r} + \Delta\boldsymbol{\theta_t} + \Delta\boldsymbol{\theta_r}) + \sin(\boldsymbol{\theta_t} + \boldsymbol{\theta_r} + \Delta\boldsymbol{\theta_t} - \Delta\boldsymbol{\theta_r})]$$

Thus, the output $\boldsymbol{g(t)}$ of the matched filter,

$$\boldsymbol{g(t)} = \frac{[A+x(t)]}{2}\ \boldsymbol{cos}(\boldsymbol{\theta_t} + \boldsymbol{\theta_r} + \Delta\boldsymbol{\theta_t} - \Delta\boldsymbol{\theta_r}) - \frac{y(t)}{2}\boldsymbol{sin}(\boldsymbol{\theta_t} + \boldsymbol{\theta_r} + \Delta\boldsymbol{\theta_t} - \Delta\boldsymbol{\theta_r}) \qquad (2)$$

Equation 2 shows the output of the matched filter with the added noise. Clearly, the noise deviates the recovered carrier, which rotates the constellation points as discussed in section I D, thus making it more likely that the VCO will lock onto a false quadrant phase. Consequently, the decision maker of the demodulator could mistake the detected angle and hence make an error in decoding the received data.

PERFORMANCE OF THE PROPOSED TECHNIQUE

The performance of the cross-correlation approach can be derived by adding narrowband noise $\boldsymbol{n_{nb}(t)}$ and its delayed version $\boldsymbol{n_{nb}(t - T_c)}$ to the signal as shown in fig. 8 when a continuous sinusoidal signal is received. The added noise deviates the phase of the transmitted angle by $\Delta\boldsymbol{\theta_t}$. Consequently the complement angle $(-\boldsymbol{\theta_r})$ of the cross correlation suffers from the jitter noise $\Delta\boldsymbol{\theta_r}$ caused by the delayed version of $\Delta\boldsymbol{\theta_t}$.

So, the correlated signal,

$$\boldsymbol{S_o(t)} = [\boldsymbol{A}\ \boldsymbol{cos}(\boldsymbol{\omega_c t} + \boldsymbol{\theta_t} + \Delta\boldsymbol{\theta_t}) + \boldsymbol{n_{nb}(t)}][\boldsymbol{A}\ \boldsymbol{cos}(\boldsymbol{\omega_c t} - \boldsymbol{\theta_r} + \Delta\boldsymbol{\theta_r}) + \boldsymbol{n_{nb}(t - T_c)}] \quad (3)$$

Expanding (3) using the quadrature components of the noise, $\boldsymbol{n_{nb}(t)}$:

$$\boldsymbol{S_o(t)} = \begin{bmatrix} \boldsymbol{A\ cos(\omega_c t + \theta_t + \Delta\theta_t) + x(t)\, cos(\omega_c t + \theta_t + \Delta\theta_t)} \\ \boldsymbol{-y(t)\, sin(\omega_c t + \theta_t + \Delta\theta_t)} \end{bmatrix}$$

$$\times \begin{bmatrix} \boldsymbol{A\ cos(\omega_c t - \theta_r + \Delta\theta_r) + x(t - T_c)\, cos(\omega_c t - \theta_r + \Delta\theta_r)} \\ \boldsymbol{-y(t - T_c)\, sin(\omega_c t - \theta_r + \Delta\theta_r)} \end{bmatrix}$$

$$= \boldsymbol{[A + x(t)][A + x(t - T_c)]\, cos(\omega_c t + \theta_t + \Delta\theta_t)\ cos(\omega_c t - \theta_r + \Delta\theta_r)}$$

$$\boldsymbol{- [A + x(t)]\, y(t - T_c)\ cos(\omega_c t + \theta_t + \Delta\theta_t)\ sin(\omega_c t - \theta_r + \Delta\theta_r)}$$

$$\boldsymbol{- y(t)[A + x(t - T_c)]\, sin(\omega_c t + \theta_t + \Delta\theta_t)\ cos(\omega_c t - \theta_r + \Delta\theta_r)}$$

$$\boldsymbol{+ y(t) y(t - T_c)\, sin(\omega_c t + \theta_t + \Delta\theta_t)\ sin(\omega_c t - \theta_r + \Delta\theta_r)}$$

The $\boldsymbol{\Delta\theta_r}$ is a delayed version of a random phase noise $\boldsymbol{\Delta\theta_t}$, which is minimised by the pre-filtering unit. The remaining noise affects the carrier amplitude at frequencies higher than those that make fake quadrant lock in carrier recovery systems. The $\boldsymbol{\Delta\theta_r}$ is cancelled with $\boldsymbol{\Delta\theta_t}$ when cross-correlated using the proposed approach. So,

$$\boldsymbol{S_o(t)} = \frac{\boldsymbol{[A+x(t)][A+x(t-T_c)]}}{\boldsymbol{2}} \boldsymbol{[cos(2\omega_c t + \theta_t - \theta_r + 2\Delta\theta_t) + cos(\theta_t + \theta_r)]}$$

$$- \frac{\boldsymbol{[A+x(t)]\, y(t-T_c)}}{\boldsymbol{2}} \boldsymbol{[sin(2\omega_c t + \theta_t - \theta_r + 2\Delta\theta_t) - sin(\theta_t + \theta_r)]}$$

$$- \frac{\boldsymbol{y(t)\, [A+x(t-T_c)]}}{\boldsymbol{2}} \boldsymbol{[sin(2\omega_c t + \theta_t - \theta_r + 2\Delta\theta_t) + sin(\theta_t + \theta_r)]}$$

$$+ \frac{\boldsymbol{y(t)\, y(t-T_c)}}{\boldsymbol{2}} \boldsymbol{[cos(\theta_t + \theta_r) - cos(2\omega_c t + \theta_t - \theta_r + 2\Delta\theta_t)]}$$

Thus,

$$g(t) = \frac{[A+x(t)]\,[A+x(t-T_c)] + y(t)\, y(t-T_c)}{2} \cos(\theta_t + \theta_r) \quad (4)$$

$$+ \frac{\boldsymbol{[A+x(t)]y(t-T_c) - y(t)[A+ x(t-T_c)]}}{\boldsymbol{2}} \sin(\theta_t + \theta_r)$$

When a symbol is phase $(\boldsymbol{\theta_t})$ transmitted, the complement angle at the receiver is $(\boldsymbol{-\theta_t})$,

$$\boldsymbol{\therefore\ g(t)} \approx \frac{\boldsymbol{[A+x(t)]\,[A+x(t-T_c)] + y(t)\, y(t-T_c)}}{\boldsymbol{2}} \quad (5)$$

Clearly, carrier recovery systems suffer from phase and amplitude noise as shown in (2) whereas the proposed approach suffers from amplitude noise only as shown in (5). The direct cross-correlation results in a guaranteed phase difference as shown by (4). The $x(t), x(t - T_c)$, $y(t)$ and $y(t - T_c)$ amplitude noise in (4) deflect and rotate the constellation points away from the origin. However, an AGC and pre-filtering units keep the SNR at a reasonable level and the highest cross-correlated points within the bounded area of the detected angle shown in fig. 1 over the symbol period.

IMPLEMENTATION AND RESULTS

With reference to fig. 6, the receiver test rig is summarised in a flowchart shown in fig. 9. It was implemented using Altera Quartus II, Altera-DSP Builder and Matlab-Simulink. VHDL language was used to design the Sign Slicer, Peak Detector, Comparator and Error Calculator.

Fig. 10 shows the 8-PSK input (top) to $\mathbf{45^0/225^0}$ correlator where yellow and magenta traces show the received and complement angle respectively. Fig. 10 also shows the output (bottom) of the correlator. The positive part indicates the detected in-phase angle and the negative part indicates the detected $\mathbf{180^0}$ out of phase angle.

The Sign Slicer VHDL code slices the positive/negative output of the 4 correlators. The absolute value of the negative parts was taken as shown in fig. 11. That is how the angles are separated equally to 8 angles using 4 detectors.

Fig. 12 shows the cross-correlated signals of the 4 detectors where the absolute value of the negative parts were taken. The correlated signals result in twice the carrier frequency.

The Peak Detector VHDL code was used to observe the peaks of the cross correlated signal as shown in fig. 13. Note that, in fig. 13, the detected peaks were slightly delayed to better explain the concept. In practice there should be no delay for direct comparison of angles and data outputting.

Clearly, the output of the Peak Detector sliced the angles where the $\mathbf{0^0}$ angle is the reference to the received angles and the highest cross-correlated point in fig. 13 reflects the detected angle. This is evident by using the "Cross Correlation Comparator" code by checking the opposite angle, $\mathbf{45^0}$ in this case.

Fig. 14 shows the cross correlated signals at the presence of AWGN. The Peak Detector code observes the peaks of angles every half cycle of the carrier as shown in fig. 13. Then, the Cross Correlation Comparator code compares the highest (detected angle) to the minimum (opposite angle) peaks, retimes any new data and eventually outputs the received data as shown in fig. 15. A delayed version of the transmitted data is displayed in fig. 15 for comparison purposes.

ANALYSIS AND DISCUSSION

An Altera CYCLONE III EP3C120F780C7N based DSP development board was used to implement the test rig shown in fig. 9. An Altera Quartus II analysis showed that the system utilises only 2% out of 119,088 Total Logic Elements, less than 1% out of 4 Mb Total Memory Bits and 1% out of 576 Embedded Multiplier 9-bit Elements. In contrast to the system of that utilises 800 Look-Up-Tables (LUTs), the system presented in this paper utilises 678 LUTs. In addition, this system used no filters compared to the conventional demodulation technique of, that uses a set of Finite Impulse Response (FIR) Low Pass Filters (LPFs) to get rid of the carrier components at the output of the correlators.

A ROHDE & SCHWARZ Noise Generator was used to introduce noise across the channel of the 8-PSK transmitter-receiver link over a range of SNR 0-25dB. A VHDL code based error calculator computed the differences between the transmitted and received symbols/bits. Fig. 16 shows the performance of the 8-PSK demodulator with no error coding using cross-correlation. Tests were performed 4 times: Carrier-to-Noise-Ratio (CNR); Bit-to-Noise-Ratio (EbNR); Symbol-to-Noise-Ratio (EsNR); and limitless noise.

The optimum error rate is 10^{-5} that provides maximum performance for 16-bit and lower resolutions. However, the presented system achieves 10^{-5} error rate at least 21 dB above noise level as shown in fig. 16. As discussed in Section IV, the system requires pre-filtering units to keep CNR with respect to phase response at a reasonable level and the highest cross correlated points within the bounded area of the detected angle.

P. K. Vitthaladevuni., and M. S. Alouini, (2005, Jul.). Effect of imperfect phase and timing synchronization on the bit-error rate performance of PSK modulations. ***IEEE Trans. Commun.*** and **P. K. Vitthaladevuni., and M. S. Alouini., (2003, Dec.). Exact BER computation of generalized hierarchical PSK constellations.** ***IEEE Trans. Commun.*** discloses a Hierarchical 8-PSK constellation and used Monte Carlo algorithms to analyse the Bit Error Rate (BER) over a range of CNR 0-24dB with an assumption of perfect carrier recovery and ability of tracking phase fluctuations. A direct comparison of the error rate in this work shows in fig. 16 that the Monte Carlo analysis delivers a maximum 8×10^{-4} BER at 24dB of CNR whereas the cross-correlation scheme delivers the same BER with only 16dB of CNR. In addition, the performance of the cross-correlation scheme is still better than that cited by **P. K. Vitthaladevuni** *et al.* for

limitless noise across the channel. The use of error coding should enhance the performance further.

V. K. Velkuru., and A. Samant, "A design for software defined M-PSK radio on FPGA for low SNRs and symbol rates upto 10MS/s," in *Proc. ICSIPA 2011, IEEE.* Kuala Lumpur, 2011, pp. 574-578 discloses a receiver on FPGA to comply with the IESS 308/310 Satellite Communication Standards based on PSK modulation scheme. The 8-PSK scheme in these standards requires 6dB, EbNR to attain lock to the carrier. In contrast, cross-correlation does not require carrier recovery and can deliver a maximum 9×10^{-3} BER at lower than 6dB compared to **V. K. Velkuru** *et al.* that requires at least 6dB to attain lock.

IEEE 802.11b-1999, 802.11g-2003 and IEEE 802.15.4 standards use adaptive systems to compensate the error rate at low SNR by switching between DPSK, BPSK and QPSK. Applications of these standards include WCDMA, HSDPA, WiMAX and WLAN broadband wireless access technologies. This leads us to propose an adaptive system, in parallel with error coding, to use cross-correlation at low SNR and back to normal operation at high SNR for the Satellite and Broadband standards.

CONCLUSION AND FURTHER WORK

Cross-correlation has been used, for the first time to demodulate 8-PSK. It has been designed and prototyped on an FPGA. The proposed scheme is very simple compared to alternative methods and requires less hardware for the realization, and thus lower power consumption. As it does not extract the carrier for demodulation purposes; the proposed detection scheme offers improved phase detection performance as well as superior resistance to AWGN compared to a carrier recovery scheme operating at low SNR. No filters were used

compared to conventional demodulation techniques that require them to get rid of the carrier components at the output of the correlators. We observed that the system requires an AGC and pre-filtering units to keep CNR with respect to phase response at reasonable level and the highest cross-correlated points within the bounded area. The presented results with no error coding provide maximum performance for 10-bit and 16-bit at CNR of 16dB and 21dB respectively. Use of the present invention with error coding can enhance the error rate at low SNR for the applications of mobile and fixed wireless broadband internet devices, 3G connections and Digital Video Broadcasting (DVB) receivers.

Demodulation of QAM signals using cross-correlation techniques

Quadrature Amplitude Modulation (QAM) is considered to be one of the highly bandwidth efficient modulation schemes in wireless communication. QAM has a noise bandwidth that is relatively smaller than that of the phase shift keying (PSK). Two types of 16-QAM are discussed in this paper, namely Star (Circular) and Square. Star 16-QAM is preferred to Square QAM in Orthogonal Frequency Division Multiplex (OFDM) systems to keep the effects of peak-to-average-power-ratios (PAPR) low. OFDM is widely used in Digital Video Broadcasting (DVB), Digital Audio Broadcasting (DAB) and Broadband internet. System integrators use ATAN computation in parallel with digital Phase-Locked-Loop (DPLL) to demodulate QAM signal. As will be shown in this paper, such a demodulation scheme requires high number of Field Programmable Gate Array (FPGA) implementation resources.

We propose a novel cross-correlation function to replace ATAN and DPLL for 16-QAM signal demodulation. As will be shown, this novel function is simple to realise, yields a significant reduction in terms of complexity and hence less use of available silicon. This technique will

yield cost reduction in products using 16-QAM demodulators, namely Broadband internet and, Digital TV and Radio.

I. INTRODUCTION

Star and Square QAM techniques are widely used to transmit m-bit symbols via a 2^M signal point constellation, distributed on a complex plane. However, the higher the M, the more bandwidth efficient the modulation scheme. 16-QAM is one of the standard modulation schemes in OFDM applications such as DAB, DVB, and High Performance Local Area Network (HIPERLAN). In addition, 16-QAM is widely used in Wide-band Code Division Multiple Access (WCDMA), High-Speed Downlink Packet Access (HSDPA), World-wide Inter-operability for Microwave Access (WiMAX), Wireless Local Area Network (WLAN), Asynchronous Digital Subscriber Line (ADSL) and High-bit-rate Digital Subscriber Line (HDSL) broadband technologies.

We present as follows: the rest of this section presents a background on Star and Square 16-QAM modulation, receiver, and carrier recovery as well as presenting the novel and inventive method of demodulating 16-QAM; section II presents the implementation of the proposed technique; section III analyses and discusses the proposed system and compares results to the prior works; and section IV summaries the findings.

A. STAR 16-QAM

Star 16-QAM has two amplitude levels that are two circles around the origin as shown in fig. 17. The outer ring is 3 times greater than the inner ring. It is considered as a two 8-PSK with different amplitude level– a combination of 8-PSK and Binary Amplitude Shift Keying (BASK). 8-PSK and 16-QAM occupies the same bandwidth since they share the same symbol rate e.g. $4\ symbols/s$. 16-QAM has a noise bandwidth that is smaller than that of 8-PSK. BASK data (a_n) is

differentially encoded and 8-PSK data ($\boldsymbol{b_n}$, $\boldsymbol{c_n}$, $\boldsymbol{d_n}$) are phase modulated on the carrier. The transmitted 16-QAM signal can be represented as (1),

$$\boldsymbol{S_{QAM}(t) = A\ \cos(\omega_c t + \theta_t)} \qquad (1)$$

The amplitude A in (1) represents BASK data whereas $\boldsymbol{\theta_t}$ represents 8-PSK data.

B. SQUARE 16-QAM

In contrast to Star 16-QAM, Square 16-QAM has three amplitude levels. The constellation points are distributed on 3 circles of the signal plane as shown in fig. 18. The points are separated in uniform square arrays. Square and Star QAM occupy the same bandwidth for the same transmission rate. Square 16-QAM signal is modulated by dividing the data source to 4 *bit/symbol* ($\boldsymbol{a_n}$, $\boldsymbol{b_n}$, $\boldsymbol{c_n}$, $\boldsymbol{d_n}$). A demultiplexer splits the data into Even and Odd Non-Return-to-Zero (NRZ) parts. The Odd and Even parts control the amplitude level of the in-phase and quadrature carriers respectively. Equation (1) formulates the transmitter output.

C. 16-QAM RECEIVER

The transmitted 16-QAM signal is a suppressed carrier where half the power is concentrated in the carrier and the other half is QAM modulated data. Demodulation of 16-QAM is crucial where 2 vectors have to be tracked, phase and amplitude. The phase can be tracked using complex number, Costas loop or DPLL and *ATAN* function using a Digital Signal Processing (DSP) processor. The amplitude can be tracked easily in the case of Star 16-QAM by comparing the absolute values of a current sample with a delayed full carrier cycle to differentially decode BASK data ($\boldsymbol{a_n}$) where an 8-PSK receiver can be used to demodulate the phase data. In contrast, the symbols in Square 16-QAM are strictly dependent on A and $\boldsymbol{\theta_t}$. This requires coherent

detection which requires phase knowledge. Unfortunately the phase noise causes the constellation points to rotate, and so an absolute phase reference must be maintained or estimated.

D. CARRIER RECOVERY AND PHASE DEMODULATION SCHEMES

One way of recovering the carrier is to use a Costas loop. It suffers from a long acquisition time; possibility of a false lock; a 180^0 phase ambiguity and hence a preamble sequence is needed to aid carrier recovery. Matched filters are to be used to slice the phases using the recovered carrier. Phase data can also be demodulated using the complex number approach. This requires Real-Imaginary to Complex conversion which needs to be performed using a high specification processor.

ATAN computation is an advanced version of Costas loop, using a DPLL. It measures the angle between the baseband signal complex envelope and the nearest constellation point. A high accuracy ATAN computation resists the noise but a high level of FPGA resources is required to perform such an operation.

Coherent detection is severely affected by multipath fading, mainly because of carrier recovery issues in a fast-fading environment where the PLL locks onto a different quadrant than that required. The carrier recovery is not efficient as the exact phase cannot be guaranteed or maintained. However, with DSP processors the carrier recovery requires LUTs to slice and scale the phases. Mainly, system integrators use *ATAN* function in parallel with DPLL to detect the phase changes. Consequently, high implementation resources are needed to perform such an operation.

We have shown previously that carrier recovery systems experience jitter noise caused by the narrowband noise deviation. This leads the

constellation points to rotate and hence make an error in decoding the received data. Alternatively, we discussed the aforementioned use of cross-correlation to demodulate 8-PSK signal compared to the schemes that use carrier recovery as part of extracting the phase data. It was concluded that the cross correlation provides great immunity at low SNR. This requires an Automatic-Gain-Control (AGC) and pre-filtering units to keep the SNR at reasonable level and the highest cross correlated points within the bounded area of the detected point over the symbol period.

E. PROPOSED SCHEME

The concept of the cross-correlation theory will be further applied to demodulate 16-QAM signal using the test rig shown in fig. 19 and compare it with prior work as will be seen later. The general operation of the 16-QAM receiver is; four detectors cross correlate the carrier by the complement transmitted angles to detect 8 separate phase angles and a timer to update and compare the cross correlated angles every half carrier cycle interval for instant observations. The cross correlated signals are separated into 2 parts and then the absolute value of both parts are obtained with the highest absolute value identifying the received data phase angle. In addition, the received signal is delayed by 360^0 to compare it with current samples. These two signals are now differentially decoded to output BASK data. The peak detector observes the peaks of detected angles and triggers the AM timer once an AM signal is detected. The AM timer feeds back a pulse width over a carrier cycle which multiplexes the amplitude by a factor of 3. This balances the amplitude inputs of the correlators which in turn maximise the precision of cross-correlation. Eventually, the Cross Correlation Comparator compares the correlated points and output the received data.

II. IMPLEMENTATION AND RESULTS

With reference to the receiver test rig shown in fig. 19, the receiver was implemented using Altera Quartus II, Altera-DSP Builder and Matlab-Simulink. The VHDL language was used to design the Sign Slicer, Peak Detector, Cross Correlation Comparator and Amplitude Modulation (AM) timer. The design was tested using a PRBS data source.

Fig. 20 shows the output of 16-QAM correlators. The phases are clearly sliced even in the presence of AM signal. This is apparent on the highest and lowest peaks as will be discussed later.

The correlated signals in fig. 20 are now separated. The absolute values of the negative parts were taken as shown in fig. 21.

The peak detector observes the AM and phase peaks separately. The phase peaks are observed over half the carrier cycle while the AM peaks are observed over quarter the carrier cycle whenever the current sample is greater than the previous sample. Any AM transitions would trigger the AM timer and also indicates BASK data reception. Once the phase timer overflowed, the highest detected phase peaks and BASK data are sent to the Cross Correlation Comparator.

Fig. 22 shows the detect peaks of 16-QAM correlated in fig. 20 and sliced in fig. 21. The detected peaks were slightly delayed by the author in fig. 22 to better explain the idea but practically there should be no delay for direct comparison of angles and data outputting.

The highest peak in fig. 22 indicates the detected angle i.e. $\mathbf{315^0}$. This is evident by checking the minimum peak which is the opposite angle i.e. $\mathbf{135^0}$. The peak detector could detect a leakage from the neighbouring angles. Such a leakage is cancelled out when compared by the Cross Correlation Comparator as the opposite angle is not confirmed.

Fig. 23 shows all the correlated and separated signals of 16-QAM signal in the presence of Additive White Gaussian Noise (AWGN). The zoomed-in area in fig. 23 shows that the red ($\mathbf{135^o}$) trace is dominant among all traces where the cyan ($\mathbf{90^o}$) and green ($\mathbf{180^o}$) are just close the red trace. This confirms that the cross correlated point is within the bounded area of the detected angle. Clearly, the AWGN affected the peaks of the cross correlated points. The cross correlation comparator compares the highest (detected angle) to the minimum (opposite angle) peaks, combines it with BASK data, retimes any new data and eventually outputs the received data. The new angle is $\mathbf{135^0}$ (maximum) and evident by the opposite angle $\mathbf{315^0}$ (minimum). Since the transmitter is sending the data at rate of 0.25 s, the comparator is updated regulary almost every 0.25 s.

A direct comparison of the transmitted and recovered data is shown in fig. 24. A delayed version of the transmitted data was displayed on fig. 24 for the comparison. The receiver missed two symols at startup and then fully recovered the data.

III. ANALYSIS AND DISCUSSION

The constellation points of Square QAM optimise the transmission over Gaussian channel compared to Star QAM. Square QAM requires AGC and carrier recovery for coherent detection. The carrier recovery is severely affected by fading channel. In contrast, Star QAM reduces the effects of Rayleigh fading. The AGC in Square QAM has to maintain stability fast enough to decode the AM data. The symbols in Square QAM are strictly dependent on A and $\boldsymbol{\theta_t}$. On the other hand, the amplitude can be tracked easily in the case of Star 16-QAM to decode BASK data separately from the phase data $\boldsymbol{\theta_t}$. Star QAM does not experience false lock positions and the transmitted mean power is relatively small compared to Square QAM. In addition, it has the property that PAPR is less than that for Square QAM. For this reason,

Star 16-QAM is preferred to Square QAM in OFDM systems to keep the effects of PAPR low. Moreover, the coded Star 16-QAM symbol error rate is better than that of Square 16-QAM.

An Altera CYCLONE III EP3C120F780C7N based DSP development board was used to implement the test rig. The authors of implemented a carrier recovery system for Square 16-QAM and the authors of implemented Square 16-QAM receiver based on FPGA using the *ATAN* function and DPLL. Hence, a direct comparison, of the number of FPGA system resources, to these works, is given in Table I. Clearly, the proposed demodulation scheme significantly reduced the number of Embedded Multipliers to demodulate 16-QAM compared to. In addition, the prototyped scheme does not need carrier recovery and uses only 4 Embedded Multipliers compared to that uses 8 Embedded Multipliers just to extract the carrier prior demodulation.

Table I
16-QAM Implementation Resources Requirements

Type of resources	Resources used by carrier recovery *	Resources used by Square 16-QAM receiver **	Resources used by Star 16-QAM [this work]
Embedded Multipliers	8	48	4
LUTs	Not presented by *	4674	1858

*** C. Dick., F. Harris., and M. Rice (2004, Jan.). FPGA implementation of carrier synchronization for QAM receivers. *Journal of VLSI Signal Processing*. [Online]. *36(1)*, pp. 57-71.**

**** X. Vu., N. A. Duc,, and T. A. Vu, "16-QAM transmitter and receiver design based on FPGA," in *Proc. DELTA'10, IEEE*. Ho Chi Minh City, 2010, pp. 95-98.**

If cross-correlation is used in Square 16-QAM, then 6 correlators are required to detect 12 angles positions and the amplitude data are to be differentially decoded. This consumes more implementation resources than Star 16-QAM. The concept of using cross correlation to demodulate 16-QAM signal was proven by using Matlab-Simulink and practical implementations of FPGA. The cross correlation has been used for the first time in Star 16-QAM demodulator system, replacing the *ATAN* function and DPLL to detect the phase changes on the received signal. This yields a significant reduction in terms of complexity and the silicon required to integrate Star 16-QAM receiver onto an IC. The reduced complexity of the receiver leads to a reduced number of resources required, for the design, and thus power consumptions of the system. This technique will yield cost reduction in products using 16-QAM demodulators, namely broadband internet and, Digital TV and Radio.

IV. CONCLUSION AND FURTHER WORK

The concept of using cross correlation to demodulate 16-QAM signal was proven using simulations and practical implementations of FPGA. The cross correlation has been used for the first time in the Star 16-QAM demodulator system, replacing the ATAN function and DPLL to detect the phase changes on the received signal. The technique requires less hardware implementation compared to alternative methods. In contrast to conventional schemes, no filters were used to get rid of the carrier components at the output of the correlators. This technique will yield cost reduction in products using 16-QAM demodulators, namely broadband internet and Digital TV.

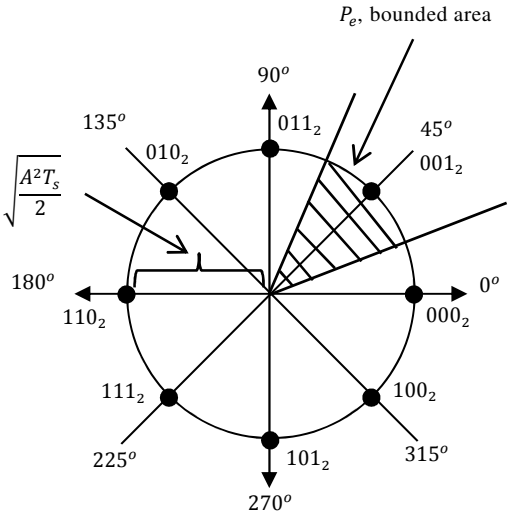

Fig. 1. 8-PSK constellation points

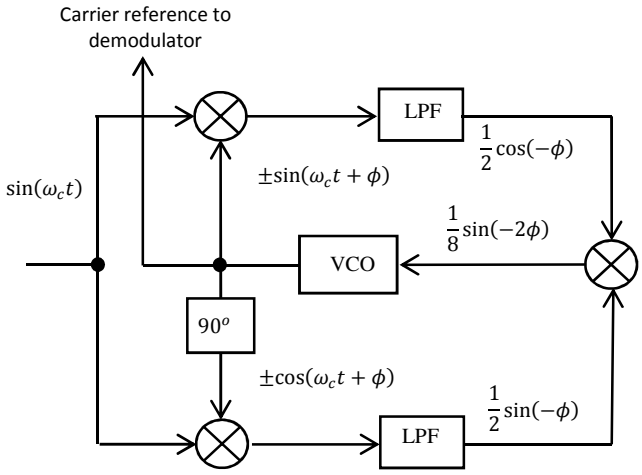

Fig. 2. Costas loop

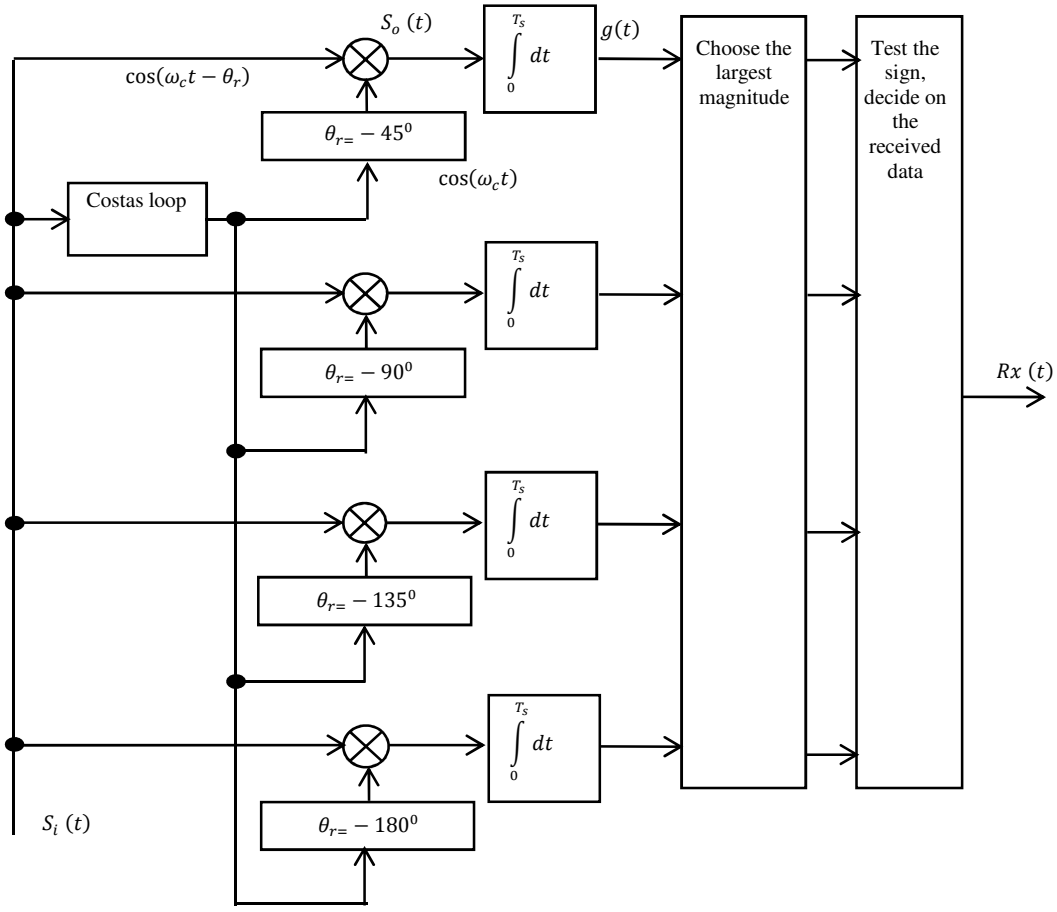

Fig. 3. 8-PSK receiver using Costas loop [14]

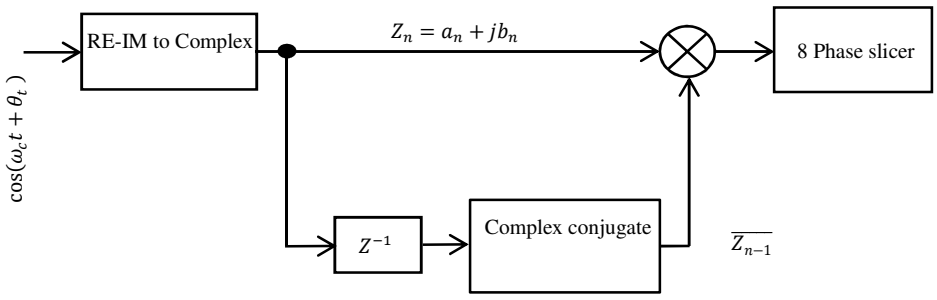

Fig. 4. 8-PSK receiver using complex number [16]

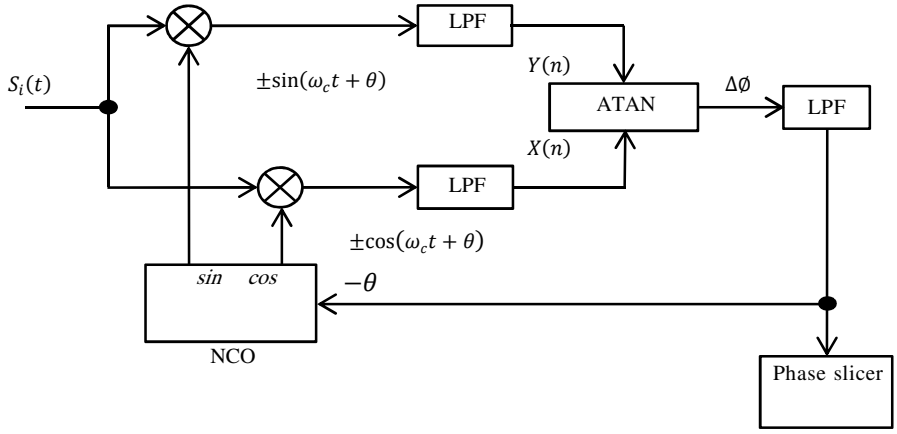

Fig. 5. Phase demodulator using *ATAN* function and digital PLL [6], [11]

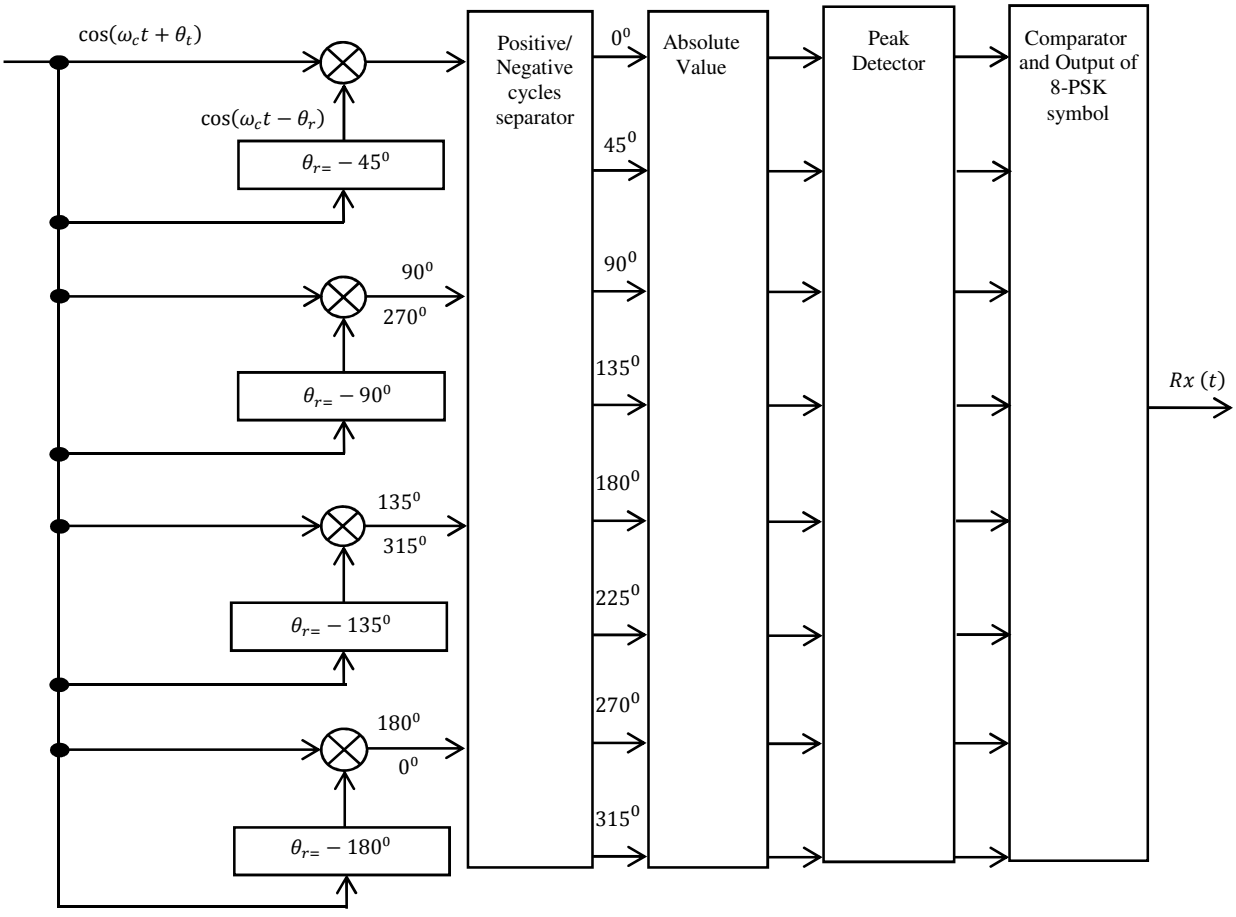

Fig. 6. 8-PSK receiver design using cross correlation

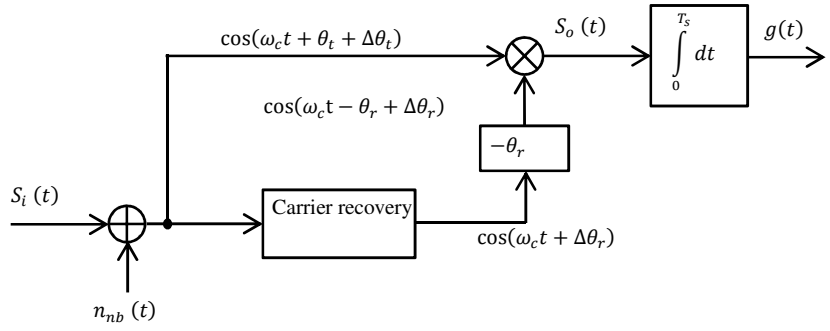

Fig. 7. Effect of added narrowband noise on matched filter using carrier recovery

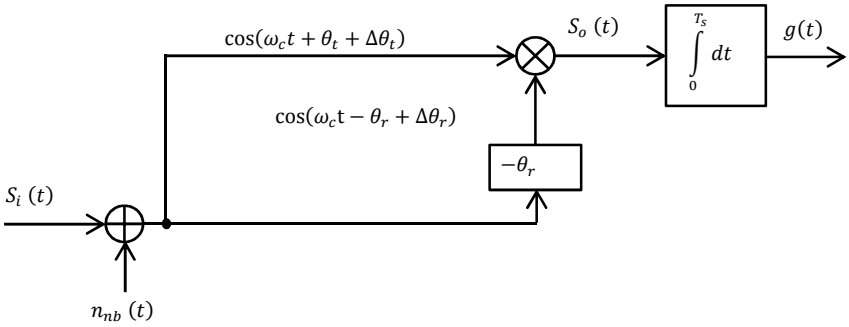

Fig. 8. Effect of added narrowband noise on cross-correlation approach

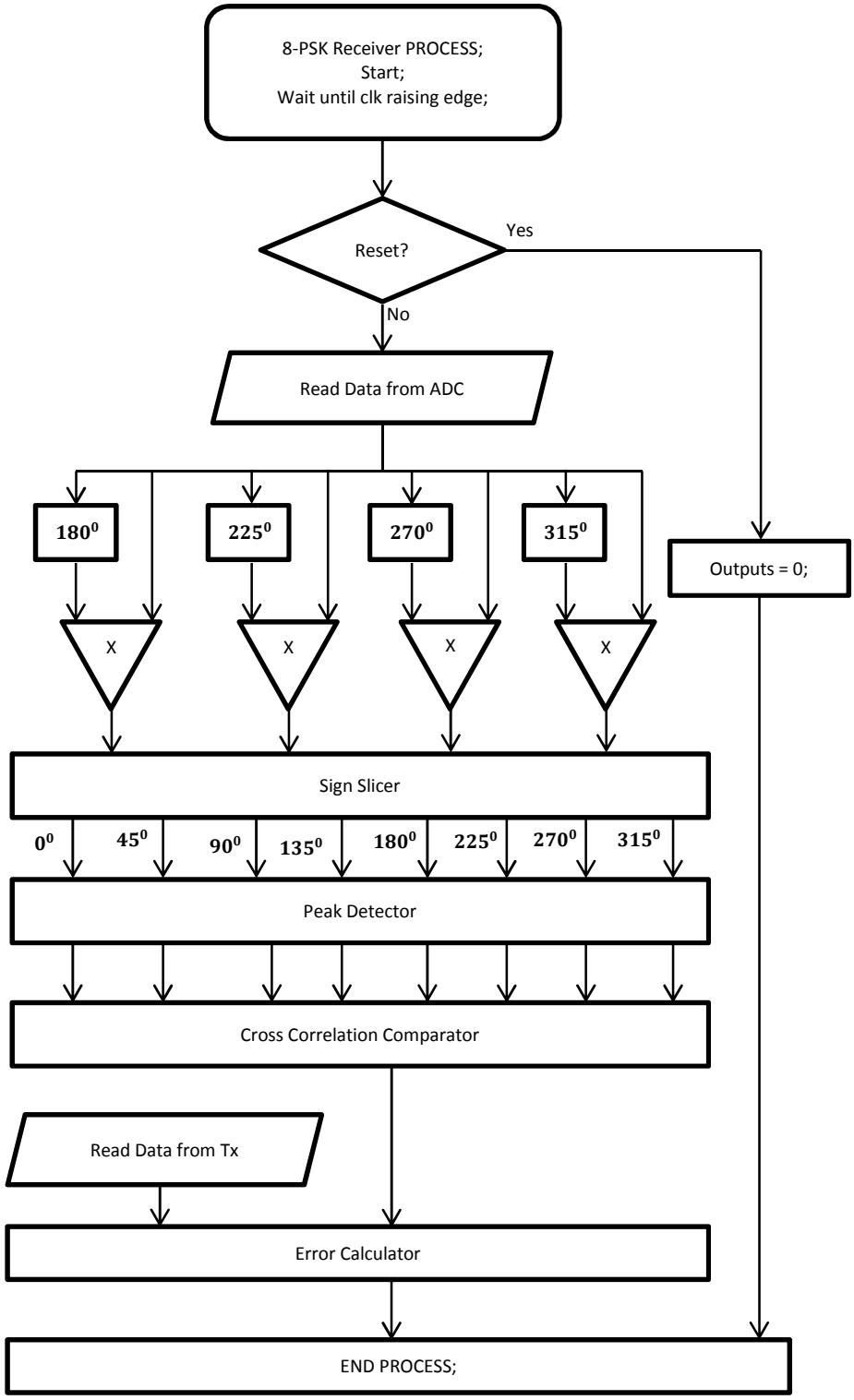

Fig. 9. 8-PSK receiver test rig using cross correlation

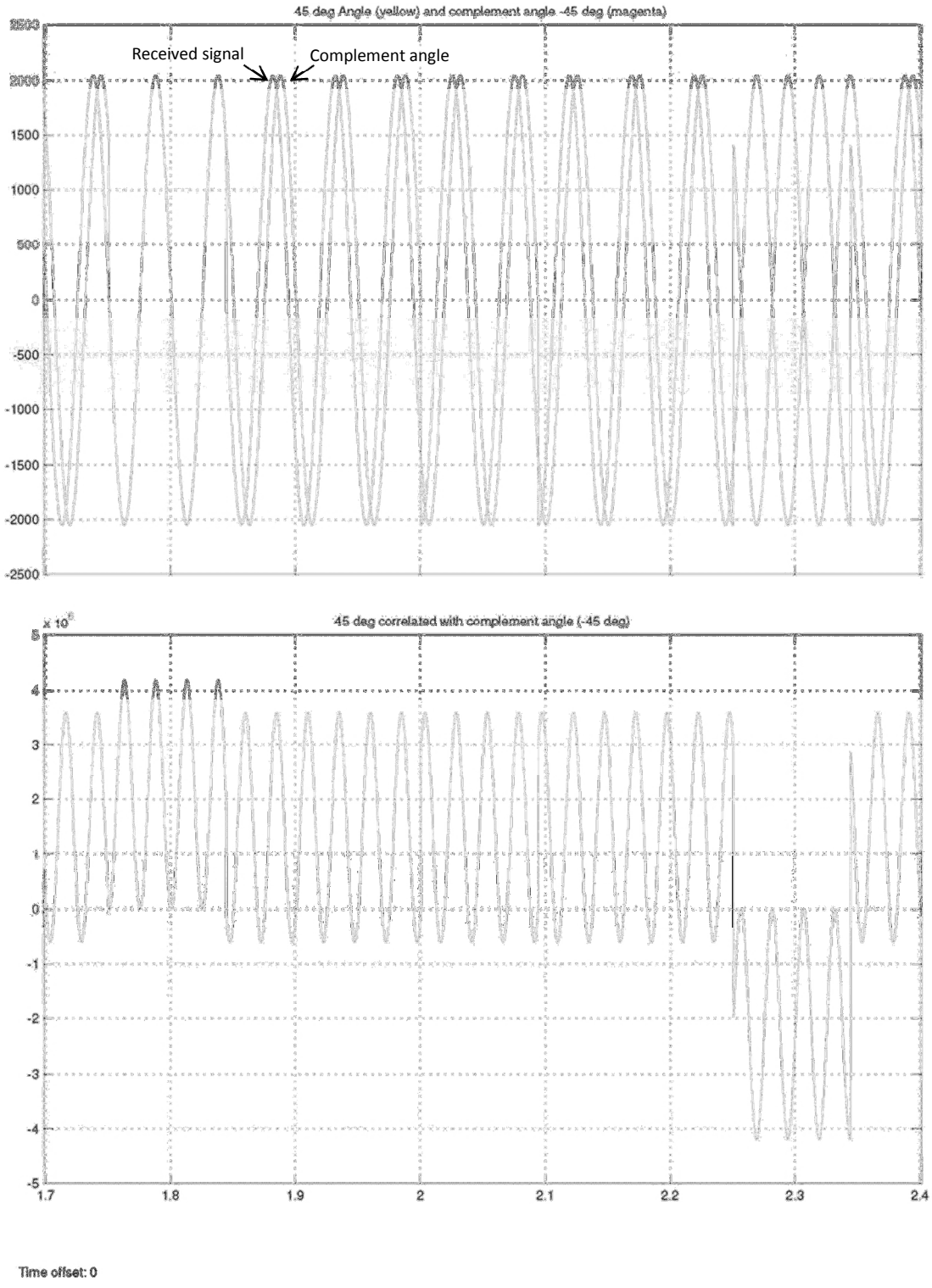

Fig. 10. The input (complement angle-magenta) and output of the 45^{o} angle detector

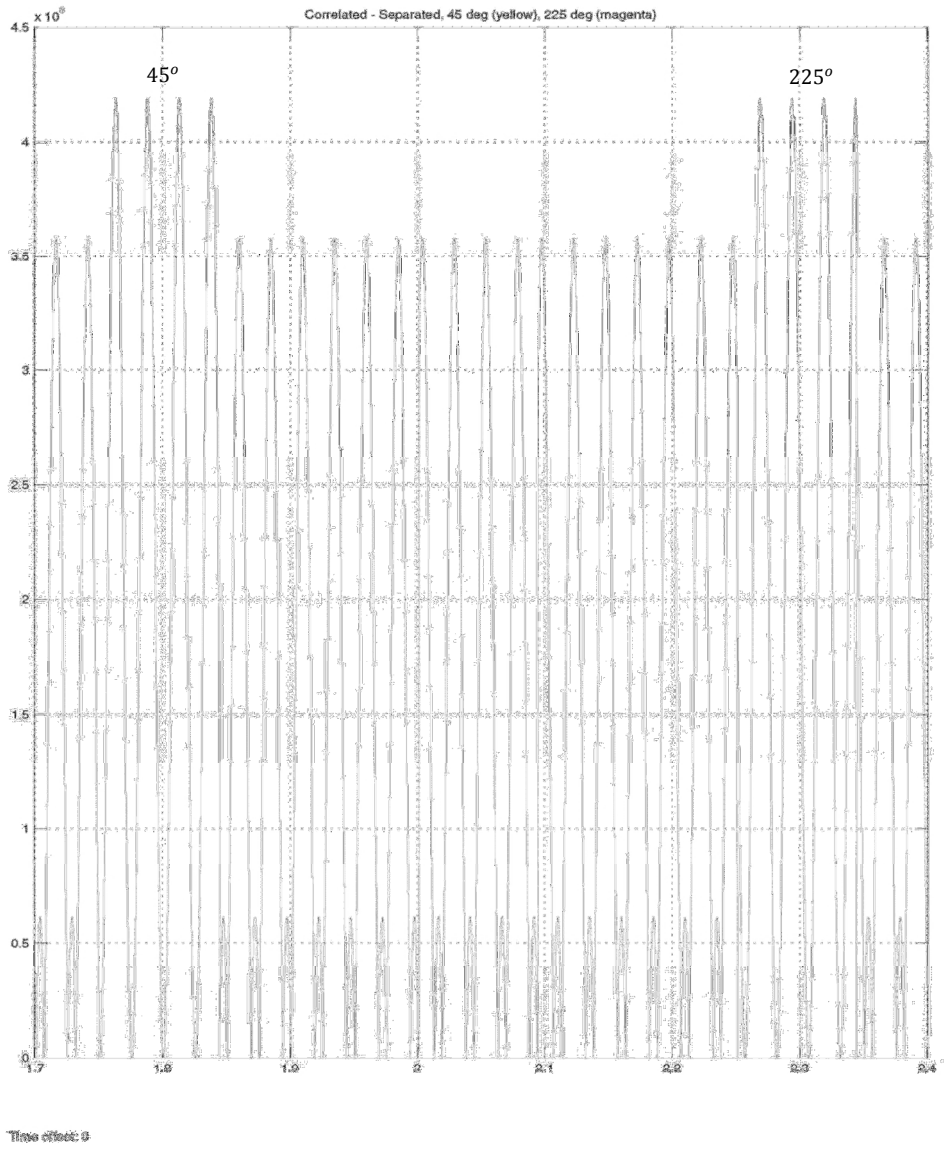

Fig. 11. Cross correlated signals are separated; 45^{o} and 225^{o}

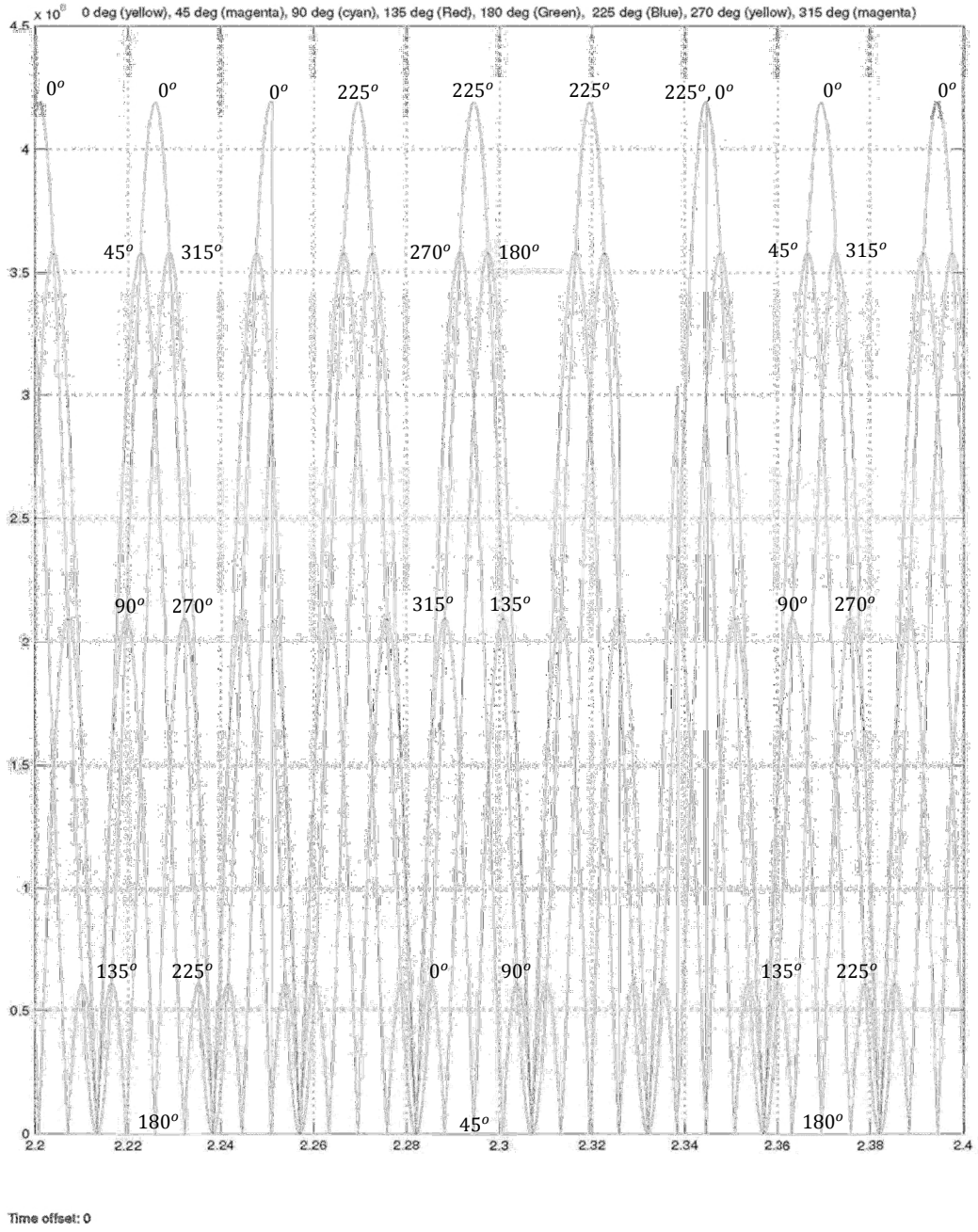

Fig. 12. Correlated - Separated, 0º, 45º, 90º, 135º, 180º, 225º, 270º, 315º

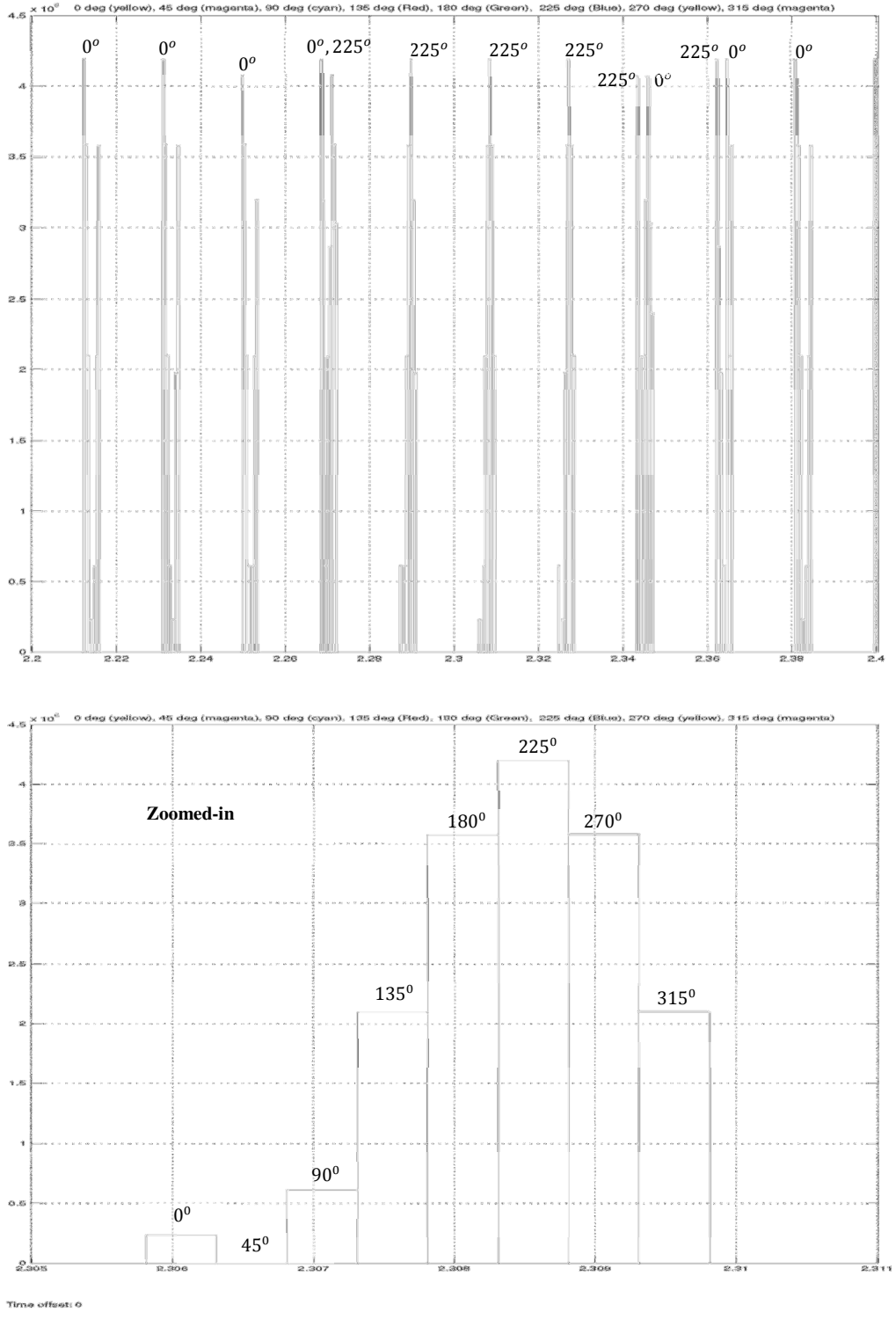

Fig. 13. Detected Peaks where 225° is dominant and 45° is the weakest

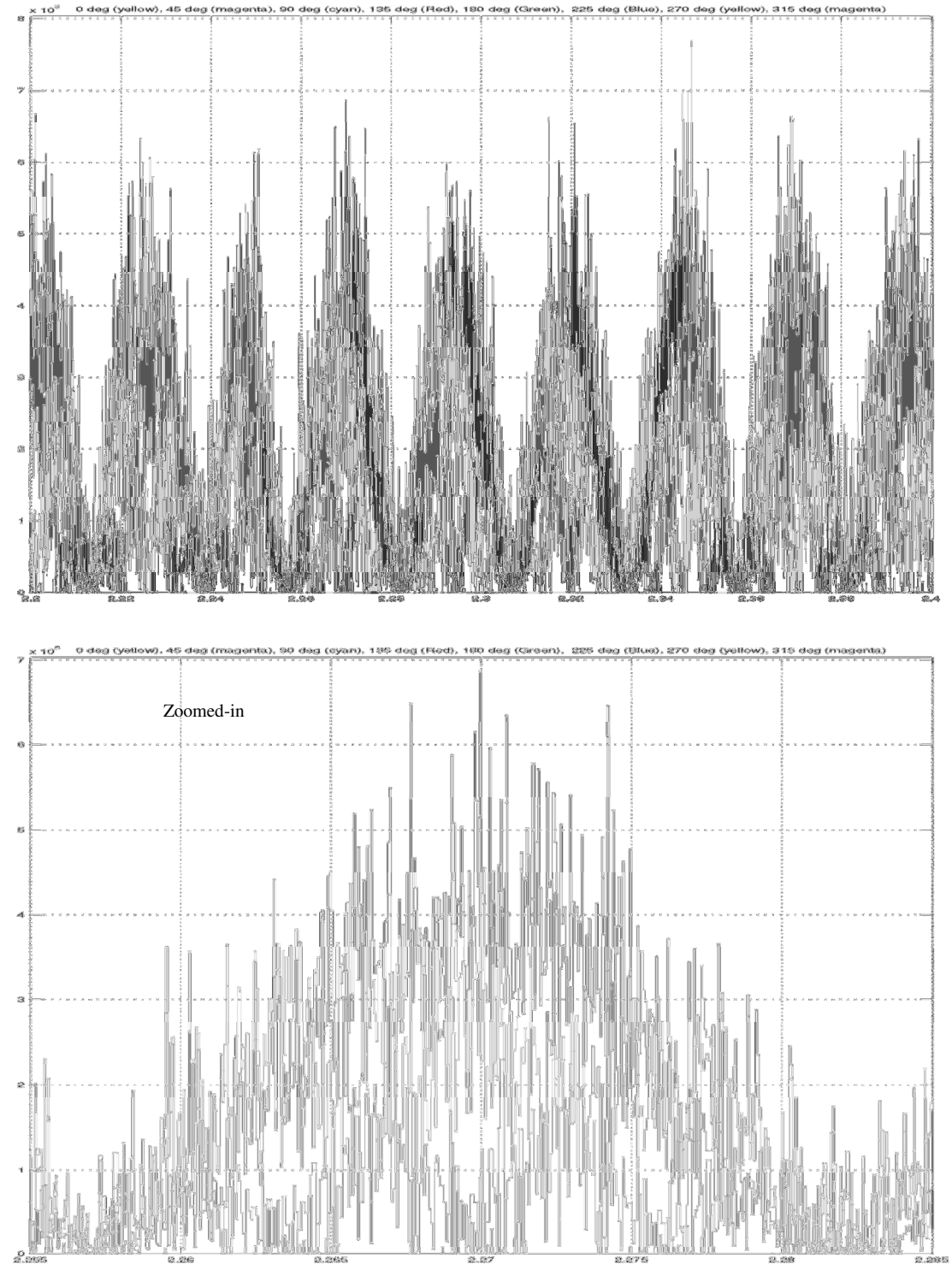

Fig. 14. Correlated-separated, all angles at the presence of AWGN

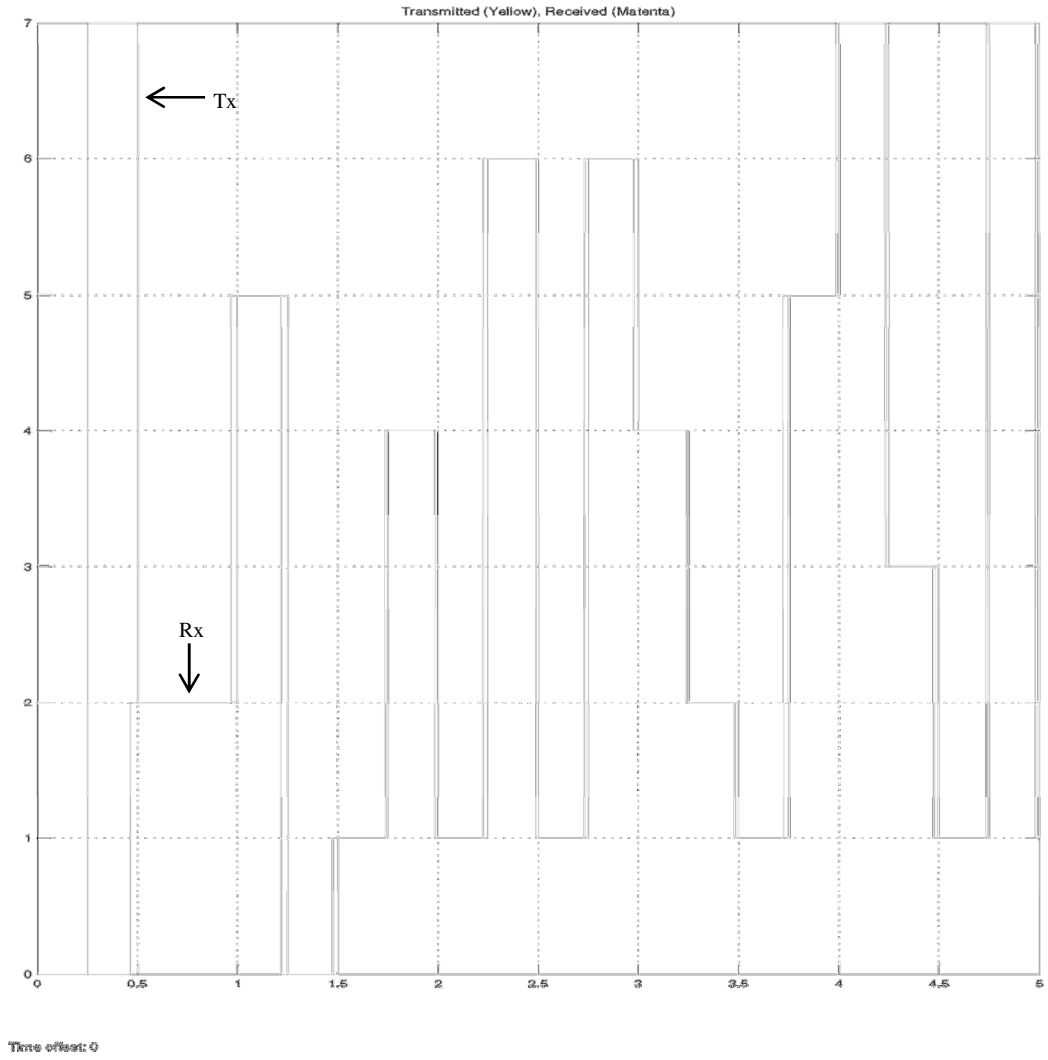

Fig. 15. Comparison of the transmitted and received data at 4 symbols/s

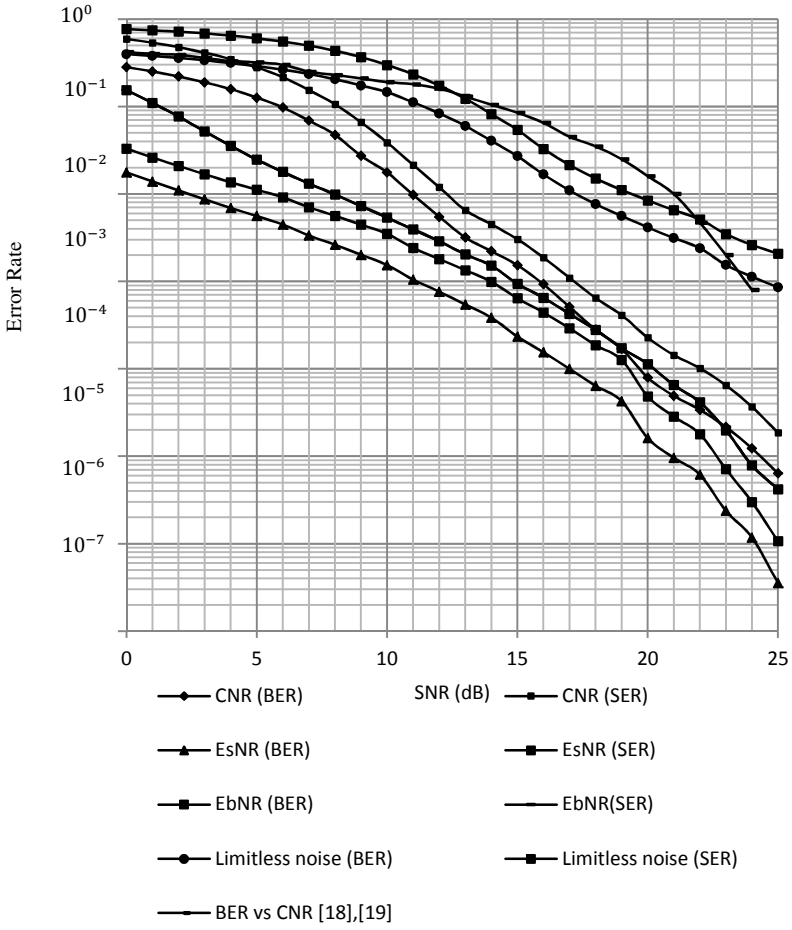

Fig. 16. Performance of 8-PSK using cross correlation versus Monte Carlo simulations

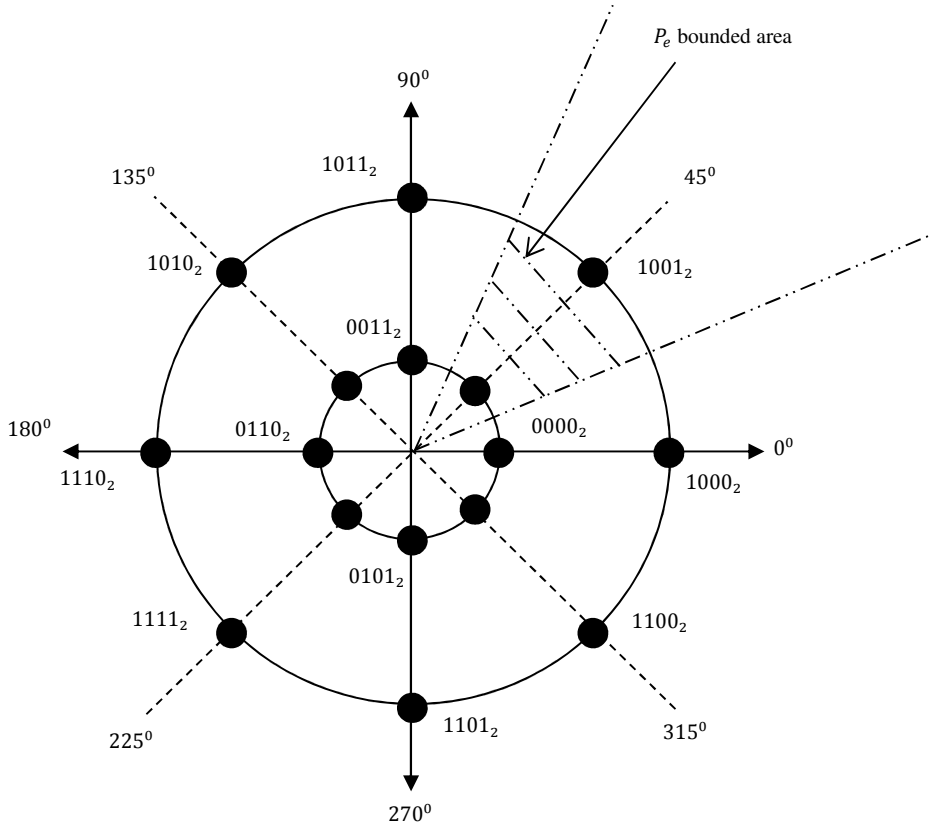

Fig. 17. Star 16-QAM Gray coding constellation

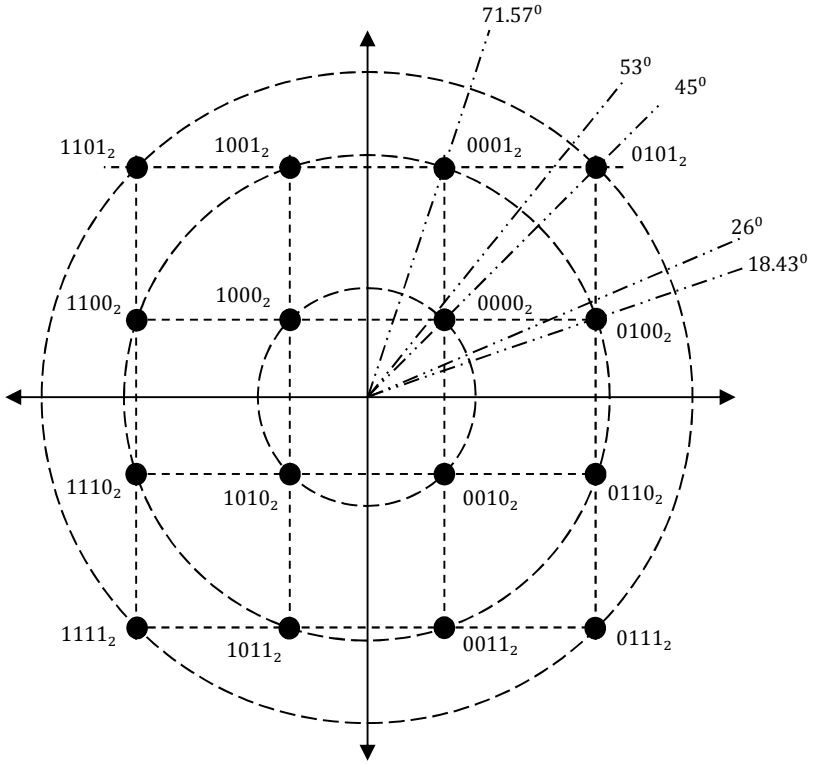

Fig. 18. Square 16-QAM Gray coding constellation

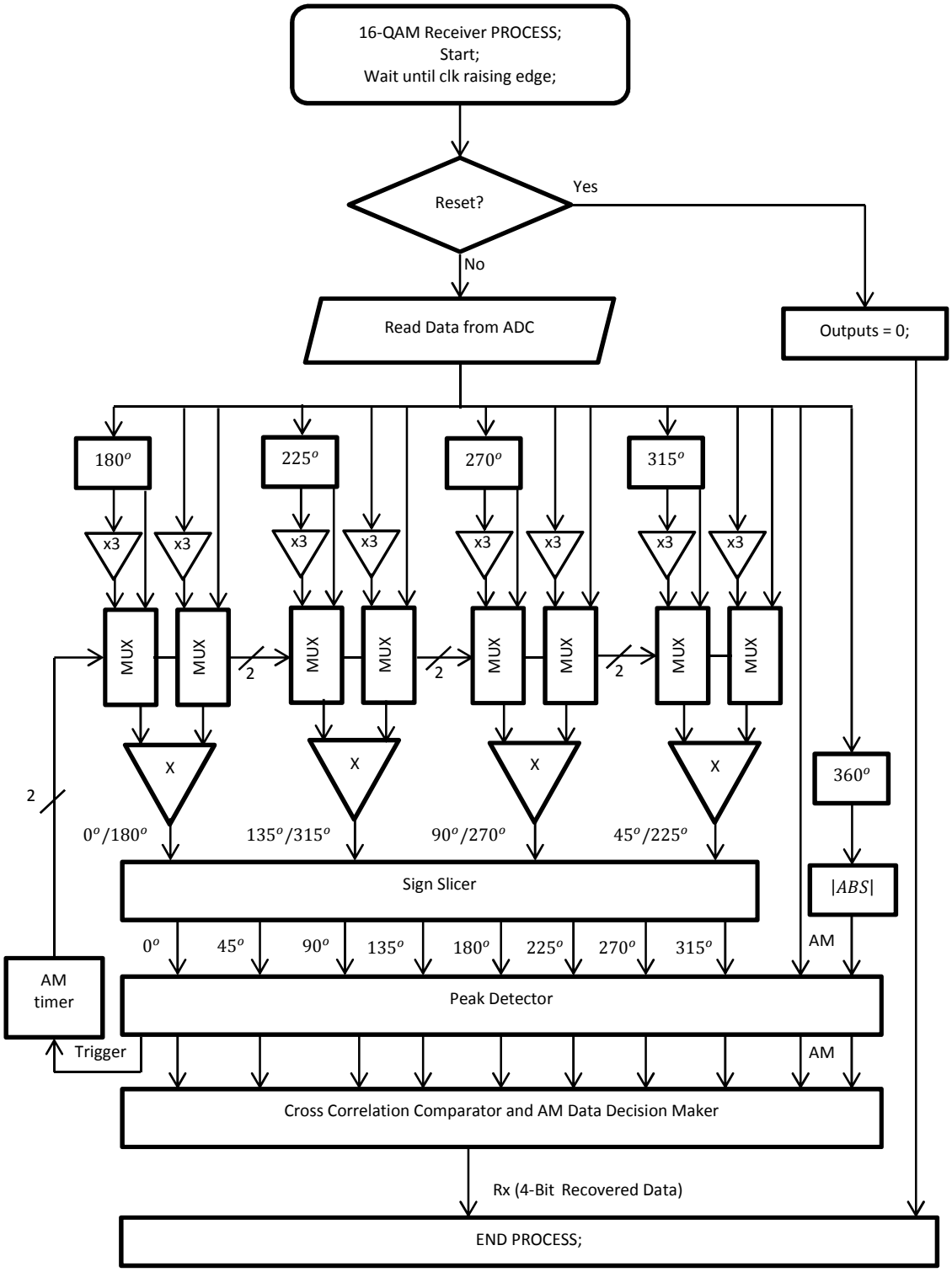

Fig. 19. 16-QAM receiver test rig using cross correlation

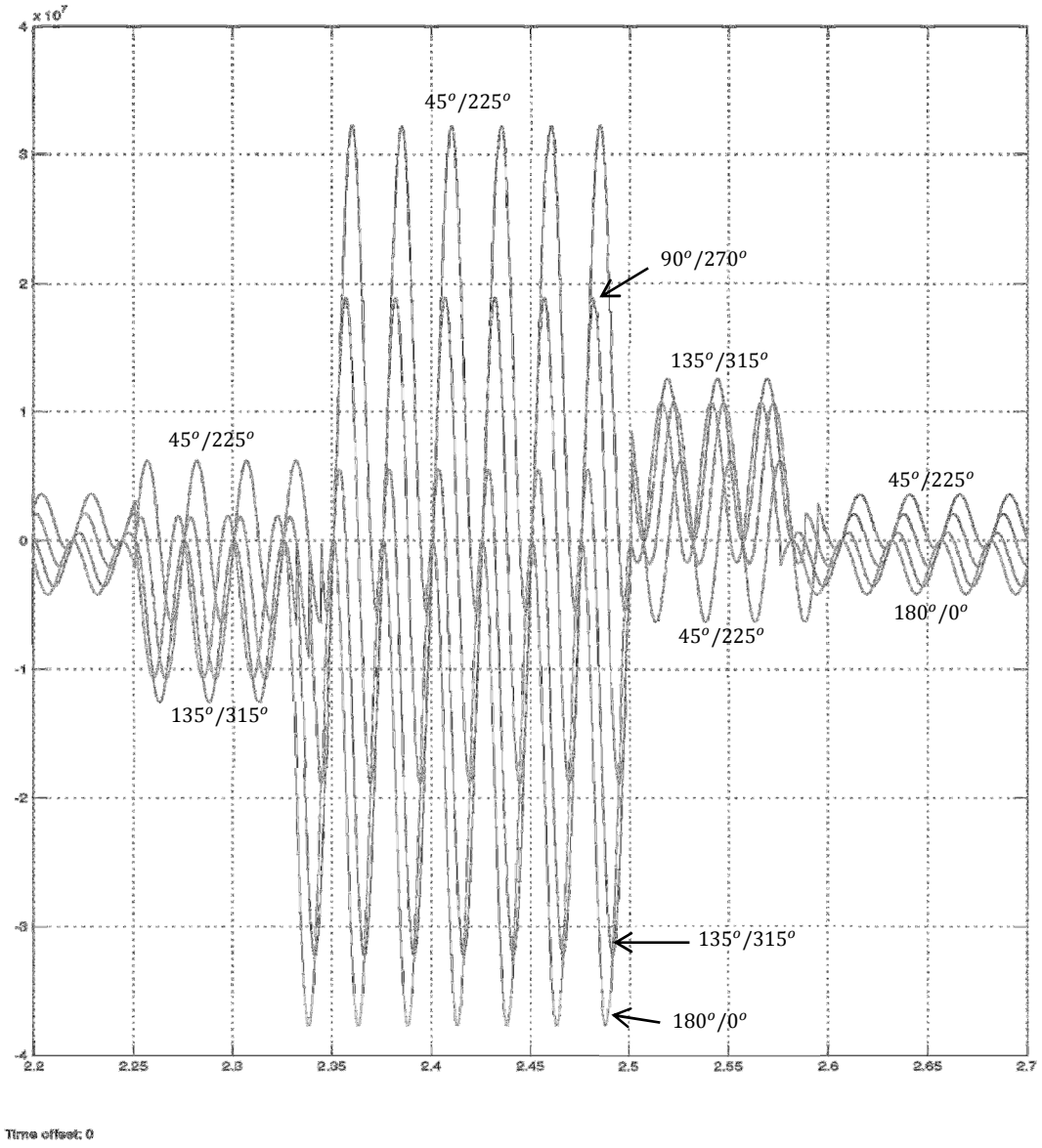

Fig. 20. 16-QAM correlators' outputs; $0^0/180^0$, $45^0/225^0$, $90^0/270^0$, $135^0/315^0$

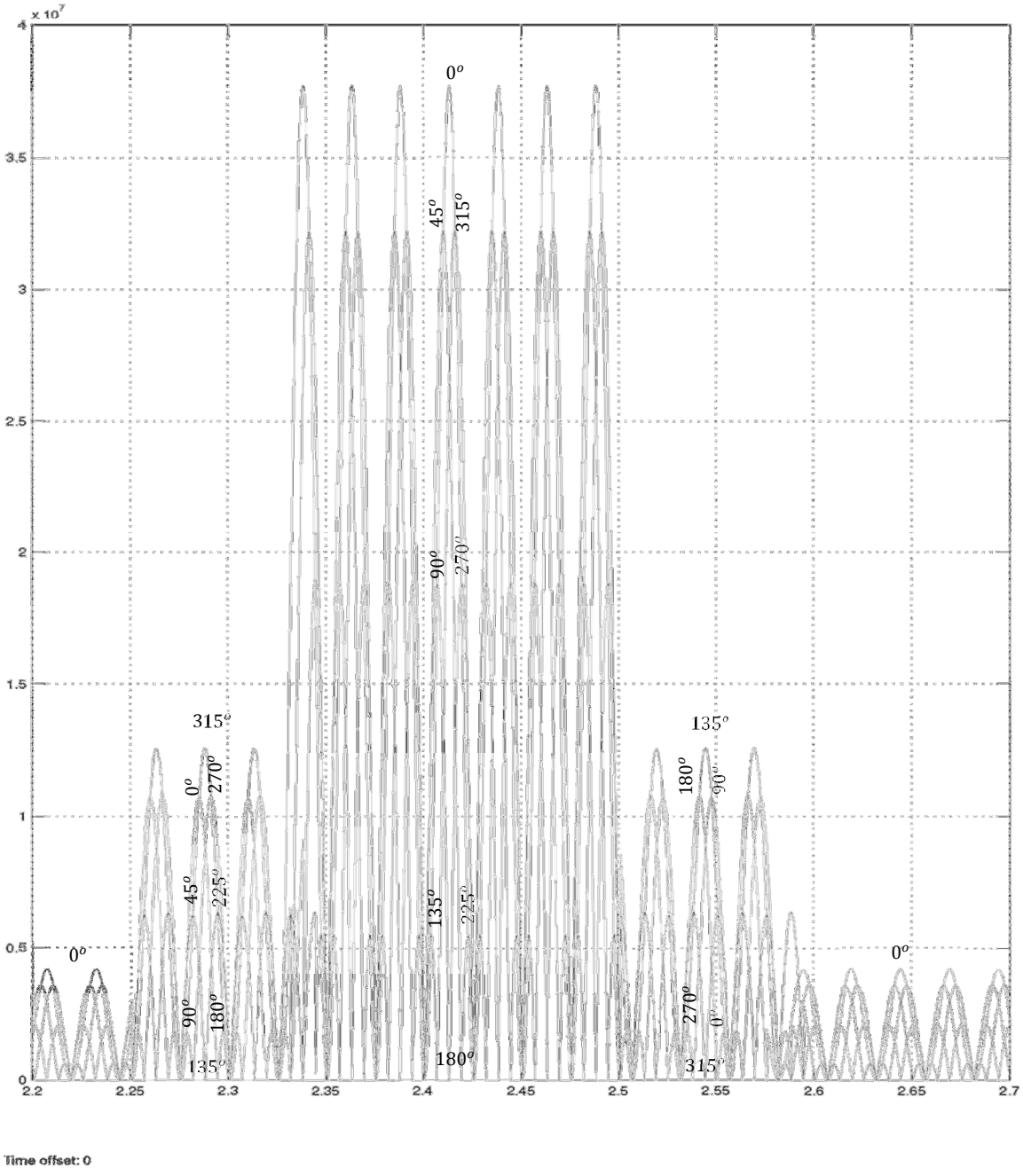

Fig. 21. Correlated - Separated, 0^o, 45^o, 90^o, 135^o, 180^o, 225^o, 270^o, 315^o

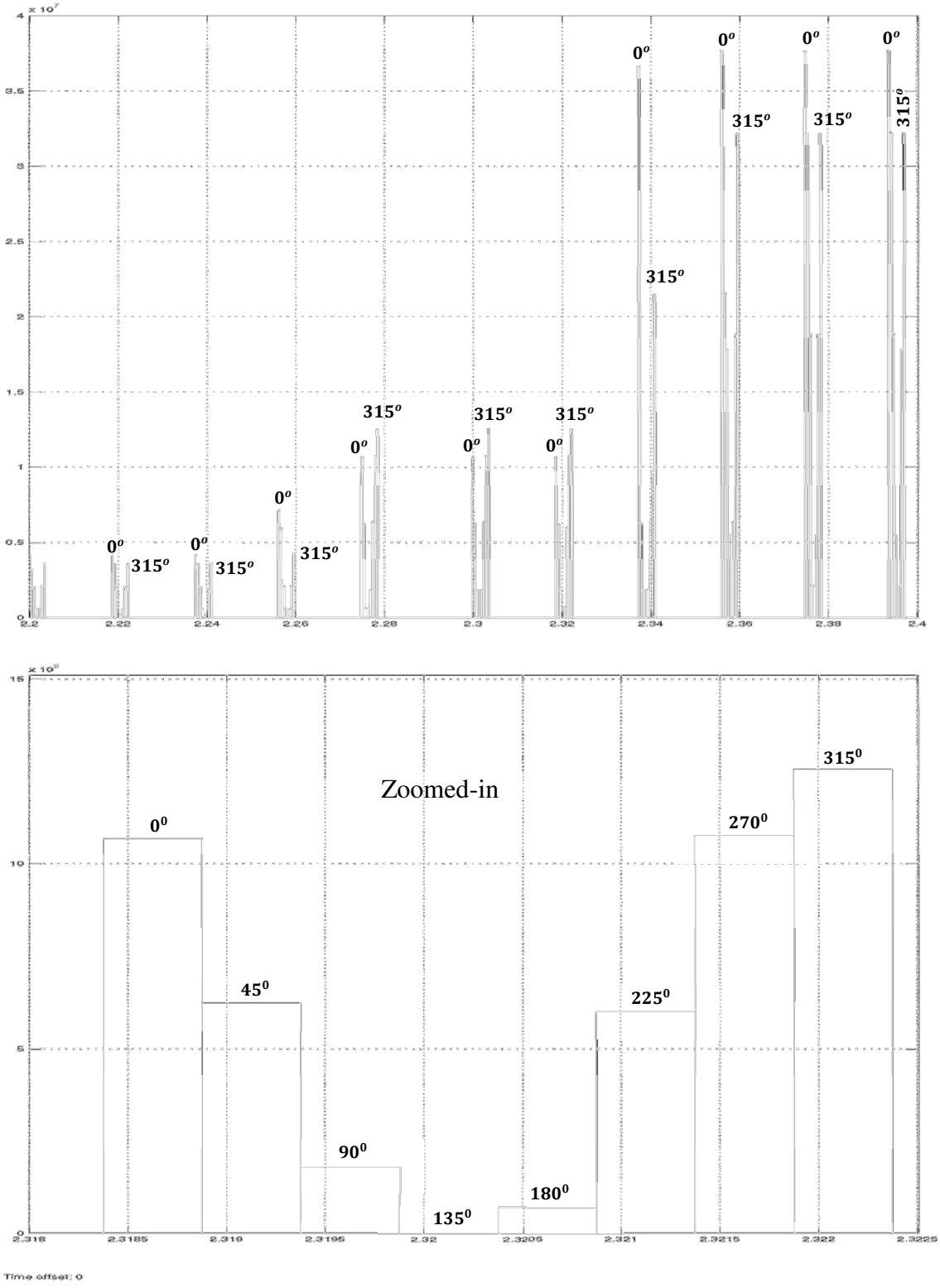

Fig. 22. Detected peaks, where 315^0 is dominant and 135^0 is the weakest

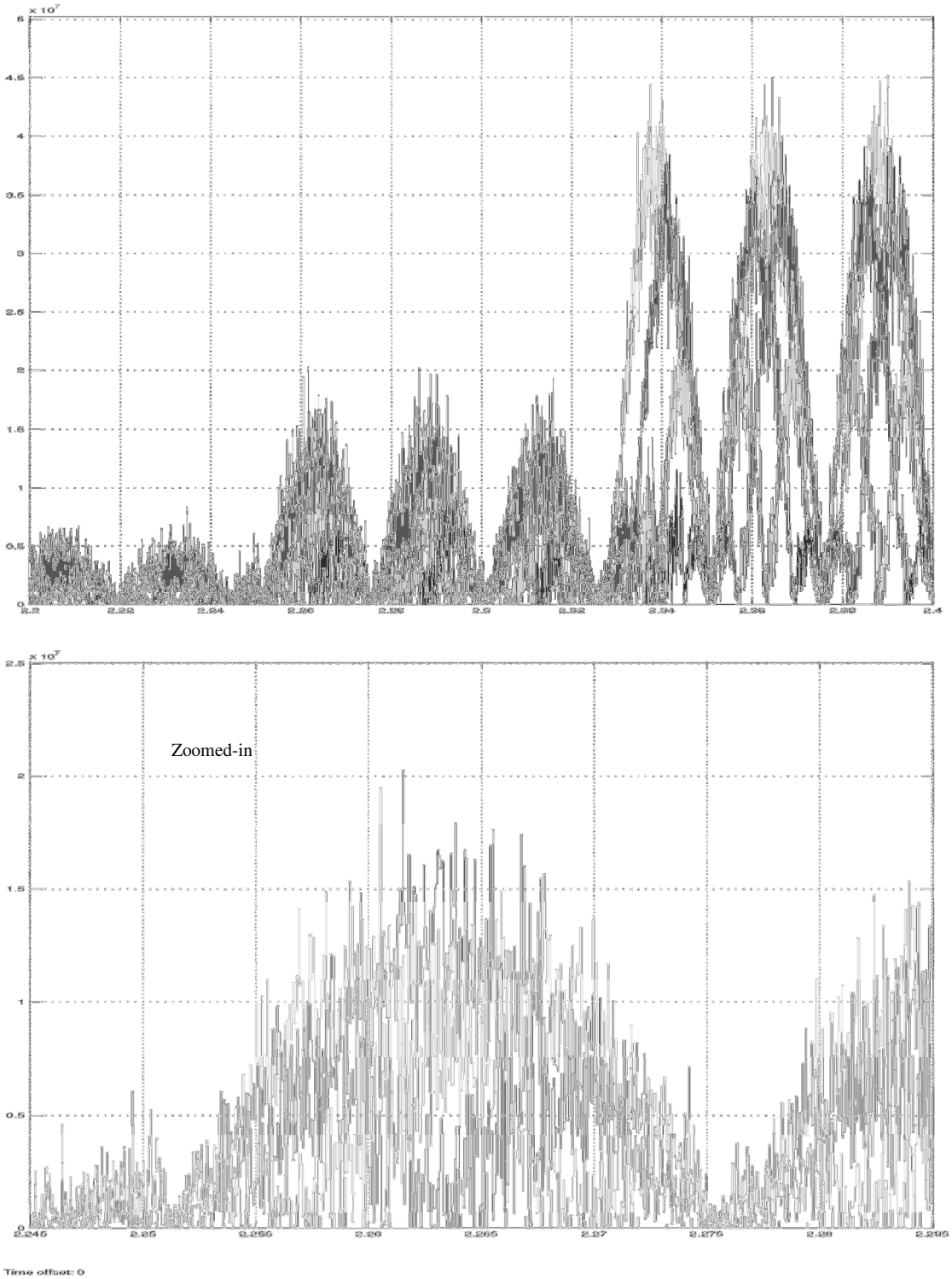

Fig. 23. 16-QAM Correlated - Separated, all angles in the presence of 15dB AWGN

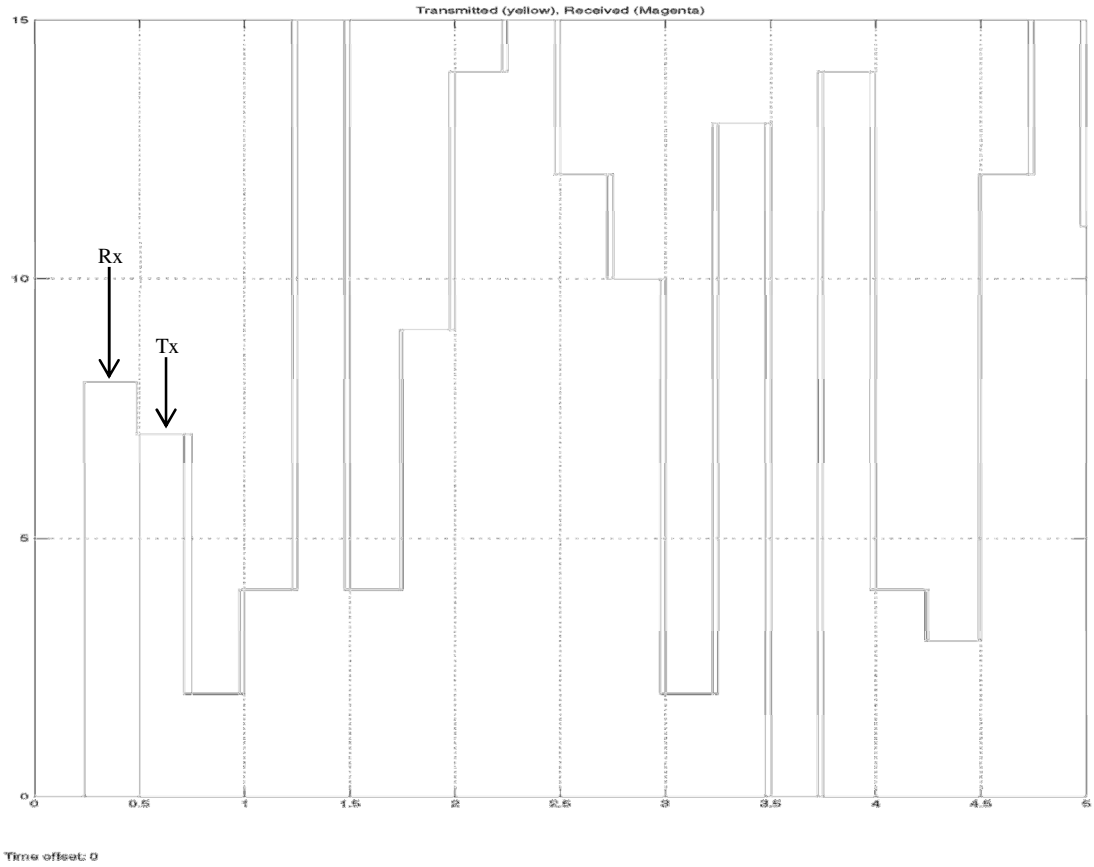

Fig. 24. Comparison of 16-QAM transmitted and received data over 5 s

Demodulation of PSK signals using cross-correlation techniques

A. Alaiwi, M.J.N. Sibley and P. J. Mather (Department of Engineering and Technology, University of Huddersfield, Queensgate, Huddersfield, HD1 3DH, UK)

E-mail: ayman.alaiwi@hud.ac.uk, m.j.n.sibley@hud.ac.uk, p.j.mather@hud.ac.uk

Abstract—Phase shift keying (PSK) is considered to be one of the highly efficient modulation schemes in terms of wireless communication system noise immunity. Demodulation of PSK signals generally requires the use of an 'atan' operator and carrier recovery using a Phase Locked Loop (PLL). As will be shown in this paper, such a demodulation scheme is highly complex and susceptible to noise.

In this paper we propose a novel demodulation technique for PSK signals. Instead of using the atan function, the new technique presented here uses the cross-correlation method to demodulate the signals. As will be shown, this novel method of demodulation results in a considerable reduction in circuit complexity and hence less use of available silicon.

Index terms - atan, BER, carrier recovery, Costas loop, cross correlation, DSP, FPGA, PLL, PSK, VHDL.

I. INTRODUCTION

Fig. 1 shows a Phase Shift Keying (PSK) signal with 8 possible positions - 8-PSK. It is a popular form of digital modulation because M-PSK has a much higher spectral efficiency than conventional Intensity Modulation (IM) by a factor $\mathbf{log_2}(\boldsymbol{M})$. Thus the bandwidth of 8-PSK is three times narrower than standard intensity modulation [1] which makes PSK modulation formats particularly useful in bandwidth limited channels. In addition, PSK has been often used for digital modulation of satellite link because of its good noise resistance [2].

Several different forms of PSK are used in the IEEE 802.11b-1999 standard [3] with Differential PSK (DPSK) being used at low data rates and Quadrature PSK (QPSK) being used at 11 Mb/s. The IEEE 802.11g-2003 standard [3] uses Binary PSK (BPSK) and QPSK at faster transmission speeds. BPSK is also used in the IEEE 802.15.4, or ZigBee, standard. Applications of these standards include Wide-band Code Division Multiple Access (WCDMA), High-Speed Downlink Packet Access (HSDPA), World-wide Inter-operability for Microwave Access (WiMAX) and Wireless Local Area Network (WLAN) broadband wireless access technologies. The HDSPA is part of the 3rd Generation Partnership Project (3GPP) WCDMA [3].

Demodulation of phase data is generally performed using a carrier, which is recovered from the received signal, to determine the phase difference between the original and recovered carrier. A complication is that the exact phase and frequency of the carrier have to be recovered to track the abrupt changes of phase caused by data changes. This makes the receiver sensitive to noise and changes in the signal [1].

This paper is presented as follows: the rest of this section presents various demodulation techniques and methods of carrier recovery as well as presenting the novel method of demodulating M-PSK; section II presents the mathematics of carrier recovery and derives the performance of the proposed technique; section III presents the implementation of the proposed technique and performance results; section IV analyses and discusses the proposed system and results compared to the prior works; and section V summaries the findings and comes up with possible applications.

A. COSTAS LOOP

The phase detector used in receivers for phase modulated signals must produce a signal proportional to the phase difference between the received signal and the recovered carrier [4]-[12]. One way of recovering the carrier is to use a Costas loop [4], [6], [10], [11] as shown in fig. 2. The outputs of the Low Pass Filters (LPFs) are proportional to the cosine and sine of the phase difference, ϕ. When the two output terms are multiplied together, the result deviates the Voltage Controlled Oscillator (VCO) operating at the carrier frequency ($\boldsymbol{\omega_c}$) until the VCO and received frequency are matched and locked. There are some practical problems associated with the Costas loop: a long acquisition time; possibility of a false lock; a $\mathbf{180^0}$ phase ambiguity due to the squaring loop; preamble sequence to aid carrier recovery [2], [13], [14].

B. M-PSK DEMODULATION USING MATCHED FILTERS

Fig. 3 shows an M-PSK coherent detector consisting of $\mathbf{2^M}$ matched filters or correlators. Each correlator is responsible for an angle where it correlates the received signal $\boldsymbol{S_i}$ $(\boldsymbol{t})$ with a delayed complement phase ($\boldsymbol{\theta_r}$) of that angle($\boldsymbol{\theta_t}$). Decisions about the received data, $\boldsymbol{Rx}$ $(\boldsymbol{t})$, are made by finding the largest magnitude over the symbol period ($\boldsymbol{T_s}$). Since two pairs of the transmitted angles are opposite each other, as shown in fig. 1, the number of correlators can be reduced to $\mathbf{2^{M-1}}$ as shown in fig. 3 where 8-PSK has been used as an example.

C. COMPLEX NUMBER DEMODULATOR

Phase ($\boldsymbol{\theta_t}$) data can be demodulated using the complex number approach [8], [16]. The delayed sample undergoes a complex conjugate conversion $\overline{\boldsymbol{Z_{n-1}}}$ and is then multiplied by the received signal $\boldsymbol{Z_n}$ [8], [16]. Fig. 4 shows an 8-PSK demodulator using the technique.

The advantage of this technique is that a simple multiplication function is required. However it requires Real-Imaginary to Complex conversion which needs to be performed using a high specification processor. The sampling frequency has to be a multiple of the *M* carrier frequency to slice the phase angles equally. In addition, the output of the mixer needs to be interpreted through a complex phase slicer circuitry before outputting the received data. This phase slicer needs continual calibration depending on the peak-to-peak amplitude of the received signal.

D. ATAN DEMODULATOR

An alternative PSK demodulation technique is to measure the angle between the baseband signal complex envelope and the nearest constellation point using an *ATAN* computation [6], [8], [11]. The *ATAN* approach is an advanced version of the Costas loop, using a digital PLL in parallel with the *ATAN* [6], [11] function as shown in fig. 5. This technique replaces the matched filters of fig. 3. The *ATAN* function is implemented using a Look-Up Table (LUT) and the whole can be implemented using Field Programmable Gate Arrays (FPGAs) with Digital Signal Processing (DSP) capabilities [6], [11]. This technique is very useful for higher M-PSK and M-QAM orders as it can be used to reduce the number of implementation resources required to implement $\mathbf{2^{M-1}}$ matched filters.

This technique is similar to the complex number approach in that the output of the *ATAN* function needs to be interpreted through an LUT phase slicer before outputting the received data. The digital PLL uses a Numerically Controlled Oscillator (NCO) which experiences jitter noise when narrowband noise is added to the received signal. This causes the received constellation to rotate [16]. The noise can be minimised by using high accuracy *ATAN* computation but a high level of FPGA resources are required to perform such an operation.

E. PROPOSED ALTERNATIVE SOLUTION

A new approach to the demodulation of phase data of a M-PSK signal using cross-correlation has been developed. As discussed, current technology generally incorporates a complex *ATAN* function to detect the phase changes of a phase modulated signal. This requires carrier signal recovery circuitry and LUTs to distinguish phase levels and changes in the received signals. However, the dynamic gain at the phase detector inputs has to be linked to an Automatic Gain Control (AGC) circuit to compensate the changes or otherwise the NCO/VCO characteristics will change accordingly [15]. Consequently, large memory blocks are required to perform the demodulation processes which requires complex and large circuits. By contrast, the cross-correlation technique, described here, does not require carrier recovery circuitry or LUTs to detect the phase changes.

Fig. 6 shows a block diagram of the technique as applied to the detection of 8-PSK. Four detectors are used to detect 8 separate phase angles and a timer is used to update and compare the cross-correlated angles every half cycle of the carrier. The cross correlated signals are separated into 2 parts and then the absolute value of both parts are obtained, with the highest absolute value identifying the received data phase angle. The absolute values of separated signals are then recorded and updated every half carrier cycles through the peak detector.

When compared to conventional schemes such as the Costas loop, the proposed scheme is very simple and requires less hardware for the realization. Also, as the scheme does not extract the carrier for demodulation purposes, this new method is more tolerant of noise. The proposed cross-correlation technique optimises the number of implementation resources required to demodulate the PSK data, compared to the other techniques discussed, by omitting the carrier recovery circuitry, filters and LUTs to slice the phase data.

II. MATHEMATICAL DERIVATION AND PERFORMANCE

A. PERFORMANCE OF CARRIER RECOVERY

The performance of the coherent carrier recovery can be tested by introducing narrowband noise $\boldsymbol{n_{nb}(t)}$ on the received data as shown in fig. 7. The added noise deviates the phase of the transmitted angle by $\boldsymbol{\Delta\theta_t}$. Consequently, the recovered carrier phase suffers from the jitter noise $\boldsymbol{\Delta\theta_r}$ of the VCO.

So, the correlated signal,

$$\boldsymbol{S_o(t) = [A\ cos(\omega_c t + \theta_t + \Delta\theta_t) + n_{nb}(t)][cos(\omega_c t - \theta_r + \Delta\theta_r)]} \quad (1)$$

Expanding (1) using the quadrature components of $\boldsymbol{n_{nb}(t)}$:

$$\boldsymbol{S_o(t) = \begin{bmatrix} A\ \cos(\omega_c t + \theta_t + \Delta\theta_t) + x(t)\cos(\omega_c t + \theta_t + \Delta\theta_t) \\ -y(t)\sin(\omega_c t + \theta_t + \Delta\theta_t) \end{bmatrix} \times [\cos(\omega_c t - \theta_r + \Delta\theta_r)]}$$

$$\boldsymbol{= [A + x(t)]\cos(\omega_c t + \theta_t + \Delta\theta_t)\ \cos(\omega_c t - \theta_r + \Delta\theta_r)}$$

$$\boldsymbol{- y(t)\sin(\omega_c t + \theta_t + \Delta\theta_t)\ \cos(\omega_c t - \theta_r + \Delta\theta_r)}$$

$$\boldsymbol{S_o(t) = \frac{[A + x(t)]}{2}[\cos(2\omega_c t + \theta_t - \theta_r + \Delta\theta_t + \Delta\theta_r) + \cos(\theta_t + \theta_r + \Delta\theta_t - \Delta\theta_r)]}$$

$$-\frac{\boldsymbol{y(t)}}{\mathbf{2}}[\mathbf{sin}(\mathbf{2}\boldsymbol{\omega_c t}+\boldsymbol{\theta_t}-\boldsymbol{\theta_r}+\Delta\boldsymbol{\theta_t}+\Delta\boldsymbol{\theta_r})+\mathbf{sin}(\boldsymbol{\theta_t}+\boldsymbol{\theta_r}+\Delta\boldsymbol{\theta_t}-\Delta\boldsymbol{\theta_r})]$$

Thus, the output $\boldsymbol{g(t)}$ of the matched filter,

$$\boldsymbol{g(t)}=\frac{[\boldsymbol{A}+\boldsymbol{x(t)}]}{\mathbf{2}}\ \boldsymbol{cos}(\boldsymbol{\theta_t}+\boldsymbol{\theta_r}+\Delta\boldsymbol{\theta_t}-\Delta\boldsymbol{\theta_r})-\frac{\boldsymbol{y(t)}}{\mathbf{2}}\boldsymbol{sin}(\boldsymbol{\theta_t}+\boldsymbol{\theta_r}+\Delta\boldsymbol{\theta_t}-\Delta\boldsymbol{\theta_r}) \quad (2)$$

Equation 2 shows the output of the matched filter with the added noise. Clearly, the noise deviates the recovered carrier, which rotates the constellation points as discussed in section I D, thus making it more likely that the VCO will lock onto a false quadrant phase. Consequently, the decision maker of the demodulator could mistake the detected angle and hence make an error in decoding the received data.

B. PERFORMANCE OF THE PROPOSED TECHNIQUE

The performance of the cross-correlation approach can be derived by adding narrowband noise $\boldsymbol{n_{nb}(t)}$ and its delayed version $\boldsymbol{n_{nb}(t-T_c)}$ to the signal as shown in fig. 8 when a continuous sinusoidal signal is received. The added noise deviates the phase of the transmitted angle by $\Delta\boldsymbol{\theta_t}$. Consequently the complement angle $(-\boldsymbol{\theta_r})$ of the cross correlation suffers from the jitter noise $\Delta\boldsymbol{\theta_r}$ caused by the delayed version of $\Delta\boldsymbol{\theta_t}$.

So, the correlated signal,

$$\boldsymbol{S_o(t)}=[\boldsymbol{A}\ \mathbf{cos}(\boldsymbol{\omega_c t}+\boldsymbol{\theta_t}+\Delta\boldsymbol{\theta_t})+\boldsymbol{n_{nb}(t)}][\boldsymbol{A}\ \mathbf{cos}(\boldsymbol{\omega_c t}-\boldsymbol{\theta_r}+\Delta\boldsymbol{\theta_r})+\boldsymbol{n_{nb}(t-T_c)}] \quad (3)$$

Expanding (3) using the quadrature components of the noise, $\boldsymbol{n_{nb}(t)}$:

$$\boldsymbol{S_o(t)}=\begin{bmatrix}\boldsymbol{A}\ \boldsymbol{cos}(\boldsymbol{\omega_c t}+\boldsymbol{\theta_t}+\Delta\boldsymbol{\theta_t})+\ \boldsymbol{x(t)}\,\boldsymbol{cos}(\boldsymbol{\omega_c t}+\boldsymbol{\theta_t}+\Delta\boldsymbol{\theta_t}) \\ -\boldsymbol{y(t)}\,\boldsymbol{sin}(\boldsymbol{\omega_c t}+\boldsymbol{\theta_t}+\Delta\boldsymbol{\theta_t})\end{bmatrix}$$

$$\times\begin{bmatrix}\boldsymbol{A}\ \boldsymbol{cos}(\boldsymbol{\omega_c t}-\boldsymbol{\theta_r}+\Delta\boldsymbol{\theta_r})+\ \boldsymbol{x(t-T_c)}\,\boldsymbol{cos}(\boldsymbol{\omega_c t}-\boldsymbol{\theta_r}+\Delta\boldsymbol{\theta_r}) \\ -\boldsymbol{y(t-T_c)}\,\boldsymbol{sin}(\boldsymbol{\omega_c t}-\boldsymbol{\theta_r}+\Delta\boldsymbol{\theta_r})\end{bmatrix}$$

$$=[\boldsymbol{A}+\boldsymbol{x(t)}][\boldsymbol{A}+\boldsymbol{x(t-T_c)}]\,\boldsymbol{cos}(\boldsymbol{\omega_c t}+\boldsymbol{\theta_t}+\Delta\boldsymbol{\theta_t})\ \boldsymbol{cos}(\boldsymbol{\omega_c t}-\boldsymbol{\theta_r}+\Delta\boldsymbol{\theta_r})$$

$$-[\boldsymbol{A}+\boldsymbol{x(t)}]\,\boldsymbol{y(t-T_c)}\ \boldsymbol{cos}(\boldsymbol{\omega_c t}+\boldsymbol{\theta_t}+\Delta\boldsymbol{\theta_t})\ \boldsymbol{sin}(\boldsymbol{\omega_c t}-\boldsymbol{\theta_r}+\Delta\boldsymbol{\theta_r})$$

$$-\boldsymbol{y(t)}[\boldsymbol{A}+\boldsymbol{x(t-T_c)}]\,\boldsymbol{sin}(\boldsymbol{\omega_c t}+\boldsymbol{\theta_t}+\Delta\boldsymbol{\theta_t})\ \boldsymbol{cos}(\boldsymbol{\omega_c t}-\boldsymbol{\theta_r}+\Delta\boldsymbol{\theta_r})$$

$$+\boldsymbol{y(t)y(t-T_c)}\,\boldsymbol{sin}(\boldsymbol{\omega_c t}+\boldsymbol{\theta_t}+\Delta\boldsymbol{\theta_t})\ \boldsymbol{sin}(\boldsymbol{\omega_c t}-\boldsymbol{\theta_r}+\Delta\boldsymbol{\theta_r})$$

The $\Delta\boldsymbol{\theta_r}$ is a delayed version of a random phase noise $\Delta\boldsymbol{\theta_t}$, which is minimised by the pre-filtering unit. The remaining noise affects the carrier amplitude at frequencies higher than those that make fake quadrant lock in carrier recovery systems. The $\Delta\boldsymbol{\theta_r}$ is cancelled with $\Delta\boldsymbol{\theta_t}$ when cross-correlated using the proposed approach. So,

$$\boldsymbol{S_o(t)} = \frac{[A+x(t)][A+x(t-T_c)]}{2}[\boldsymbol{cos}(2\omega_c t + \theta_t - \theta_r + 2\Delta\theta_t) + \boldsymbol{cos}(\theta_t + \theta_r)]$$
$$- \frac{[A+x(t)]\, y(t-T_c)}{2}[\boldsymbol{sin}(2\omega_c t + \theta_t - \theta_r + 2\Delta\theta_t) - \boldsymbol{sin}(\theta_t + \theta_r)]$$
$$- \frac{y(t)\,[A+x(t-T_c)]}{2}[\boldsymbol{sin}(2\omega_c t + \theta_t - \theta_r + 2\Delta\theta_t) + \boldsymbol{sin}(\theta_t + \theta_r)]$$
$$+ \frac{y(t)\, y(t-T_c)}{2}[\boldsymbol{cos}(\theta_t + \theta_r) - \boldsymbol{cos}(2\omega_c t + \theta_t - \theta_r + 2\Delta\theta_t)]$$

Thus,

$$\boldsymbol{g(t)} = \frac{[A+x(t)]\,[A+x(t-T_c)] + y(t)\, y(t-T_c)}{2}\boldsymbol{cos}(\theta_t + \theta_r) \quad (4)$$
$$+ \frac{[A+x(t)]y(t-T_c) - y(t)[A+x(t-T_c)]}{2}\boldsymbol{sin}(\theta_t + \theta_r)$$

When a symbol is phase $(\boldsymbol{\theta_t})$ transmitted, the complement angle at the receiver is $(-\boldsymbol{\theta_t})$,

$$\therefore\ \boldsymbol{g(t)} \approx \frac{[A+x(t)]\,[A+x(t-T_c)] + y(t)\, y(t-T_c)}{2} \quad (5)$$

Clearly, carrier recovery systems suffer from phase and amplitude noise as shown in (2) whereas the proposed approach suffers from amplitude noise only as shown in (5). The direct cross-correlation results in a guaranteed phase difference as shown by (4). The $\boldsymbol{x(t)}$, $\boldsymbol{x(t-T_c)}$, $\boldsymbol{y(t)}$ and $\boldsymbol{y(t-T_c)}$ amplitude noise in (4) deflect and rotate the constellation points away from the origin. However, an AGC and pre-filtering units keep the SNR at a reasonable level and the highest cross-correlated points within the bounded area of the detected angle shown in fig. 1 over the symbol period.

III. IMPLEMENTATION AND RESULTS

With reference to fig. 6, the receiver test rig is summarised in a flowchart shown in fig. 9. It was implemented using Altera Quartus II, Altera-DSP Builder and Matlab-Simulink. VHDL language was used to design the Sign Slicer, Peak Detector, Comparator and Error Calculator.

Fig. 10 shows the 8-PSK input (top) to $\mathbf{45^0/225^0}$ correlator where yellow and magenta traces show the received and complement angle respectively. Fig. 10 also shows the output (bottom) of the correlator. The positive part indicates the detected in-phase angle and the negative part indicates the detected $\mathbf{180^0}$ out of phase angle.

The Sign Slicer VHDL code slices the positive/negative output of the 4 correlators. The absolute value of the negative parts was taken as shown in fig. 11. That is how the angles are separated equally to 8 angles using 4 detectors.

Fig. 12 shows the cross-correlated signals of the 4 detectors where the absolute value of the negative parts were taken. The correlated signals result in twice the carrier frequency.

The Peak Detector VHDL code was used to observe the peaks of the cross correlated signal as shown in fig. 13. Note that, in fig. 13, the detected peaks were slightly delayed to better explain the concept. In practice there should be no delay for direct comparison of angles and data outputting.

Clearly, the output of the Peak Detector sliced the angles where the $\mathbf{0^0}$ angle is the reference to the received angles and the highest cross-correlated point in fig. 13 reflects the detected angle. This is evident by using the "Cross Correlation Comparator" code by checking the opposite angle, $\mathbf{45^0}$ in this case.

Fig. 14 shows the cross correlated signals at the presence of AWGN. The Peak Detector code observes the peaks of angles every half cycle of the carrier as shown in fig. 13. Then, the Cross Correlation Comparator code compares the highest (detected angle) to the minimum (opposite angle) peaks, retimes any new data and eventually outputs the received data as shown in fig. 15. A delayed version of the transmitted data is displayed in fig. 15 for comparison purposes.

IV. ANALYSIS AND DISCUSSION

An Altera CYCLONE III EP3C120F780C7N based DSP development board was used to implement the test rig shown in fig. 9. An Altera Quartus II analysis showed that the system utilises only 2% out of 119,088 Total Logic Elements, less than 1% out of 4 Mb Total Memory Bits and 1% out of 576 Embedded Multiplier 9-bit Elements. In contrast to the system of [17] that utilises 800 Look-Up-Tables (LUTs), the system presented in this paper utilises 678 LUTs. In addition, this system used no filters compared to the conventional demodulation technique of [17], that uses a set of Finite Impulse Response (FIR) Low Pass Filters (LPFs) to get rid of the carrier components at the output of the correlators.

A ROHDE & SCHWARZ Noise Generator was used to introduce noise across the channel of the 8-PSK transmitter-receiver link over a range of SNR 0-25dB. A VHDL code based error calculator computed the differences between the transmitted and received symbols/bits. Fig. 16 shows the performance of the 8-PSK demodulator with no error coding using cross-correlation. Tests were performed 4 times: Carrier-to-Noise-Ratio (CNR); Bit-to-Noise-Ratio (EbNR); Symbol-to-Noise-Ratio (EsNR); and limitless noise.

The optimum error rate is $\mathbf{10^{-5}}$ that provides maximum performance for 16-bit and lower resolutions. However, the presented system achieves $\mathbf{10^{-5}}$ error rate at least 21 dB above noise level as shown in fig. 16. As discussed in Section IV, the system requires pre-filtering units to keep CNR with respect to phase response at a reasonable level and the highest cross correlated points within the bounded area of the detected angle.

References [18] and [19] implemented a Hierarchical 8-PSK constellation and used Monte Carlo algorithms to analyse the Bit Error Rate (BER) over a range of CNR 0-24dB with an assumption of perfect carrier recovery and ability of tracking phase fluctuations. A direct comparison of the error rate in this work shows in fig. 16 that the Monte Carlo analysis of [18] and [19] delivers a maximum $\mathbf{8 \times 10^{-4}}$ BER at 24dB of CNR whereas the cross-correlation scheme delivers the same BER with only 16dB of CNR. In addition, the performance of the cross-correlation scheme is still better than [18] and [19] for limitless noise across the channel. The use of error coding should enhance the performance further.

Reference [20] designed a receiver on FPGA to comply with the IESS 308/310 Satellite Communication Standards based on PSK modulation scheme. The 8-PSK scheme in these standards requires 6dB, EbNR to

attain lock to the carrier. In contrast, cross-correlation does not require carrier recovery and can deliver a maximum $\mathbf{9 \times 10^{-3}}$ BER at lower than 6dB compared to [20] that requires at least 6dB to attain lock.

IEEE 802.11b-1999, 802.11g-2003 and IEEE 802.15.4 standards [3] use adaptive systems to compensate the error rate at low SNR by switching between DPSK, BPSK and QPSK. Applications of these standards include WCDMA, HSDPA, WiMAX and WLAN broadband wireless access technologies. This leads us to propose an adaptive system, in parallel with error coding, to use cross-correlation at low SNR and back to normal operation at high SNR for the Satellite and Broadband standards.

V. CONCLUSION AND FURTHER WORK

Cross-correlation has been used, for the first time to demodulate 8-PSK. It has been designed and prototyped on an FPGA. The proposed scheme is very simple compared to alternative methods and requires less hardware for the realization, and thus lower power consumption. As it does not extract the carrier for demodulation purposes; the proposed detection scheme offers improved phase detection performance as well as superior resistance to AWGN compared to a carrier recovery scheme operating at low SNR. No filters were used compared to conventional demodulation techniques that require them to get rid of the carrier components at the output of the correlators. We observed that the system requires an AGC and pre-filtering units to keep CNR with respect to phase response at reasonable level and the highest cross-correlated points within the bounded area. The presented results with no error coding provide maximum performance for 10-bit and 16-bit at CNR of 16dB and 21dB respectively. Further work includes error coding to enhance the performance of the cross-correlation technique. Use of the scheme with error coding can enhance the error rate at low SNR for the applications of mobile and fixed wireless broadband internet devices, 3G connections and Digital Video Broadcasting (DVB) receivers.

References

1. S. Camatel. and V. Ferrero. (2006, Jan.). Homodyne coherent detection of ASK and PSK signals performed by a subcarrier optical phase-locked loop. *IEEE Photonics Technol. Lett.* [Online]. *18(1)*, pp. 142-144. Available: http://dx.doi.org/10.1109/LPT.2005.860377

2. P. Balasubramanian., P. M. Aravindakshan., K. Parameswaran., and V. K. Agrawal. (2004, Sep.). A simple scheme for PSK demodulation. *Microprocessors and Microsystems.* [Online]. *28(7)*, pp. 351-355. Available: http://dx.doi.org/10.1016/j.micpro.2003.08.002

3. R. Esmailzadeh, *Broadband Wireless Communications Business: An Introduction to the Costs and Benefits of New Technologies*. Chichester: John Wiley & Sons, 2006.

4. A. N. D'Andrea., and M. Luise. (1996, Mar.). Optimization of symbol timing recovery for QAM data demodulators. *IEEE Trans. Commun.* [Online]. *44(3)*, pp. 399-406. Available: http://dx.doi.org/10.1109/26.486334

5. A. M. P., de Lucena., J. C. M., Mota., and C. C., Cavalcante., (2009, Feb.). Optimum detection of non-orthogonal QAM signals with spectral overlapping. *IET Commun.* [Online]. *3(2),* pp. 249-256. Aavailable: http://dx.doi.org/10.1049/iet-com:20080157

6. C. Dick., F. Harris., and M. Rice (2004, Jan.). FPGA implementation of carrier synchronization for QAM receivers. *Journal of VLSI Signal Processing*. [Online]. *36(1)*, pp. 57-71. Available: http://dx.doi.org/10.1023/B:VLSI.0000008070.30837.e1

7. A. Metref., D. Le Guennec., and J. Palicot, "Optimized decision-directed carrier recovery loop for 16-QAM constellations," in *Proc. GLOBECOM '07, IEEE*. Washington, DC, 2007, pp. 3112-3117. [Online]. Available: http://dx.doi.org/10.1109/GLOCOM.2007.589

8. F. Rice., M. Rice., and B. Cowley., (2003, Feb.). A new bound and algorithm for Star 16-QAM carrier phase estimation. *IEEE Trans. Commun.* [Online]. *51(2)*, pp. 161-165. Available: http://dx.doi.org/10.1109/TCOMM.2003.809235

9. T. Toeda., R. Okuizumi., and M. Muraguchi, "Demodulation of 16-QAM signals using RF direct orthogonal phase under-sampling technique," in *Proc. APMC 2009, IEEE*. Singapore, 2009, pp. 508-511. [Online]. Available: http://dx.doi.org/10.1109/APMC.2009.5384187

10. X. H. Wang., X. Z. Qiu., P. Lambrecht., J. Vandewege., K. De Meyer., and W. Trog, "Burst-mode 16 QAM receiver for upstream transmission over CATV networks," in *Proc. MWSCAS 1996, IEEE*. Ames, IA, 1996, pp. 1260-1263. [Online]. Available: http://dx.doi.org/10.1109/MWSCAS.1996.593146

11. X. Vu., N. A. Duc,, and T. A. Vu, "16-QAM transmitter and receiver design based on FPGA," in *Proc. DELTA'10, IEEE*. Ho Chi Minh City, 2010, pp. 95-98. [Online]. Available: http://dx.doi.org/10.1109/DELTA.2010.34

12. Y. Park., and J. Ahn, "A new carrier recovery method for 16-QAM signal," in *Proc. ICPWC'97, IEEE.* Mumbai, India, 1997, pp. 194-197. [Online]. Available: http://dx.doi.org/10.1109/ICPWC.1997.655506

13. J. G. Proakis., and M. Salehi, *Communication systems engineering*. Englewood Cliffs: Prentice Hall, 1994.

14. M. S. Roden, *ANALOG AND DIGITAL COMMUNICATION SYSTEMS*. London: Prentice-Hall International Inc, 1996.

15. Y. Linn, "A robust phase detection structure for M-PSK: Theoretical derivations, simulation results, and system identification analysis," in *Proc. CCECE'05, IEEE.* Saskatoon, Sask, 2005, pp. 869 - 883. [Online]. Available: http://dx.doi.org/10.1109/CCECE.2005.1557117

16. I. A. Z. Qatawneh, "The use of orthogonal frequency division multiplex (OFDM) techniques in mobile broadband applications," Ph.D. dissertation, Dept. Eng., Huddersfield Uni., Huddersfield, UK, 1997.

17. K. A. Arun Kumar, "FPGA implementation of PSK modems using partial re-configuration for SDR and CR applications," in *Proc. INDICON 2012*, *Annual IEEE.* Kochi, 2012, pp. 205-209. [Online]. Available: http://dx.doi.org/10.1109/INDCON.2012.6420616

18. P. K. Vitthaladevuni., and M. S. Alouini, (2005, Jul.). Effect of imperfect phase and timing synchronization on the bit-error rate performance of PSK modulations. *IEEE Trans. Commun.* [Online]. *53(7)*, pp. 1096-1099. Available: http://dx.doi.org/10.1109/TCOMM.2005.851616

19. P. K. Vitthaladevuni., and M. S. Alouini., (2003, Dec.). Exact BER computation of generalized hierarchical PSK constellations. *IEEE Trans. Commun.* [Online]. *51(12)*, pp. 2030-2037. Available: http://dx.doi.org/10.1109/TCOMM.2003.820748

20. V. K. Velkuru., and A. Samant, "A design for software defined M-PSK radio on FPGA for low SNRs and symbol rates upto 10MS/s," in *Proc. ICSIPA 2011, IEEE.* Kuala Lumpur, 2011, pp. 574-578. [Online]. Available: http://dx.doi.org/10.1109/ICSIPA.2011.6144169

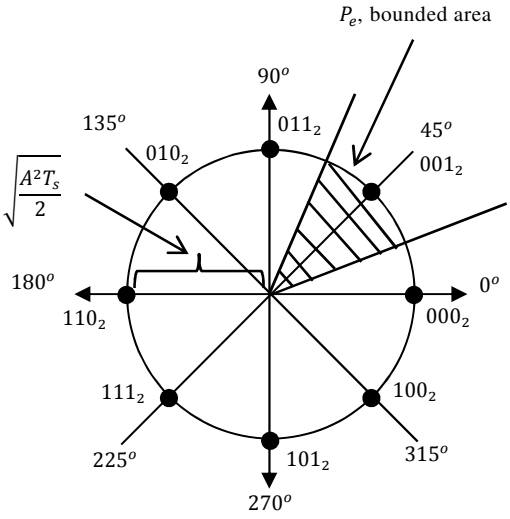

Fig. 1. 8-PSK constellation points

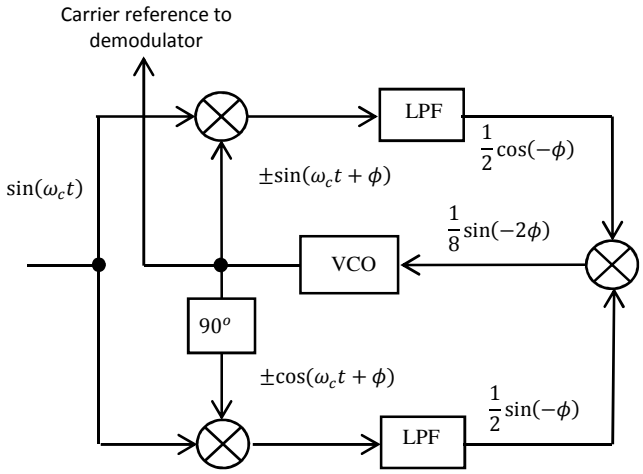

Fig. 2. Costas loop [4], [6], [10], [11], [15]

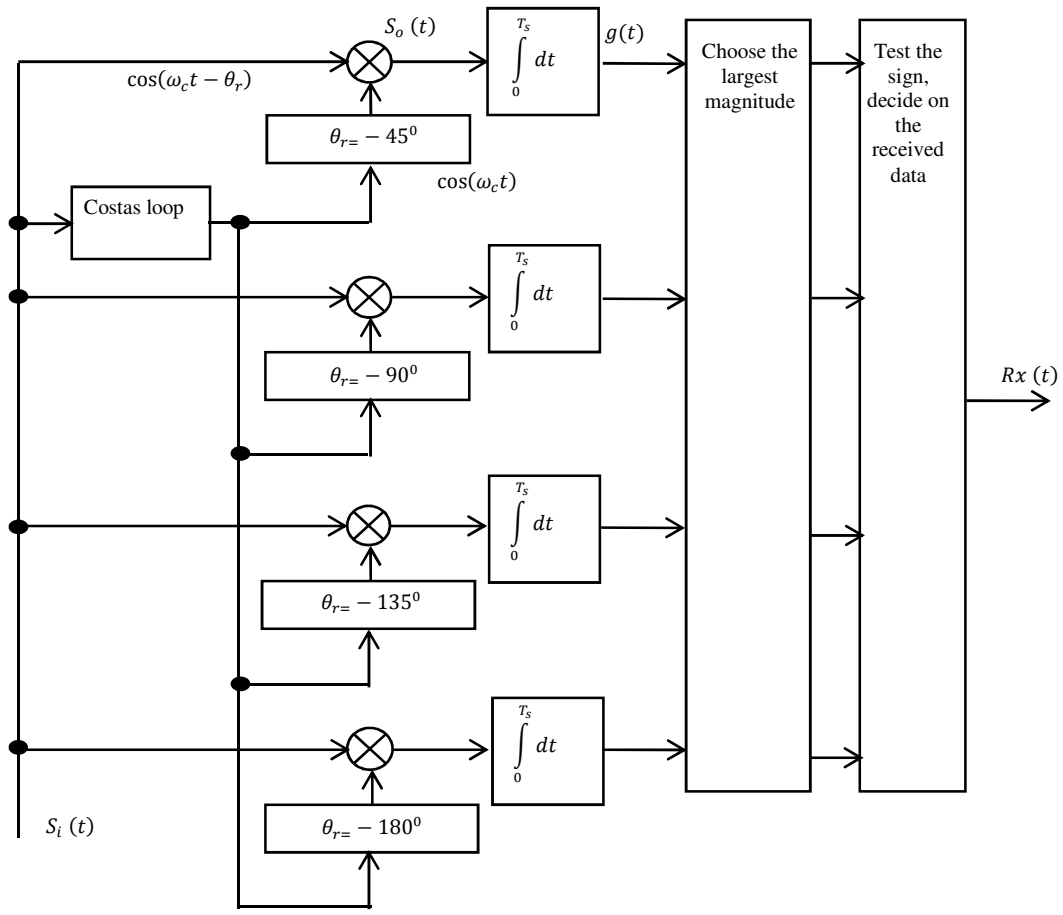

Fig. 3. 8-PSK receiver using Costas loop [14]

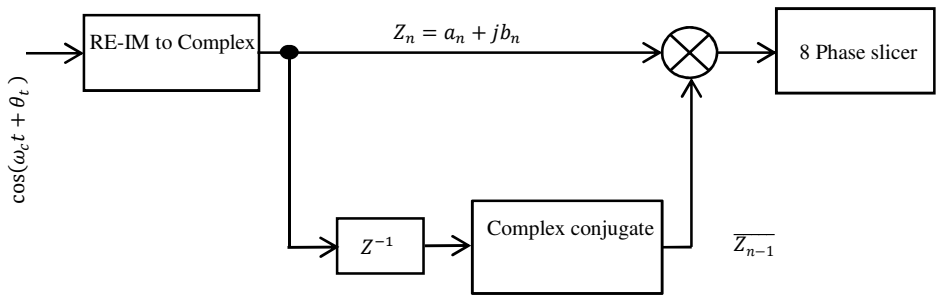

Fig. 4. 8-PSK receiver using complex number [16]

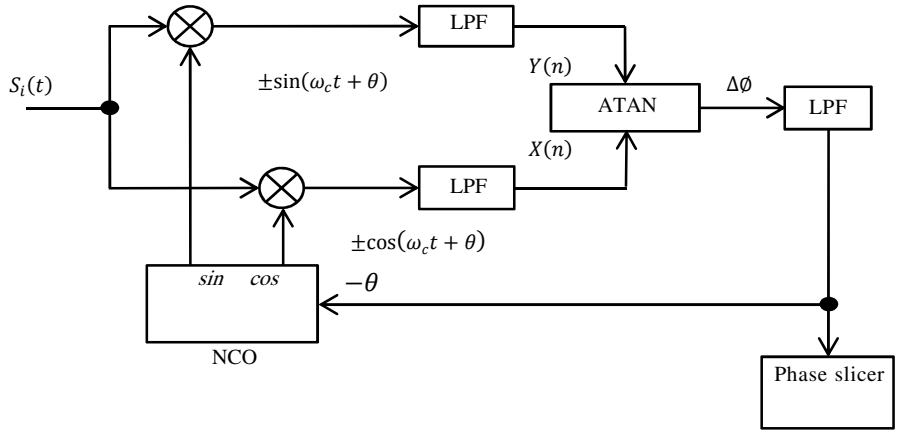

Fig. 5. Phase demodulator using *ATAN* function and digital PLL [6], [11]

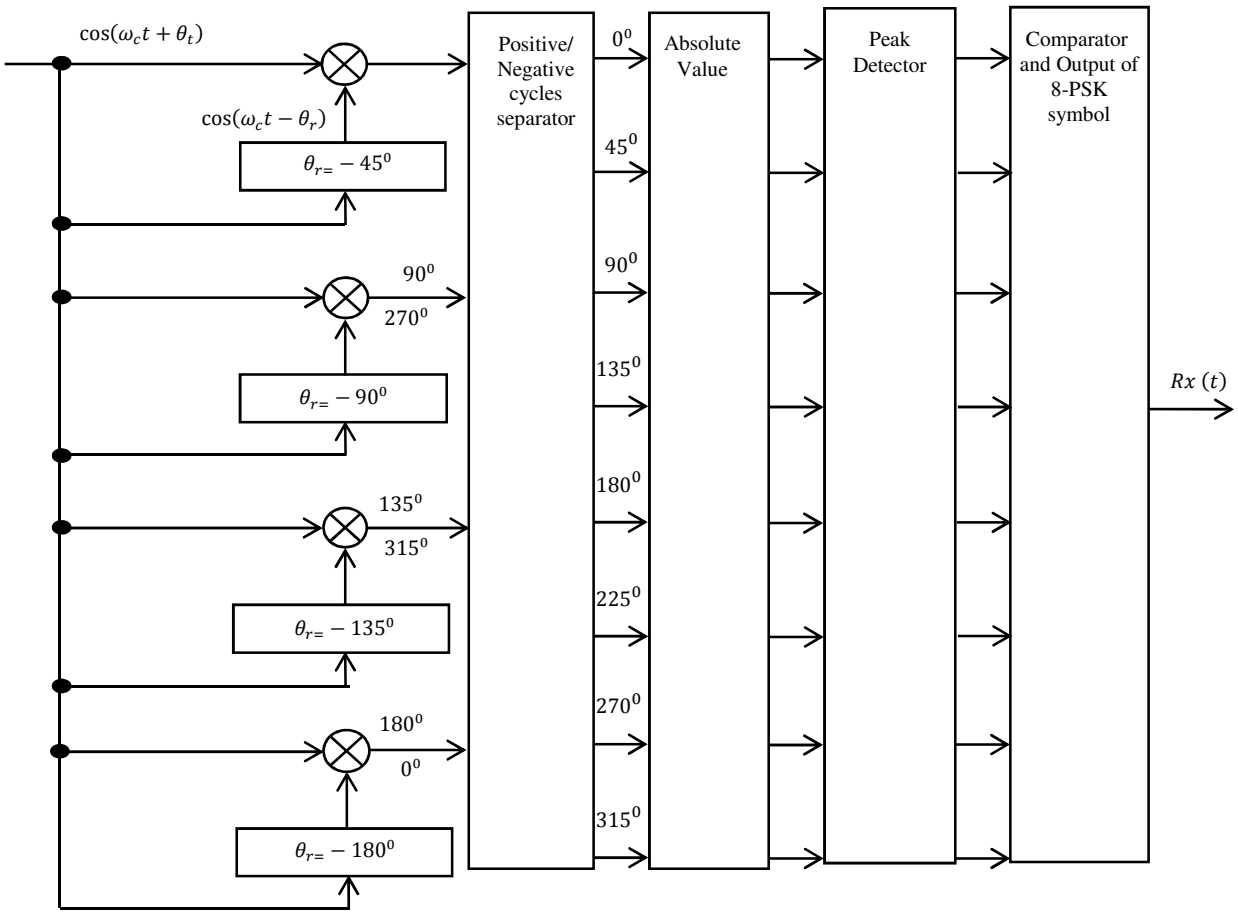

Fig. 6. 8-PSK receiver design using cross correlation

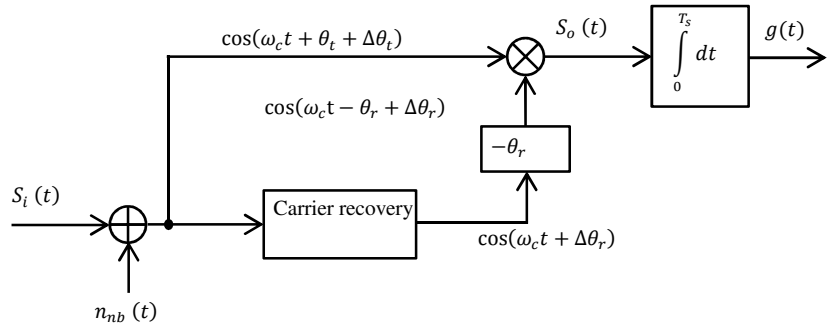

Fig. 7. Effect of added narrowband noise on matched filter using carrier recovery

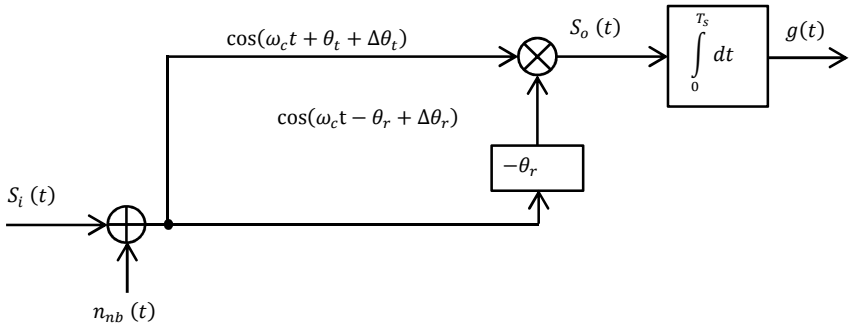

Fig. 8. Effect of added narrowband noise on cross-correlation approach

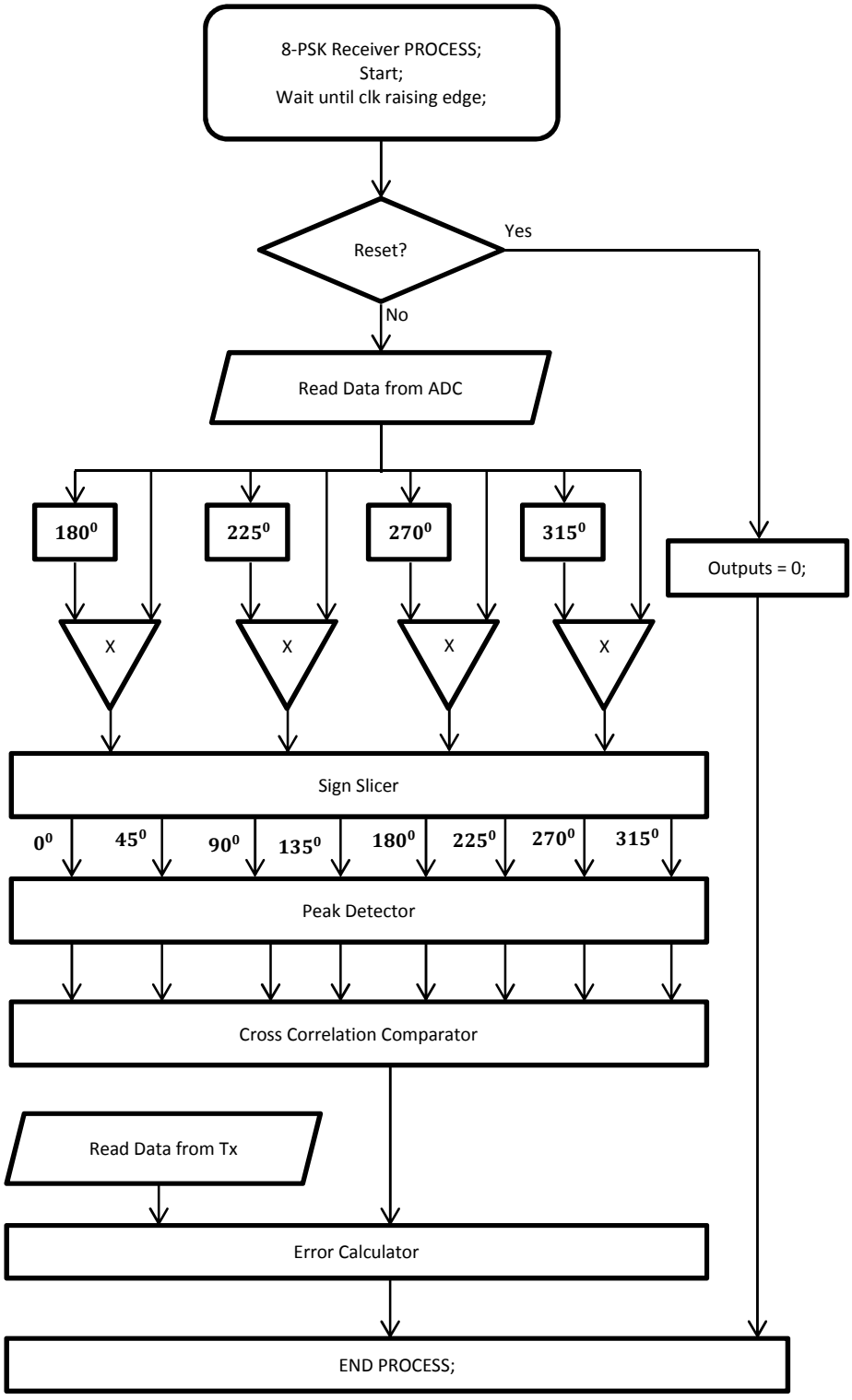

Fig. 9. 8-PSK receiver test rig using cross correlation

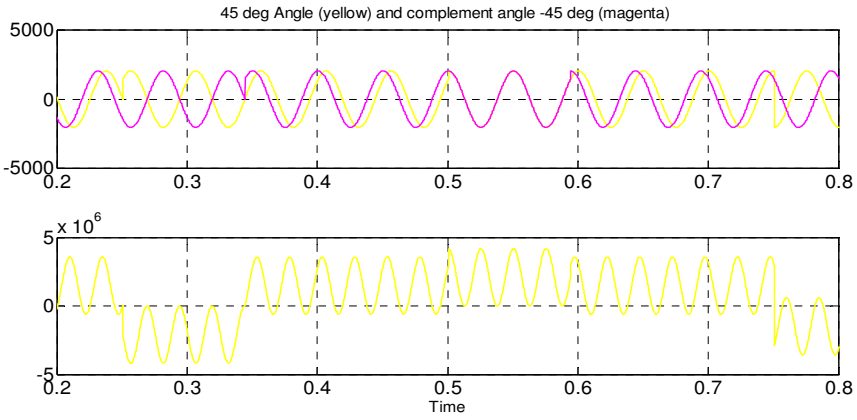

Fig. 10. The input (complement angle-magenta) and output of the **45º** angle detector

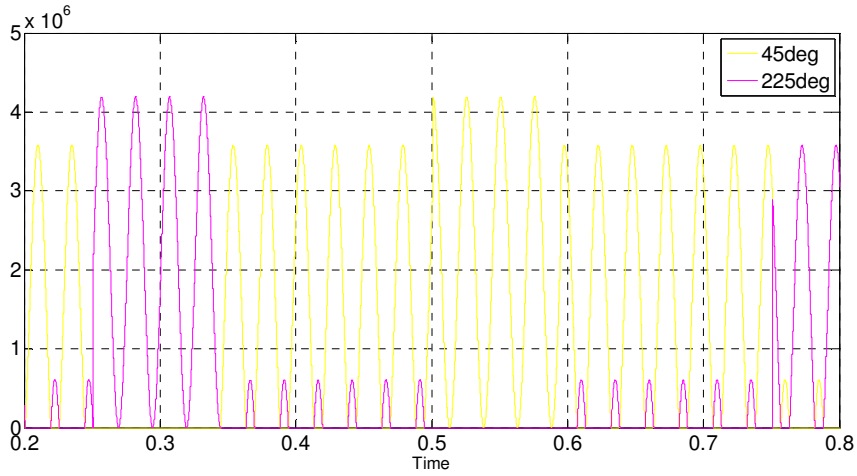

Fig. 11. Cross correlated signals are separated; **45º** (yellow) and **225º** (magenta)

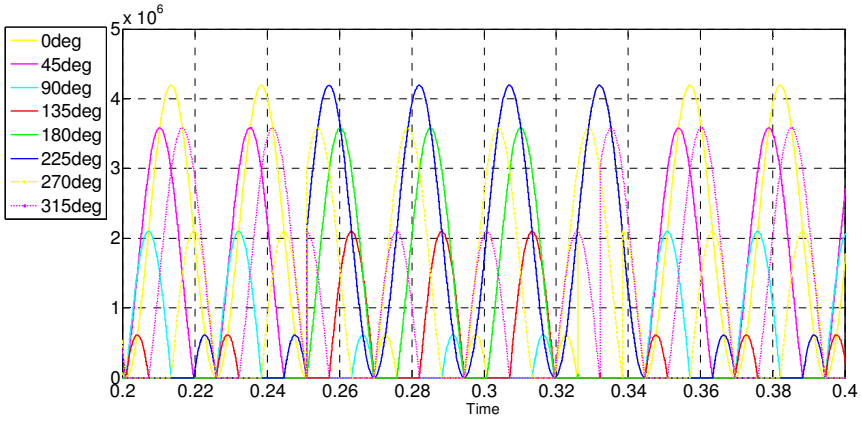

Fig. 12. Correlated - Separated, **0º** (yellow), **45º** (magenta), **90º** (cyan), **135º** (Red), **180º** (Green), **225º** (Blue), **270º** (yellow), **315º** (magenta)

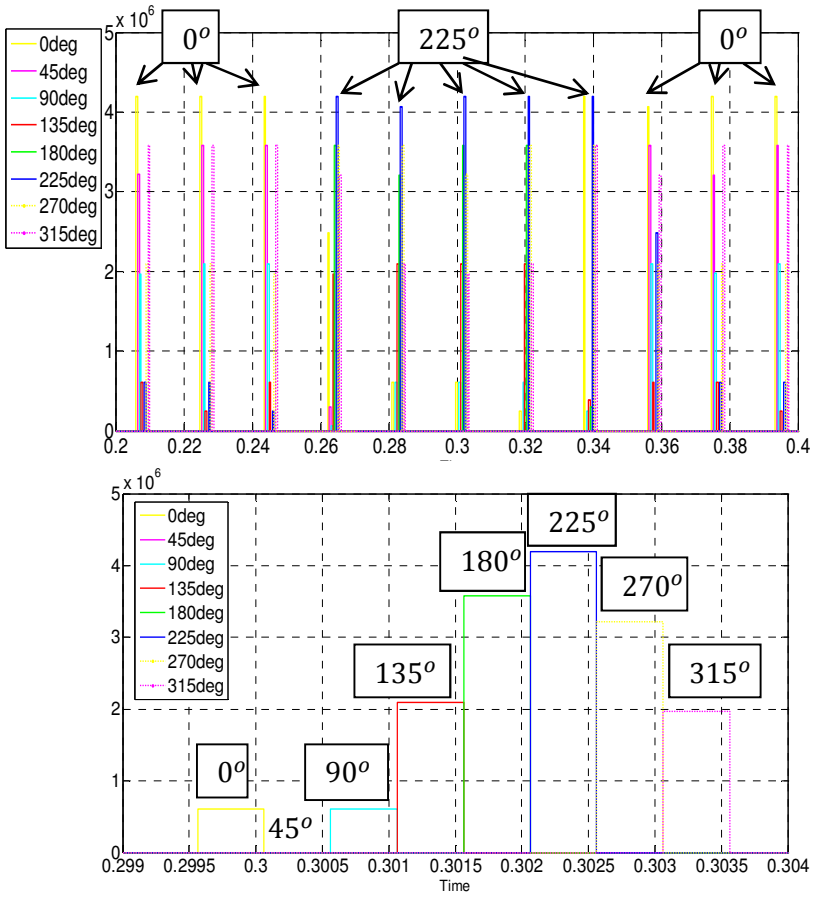

Fig. 13. Detected Peaks where **225°** is dominant and **45°** is the weakest

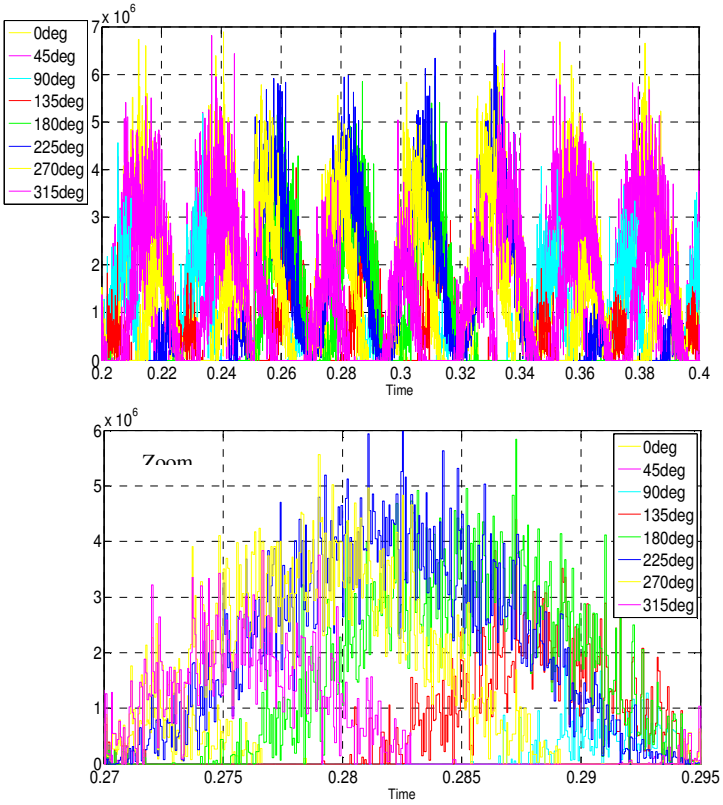

Fig. 14. Correlated-separated, all angles at the presence of AWGN

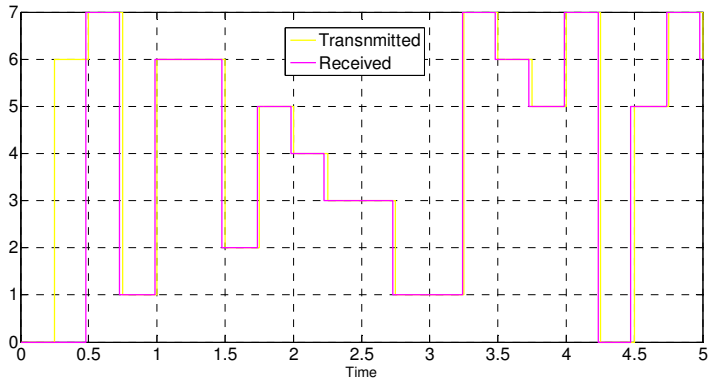

Fig. 15. Comparison of the transmitted and received data at 4 symbols/s

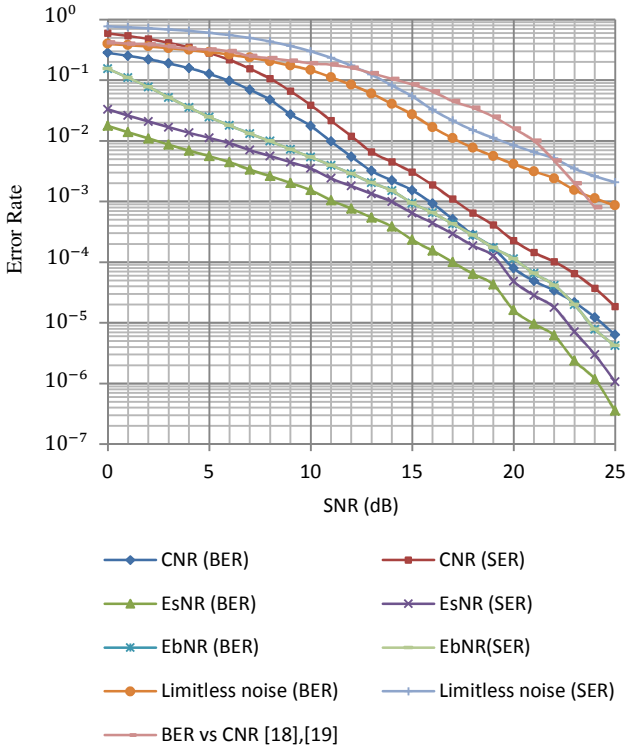

Fig. 16. Performance of 8-PSK using cross correlation versus Monte Carlo simulations by [18] and [19]

Demodulation of QAM signals using cross-correlation techniques

A. Alaiwi, M.J.N. Sibley and P. J. Mather (Department of Engineering and Technology, University of Huddersfield, Queensgate, Huddersfield, HD1 3DH, UK)

E-mail: ayman.alaiwi@hud.ac.uk, m.j.n.sibley@hud.ac.uk, p.j.mather@hud.ac.uk

Abstract—Quadrature Amplitude Modulation (QAM) is considered to be one of the highly bandwidth efficient modulation schemes in wireless communication. QAM has a noise bandwidth that is relatively smaller than that of the phase shift keying (PSK). Two types of 16-QAM are discussed in this paper, namely Star (Circular) and Square. Star 16-QAM is preferred to Square QAM in Orthogonal Frequency Division Multiplex (OFDM) systems to keep the effects of peak-to-average-power-ratios (PAPR) low. OFDM is widely used in Digital Video Broadcasting (DVB), Digital Audio Broadcasting (DAB) and Broadband internet. System integrators use ATAN computation in parallel with digital Phase-Locked-Loop (DPLL) to demodulate QAM signal. As will be shown in this paper, such a demodulation scheme requires high number of Field Programmable Gate Array (FPGA) implementation resources.

In this paper we propose a novel cross-correlation function to replace ATAN and DPLL for 16-QAM signal demodulation. As will be shown, this novel function is simple to realise, yields a significant reduction in terms of complexity and hence less use of available silicon. This technique will yield cost reduction in products using 16-QAM demodulators, namely Broadband internet and, Digital TV and Radio.

Index terms - atan, AWGN, carrier recovery, Costas loop, cross correlation, DSP, FPGA, OFDM, PLL, PSK, QAM, VHDL.

I. INTRODUCTION

Star and Square QAM techniques are widely used to transmit *m*-bit symbols via a $\mathbf{2^M}$ signal point constellation, distributed on a complex plane [1]-[4]. However, the higher the *M*, the more bandwidth efficient the modulation scheme [1]-[3], [5]. 16-QAM is one of the standard modulation schemes in OFDM [6] applications such as DAB, DVB, and High Performance Local Area Network (HIPERLAN) [7], [8]. In addition, 16-QAM is widely used in Wide-band Code Division Multiple Access (WCDMA), High-Speed Downlink Packet Access (HSDPA), World-wide Inter-operability for Microwave Access (WiMAX), Wireless Local Area Network (WLAN), Asynchronous Digital Subscriber Line (ADSL) and High-bit-rate Digital Subscriber Line (HDSL) broadband technologies [9].

This paper is presented as follows: the rest of this section presents a background on Star and Square 16-QAM modulation, receiver, and carrier recovery as well as presenting the novel method of demodulating 16-QAM; section II presents the implementation of the proposed technique; section III analyses and discusses the proposed system and compares results to the prior works; and section IV summaries the findings.

A. STAR 16-QAM

Star 16-QAM has two amplitude levels that are two circles around the origin as shown in fig. 1. The outer ring is 3 times greater than the inner ring. It is considered as a two 8-PSK with different amplitude level [4] – a combination of 8-PSK and Binary Amplitude Shift Keying (BASK). 8-PSK and 16-QAM occupies the same bandwidth since they share the same symbol rate e.g. *4 symbols/s*. 16-QAM has a noise bandwidth that is smaller than that of 8-PSK [1], [4]. BASK data ($\boldsymbol{a_n}$) is differentially encoded and 8-PSK data ($\boldsymbol{b_n}$, $\boldsymbol{c_n}$, $\boldsymbol{d_n}$) are phase modulated on the carrier. The transmitted 16-QAM signal can be represented as (1),

$$\boldsymbol{S_{QAM}(t) = A\ \cos(\omega_c t + \theta_t)} \qquad (1)$$

The amplitude *A* in (1) represents BASK data whereas $\boldsymbol{\theta_t}$ represents 8-PSK data.

B. SQUARE 16-QAM

In contrast to Star 16-QAM, Square 16-QAM has three amplitude levels. The constellation points are distributed on 3 circles of the signal plane as shown in fig. 2. The points are separated in uniform square arrays. Square and Star QAM occupy the same bandwidth for the same transmission rate. Square 16-QAM signal is modulated by dividing the data source to 4 *bit/symbol* ($\boldsymbol{a_n}$, $\boldsymbol{b_n}$, $\boldsymbol{c_n}$, $\boldsymbol{d_n}$). A demultiplexer splits the data into Even and Odd Non-Return-to-Zero (NRZ) parts. The Odd and Even parts control the amplitude level of the in-phase and quadrature carriers respectively. Equation (1) formulates the transmitter output.

C. 16-QAM RECEIVER

The transmitted 16-QAM signal is a suppressed carrier where half the power is concentrated in the carrier and the other half is QAM modulated data. Demodulation of 16-QAM is crucial where 2 vectors have to be tracked, phase and amplitude [1], [2], [4], [5], [10]-[14]. The phase can be tracked using complex number [1], Costas loop [3] or DPLL and *ATAN* function [11], [13] using a Digital Signal Processing (DSP) processor. The amplitude can be tracked easily in the case of Star 16-QAM by comparing the absolute values of a current sample with a delayed full carrier cycle to differentially decode BASK data ($\boldsymbol{a_n}$) where an 8-PSK receiver can be used to demodulate the phase data. In contrast, the symbols in Square 16-QAM are strictly dependent on *A* and $\boldsymbol{\theta_t}$. This requires coherent detection which requires phase knowledge. Unfortunately the phase noise causes the constellation points to rotate, and so an absolute phase reference must be maintained or estimated [1], [2], [4], [5], [10]-[14].

D. CARRIER RECOVERY AND PHASE DEMODULATION SCHEMES

One way of recovering the carrier is to use a Costas loop [5], [10], [11], [13]. It suffers from a long acquisition time; possibility of a false lock; a $\mathbf{180^0}$ phase ambiguity and hence a preamble sequence is needed to aid carrier recovery [3], [15]. Matched filters are to be used to slice the phases using the recovered carrier. Phase data can also be demodulated using the complex number approach [1], [2]. This requires Real-Imaginary to Complex conversion which needs to be performed using a high specification processor.

ATAN computation is an advanced version of Costas loop, using a DPLL. It measures the angle between the baseband signal complex envelope and the nearest constellation point [2], [11], [13]. A high accuracy ATAN computation resists the noise but a high level of FPGA resources is required to perform such an operation.

Coherent detection is severely affected by multipath fading, mainly because of carrier recovery issues in a fast-fading environment [1], [4], [5], [14] where the PLL locks onto a different quadrant than that required [1], [4], [5], [14]. The carrier recovery is not efficient as the exact phase cannot be guaranteed or maintained. However, with DSP processors the carrier recovery requires LUTs to slice and scale the phases. Mainly, system integrators use *ATAN* function in parallel with DPLL to detect the phase changes [11]-[13], [15]. Consequently, high implementation resources are needed to perform such an operation.

Reference [16] showed that carrier recovery systems experience jitter noise caused by the narrowband noise deviation. This leads the constellation points to rotate and hence make an error in decoding the received data. Alternatively, reference [16] discussed the use of cross-correlation to demodulate 8-PSK signal compared to the schemes that use carrier recovery as part of extracting the phase data. It was concluded that the cross correlation provides great immunity at low SNR. This requires an Automatic-Gain-Control (AGC) and pre-filtering units to keep the SNR at reasonable level and the highest cross correlated points within the bounded area of the detected point over the symbol period.

E. PROPOSED SCHEME

The concept of the cross-correlation theory will be applied in this paper to demodulate 16-QAM signal using the test rig shown in fig. 3 and compare it with prior work as will be seen later. The general operation of the 16-QAM receiver is; four detectors cross correlate the carrier by the complement transmitted angles to detect 8 separate phase angles and a timer to update and compare the cross correlated angles every half carrier cycle interval for instant observations. The cross correlated signals are separated into 2 parts and then the absolute value of both parts are obtained with the highest absolute value identifying the received data phase angle. In addition, the received signal is delayed by $\mathbf{360^0}$ to compare it with current samples. These two signals are now differentially decoded to output BASK data. The peak detector observes the peaks of detected angles and triggers the AM timer once an AM signal is detected. The AM timer feeds back a pulse width over a carrier cycle which multiplexes the amplitude by a factor of 3. This balances the amplitude inputs of the correlators which in turn maximise the precision of cross-correlation. Eventually, the Cross Correlation Comparator compares the correlated points and output the received data.

II. IMPLEMENTATION AND RESULTS

With reference to the receiver test rig shown in fig. 3, the receiver was implemented using Altera Quartus II, Altera-DSP Builder and Matlab-Simulink. The VHDL language was used to design the Sign Slicer, Peak Detector, Cross Correlation Comparator and Amplitude Modulation (AM) timer. The design was tested using a PRBS data source.

Fig. 4 shows the output of 16-QAM correlators. The phases are clearly sliced even in the presence of AM signal. This is apparent on the highest and lowest peaks as will be discussed later.

The correlated signals in fig. 4 are now separated. The absolute values of the negative parts were taken as shown in fig. 5.

The peak detector observes the AM and phase peaks separately. The phase peaks are observed over half the carrier cycle while the AM peaks are observed over quarter the carrier cycle whenever the current sample is greater than the previous sample. Any AM transitions would trigger the AM timer and also indicates BASK data reception. Once the phase timer overflowed, the highest detected phase peaks and BASK data are sent to the Cross Correlation Comparator.

Fig. 6 shows the detect peaks of 16-QAM correlated in fig. 4 and sliced in fig. 5. The detected peaks were slightly delayed by the author in fig. 6 to better explain the idea but practically there should be no delay for direct comparison of angles and data outputting.

The highest peak in fig. 6 indicates the detected angle i.e. $\mathbf{315^0}$. This is evident by checking the minimum peak which is the opposite angle i.e. $\mathbf{135^0}$. The peak detector could detect a leakage from the neighbouring angles. Such a leakage is cancelled out when compared by the Cross Correlation Comparator as the opposite angle is not confirmed.

Fig. 7 shows all the correlated and separated signals of 16-QAM signal in the presence of Additive White Gaussian Noise (AWGN). The zoomed-in area in fig. 7 shows that the red ($\mathbf{135^o}$) trace is dominant among all traces where the cyan ($\mathbf{90^o}$) and green ($\mathbf{180^o}$) are just close the red trace. This confirms that the cross correlated

point is within the bounded area of the detected angle. Clearly, the AWGN affected the peaks of the cross correlated points. The cross correlation comparator compares the highest (detected angle) to the minimum (opposite angle) peaks, combines it with BASK data, retimes any new data and eventually outputs the received data. The new angle is $\mathbf{135^0}$ (maximum) and evident by the opposite angle $\mathbf{315^0}$ (minimum). Since the transmitter is sending the data at rate of 0.25 s, the comparator is updated regulary almost every 0.25 s.

A direct comparison of the transmitted and recovered data is shown in fig. 8. A delayed version of the transmitted data was displayed on fig. 8 for the comparison. The receiver missed two symols at startup and then fully recovered the data.

III. ANALYSIS AND DISCUSSION

The constellation points of Square QAM optimise the transmission over Gaussian channel compared to Star QAM [4]. Square QAM requires AGC and carrier recovery for coherent detection [1], [4], [5], [14]. The carrier recovery is severely affected by fading channel [1], [4], [5], [12], [14]. In contrast, Star QAM reduces the effects of Rayleigh fading [1], [4]. The AGC in Square QAM has to maintain stability fast enough to decode the AM data [1], [4], [5]. The symbols in Square QAM are strictly dependent on A and $\boldsymbol{\theta_t}$. On the other hand, the amplitude can be tracked easily in the case of Star 16-QAM to decode BASK data separately from the phase data $\boldsymbol{\theta_t}$. Star QAM does not experience false lock positions and the transmitted mean power is relatively small compared to Square QAM [17]. In addition, it has the property that PAPR is less than that for Square QAM [2]. For this reason, Star 16-QAM is preferred to Square QAM in OFDM systems to keep the effects of PAPR low [7]. Moreover, the coded Star 16-QAM symbol error rate is better than that of Square 16-QAM [2].

An Altera CYCLONE III EP3C120F780C7N based DSP development board was used to implement the test rig. The authors of [11] implemented a carrier recovery system for Square 16-QAM and the authors of [13] implemented Square 16-QAM receiver based on FPGA using the *ATAN* function and DPLL. Hence, a direct comparison, of the number of FPGA system resources, to these works, is given in Table I. Clearly, the proposed demodulation scheme significantly reduced the number of Embedded Multipliers to demodulate 16-QAM compared to [11], [13]. In addition, the prototyped scheme does not need carrier recovery and uses only 4 Embedded Multipliers compared to [11] that uses 8 Embedded Multipliers just to extract the carrier prior demodulation.

Table I
16-QAM Implementation Resources Requirements

Type of resources	Resources used by carrier recovery [11]	Resources used by Square 16-QAM receiver [13]	Resources used by Star 16-QAM [this work]
Embedded Multipliers	8	48	4
LUTs	Not presented by [11]	4674	1858

If cross-correlatoin is used in Square 16-QAM, then 6 correlators are required to detect 12 angles positions and the amplitude data are to be differentially decoded. This consumes more implmentation resources than Star 16-QAM. The concept of using cross correlation to demodulate 16-QAM signal was proven by using Matlab-Simulink and practical implementations of FPGA. The cross correlation has been used for the first time in Star 16-QAM demodulator system, replacing the *ATAN* function and DPLL to detect the phase changes on the received signal. This yields a significant reduction in terms of complexity and the silicon required to integrate Star 16-QAM receiver onto an IC. The reduced complexity of the receiver leads to a reduced number of resources required, for the design, and thus power consumptions of the system. This technique will yield cost reduction in products using 16-QAM demodulators, namely broadband internet and, Digital TV and Radio.

IV. CONCLUSION AND FURTHER WORK

The concept of using cross correlation to demodulate 16-QAM signal was proven using simulations and practical implementations of FPGA. The cross correlation has been used for the first time in the Star 16-QAM demodulator system, replacing the ATAN function and DPLL to detect the phase changes on the received signal. The technique requires less hardware implementation compared to alternative methods. In contrast to conventional schemes, no filters were used to get rid of the carrier components at the output of the correlators. This technique will yield cost reduction in products using 16-QAM demodulators, namely broadband internet and Digital TV.

References

1. I. A. Z. Qatawneh, "The use of orthogonal frequency division multiplex (OFDM) techniques in mobile broadband applications," Ph.D. dissertation, Dept. Eng., Huddersfield Uni., Huddersfield, UK, 1997.

2. F. Rice., M. Rice., and B. Cowley., (2003, Feb.). A new bound and algorithm for Star 16-QAM carrier phase estimation. *IEEE Trans. Commun.* [Online]. *51(2)*, pp. 161-165. Available: http://dx.doi.org/10.1109/TCOMM.2003.809235

3. M. S. Roden, *ANALOG AND DIGITAL COMMUNICATION SYSTEMS*. London: Prentice-Hall International Inc, 1996.

4. W. T. Webb., L. Hanzo., and R. Steele., (1991, Jun.). Bandwidth-efficient QAM schemes for Rayleigh fading channels. *IEE PROCEEDING-I COMMUNICATIONS SPEECH AND VISION*. [Online]. *138(3)*, pp. 169-175. Available: http://eprints.soton.ac.uk/257020/1/wtw-lh-rs-IEEproc-june-1991.pdf

5. X. H. Wang., X. Z. Qiu., P. Lambrecht., J. Vandewege., K. De Meyer., and W. Trog, "Burst-mode 16 QAM receiver for upstream transmission over CATV networks," in *Proc. MWSCAS 1996, IEEE*. Ames, IA, 1996, pp. 1260-1263. [Online]. Available: http://dx.doi.org/10.1109/MWSCAS.1996.593146

6. A. M. P., de Lucena., J. C. M., Mota., and C. C., Cavalcante., (2009, Feb.). Optimum detection of non-orthogonal QAM signals with spectral overlapping. *IET Commun.* [Online]. *3(2),* pp. 249-256. Aavailable: http://dx.doi.org/10.1049/iet-com:20080157

7. K. Abdullah., S. S. Mahmoud., and Z. M. Hussain., (2009, Dec.). Performance Analysis of an Optimal Circular 16-QAM for Wavelet Based OFDM Systems. *International Journal of Communications, Network and System Sciences*. [Online] *2(9)*, pp. 836-844. Available: http://dx.doi.org/10.4236/ijcns.2009.29097

8. R. D. Bruin., and J. Smits, "Digital transmission," in *Digital video broadcasting: technology, standards, and regulations*. Boston, Mass: Artech House, 1999. pp. 167-201.

9. R. Esmailzadeh, *Broadband Wireless Communications Business: An Introduction to the Costs and Benefits of New Technologies*. Chichester: John Wiley & Sons, 2006.

10. A. N. D'Andrea., and M. Luise. (1996, Mar.). Optimization of symbol timing recovery for QAM data demodulators. *IEEE Trans. Commun.* [Online]. *44(3)*, pp. 399-406. Available: http://dx.doi.org/10.1109/26.486334

11. C. Dick., F. Harris., and M. Rice (2004, Jan.). FPGA implementation of carrier synchronization for QAM receivers. *Journal of VLSI Signal Processing*. [Online]. *36(1)*, pp. 57-71. Available: http://dx.doi.org/10.1023/B:VLSI.0000008070.30837.e1

12. A. Metref., D. Le Guennec., and J. Palicot, "Optimized decision-directed carrier recovery loop for 16-QAM constellations," in *Proc. GLOBECOM '07, IEEE*. Washington, DC, 2007, pp. 3112-3117. [Online]. Available: http://dx.doi.org/10.1109/GLOCOM.2007.589

13. X. Vu., N. A. Duc,, and T. A. Vu, "16-QAM transmitter and receiver design based on FPGA," in *Proc. DELTA'10, IEEE*. Ho Chi Minh City, 2010, pp. 95-98. [Online]. Available: http://dx.doi.org/10.1109/DELTA.2010.34

14. Y. Park., and J. Ahn, "A new carrier recovery method for 16-QAM signal," in *Proc. ICPWC'97, IEEE.* Mumbai, India, 1997, pp. 194-197. [Online]. Available: http://dx.doi.org/10.1109/ICPWC.1997.655506

15. P. Balasubramanian., P. M. Aravindakshan., K. Parameswaran., and V. K. Agrawal. (2004, Sep.). A simple scheme for PSK demodulation. *Microprocessors and Microsystems.* [Online]. *28(7)*, pp. 351-355. Available: http://dx.doi.org/10.1016/j.micpro.2003.08.002

16. A. Alaiwi., M. J. N. Sibley., and P. J. Mather., (2013, Month.). Demodulation of PSK signals using cross-correlation techniques. *IEEE Trans. Commun, Vol(issue)*, pp. xx-xx. Available: website To be confirmed

17. J. G. Proakis, *Digital communications*. New York: McGraw-Hill, 1995.

Figures

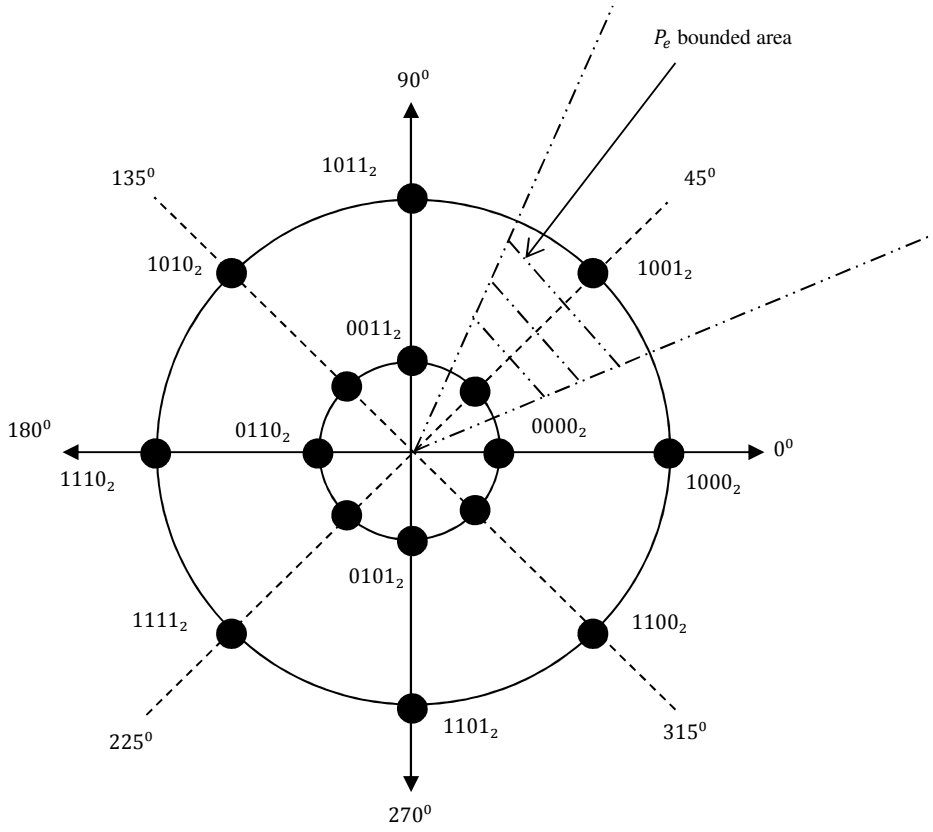

Fig. 1. Star 16-QAM Gray coding constellation

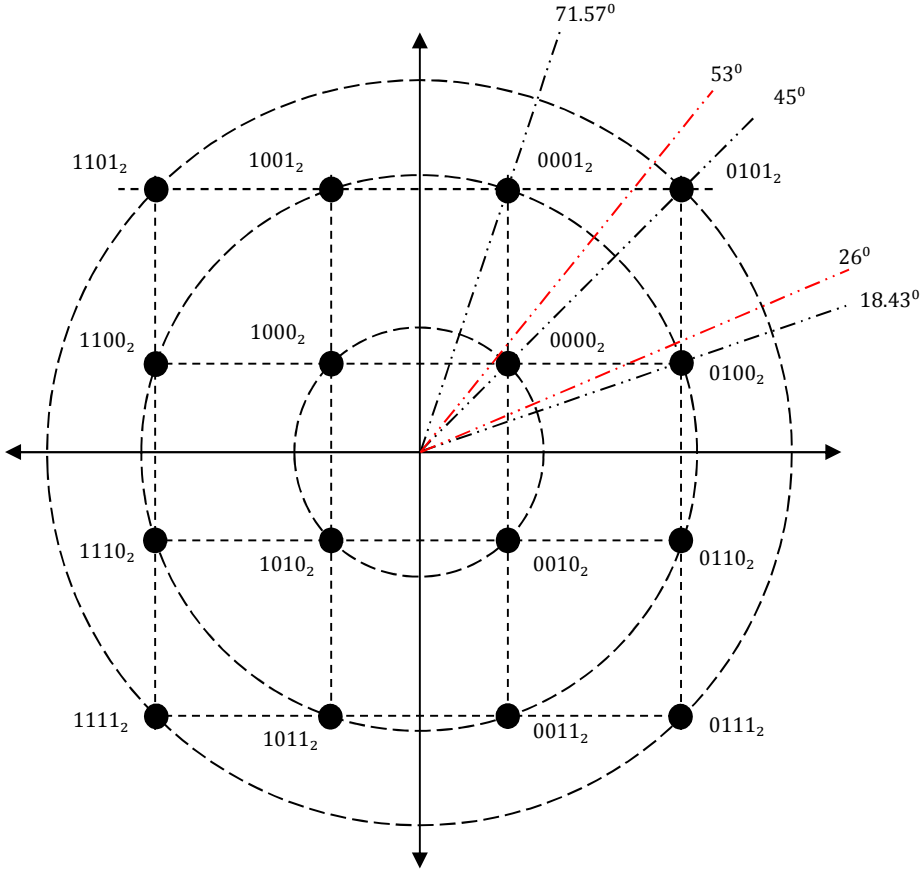

Fig. 2. Square 16-QAM Gray coding constellation

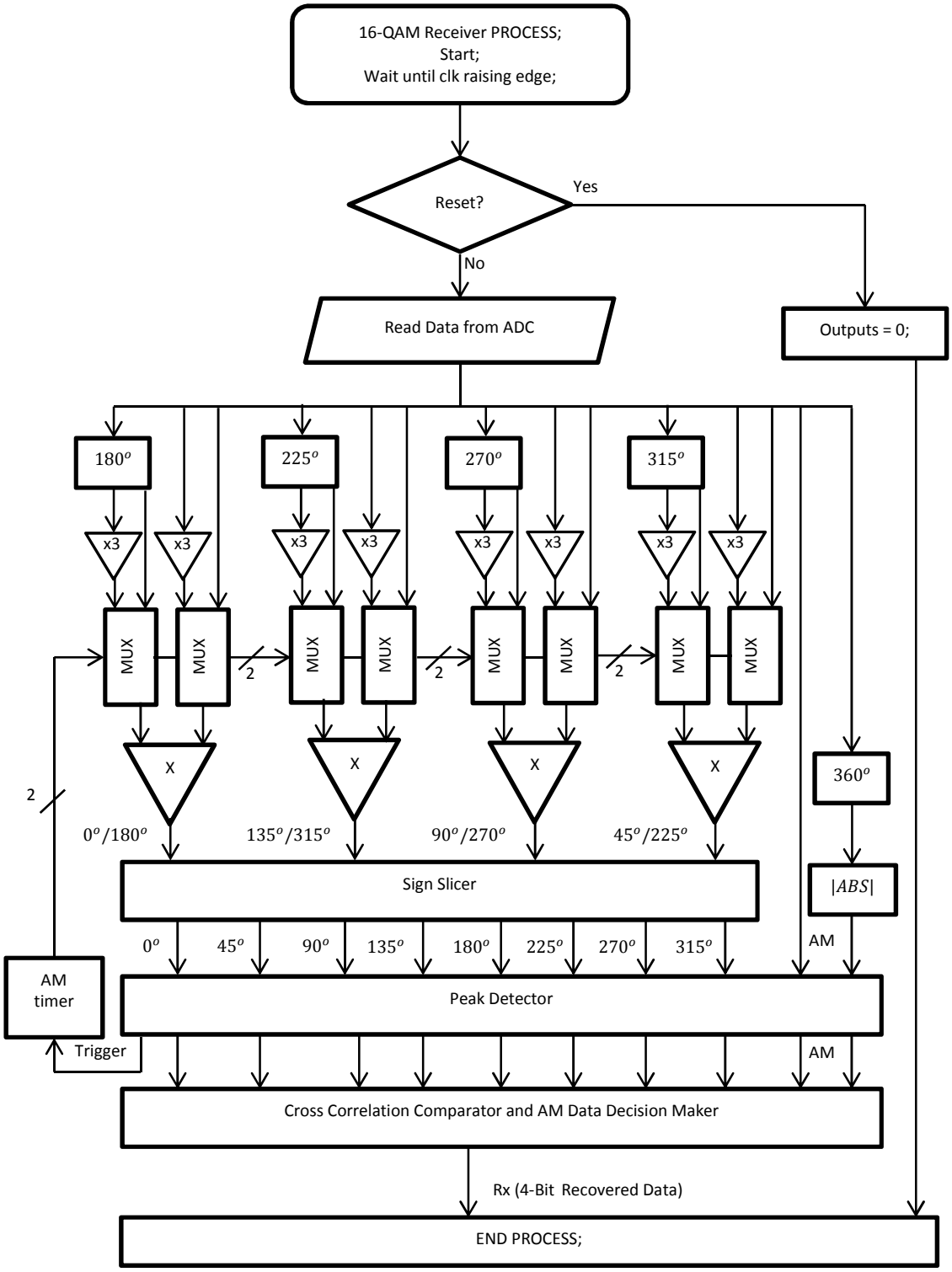

Fig. 3. 16-QAM receiver test rig using cross correlation

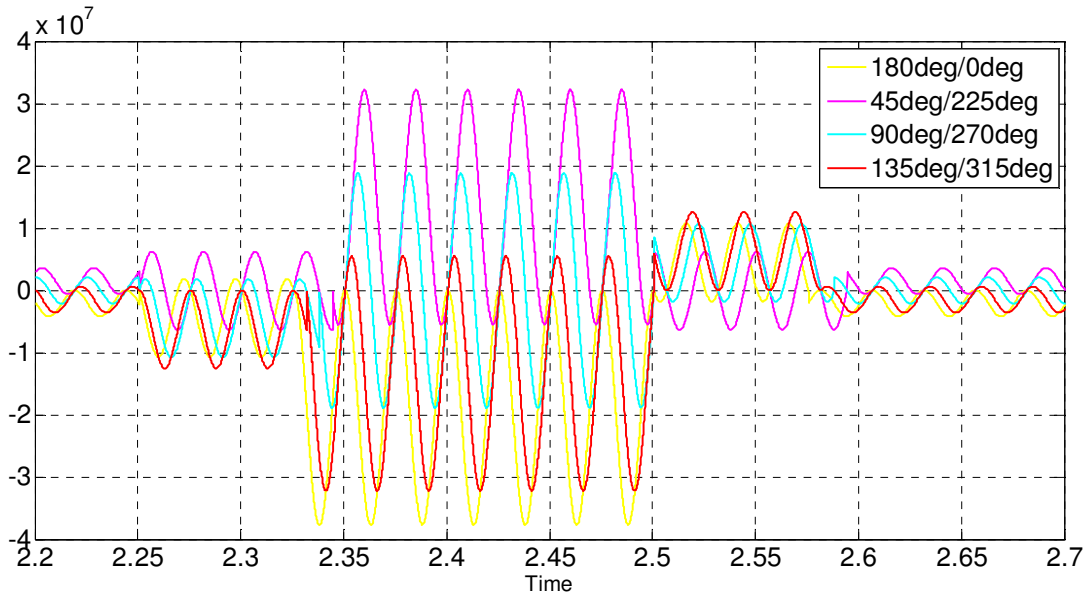

Fig. 4. 16-QAM correlators' outputs; $\mathbf{0^0/180^0}$ (yellow), $\mathbf{45^0/225^0}$ (magenta), $\mathbf{90^0/270^0}$ (cyan), $\mathbf{135^0/315^0}$ (red)

Fig. 5. Correlated - Separated, $\mathbf{0^o}$ (yellow), $\mathbf{45^o}$ (magenta), $\mathbf{90^o}$ (cyan), $\mathbf{135^o}$ (Red), $\mathbf{180^o}$ (Green), $\mathbf{225^o}$ (Blue), $\mathbf{270^o}$ (yellow), $\mathbf{315^o}$ (magenta)

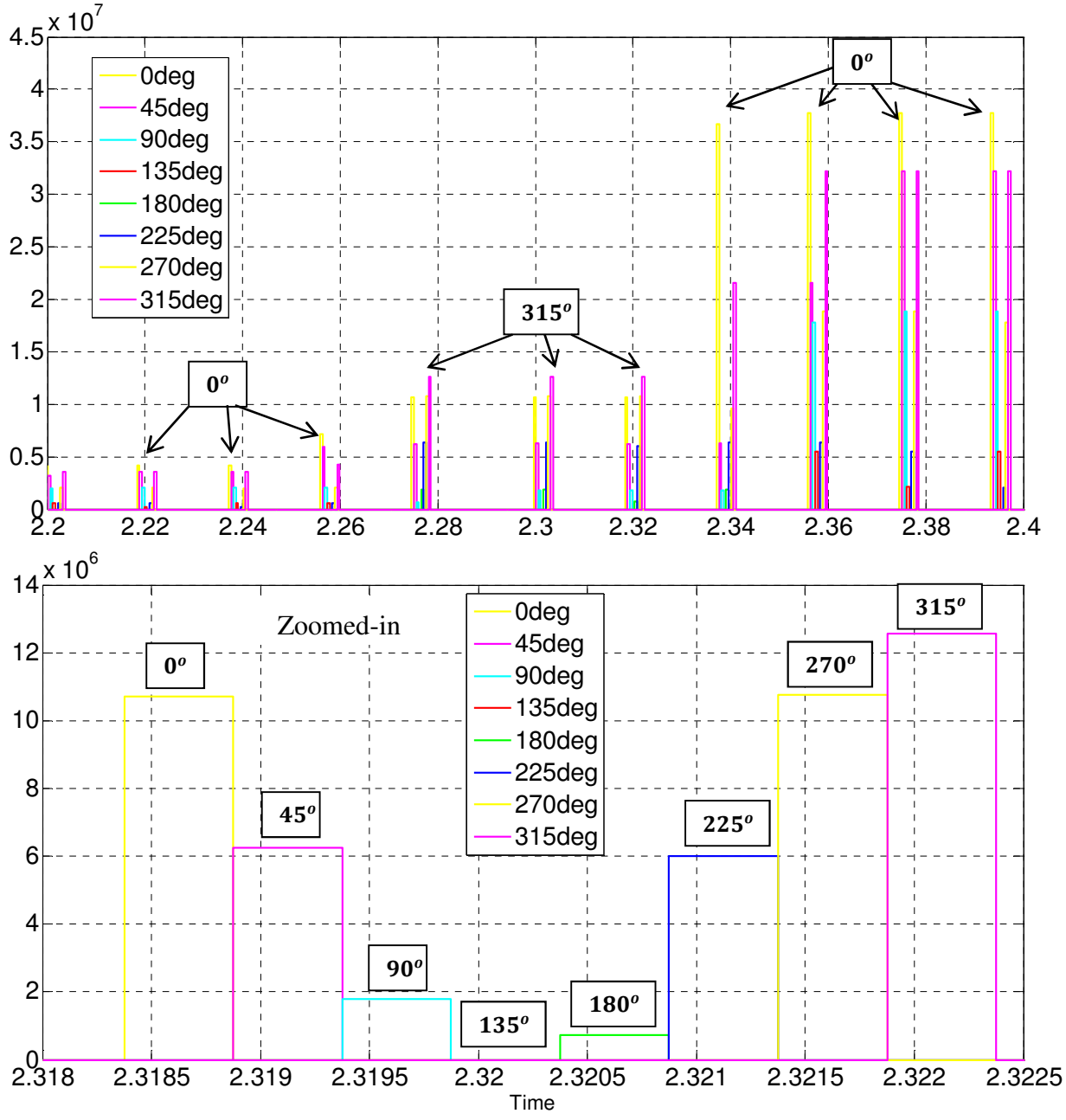

Fig. 6. Detected peaks, where $\mathbf{315^0}$ is dominant and $\mathbf{135^0}$ is the weakest

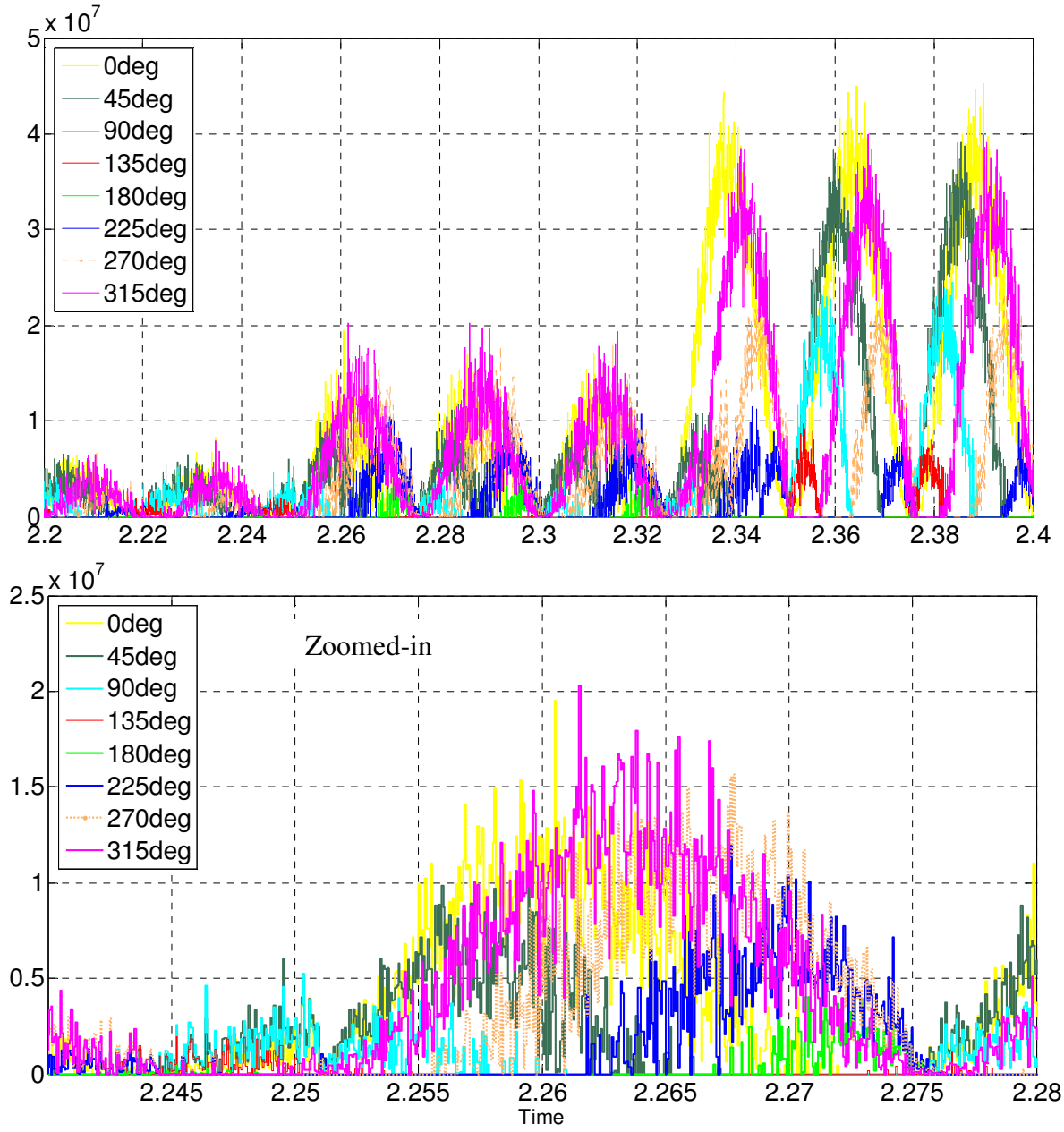

Fig. 7. 16-QAM Correlated - Separated, all angles in the presence of 15dB AWGN

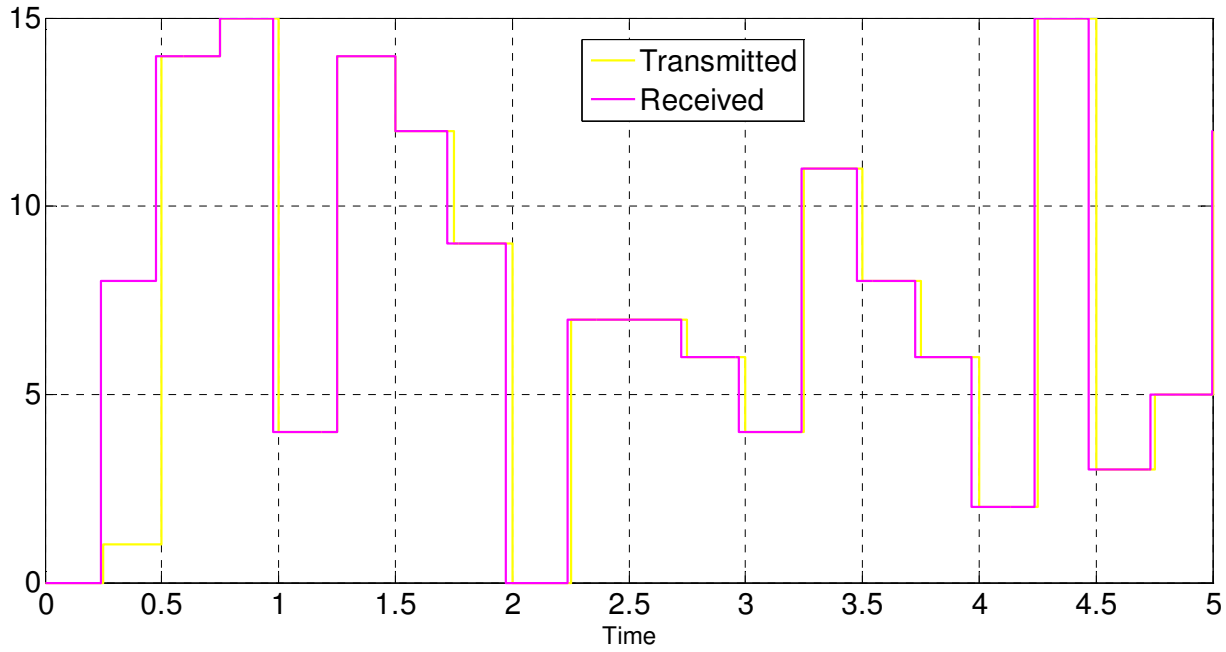

Fig. 8. Comparison of 16-QAM transmitted (yellow) and received (magenta) data over 5 s